APS SCIENCE 2011

RESEARCH AND ENGINEERING HIGHLIGHTS
FROM THE
ADVANCED PHOTON SOURCE
AT
ARGONNE NATIONAL LABORATORY

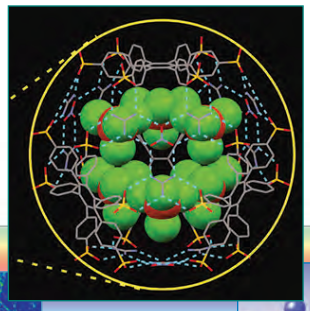

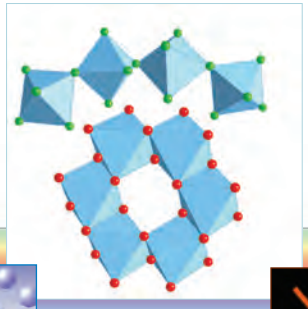

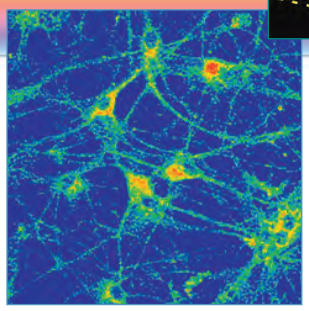

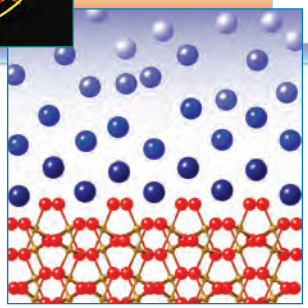

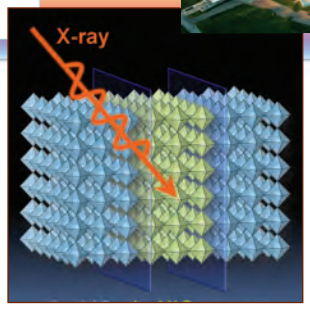

ANL-11/49
ISSN 1931-5007
May 2012

Argonne NATIONAL LABORATORY

ANL-11/49
ISSN 1931-5007
May 2012

The Advanced Photon Source at Argonne National Laboratory is supported by the U.S. Department of Energy, Office of Science, Office of Basic Energy Sciences, under Contract No. DE-ACO2-06CH11357.

ANL-11/49
ISSN 1931-5007
May 2012

APS SCIENCE 2011

Research and Engineering Highlights from the Advanced Photon Source at Argonne National Laboratory

Argonne is a U.S. Department of Energy laboratory managed by UChicago Argonne, LLC
The Advanced Photon Source is an Office of Science User Facility operated for the U.S. Department of Energy Office of Science by Argonne National Laboratory

For links to online content including animations, videos, etc., look for URLS or (for readers of the print version of this book) QR codes (below). QR codes quickly link smartphone users to the content.
A code reader can be downloaded from, for instance, http://www.quickmark.com.tw/En/basic/download.asp
Adobe Flash may be required for some films.

For news from, and information about, light sources worldwide, visit www.lightsources.org

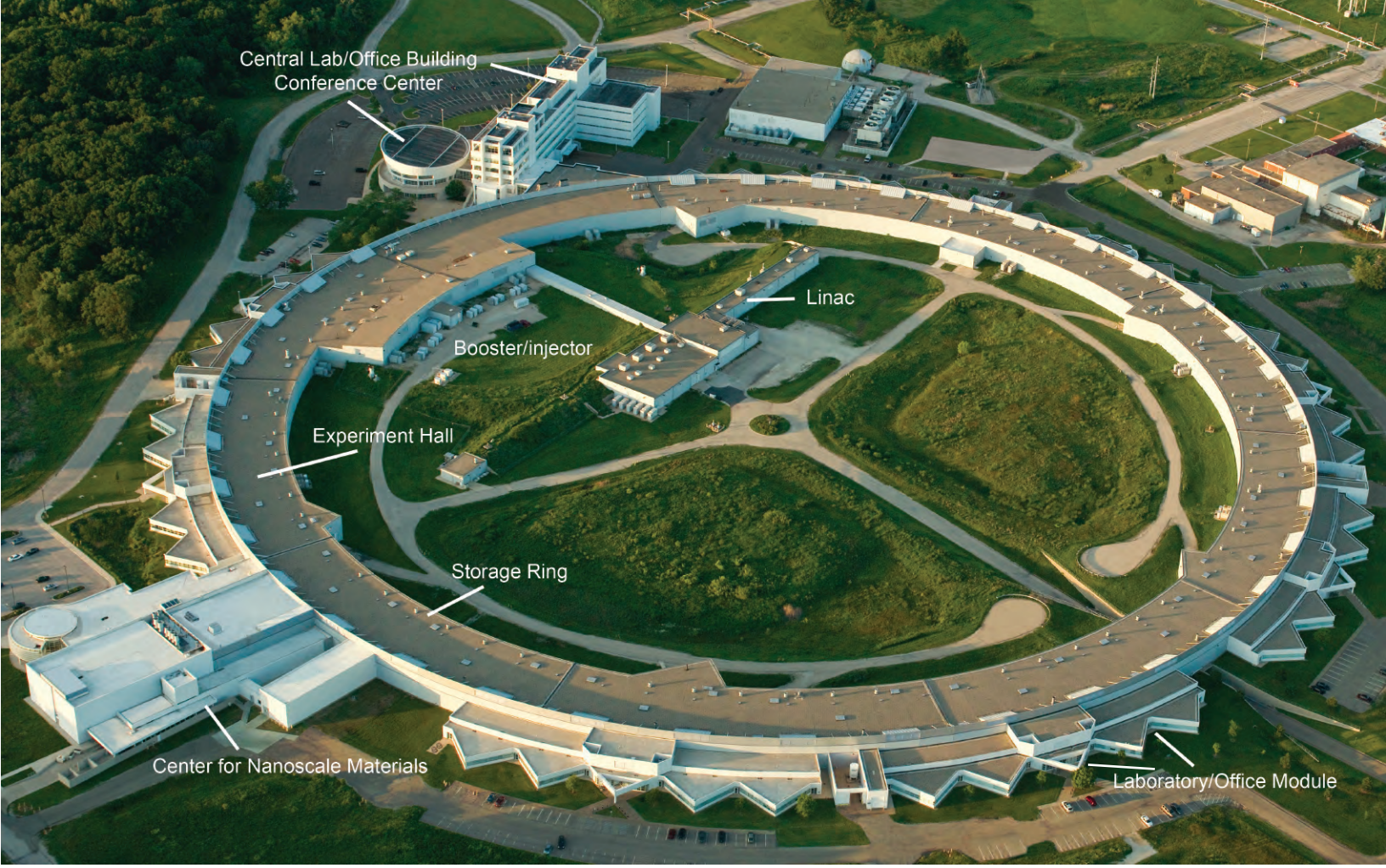

The Advanced Photon Source facility at Argonne National Laboratory

The Advanced Photon Source (APS) occupies an 80-acre site on the Argonne National Laboratory campus, about 25 miles from downtown Chicago, Illinois.
For directions to Argonne, see http://www.anl.gov/directions-and-visitor-information.

The APS, a national synchrotron radiation research facility operated by Argonne for the U.S. Department of Energy (DOE) Office of Science, provides this nation's brightest high-energy x-ray beams for science. Research by APS users extends from the center of the Earth to outer space, from new information on combustion engines and microcircuits to new drugs and nanotechnologies whose scale is measured in billionths of a meter. The APS helps researchers illuminate answers to the challenges of our high-tech world, from developing new forms of energy, to sustaining our nation's technological and economic competitiveness, to pushing back against the ravages of disease. Research at the APS promises to have far-reaching impact on our technology, our economy, our health, and fundamental knowledge of the materials that make up our world.

Contact us

For more information about the APS or to order additional copies of this, or previous, issues of *APS Science*, send an e-mail to apsinfo@aps.anl.gov, or write to APS Info, Bldg. 401, Rm. A4115, Argonne National Laboratory, 9700 S. Cass Ave., Argonne, IL 60439, or go to http://www.aps.anl.gov/Science/Reports/ to download PDF versions.

Visit the APS on the Web at www.aps.anl.gov

Table of Contents

Welcome

Brian Stephenson

May 2012

While one might have expected some tempering in the pace of the revolution that was sparked by the advent of accelerator-based x-ray facilities nearly 40 years ago, instead the future has never looked brighter for x-ray science.

Internationally, new storage-ring and free-electron-laser (FEL) x-ray facilities are being planned, built, and commissioned for user operations at an increasing pace. Nationally, the U. S. Department of Energy (DOE) has built the world's first FEL source to reach the x-ray region of the spectrum, the Linac Coherent Light Source at SLAC National Accelerator Laboratory, and will soon be commissioning a next-generation storage ring source for high-brilliance medium-energy x-rays, the National Synchrotron Light Source II at Brookhaven National Laboratory. Here at Argonne, we are in the design phase for a major upgrade to DOE's premier high-energy x-ray source, the Advanced Photon Source (APS).

In September of 2011 I was honored by Argonne Director Eric Isaacs to be appointed Director of this remarkable facility at such an exciting time. While my background is in development of x-ray techniques for materials science, and I've been involved in building several beamlines at APS and elsewhere, it is a new challenge and pleasure to facilitate research across the full spectrum of disciplines represented at APS. The science highlights in this book are just a sample of the stream of knowledge produced by our users in the past year. The APS Upgrade Project will move that knowledge forward as we provide our users with new tools and capabilities. A progress report by Upgrade Project Director George Srajer follows this "Welcome."

The year 2011 has been eventful. In addition to developing the conceptual design for the APS Upgrade Project, the scientific output of the APS continues to increase and the APS accelerator systems achieved new records for x-ray availability and machine reliability, building on what has been a gold standard for light source operation.

The life sciences are an important part of the APS research portfolio. Life science researchers are the largest segment of our user community, and approximately half of our operating beamlines are devoted to the life sciences. To forge stronger links with that community, and in the wake of strong recommendations for such action by several review committees, we have created a new part-time position, Senior Advisor for Life Sciences at the APS. Prof. Keith Moffat of the University of Chicago, a long-time leader in life science research at synchrotron x-ray facilities and a pioneer of time-resolved x-ray studies, has agreed to take on this responsibility. He is advising APS management, coordinating the development of a long-range strategy for life science at the APS, interacting with his counterparts at other facilities, and working with groups in the life science community to advocate for the field.

Even while planning for our upgrade, we've continued to augment our current facility. At the time of this writing the APS has 64 simultaneously operating end stations. A new canted beamline is being added at Sector 13. The 7-BM end station dedicated to ultrafast x-ray radiography and tomography experiments for fuel sprays and associated phenomena is undergoing commissioning. A new beamline for intermediate energy x-rays nearing completion at Sector 29 will operate at energies between 250 and 2500 eV to provide capabilities for angular resolved photoemission spectroscopy and soft x-ray resonant scattering. And a new beamline for dynamic compression studies is in the design stage. Users there will examine and understand, at the microscopic level, the dynamic response of materials subjected to large compressions, high temperatures, and large deformations on short time scales (picoseconds to microseconds).

Our user program continues to grow. The total number of APS users of all kinds (visitors, remote, mail-in, and co-proposers) reached 4713 in fiscal year (FY) 2011, an increase of 7% over FY2010. More users, in this case, meant more experiments. These exceed 4400 in FY11, 11% higher than in FY10. These increases come as our scheduled x-ray hours have stayed the same, indicating that we are learning to be more efficient in the way we run our user program. And the increase in users can also be taken as an indicator of the increasing number of researchers who are turning to synchrotron x-ray techniques to answer their questions.

Brian Stephenson
Associate Laboratory Director,
Photon Sciences;
and Director, Advanced Photon Source

The Advanced Photon Source Upgrade Project

George Srajer

May 2012

On Thursday, September 15, 2011, William Brinkman, Director of the U.S. Department of Energy (DOE) Office of Science gave his approval for Critical Decision 1 (CD-1) for the Advanced Photon Source Upgrade (APS-U) Project.

This action signaled DOE's formal approval of the alternative selection and cost range for the APS-U Project, established the preliminary technical scope of the project, and authorized the detailed preliminary design and initial research and development activities.

The awarding of CD-1 to the APS-U followed a rigorous and ultimately successful DOE review of a conceptual design for the APS-U on May 17-19, 2011. That review culminated in a unanimous review committee recommendation for approval of CD-1. We were all gratified that the committee members commended the work our staff had done, and the recognition of our staff's professionalism and dedication. In addition, the review provided comments and recommendations that will be incorporated into the preliminary design for the APS-U Project. The final conceptual design report has now been made publicly available at: http://www.aps.anl.gov/Upgrade/Documents/CDR/.

That was not the only review of the APS-U in 2011.

The APS Scientific Advisory Committee (SAC) held a review of Upgrade proposals on March 7-9. That review produced endorsement by the SAC of all 35 of the beamline proposals and their prioritization into three categories: Very Strongly Recommended, Strongly Recommended, and Recommended. This scientific prioritization has been extremely useful in planning for the Upgrade and associated long-term improvements to the APS. This review was followed almost immediately by the Argonne Director's Review of APS-U on March 14-16. This group reviewed the draft Conceptual Design Report and the project's scope, cost, schedule, and management in preparation for the May DOE review. The review also produced valuable advice that will help us carry the project forward.

At the time of this writing we have developed a "roadmap," a long-term plan for the locations of current and potential future programs/beamlines at the APS. Our approach was centered on the premise that a roadmap must incorporate not only the activities included in the base and contingent scope of the APS Upgrade Project, but also proposed activities outside of the Upgrade. Also, the goal is to minimize disruption or relocation of the existing collaborative access team or X-ray Science Division beamlines.

We presented roadmap scenarios to the Stakeholder Committee, resident users, XSD staff, the Project Science Advisory Committee (PSAC), the SAC, and Argonne's Laboratory Director. We also created a Web page for user input. Based on constructive and thoughtful feedback, we are in the process of narrowing the roadmap to one base scenario and several options.

We are growing the project team in anticipation of ever-increasing Upgrade-related effort and in preparation for upcoming milestones. The first one is the DOE Office of Science status review of the project scheduled for June 13, 2012. The purpose of this review is to assess the project's progress toward the Critical Decision 2, "Approve Performance Baseline" review in early fiscal year 2013. Our scientific and engineering staff continues the development of short-pulse x-ray capability and superconducting undulators, the innovative technologies that will complement and support the new and improved beamlines.

In February of 2012, Argonne Director Eric Isaacs appointed me APS Upgrade Project Director. By way of introduction, I have been with the APS since joining Argonne as an assistant physicist in 1991 during the original APS construction project. I have been involved in developing and managing x-ray science programs and facilities, most recently as Associate Division Director in XSD, as the leader for Argonne's Hard X-ray Sciences Strategic Initiative, and as a group leader for polarization studies.

Bringing the APS-U to fruition promises to be an exciting and fulfilling process for all of us. As noted on the Upgrade web site, "The … APS-U… Project… will enhance the capacity and capabilities of the … DOE's… largest national synchrotron x-ray research facility. Innovative physics and technologies developed and implemented by Argonne scientists and engineers will result in an improved world-class source of high-energy, high-brightness, tunable x-rays for scientific research. With nanometers of spatial resolution for imaging and picoseconds of timing resolution for dynamics research, the upgraded Advanced Photon Source will enhance our support of the DOE research missions in energy, the environment, and national security for the coming decades."

George Srajer

Deputy Associate Laboratory Director, Facility Development, Photon Sciences; and Director, Advanced Photon Source Upgrade Project

APS Sectors: At the APS, a "sector" comprises the radiation sources (one bending magnets and one insertion device, although the number of insertion devices in the straight sections of the storage ring can vary), and the beamlines, enclosures, and instrumentation that are associated with a particular storage ring sector. The APS has 35 sectors, 34 of which are dedicated to user science and experimental apparatus. The 35th has limited space for instrumentation and is used primarily for accelerator-related studies. **X-ray Science Division** (XSD) sectors comprise those beamlines operated by the APS. **Collaborative access team** (CAT) sectors comprise beamlines operated by independent groups made up of scientists from universities, industry, and/or research laboratories. **Collaborative development teams** (CDTs) comprise an external partner group that drives the development of a beamline that will be ultimately operated by the APS.

Key to the beamline descriptions below and that accompany each science highlight: Beamline designation • Sector operator • Disciplines • Techniques • Radiation source energy • User access modes •

For detailed information, go to http://www.aps.anl.gov/Beamlines/Directory/ and click on the "Beamline" link at left on the page.

Sector 1: XSD 1 • **1-BM-B,C:** Chemistry, materials science, physics • Powder diffraction, high-pressure diamond anvil cell • 8-22 keV • On-site • **1-ID-B,C,E:** Materials science, physics, chemistry • High-energy x-ray diffraction, radiography, small-angle x-ray scattering, fluorescence spectroscopy, Pair distribution function • 50-90 keV, 50-150 keV • On-site •

Sector 2: XSD 2 • **2-BM-A,B:** Physics, life sciences, geoscience, materials science • Tomography, phase contrast imaging • 5-30 keV, 0-30 keV • On-site • **2-ID-B:** Materials science, environmental science, physics • Coherent x-ray scattering (soft x-ray), microfluorescence (soft x-ray) • 635-2900 eV • On-site • **2-ID-D:** Life sciences, materials science, environmental science • Microfluorescence (hard x-ray), microdiffraction, micro x-ray absorbtion fine structure • 5-30 keV • On-site • **2-ID-E:** Life sciences, environmental science, materials science • Microfluorescence (hard x-ray) • 7-10.5 keV, 11-17 keV • On-site •

Sector 3: XSD 3 • **3-ID-B,C,D:** Physics • High-pressure diamond anvil cell, inelastic x-ray scattering, nuclear resonant scattering • 7-27 keV, 14.41-14.42 keV • On-site •

Sector 4: XSD 4 • **4-ID-C:** Physics, materials science • Magnetic circular dichroism (x-ray magnetic circular dichroism, soft x-ray), x-ray magnetic linear dichroism, x-ray photoemission spectroscopy, x-ray photoemission electron microscopy, anomalous and resonant scattering (soft x-ray) • 500-2800 eV • On-site • **4-ID-D:** Physics, materials science • Anomalous and resonant scattering (hard x-ray), magnetic x-ray scattering, magnetic circular dichroism (x-ray magnetic circular dichroism, hard x-ray) • 2.7-40 keV • On-site •

Sector 5: DuPont-Northwestern-Dow CAT • **5-BM-C:** Materials science, polymer science • Powder diffraction, tomography • 10-42 keV • On-site • **5-BM-D:** Materials science, polymer science • X-ray absorption fine structure, high-energy x-ray diffraction, general diffraction • 4.5-25 keV, 4.5-80 keV • On-site • **5-ID-B,C,D:** Materials science, polymer science • Powder diffraction, x-ray standing waves, x-ray optics development/techniques, small-angle x-ray scattering, surface diffraction, x-ray reflectivity, wide-angle x-ray scattering • 5-20 keV • On-site •

Sector 6: XSD 6 • **6-ID-B,C:** Physics, materials science • Magnetic x-ray scattering, anomalous and resonant scattering (hard x-ray), general diffraction, grazing incidence diffraction, surface diffraction (UHV) • 3.2-38 keV • On-site • **6-ID-D:** Physics, materials science • Magnetic x-ray scattering, high-energy x-ray diffraction, powder diffraction, pair distribution function • 27-52 keV, 50-100 keV, 67-130 keV • On-site •

Sector 7: XSD 7 • **7-BM-B:** Commissioning • **7-ID-B,C,D:** Materials science, atomic physics, chemistry • Time-resolved x-ray scattering, time-resolved x-ray absorption fine structure, phase contrast imaging • 6-21 keV • On-site •

Sector 8: XSD 8 • **8-BM-B:** Life sciences, environmental science • Microfluorescence (hard x-ray) • 5.5-20 keV, 7-17 keV • On-site • **8-ID-E:** Materials science, polymer science, physics • Grazing incidence small-angle scattering, x-ray photon correlation spectroscopy, intensity fluctuation spectroscopy, grazing incidence diffraction • 7.35-7.35 keV, 12-12 keV • On-site • **8-ID-I:** Materials science, physics, polymer science • Intensity fluctuation spectroscopy, small-angle x-ray scattering, x-ray photon correlation spectroscopy • 6-12.5 keV, 7.35-7.35 keV, 7.35 keV • On-site •

Sector 9: XSD 9 • **9-BM-B,C:** Materials science, chemistry • X-ray absorption fine structure • 2.1-23 keV • On-site • **9-ID-B,C:** Physics, materials science • Resonant inelastic x-ray scattering, inelastic x-ray scattering, liquid scattering • 4.5-24 keV • On-site •

Sector 10: Materials Research CAT (MR-CAT) • **10-BM-A,B:** Materials science, chemistry, environmental science, physics • X-ray absorption fine structure, x-ray lithography, tomography • 3-200 keV, 4-32 keV • On-site • **10-ID-B:** Materials science, environmental science, chemistry • X-ray absorption fine structure, time-resolved x-ray absorption fine structure, micro x-ray absorption fine structure, microfluorescence (hard x-ray) • 4.3-27 keV, 4.3-32 keV, 15-90 keV • On-site •

Sector 11: XSD 11 • **11-BM-B:** Chemistry, materials science, physics • Powder diffraction • 15-35 keV • On-site, mail-in • **11-ID-B:** Chemistry, environmental science, materials science • Pair distribution function • 58-60 keV, 90-91 keV • On-site • **11-ID-C:** Materials science • High-energy x-ray diffraction, diffuse x-ray scattering, pair distribution function • 115 keV • On-site **11-ID-D:** XSD • Chemistry • X-ray absorption fine structure, general diffraction, time-resolved x-ray absorption fine structure • 4-40 keV • On-site •

Sector 12: XSD 12 • **12-BM-B:** Materials science • X-ray absorption fine structure, powder diffraction, general diffraction, x-ray reflectivity, fluorescence spectroscopy, small-angle x-ray scattering • 5-23 keV • On-site • **12-ID-B:** Chemistry, materials science, life sciences, geoscience, polymer science • Small-angle x-ray scattering, grazing incidence small-angle scattering, wide-angle x-ray scattering • 7.9-14 keV • On-site • **12-ID-C,D:** Chemistry, physics, materials science • Small-angle x-ray scattering, grazing incidence small-angle scattering, wide-angle x-ray scattering, surface diffraction • 4.5-36 keV • On-site •

Sectors 13 through 15: Center for Advanced Radiation Sources (CARS)

Sector 13: GeoSoilEnviro(GSE)CARS-CAT • **13-BM-C:** Geoscience, environmental science • Surface diffraction, high-pressure diamond anvil cell, single-crystal diffraction • 10-10 keV, 18-18 keV, 30-30 keV • On-site • **13-BM-D:** Geoscience, environmental science • tomography, high-pressure diamond anvil cell, high-pressure multi-anvil press, x-ray absorption fine structure • 4.5-70 keV • On-site • **13-ID-C,D:** Geoscience, environmental science • Inelastic x-ray scattering, small x-ray absorbtion fine structure, microdiffraction, x-ray absorption fine structure, microfluorescence (hard x-ray), high-pressure diamond anvil cell, high-pressure multi-anvil press • 4-45 keV • On-site • ***Continued on page 10***

Argonne NATIONAL LABORATORY

THE ADVANCED PHOTON SOURCE

Sector Allocations & Disciplines

Source Configuration

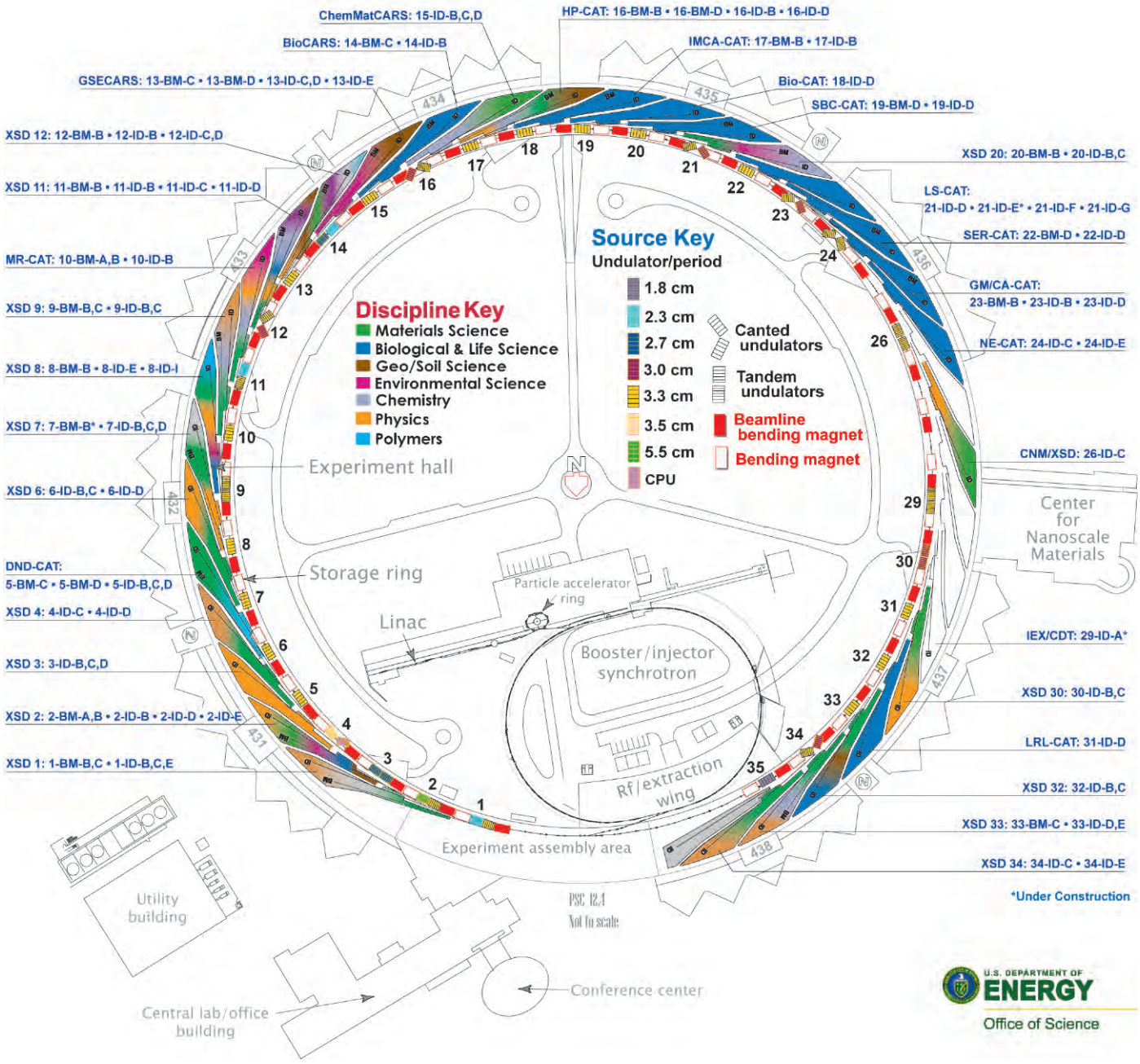

Continued from page 8

Sector 14: BioCARS-CAT • **14-BM-C:** Life sciences • Macromolecular crystallography, fiber diffraction, biohazards at the BSL2/3 level, subatomic (<0.85 Å) resolution, large unit cell crystallography • 8-14.9 keV • On-site • **14-ID-B:** Life sciences • Time-resolved crystallography, time-resolved x-ray scattering, Laue crystallography, wide-angle x-ray scattering, biohazards at the BSL2/3 level, macromolecular crystallography • 7-20 keV • On-site •

Sector15: ChemMatCARS-CAT • **15-ID-B,C,D:** Materials science, chemistry • Single-crystal diffraction, anomalous and resonant scattering (hard x-ray), wide-angle x-ray scattering, microdiffraction, liquid surface diffraction, small-angle x-ray scattering, ultra-small-angle x-ray scattering, high-pressure diamond anvil cell • 6-32 keV, 10-60 keV • On-site •

Sector 16: High Pressure CAT (HP-CAT) • **16-BM-B:** Materials science, geoscience, chemistry, physics • White Laue single-crystal diffraction, energy dispersive x-ray diffraction • 10-120 keV • On-site • **16-BM-D:** Materials science, geoscience, chemistry, physics • Powder angular dispersive x-ray diffraction, x-ray absorption near-edge structure, single-crystal diffraction, high-pressure diamond anvil cell • 6-70 keV • On-site • **16-ID-B:** Materials science, geoscience, chemistry, physics • Microdiffraction, single-crystal diffraction, high-pressure diamond anvil cell • 24-35 keV • On-site • **16-ID-D:** Materials science, geoscience, chemistry, physics • Nuclear resonant scattering, inelastic x-ray scattering (1-eV resolution), x-ray Raman scattering, x-ray emission spectroscopy, high-pressure diamond anvil cell • 6-25 keV, 14.41-14.42 keV • On-site •

Sector 17: Industrial Macromolecular Crystallography Association CAT (IMCA-CAT) • **17-BM-B:** Life sciences • Macromolecular crystallography, multi-wavelength anomalous dispersion, microbeam, single-wavelength anomalous dispersion • 7.5-14 keV • On-site, remote, mail-in • **17-ID-B:** Life sciences • Macromolecular crystallography, multi-wavelength anomalous dispersion, microbeam, single-wavelength anomalous dispersion • 6-20 keV • On-site, remote, mail-in •

Sector 18: Biophysics CAT (Bio-CAT) • **18-ID-D:** Life sciences • Fiber diffraction, microdiffraction, microfluorescence (hard x-ray), small-angle x-ray scattering, time-resolved x-ray scattering, micro x-ray absorption fine structure • 3.5-35 keV • On-site •

Sector 19: Structural Biology Center CAT (SBC-CAT) • **19-BM-D:** Life sciences, ultra-low-temperature (15K), multi-wavelength anomalous dispersion, single-wavelength anomalous dispersion • 6-13.5 keV • On-site, mail-in • **19-ID-D:** Life sciences • Large unit cell crystallography, macromolecular crystallography, microbeam, multi-wavelength anomalous dispersion, single-wavelength anomalous dispersion, subatomic (<0.85 Å) resolution, ultra-low-temperature (15K) • 6.5-19.5 keV • On-site, remote, mail-in •

Sector 20: XSD 20 • **20-BM-B:** Chemistry, environmental science, geoscience, materials science • Micro x-ray absorption fine structure, microfluorescence (hard x-ray), x-ray absorption fine structure • 2.7-25 keV, 2.7-30 keV, 2.7-35 keV • On-site • **20-ID-B,C:** Materials science, environmental science, chemistry • X-ray absorption fine structure, surface diffraction, x-ray Raman scattering, small-angle x-ray absorbtion fine structure, microfluorescence (hard x-ray), time-resolved x-ray absorption fine structure, x-ray emission spectroscopy • 4.3-27 keV, 7-52 keV • On-site •

Sector 21: Life Sciences CAT (LS-CAT) • **21-ID-D:** Life sciences • Macromolecular crystallography, microfluorescence (hard x-ray), nano-fluorescence imaging, nanotomography • 6.5-20 keV • On-site, remote, mail-in • **21-ID-F:** Life sciences • Macromolecular crystallography • 12.7 keV • On-site, remote, mail-in • **21-ID-G:** Life sciences • Macromolecular crystallography • 12.7 keV • On-site, remote, mail-in •

Sector 22: Southeast Regional CAT (SER-CAT) • **22-BM-D:** Life sciences • Macromolecular crystallography • 8-20 keV • On-site, remote • **22-ID-D:** Life sciences • Macromolecular crystallography, multi-wavelength anomalous dispersion, microbeam • 6-20 keV • On-site, remote •

Sector 23: General Medicine and Cancer Institutes CAT (GM/CA-CAT) • **23-BM-B:** Life sciences • Macromolecular crystallography • 12.5-12.75 keV • On-site • **23-ID-B:** Life sciences • Large unit cell crystallography, macromolecular crystallography, microbeam, multi-wavelength anomalous dispersion, single-wavelength anomalous dispersion, subatomic (<0.85 Å) resolution • 3.5-20 keV • Remote • **23-ID-D:** Life sciences • Macromolecular crystallography, microbeam, large unit cell crystallography, subatomic (<0.85 Å) resolution, multi-wavelength anomalous dispersion, single-wavelength anomalous dispersion • 5-20 keV • On-site, remote •

Sector 24: Northeastern CAT (NE-CAT) • **24-ID-C:** Life sciences • Macromolecular crystallography, microdiffraction, single-wavelength anomalous dispersion, single-crystal diffraction, microbeam • 6.5-23 keV • On-site • **24-ID-E:** Life sciences • Macromolecular crystallography, microbeam, microdiffraction, single-wavelength anomalous dispersion, single-crystal diffraction • 12.68 keV • On-site •

Sector 26: Center for Nanoscale Materials/X-ray Science Division (CNM/XSD) • **26-ID-C:** Physics, materials science • Microfluorescence (hard x-ray), microdiffraction, tomography • 8-12 keV • On-site •

Sector 29: Intermediate-Energy X-ray CDT (IEX/CDT) • **29-ID-A:** Commissioning •

Sector 30: XSD 30 • **30-ID-B,C:** Physics, materials science • Inelastic x-ray scattering, resonant inelastic x-ray scattering • 5-14 keV, 5-30 keV, 23.7-23.9 keV • On-site •

Sector 31: Lilly Research Laboratories CAT (LRL-CAT) • **31-ID-D:** Life sciences • Macromolecular crystallography, single-wavelength anomalous dispersion, single-crystal diffraction • 4.7-28 keV • Mail-in •

Sector 32: XSD 32 • **32-ID-B,C:** Materials science, life sciences, geoscience • Phase contrast imaging, radiography, transmission x-ray microscopy, tomography • 7-40 keV • On-site •

Sector 33: XSD 33 • **33-BM-C:** Materials science, physics, chemistry • Diffuse x-ray scattering, general diffraction, powder diffraction, x-ray reflectivity, grazing incidence diffraction, anomalous and resonant scattering (hard x-ray) • 5-35 keV • On-site • **33-ID-D,E:** Materials science, physics, chemistry • Anomalous and resonant scattering (hard x-ray), diffuse x-ray scattering, general diffraction, surface diffraction, x-ray reflectivity, x-ray standing waves • 4-40 keV, 6-21 keV • On-site •

Sector 34: XSD 34 • **34-ID-C:** Materials science, physics • Coherent x-ray scattering • 5-15 keV, 7-25 keV • On-site • **34-ID-E:** Materials science, physics • Microdiffraction, Laue crystallography, microbeam • 7-30 keV • On site •

Access to Beam Time at the APS

All beam time at the APS must be requested each cycle through the web-based Beam Time Request System. Five types of requests are possible: General User (a researcher not associated with a particular beamline), Partner User (a member of a collaborative access team [CAT], a partner user proposer, or a member of a collaborative development team), CAT member, CAT staff, and APS staff. Each beam time request (BTR) must be associated with a proposal, but the requirements for each proposal type differ.

The new APS User Portal (http://www.aps.anl.gov/Users/aps_userPortal.html) provides access to comprehensive information for prospective and current APS users.

General User proposals and BTRs

Proposals are peer reviewed and scored by a General User Proposal Review Panel, and time is allocated on the basis of scores and feasibility. A new BTR must be submitted each cycle, and for each cycle, allocation is competitive. Proposals expire in two years or when the number of shifts recommended in the peer review have been used, whichever comes first.

Partner User proposals and BTRs

Proposals are peer reviewed by a General User Proposal Review Panel and reviewed further by a subcommittee of the APS Scientific Advisory Committee; the final decision on acceptance is made by the APS Deputy Director. Although a new BTR must be submitted each cycle, a specific amount of beam time is guaranteed for up to three years.

CAT member proposals and BTRs

Proposals from CAT members are much shorter, do not expire, and are reviewed by processes developed by individual CATs. A new BTR must be submitted against these proposals for each cycle during which the proposal needs beam time, and allocation/scheduling is determined by the CAT.

CAT and APS staff member proposals and BTRs

Proposals of this type are also very short, do not expire, and are reviewed through processes developed by either the CAT or the APS. A new BTR must be submitted against such proposals for each cycle during which the proposal needs beam time. Each CAT/beamline determines how these BTRs are allocated/scheduled.

Industrial users

Improving industrial-user access to beam time is the focus of an APS pilot plan under the rubric "Measurement Access Mode" (MAM). Initially, several sectors agreed to participate in the MAM pilot. This involved setting aside three rapid-access beam-time shifts, at approximately two-week intervals (some 5% of the beam time). Qualifying MAM projects are then scheduled during each running cycle into the next available rapid-access period on the appropriate beamline. Concurrently, a web site (http://www.aps.anl.gov/industry/) was begun in order to make the whole access process easier for potential industrial users. An electronic contact information form filled out by the principal investigator (PI) is emailed to the APS Industrial Liaison Office for follow-up. This follow-up comprises an acknowledgement e-mail and contact with the PI for a verbal/e-mail discussion to obtain further information. If the consensus is that the proposed work meets three criteria (Can it be done here? Can it be done safely? Is there a reasonable chance that useful information can be obtained?), the office arranges contact between the PI and the beamline scientist for the APS sector where the work will be done. In addition, work on the appropriate administrative issues (user registration, user agreements, user accounts) is begun. The web site is currently being upgraded to include much more information for industrial users. For more information, contact Dennis Mills (DMM@aps.anl.gov) or the Industrial Liaison Office (aps-i@aps.anl.gov).

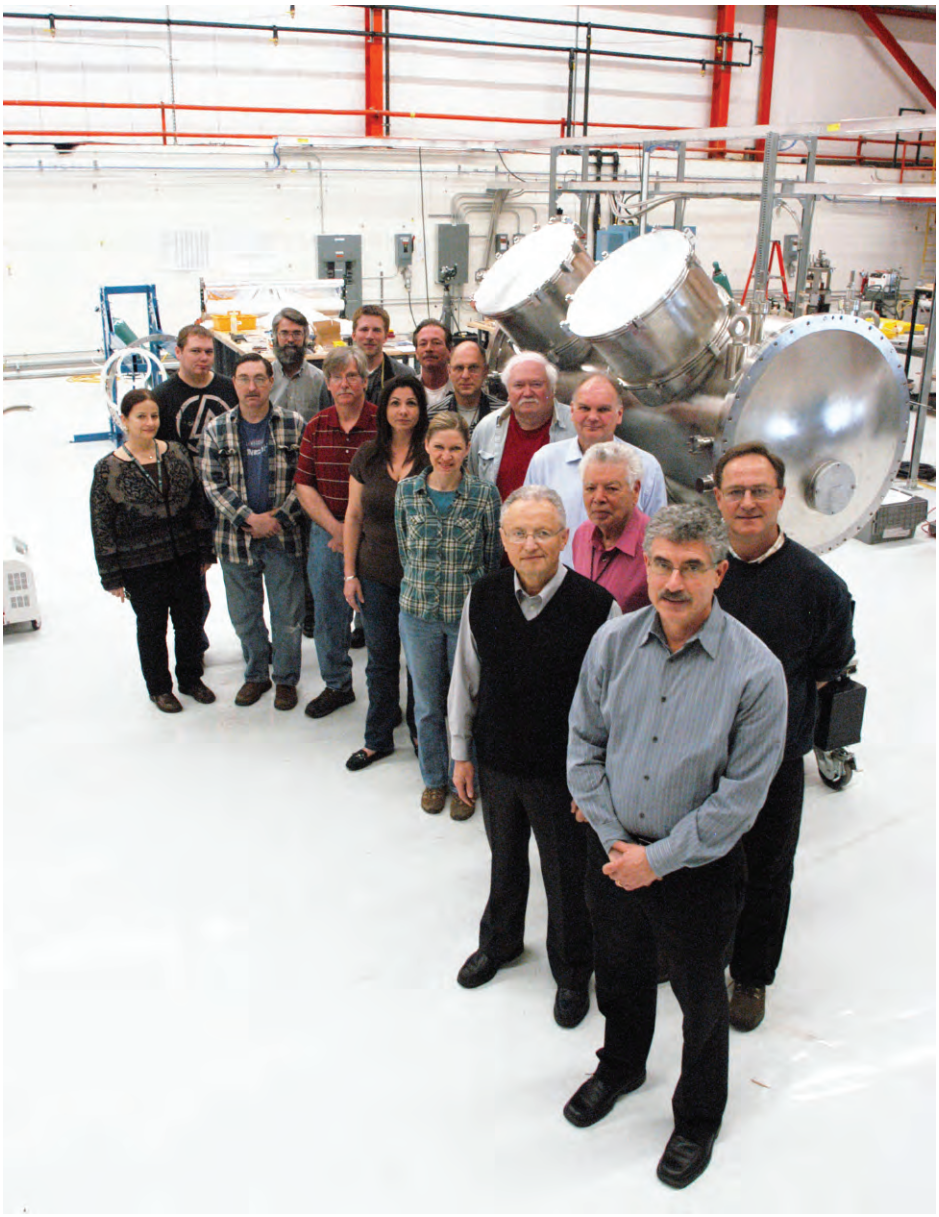

Members of the superconducting undulator and APS Upgrade (APS-U) Project teams assembled in the Bldg. 314 high bay at Argonne. Behind them is the large cryostat for the superconducting planar undulator being developed for the APS-U Project. Left to right in the photo are: Marion White (ASD-AOP and APS Upgrade Project); Joe Gagliano, Jr. (ASD-MD); John TerHAAR (ASD-MD); Joel Fuerst (ASD-MD); Chuck Doose (ASD-MD); Matthew Kasa (ASD-MD); Denise Skiadopoulos (AES-DD); Jack Burke (AES-MOM); Kurt Boerste (ASD-MD); Susan Bettenhausen (ASD-MD); Mike Merritt (ASD-MD); Yury Ivanyushenkov (ASD-MD); Emil Trakhtenberg (AES-MED); Efim Gluskin (ASD-MD); George Srajer (PSC and APS Upgrade Project); and Quentin Hasse (ASD-MD).

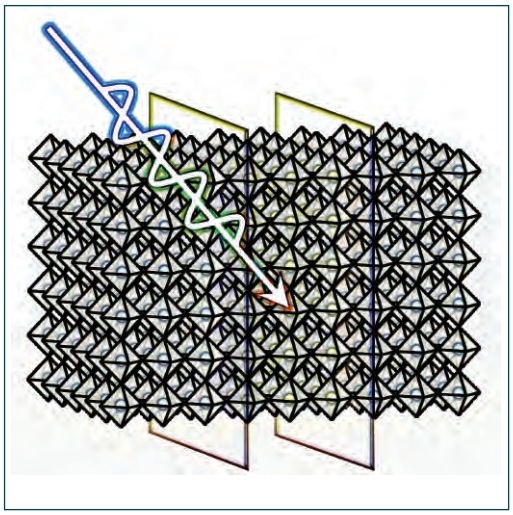

Electronic & Magnetic Materials

A NEW "TRIXS" FOR MEASURING LOW-ENERGY SURFACE AND INTERFACIAL ELECTRONIC STRUCTURE

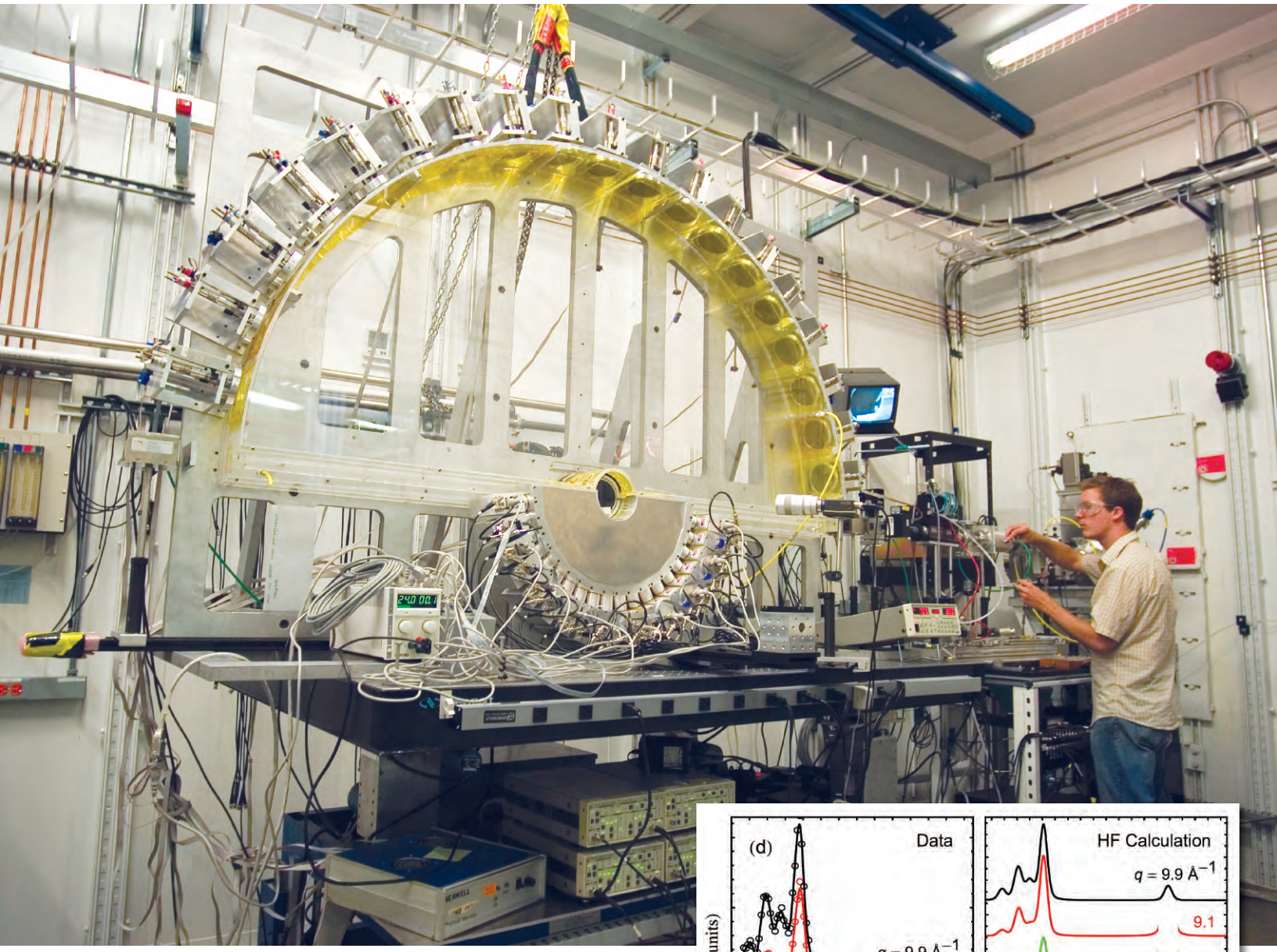

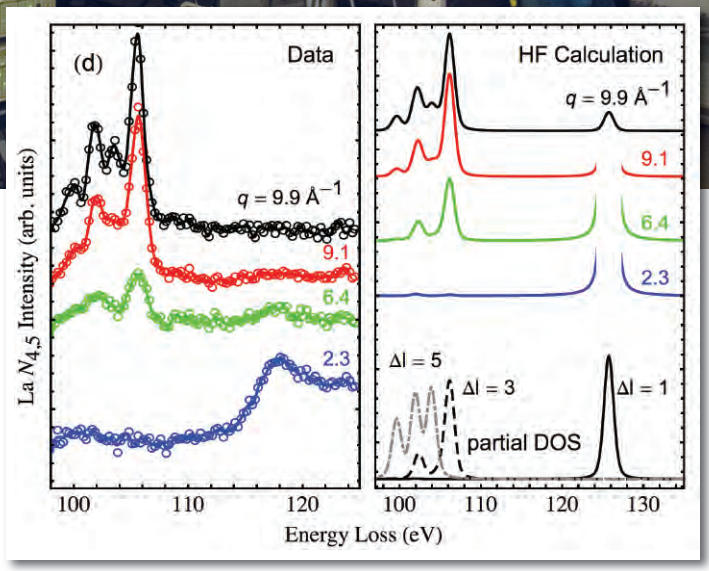

Fig. 1 (above). TRIXS measurements were performed on the LERIX spectrometer at beamline 20-ID-B,C. The outer fan of x-ray analyzers collects x-rays of a fixed scattered energy and focuses them to a corresponding array of detectors below. By scanning the incident energy, researchers collect loss spectra at 19 momentum transfers simultaneously.

Fig. 2 (right). Evolution of the La $N_{4,5}$-edge with q as measured by TRIXS (left) and by a Hartree Fock calculation for lanthanum (right). Note that the high q multiplet fine structure from lanthanum's *f*-states is quantum mechanically forbidden in dipole-limited techniques, like x-ray absorption and electron energy loss spectroscopy. The sensitivity of TRIXS to *f*-states occupation and hybridization will be useful for planned studies on lanthanides and actinides.

A variety of spectroscopy techniques have been used to probe the oftentimes complex structures found in thin films. Existing techniques have proven to be somewhat limited. Low-energy methods are constrained near the surface of the thin film and to vacuum-based environments; on the other hand, high-energy probes can access samples in extreme conditions, but are insensitive to light elements. In this research, a new high-energy x-ray technique — total reflection inelastic x-ray scattering (TRIXS) — was used at the APS to gather information about the electronic structure (i.e., the unoccupied density of states) within a thin film of $La_{0.6}Sr_{0.4}CoO_3$ (LSCO). The TRIXS method was able to probe electronic phenomena within the thin film that are hidden from other high-energy x-ray techniques, making it applicable for studying a wide range of new and interesting materials systems involving extreme environments typically inaccessible to lower-energy probes.

TRIXS is the extension of core-shell inelastic x-ray scattering (IXS) to surfaces. ("Core-shell" refers to an atom's inner electrons, as opposed to its outer, or valence, electrons). The basic idea of IXS is that when an x-ray photon inelastically strikes an atom, the energy transfer can eject a core electron. By changing the amount of energy transferred to the electron, IXS can map out the (unoccupied) density of states for a particular element, which is extremely sensitive to its local bonding and chemical state. This process, also known as x-ray Raman scattering, is analogous to more established techniques, like x-ray absorption spectroscopy or electron energy loss spectroscopy, but uses high-energy x-rays to measure sub-keV excitations. For instance, TRIXS was able to easily distinguish oxygen atoms in the LSCO thin film from its underlying $SrTiO_3$ (STO) substrate.

The TRIXS technique utilizes inelastic scattering via an incident beam of x-rays that strike a target at a very shallow angle almost parallel to the target's surface. Such a shallow, or grazing, angle of incidence results in nearly all of the x-rays being reflected from the surface. In contrast, steeper angles of incidence result in many of the x-rays being absorbed or refracted deeper into the material instead of being reflected. TRIXS uses x-ray beams that intercept the target close to its critical angle (typically a very small angle), which is the exact angle wherein all incident x-rays are (theoretically) reflected off the target.

Figure 1 shows the spectrometer used at XSD beamline 20-ID-B,C to capture the x-rays in this research. The material examined for this research was composed of a 10-nm-thick epitaxial thin film of LSCO deposited upon an STO substrate. Below the critical angle, the x-rays are expected to only penetrate 2-3-nm into the film. This surface sensitivity was confirmed by the suppression of the substrate's strong titanium signal and the enhancement of lanthanum, an element only present in the LSCO thin film. Scattering from lanthanum's 4*d* electrons (the $N_{4,5}$-edge) highlighted a unique aspect to TRIXS. At high scattering angle (corresponding to high momentum transfer, *q*), the 4*d* electrons were able to transition to open *f*-orbitals typically forbidden by low energy techniques. As seen in Fig. 2, the evolution of the spectrum with *q* arises from these new "dipole-forbidden" states with angular momentum beyond the reach of traditional spectroscopic methods. These findings will be applied to future studies of materials incorporating elements from the lanthanide and actinide groups of elements.

This research has for the first time applied the TRIXS method to a thin film, demonstrating several advantages as compared to other x-ray techniques. One advantage of TRIXS is its ability to confine x-ray interactions mostly to the thin film of interest. Another crucial advantage of TRIXS is its ability to probe electronic states that other methods cannot access. Finally, while a single type of thin-film oxide was investigated here, the TRIXS technique should be applicable to a wide array of new and interesting materials systems involving extreme environments typically inaccessible to lower energy probes. *— Philip Koth*

See: T.T. Fister[1]*, D.D. Fong[1], J.A. Eastman[1], H. Iddir[1], P. Zapol[1], P.H. Fuoss[1], M. Balasubramanian[1], R.A. Gordon[2], K.R. Balasubramaniam[3], and P.A. Salvador[3], "Total-Reflection Inelastic X-Ray Scattering from a 10-nm Thick $La_{0.6}Sr_{0.4}CoO_3$ Thin Film," Phys. Rev. Lett. **106**, 037401 (2011). DOI:10.1016/j.gca.2011.01.025
Author affiliations: [1]Argonne National Laboratory, [2]Simon Fraser University, [3]Carnegie Mellon University
Correspondence: *fister@anl.gov

Sector 20 at the APS and research at the facility are supported by the U.S. Department of Energy (DOE) Office of Science, a Major Resources Support grant from NSERC, the University of Washington, Simon Fraser University, and the APS. This research was also supported by the DOE Solid-State Energy Conversion Alliance (T.T. F., K.R.B., and P.A.S.). Use of the APS is supported by the DOE Office of Science under Contract No. DE-AC02-06CH11357.

20-ID-B,C • XSD • Materials science, environmental science, chemistry • X-ray absorption fine structure, surface diffraction, x-ray Raman scattering, small-angle x-ray absorbtion fine structure, microfluorescence (hard x-ray), time-resolved x-ray absorption fine structure, x-ray emission spectroscopy • 4.3-27 keV, 7-52 keV • On-site • Accepting general users •

WHAT DRIVES THE CHARGE DENSITY WAVE PHASE TRANSITION IN 2*H*-$NbSe_2$?

The origin of charge-density-wave (CDW) order, which is a low-energy ordered state of a solid, is a long-standing problem relevant to a number of important issues in condensed matter physics, such as the role of stripes in superconductivity of chemical compounds containing the copper anion, and charge fluctuations in the colossal magnetoresistive manganites that can change electrical resistance when introduced to a magnetic field, both of which have implications for new materials-based technologies. Researchers employing inelastic x-ray scattering experiments at the XSD 30-ID-C high-energy resolution inelastic x-ray scattering (HERIX) beamline at the APS have produced results that clarify how CDW functions in a material closely associated with the phenomenon, and could lead to investigations of other materials where electron-phonon coupling is important, and that possess unusual and often technologically useful electronic and magnetic properties.

Left to right; Ayman Said (XSD-IXN), John-Paul Castellan, Stephen Rosenkranz, and Ray Osborn (all ANL-MSD). Behind them is the HERIX spectrometer at Sector 30 of the APS. The instrument is used to study collective excitations of atoms in single crystals and disordered systems. The energy resolution of the HERIX spectrometer is 1.5 meV.

30-ID-B,C • XSD • Physics, materials science • Inelastic x-ray scattering, resonant inelastic x-ray scattering • 5-14 keV, 5-30 keV, 23.7-23.9 keV • On-site • Accepting general users •

When metals are cooled, they often undergo a phase transition to a differently ordered state. Iron and nickel, for example, become ferromagnetic below temperatures of several hundred degrees Celsius because their electronic spins spontaneously align to produce a net magnetization. Since the 1970s, several metals have been discovered to undergo a phase transition of another type, a transition to a CDW state. At high temperatures, the electronic density is the same in each crystallographic unit cell, but when the CDW state forms, the electronic density becomes non-uniform, with a periodic modulation that may not be commensurate with the underlying lattice. For many years, it was generally believed that this remarkable behavior was driven primarily by electron interactions, with the length scale of the modulation determined by the wavelength of the mobile conduction electrons. This is known as Fermi surface nesting, because the electrons that are coupled have momenta that lie on a surface of constant energy, the Fermi energy.

On the other hand, the electrons are also strongly coupled to the atomic nuclei making up the crystal lattice, so the modulation in electron density is always accompanied by a modulation of the lattice. The interactions are known as electron-phonon coupling (EPC), because the periodic lattice distortion can be thought of as a freezing of a quantized atomic vibration, or phonon. In most textbooks, it is assumed that the lattice distortion follows the electronic modulation, but they always occur simultaneously. Could it be the other way around, that is, that the lattice distortion is driving the electronic modulation?

This has become a central question in one of the most-often studied CDW materials, 2*H*-$NbSe_2$. Some theorists have questioned whether the electron-electron coupling is strong enough to produce a modulation with the observed wave vector (or inverse wavelength), and their doubts seemed to be confirmed by photoemission measurements of the electronic structure. However, there has never been any evidence of the alternative explanation, that the modulation wavelength is determined by the electron-phonon coupling.

To test this conjecture, researchers from Argonne, Karlsruhe Institute of Technology, the University of Tennessee, and the University of Colorado at Boulder measured the energies and linewidths of phonon excitations in 2*H*-$NbSe_2$ as a function of temperature and compared the measurements to *ab initio* calculations. They utilized high-energy resolution inelastic x-ray scattering at beamline 30-ID-C, which allowed them to obtain measurements of the relevant phonon excitations over a wide temperature range.

When 2*H*-$NbSe_2$ transitions to the CDW phase on cooling, acoustic phonons soften to zero energy and become overdamped over an extended region around the CDW wave vector (Fig. 1). This extended phonon collapse is dramatically different from the sharp cusp in the phonon energies expected from Fermi surface nesting. However, the energy widths of the phonons, which are proportional to the EPC, show a strong but also broad peak at the CDW wave vector $\mathbf{q}_{CDW}$ = (0.329, 0, 0) (wave vectors given in $\mathbf{q}$ = (2π/a, 2π/b, 2π/c) with $a = b$ = 3.44 Å and c = 12.55 Å). A detailed comparison between the experimental results and lattice dynamical calculations using density functional perturbation theory confirm that the periodicity of the CDW ordered state in 2*H*-$NbSe_2$ is determined entirely by the wavelength dependence of the EPC, not the electron-electron interaction.

The evidence that a wave vector-dependent EPC can drive a structural phase transition explains the enigmatic behavior of CDW ordering in 2*H*-$NbSe_2$ and may provide a new approach for understanding other strongly correlated systems for which EPC is important. The results have implications for many other strongly correlated systems, particularly CDW correlations in the form of stripes and/or checkerboard patterns that have been linked to the emergence of unusual states and physical properties, such as colossal magnetoresistance in manganites and the pseudogap state in cuprates. The observation of phonon anomalies in manganites at the wave vector of the checkerboard-type order and anomalies observed in $La_{2-x}Sr_xCu_{O4}$ at the stripe ordering wave vector demonstrate that strong EPC could be important in these materials as well.

— Vic Comello

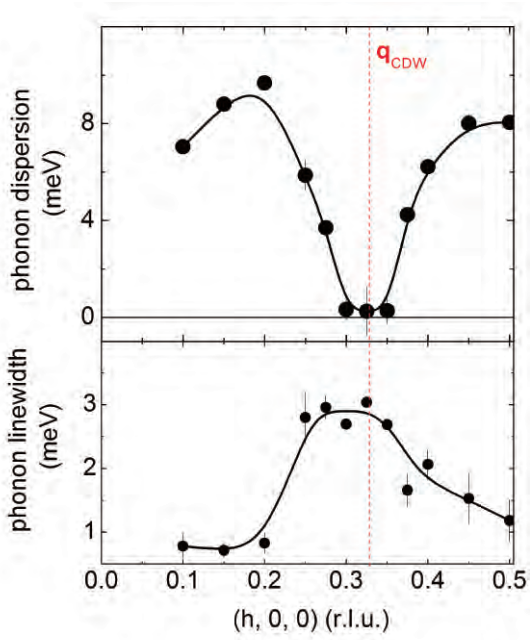

Fig. 1. Soft mode dispersion and linewidth at the CDW phase transition temperature T_{CDW} = 33K in 2H-$NbSe_2$ measured by high-resolution inelastic x-ray scattering at the HERIX spectrometer at Sector 30 of the APS. Lines are guides to the eye.

See: F. Weber[1,2*], S. Rosenkranz[1], J.-P. Castellan[1], R. Osborn[1], R. Hott[2], R. Heid[2], K.-P. Bohnen[2], T. Egami[3], A.H. Said[1], and D. Reznik[2,4], "Extended Phonon Collapse and the Origin of the Charge-Density Wave in 2*H*-$NbSe_2$," Phys. Rev. Lett. **107**, 107403 (September 2, 2011). DOI:10.1103/PhysRevLett.107.107403

Author affiliations: [1]Argonne National Laboratory, [2]Karlsruhe Institute of Technology, [3]University of Tennessee, [4]University of Colorado at Boulder
Correspondence: *frank.weber@kit.edu

Work at Argonne and use of the Advanced Photon Source was supported by the U.S. Department of Energy Office of Science under Contract No. DE-AC02-06CH11357. The construction of HERIX was partially supported by the National Science Foundation under Grant No. DMR-0115852.

STUDYING NEW MATERIALS FOR HIGH-TEMPERATURE SUPERCONDUCTORS

Researchers utilized an APS beamline to study how a nickelate-based superlattice synthesized from layers of $LaNiO_3$ and $LaAlO_3$ behaved due to quantum confinement, a situation in which electron movement is constrained to certain directions. These crystals shared electronic characteristics with cuprates, but were different enough that there was no guarantee that cuprate-like physics would be seen. The results of this study found characteristics common to both the crystals and the cuprates. In addition to holding out a tantalizing material for further study regarding potential superconductors, the ability to fine tune electron interaction in this superlattice might be a prototype for exploring a new generation of electronics based on Mott electrons. >>>

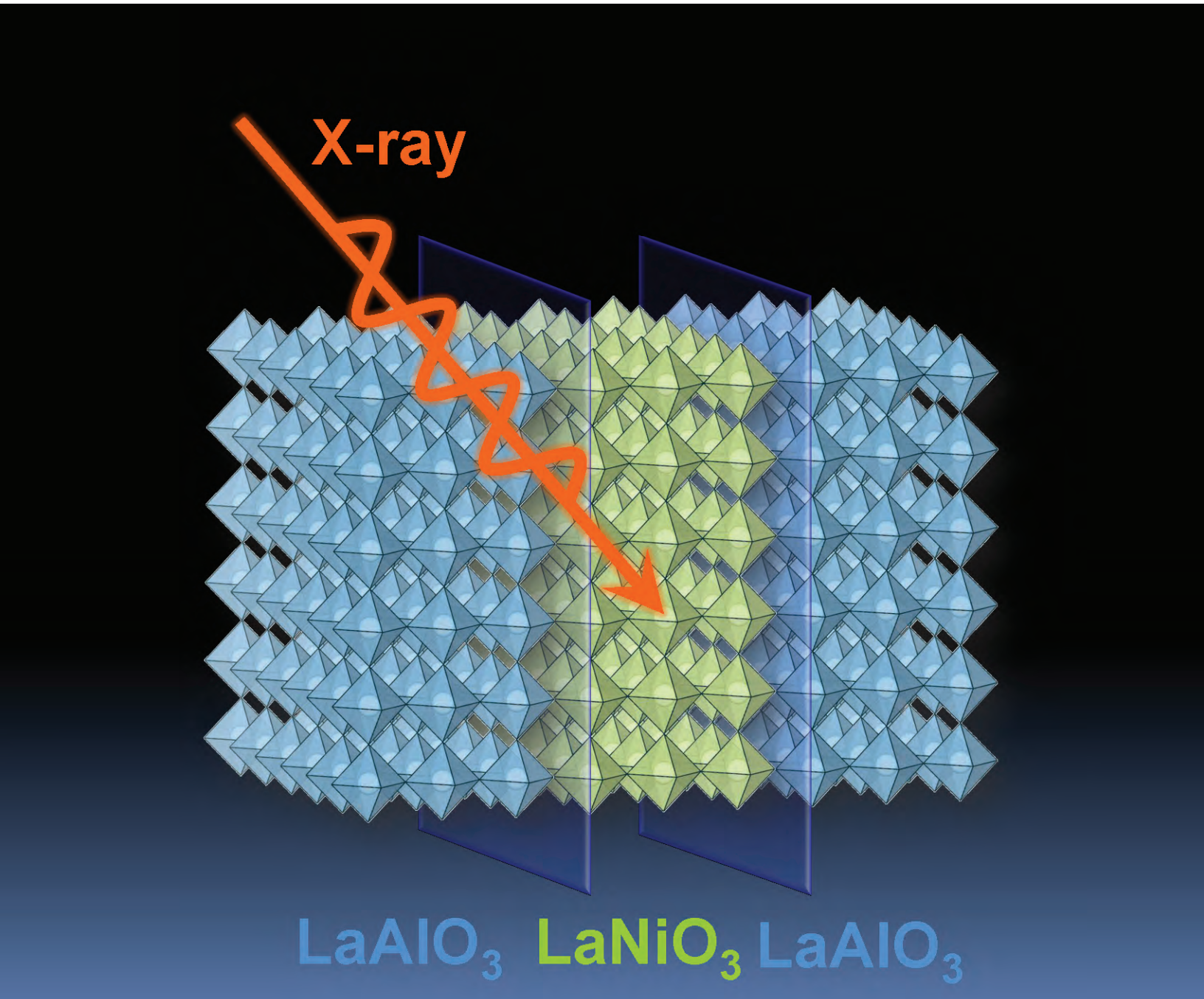

In the search for superconducting materials that don't need to be maintained in a liquid nitrogen bath — or even better but more elusive, can exist at room temperature — researchers study materials analogous to the copper oxides, or cuprates, which have been the only materials to exhibit superconductivity as high as 140K. One area of interest is nickel oxides, or nickelates, in which a nickel atom replaces the copper atom in a given material, while maintaining a similar crystal and electronic character. Such materials do not exist in nature, but recent advances in technology now exist to create layers of material as thin as a one-unit cell, creating not just a sandwich of different materials, but an entirely new crystalline material.

First, the researchers from the University of Arkansas, Lawrence Berkeley National Laboratory, Oak Ridge National Laboratory, Argonne, and Northern Illinois University performed electrical conductivity measurement on crystals with different thicknesses of the $LaNiO_3$ layer. They observed that as a change in thickness pushed the crystal toward the confinement limit — that is, electron movement being more and more constrained to a single direction — it artificially forced the material to become insulating in the vertical direction, perpendicular to the layers. This suggests that, within the plane of a single layer, this could be used to control, and indeed increase the interactivity of Mott electrons, antisocial electrons that generally prefer not to be shared between two atoms. Insulating well across layers, but increased Mott electron interaction within the layers is a characteristic shared by the cuprates.

To understand this phenomenon better, they examined what was happening to the nickel on a microscopic scale by using the XSD 4-ID-C beamline at the APS. X-rays from the beamline excited the core electron of the nickel atoms, allowing the researchers to map the nickel sites, as well as the local Mott electrons that coupled strongly to the hole left behind. From the spectra produced by the excited nickel electrons, the researchers confirmed that imposing quantum confinement in the vertical direction (that is, across the layers) enhances electron interaction in the horizontal direction, in line with the layers (Fig.1). This is further amplified by the simple fact that the aluminum in the alternating layers will not take on any extra Mott electrons in the vertical direction. Together this leads to a charge redistribution that constrains electron sharing to the horizontal direction.

Such a phenomenon is similar to what happens in superconducting cuprates. Indeed, the differentiation between electron interaction in the horizontal and vertical directions has a close relation to the temperature below which the material becomes superconducting.

The team will now attempt to "dope" — that is, remove some Mott electrons so the remaining electrons can move more freely — to mimic how the parent cuprate crystals were previously transformed into high-temperature superconductors. *— Karen Fox*

< Fig. 1. A 3-unit-cell-thick layer of $LaNiO_3$ sandwiched by two $LaAlO_3$ layers. Each octahedron cage has oxygen sitting at each corner, and the ball in the middle is either nickel or aluminum. The two planes highlight the interfaces where the electrons are constrained.

See: Jian Liu[1,2*], S. Okamoto[3], M. van Veenendaal[4,5], M. Kareev[1], B. Gray[1], P. Ryan[4], J.W. Freeland[4], and J. Chakhalian[1], "Quantum confinement of Mott electrons in ultrathin $LaNiO_3$/ $LaAlO_3$ superlattices," Phys. Rev. B **83**, 161102 (2011).
DOI:10.1103/PhysRevB.83.161102
Author affiliations: [1]University of Arkansas, [2]Lawrence Berkeley National Laboratory, [3]Oak Ridge National Laboratory, [4]Argonne National Laboratory, [5]Northern Illinois University
Correspondence: *jxl026@uark.edu

J.C. was supported by the Department of Defense-Army Research Office under Grant No. 0402-17291 and the U.S. National Science Foundation under Grant No. DMR-0747808. M.v.V. was supported by the U.S. Department of Energy (DOE) Office of Science under Contract DE-FG02-03ER46097. S.O. was supported by the U.S. DOE. Use of the Advanced Photon Source was supported by the U.S. DOE Office of Science under Contract DE-AC02-06CH11357.

4-ID-C • XSD • Physics, materials science • Magnetic circular dichroism (x-ray magnetic circular dichroism, soft x-ray), x-ray magnetic linear dichroism, x-ray photoemission spectroscopy, x-ray photoemission electron microscopy, anomalous and resonant scattering (soft x-ray) • 500-2800 eV • On-site • Accepting general users •

THE ORIGIN OF MAGNETISM IN IRON PNICTIDES AND IRON CHALOGENIDES

Efforts to resolve the age-old debate about the origin of metallic ferromagnetism have redoubled since the recent discovery that iron pnictides and chalcogenides become superconductive at relatively high temperatures, because it just may turn out that resolution of this problem with respect to these materials leads to the development of a new theory of superconductivity. At issue is whether magnetic order arises from local magnetic moments interacting through exchange interactions or whether it arises from a spin-density wave of itinerant electrons; another possibility is that magnetic order is the result of a combination of the two. Researchers utilized XSD beamline 9-ID-B,C and approached this question by studying several iron pnictides and chalcogenides in the paramagnetic regime where the presence of localized magnetism would be a telltale sign of local moments. Their results provide new clues to magnetism in iron-based superconductors. >>>

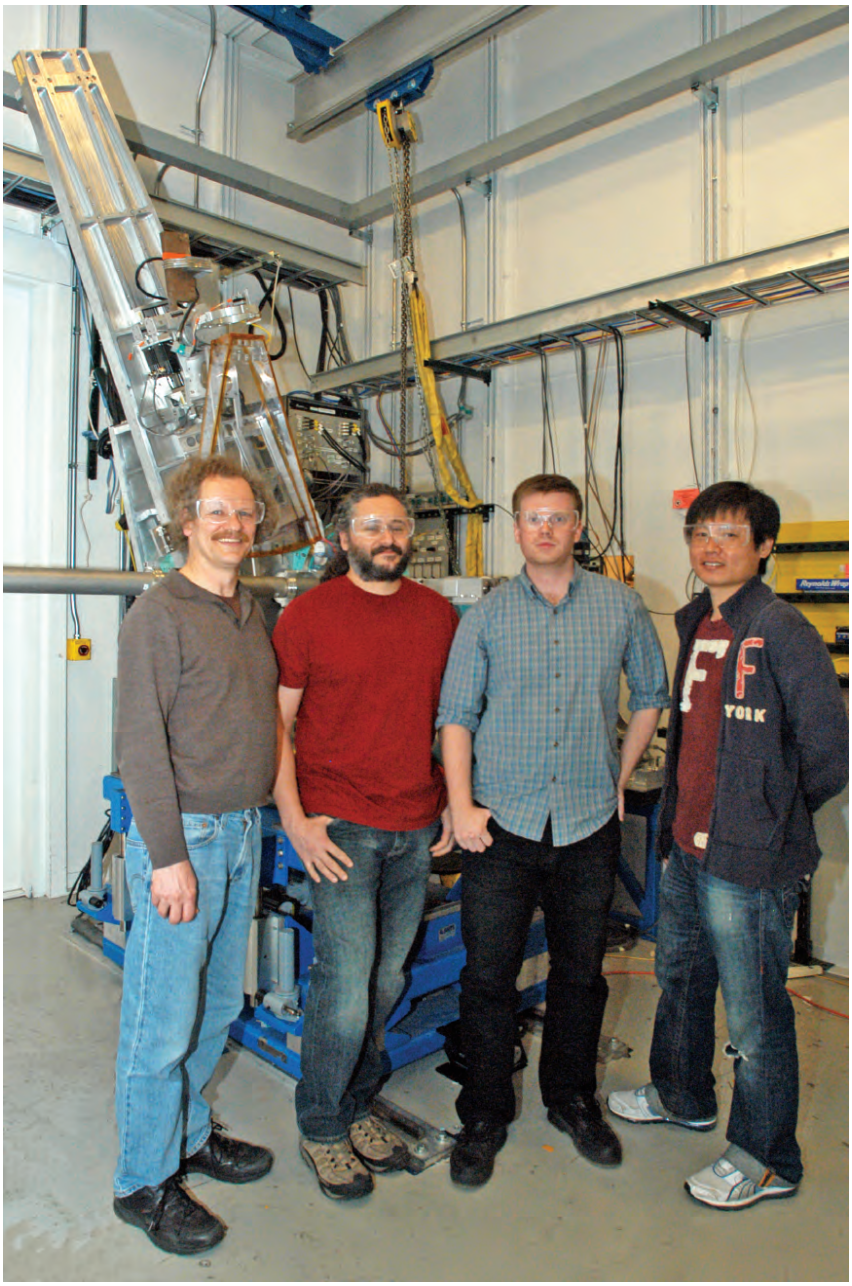

Some of the members of the research team in this study. Left to right, Thomas Gog and Diego Casa (both XSD-IXN), Hlynur Gretarsson (University of Toronto), and Jungho Kim (XSD-IXN). The instrument behind them is the "inelastic spectrometer" in APS research station 9-ID-B. It is used to perform inelastic x-ray scattering measurements with medium-energy resolution for electronic excitations in novel materials, such as high-T_c superconductors and other transition metal oxides.

The researchers, from the University of Toronto, Argonne, Brookhaven National Laboratory, the Chinese Academy of Science, Seoul National University, Japan Atomic Energy Agency, and Stanford University relied on x-ray emission spectroscopy (XES) because of its proven track record as a bulk-sensitive method for probing the spin states of iron (Fe) in minerals.

The comprehensive investigation involved the magnetic moments of PrFeAsO, $Ba(Fe,Co)_2As_2$, LiFeAs, $Fe_{1+x}(Te,Se)$, and $A_2Fe_4Se_5$ (where A = Cs, K, and Rb). The local moment sensitivity of the Kβ emission line ($3p \rightarrow 1s$) originates from a large overlap between the 3*p* and 3*d* orbitals, with the Kβ emission process involving a core-hole in the final state ($3p^5$) that interacts strongly with the $3d^6$ valence electrons by means of exchange interactions that are driven mainly by the presence of a net magnetic moment in the 3*d* valence shell. Since the 3*p*-3*d* interaction is local, this method is not sensitive to long-range order but only probes the local magnetic moment. The final states with antiparallel or parallel net spins between the $3p^5$ core-hole and $3d^6$ valence shell give rise to a main peak $K\beta_{1,3}$ and a low-energy satellite Kβ ', which has the appearance of a shoulder. Such final states are clearly seen in $K_2Fe_4Se_5$ (Fig.1b). The size of this splitting depends on the local moment, but extracting the position of the satellite peak can be difficult. In the case of $BaFe_2As_2$, for instance, the low-energy satellite Kβ ' is hard to observe (Fig.1a). So the team used integrated absolute difference analysis (IAD) in calculating the total local moment, which makes use of the whole spectrum rather than peak position.

Figure 1 shows an example of the IAD method. By subtracting each spectra from the nonmagnetic reference spectra of FeCrAs and integrating the absolute value of the difference, the corresponding IAD value can be extracted. In Fig.1c, the IAD value derived in this way can be seen for various samples. Since the IAD number is proportional to the local magnetic moment, this can be mapped onto a local magnetic moment scale (shown on the right-hand side).

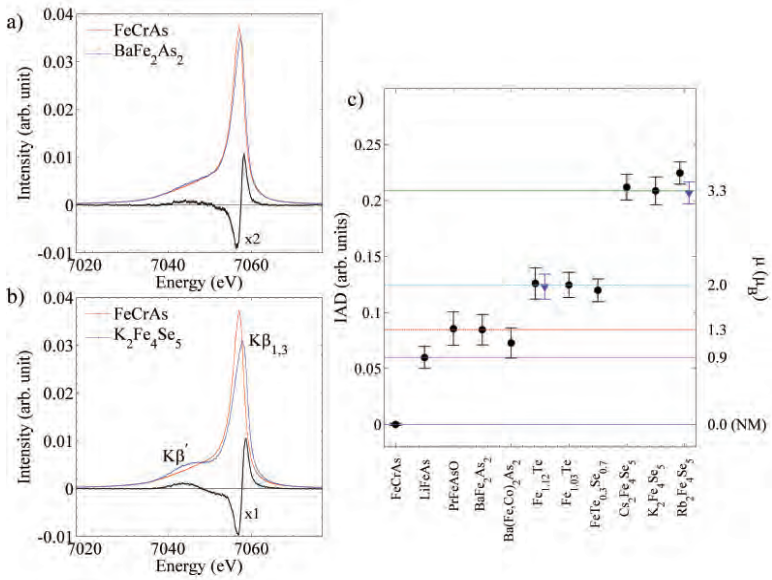

Fig. 1. (a and b) The XES spectra of the Fe Kβ emission lines for $BaFe_2As_2$ and $K_2Fe_4Se_5$; the nonmagnetic reference spectra of FeCrAs and the difference spectra are also plotted. Note that the difference spectrum for $BaFe_2As_2$ was magnified by a factor of 2. (c) The IAD values derived from the XES spectra for various samples. The room-temperature data are shown in circles, and the low-temperature IAD values at T = 15K are shown in triangles for $Fe_{1.12}Te$ and $Rb_2Fe_4Se_5$. On the right-hand side is the local magnetic moment scale.

Through this method, the researchers found local magnetic moments in the paramagnetic phase in all of the iron pnictide and chalcogenide samples. The moment size was found to be independent of temperature or carrier concentration but did vary significantly across different families. Specifically, all iron pnictide samples have local moments of about $1\mu_B$/Fe, while FeTe and $K_2Fe_4Se_5$ families have much larger local moments of ~$2\mu_B$/Fe and ~$3.3\mu_B$/Fe, respectively.

The results suggest that the magnetism in iron-based superconductors requires a description that takes into account the local moment as well as the effect of itinerant electrons. The relative importance of local-moment versus itinerant magnetism depends on the type of anions involved and the structural details. — *Vic Comello*

See: H. Gretarsson[1] , A. Lupascu[1], Jungho Kim[2], D. Casa[2], T. Gog[2], W. Wu[1], S.R. Julian[1], Z.J. Xu[3], J.S. Wen[3], G.D. Gu[3], R.H. Yuan[4], Z.G. Chen[4], N.-L. Wang[4], S. Khim[5], K.H. Kim[5], M. Ishikado[6], I. Jarrige[6], S. Shamoto[6], J.-H. Chu[7], I.R. Fisher[7], and Young-June Kim[1]*, "Revealing the dual nature of magnetism in iron pnictides and iron chalcogenides using x-ray emission spectroscopy," Phys. Rev. B **84**, 100509 (2011). DOI:10.1103/PhysRevB.84.100509

Author affiliations: [1]University of Toronto, [2]Argonne National Laboratory, [3]Brookhaven National Laboratory, [4]Chinese Academy of Sciences, [5]Seoul National University, [6]Japan Atomic Energy Agency, [7]Stanford University

Correspondence:

*yjkim@physics.utoronto.ca

Y.-J.K. was supported by the KOFST through the Brainpool program. The work at Brookhaven National Laboratory was supported by the U.S. Department of Energy (DOE) under Contract No. DE-AC02-98CH10886. N. L.W. acknowledges NSFC and the MOST 973 project from China. Work at Seoul National University was supported by the National Creative Research Initiative (2010-0018300). Work at the Japan Atomic Energy Agency was supported by JST, TRIP. Work at Stanford was supported by the U.S. DOE Office of Science under Contract No. DE-AC02-76SF00515. Use of the Advanced Photon Source at Argonne National Laboratory was supported by the U.S. DOE Office of Science under Contract No. DE-AC02-06CH11357.

9-ID-B,C • XSD • Physics, materials science • Resonant inelastic x-ray scattering, inelastic x-ray scattering, liquid scattering • 4.5-24 keV • On-site • Accepting general users

ANALYZING PTCDA MONOLAYERS ON EPITAXIAL GRAPHENE

There is great interest in graphene-based electronics because graphene has excellent and unique electronic properties that can be used for future applications such as flexible and stretchable transparent electrodes and optical modulators to significantly enhance ultrafast optical communication and computing. However, integrating graphene with other materials is difficult because it is largely chemically inert: there is no chemical handle on graphene for a reaction to take place. Thus, materials deposited on the surface, such as dielectric thin films, do not form high-quality layers. A possible solution to this problem was sought by researchers who investigated whether monolayers of a common organic semiconductor could adsorb to epitaxial graphene without disturbing its electronic properties and act as a seeding layer for growth of additional thin films. Using scanning tunneling microscopy (STM) and high-resolution x-ray reflectivity (XRR) at XSD beamline 33-BM-C at the APS, these researchers studied both the lateral and vertical structure of a substrate-graphene-semiconductor stack and found an organic semiconductor material that is a promising seed layer for depositing high-quality dielectric films. >>>

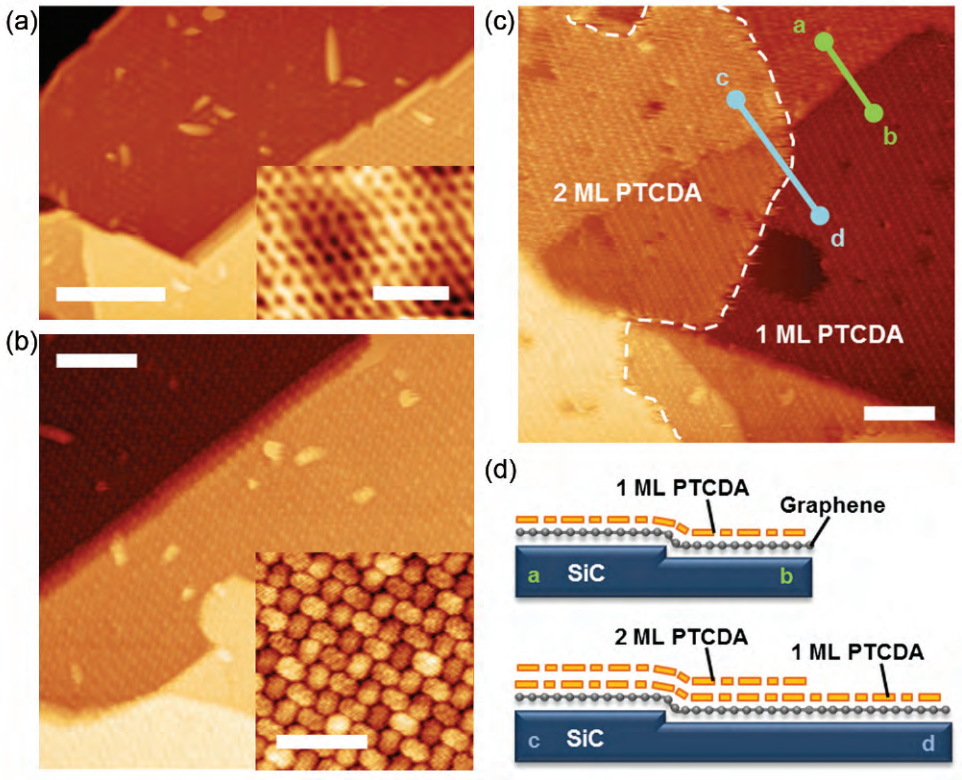

Fig.1. UHV STM images of the sample surfaces. (a) Clean epitaxial graphene (Sample bias −2.1 V, tunneling current 50 pA, scale bar 20 nm). Inset: atomically resolved image showing the honeycomb lattice of graphene (−0.4 V, 50 pA, 1 nm). (b) Single-monolayer coverage of PTCDA on epitaxial graphene (−1.9 V, 22 pA, 10 nm). Inset: Molecularly resolved image showing that the PTCDA monolayer has a herringbone arrangement (−2.0 V, 70 pA, 4 nm). (c) At ~ 1.5-ML PTCDA coverage, the sample concurrently possesses regions with 1-ML and 2-ML PTCDA (−1.9 V, 22 pA, 10 nm). The region to the left of the white dashed line has two layers of PTCDA, while the region to the right has one layer. (d) Schematic depth profiles of the two lines, a–b and c–d, indicated in (c). The SiC step edge in both profiles is the same, but is covered by one layer of PTCDA in line a–b and two layers in line c–d. From J.D. Emery et al., Surf. Sci. **605**, 1685 (2011).

Researchers have tried to overcome the graphene-integration problem by creating functional groups that are covalently bound to graphene, but this process can interfere with graphene's desirable properties. The researchers in this study instead deposited an organic semiconductor called perylene-3,4,9,10-tetracarboxylic dianhydride (PTCDA) onto the graphene. PTCDA self-assembles into a highly ordered monolayered film.

The researchers, at Northwestern University, École Supérieure de Physique et de Chimie Industrielles de la ville de Paris, and Argonne grew graphene on a SiC substrate via thermal decomposition, resulting in a surface with both single and bilayer graphene. They deposited PTCDA monolayers in an ultra-high-vacuum (UHV) system, which formed films both one and two layers thick on the graphene. The UHV system included a separate chamber for performing STM, which allowed them to image the lateral structure without breaking vacuum. Samples of varying PTCDA dose were also transferred to beamline 33-BM-C for XRR studies.

From the STM and XRR data, the researchers inferred the structure of the functionalized graphene, using a combination of Fienup-based phase-retrieval methods and model-based least-squares analyses to interpret the data. The STM data shows that PTCDA forms well-ordered monolayers with a long-range herringbone arrangement that conforms seamlessly to the surface of graphene (Fig. 1). XRR allowed them to resolve the interfacial structure of the PTCDA layers on epitaxial graphene. They employed 17-keV x-rays, with an incident flux of about 10^{10} photons/s, and a 2.0-mm × 0.1-mm beam to obtain reflectivity data (Fig. 2). The x-ray scattered intensity pattern near the specular condition was collected with a point detector for low-angle data, and with a two-dimensional charge-coupled device at high angle. From this data, full electron density profiles were developed for samples of three varying PTCDA coverages.

The interlayer spacing between PTCDA and graphene depends on the molecular interaction between layers. Based on the data, the spacing between the PTCDA and the graphene is roughly 3.40 Å (similar to the bonding distance between individual graphene layers). This supports the view that the relationship is defined by π–π^* stacking and suggests that, because of the large spatial separation, the electronic properties of the PTCDA are largely decoupled from those of epitaxial graphene.

Because it does not disrupt the electronic properties of the underlying graphene and forms well-ordered, stable monolayers, PTCDA is a promising seed layer for depositing high-quality dielectric films with a high dielectric constant. In subsequent work, the team grew and characterized highly insulating layers on top of the PTCDA and demonstrated well-behaved metal-oxide-graphene capacitors enabled by the use of PTCDA seeding layers [1].

— Yvonne Carts-Powell

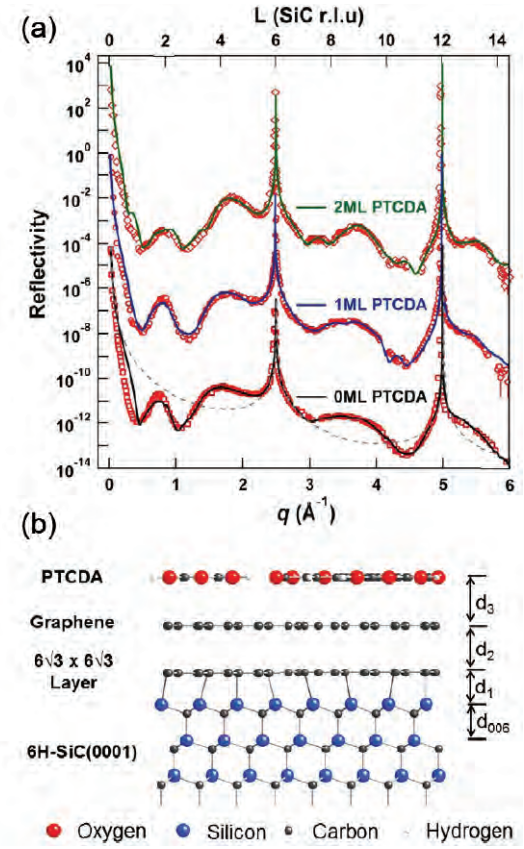

Fig. 2. (a) XRR data and fits for bare graphene (zero monolayer or 0 ML, red squares, black line), as well as a 1-ML (red circles, blue line) and 2-ML (red diamonds, green line) PTCDA grown on epitaxial graphene. These data provide information about the vertical structural profiles of the PTCDA/EG/SiC (0001) stack, allowing for the extraction of interplanar spacing of the individual layers. (b) An idealized depiction of 1-ML PTCDA on epitaxial graphene as viewed from the [1000] direction with oxgyen, silicon, carbon, and hydrogen atoms shown in red, blue, gray, and white, respectively. The interplanar spacing between the graphene sheet and the PTCDA layer is d3, approximately 3.4 Å, indicating characteristic π stacking interactions between the two layers.

REFERENCE

[1] J. M. P. Alaboson et al, "Seeding Atomic Layer Deposition of High-k Dielectrics on Epitaxial Graphene with Organic Self-Assembled Monolayers" ACS Nano. **5**(6), 5223 (2011).

See: Jonathan D. Emery[1], Qing Hua Wang[1], Marie Zarrouati[2], Paul Fenter[3], Mark C. Hersam[1]*, and Michael J. Bedzyk[1], "Structural analysis of PTCDA monolayers on epitaxial graphene with ultra-high vacuum scanning tunneling microscopy and high-resolution X-ray reflectivity," Surf. Sci. **605**, 1685 (2011). DOI:10.1016/j.susc.2010.11.008.

Author affiliations: [1]Northwestern University, [2]École Supérieure de Physique et de Chimie Industrielles de la ville de Paris, [3]Argonne National Laboratory

Correspondence:

*m-hersam@northwestern.edu

This work was partially supported by the National Science Foundation (DMR-0520513 to the MRSEC at Northwestern University and EEC-0647560), the Office of Naval Research (N00014-09-1-0180), and the Department of Energy (DOE) DEJSC0001785, DE-AC02-06CH11357 to the CEES-EFRC. X-ray characterization and analysis by P.F. was funded by DE-AC02-06CH11357 to the CEES-EFRC. Use of the Advanced Photon Source at Argonne National Laboratory was supported by the U.S. DOE Office of Science under Contract No. DE-AC02-06CH11357.

33-BM-C • XSD • Materials science, physics, chemistry • Diffuse x-ray scattering, general diffraction, powder diffraction, x-ray reflectivity, grazing incidence diffraction, anomalous and resonant scattering (hard x-ray) • 5-35 keV • On-site • Accepting general users •

Beamline scientist Steven Weigand (Northwestern University and DND-CAT) adjusting the fume exhaust prior to a small-angle x-ray scattering experiment using the Linkam thermal stage capillary flow-cell at Sector 5 of the APS.

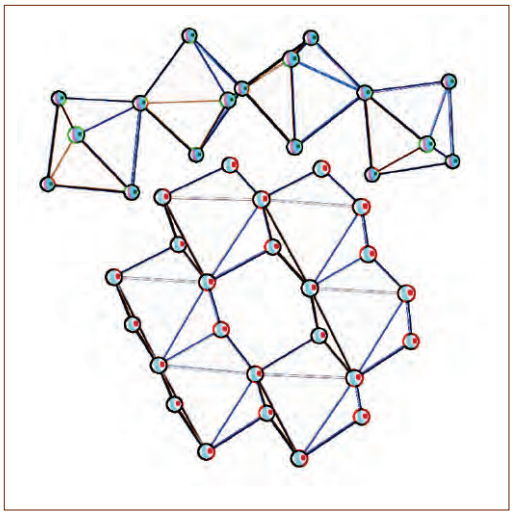

Engineering Materials & Applications

STACKING SOLAR CELLS

Photovoltaic devices that directly convert incident sunlight into electricity offer great potential as a sustainable, non-polluting energy source. Chemists hope to find inexpensive alternatives to inorganic semiconducting materials, such as silicon, cadmium telluride, and copper indium gallium selenide. Organic semiconducting polymers especially show much promise, given that they are relatively easy to make, their properties can be fine-tuned, and they can be flexible as well as inexpensive. Unfortunately, the efficiencies of organic, as opposed to inorganic semiconductors are not high. Now, a team of researchers has carried out studies at the APS on how novel copolymers stack together to boost their solar energy conversion efficiency.

Finding ways to boost efficiencies in such materials is the goal of the research team from The University of Chicago, the National Institute of Standards and Technology (NIST), the University of Delaware, and Argonne. The researchers made a series of semiconducting copolymers, known generically as PTAT-x, a polymeric version of tetrathienoanthracene. This molecular unit contains a series of alternating double bonds between carbon atoms, a conjugated system, which is a prerequisite for building a semiconducting polymer. In the polymer the conjugated system forms long chains of electron-rich bonds. Shine a light on such a system and electrons are nudged along the chains so that a current flows.

The team incorporated a second conjugated monomer unit, thieno[3,4-b]thiophene, into their copolymers. The polymer chains within the material stack together as the conjugated systems line up. Spectroscopy revealed that the material absorbs ultraviolet-visible light with three broad spectral peaks at 684-, 664-, and 665-nm wavelengths in the red part of the visible spectrum.

The team then fabricated thin layers of their semiconducting copolymers, just 100-nm thick, into a solar-cell device for testing. They carried out small-angle neutron scattering (SANS) measurements on the NG7 30-m SANS instrument at NIST (Fig. 1). The SANS measurements showed that certain polymer blends contain large domains — crystalline regions — that are detrimental to conversion of solar energy, whereas no such domains are present in the blend of PTAT-3 and $PC_{61}BM$. This allowed the team to focus on this specific blend for further investigation.

They also carried out grazing incidence wide-angle x-ray scattering (GIWAXS) measurements using XSD beamline 8-ID-E at the APS, to show how the stacking of the conjugated bonds in PTAT-3/ $PC_{61}BM$ is parallel to the surface on which the copolymer film is deposited, despite or perhaps because of the presence of the bulky 2-butyloctyl alkyl side chains on the PTAT-3 polymer chain (Fig. 2). This bodes well for the transport of "holes," the opposite of electrons, from one electrode to the second electrode at the opposite end of the film.

In addition, PTAT-3 is soluble in organic solvents and so can be handled much more easily than the other copolymers tested. Moreover, cyclic voltammetry experiments show that it can be repeatedly oxidized and reduced, the chemical process that occurs within the material during solar energy conversion, which bodes well for a long-lasting solar cell.

The team's solar cell based on a thin film of PTAT-3/ $PC_{61}BM$ on an indium tin oxide and [poly(3,4-ethylenedioxythiophene)-tetramethacrylate]: polystyrene sulfonic acid (PEDOT:PSS] sandwich showed an overall energy conversion efficiency of 5.6%. Commercial inorganic photovoltaic materials have an efficiency of around 10-12%, although one manufacturer has recently claimed to have developed an efficiency of more than 20%. Such photovoltaics are expensive and have none of the potential benefits of manufacturing ease, robustness, and flexibility of organic photovoltaics.

The team notes that the tetrathienoanthracene reinforces the stacking between conjugated chains in the solid copolymer films and it is this that boosts device efficiency because holes and electrons can be transported more easily. They concede that devices based on bigger polymers with the same 2-butyloctyl alkyl side chains as PTAT-3 have even better solar properties, but suffer from a rapidly diminishing solubility, which means they could not easily be processed into thin films for commercially viable devices.

A good solution is to balance the two conflicting effects in search of further enhancement of solar cell properties, the team concludes.

— David Bradley

See: Feng He[1], Wei Wang[1], Wei Chen[2], Tao Xu[1], Seth B. Darling[2], Joseph Strzalka[2], Yun Liu[3,4], and Luping Yu[1]*, "Tetrathienoanthracene-Based Copolymers for Efficient Solar Cells," J. Am. Chem. Soc. **133**, 3284 (2011)
DOI:10.1021/ja1110915
Author affiliations: [1]The University of Chicago, [2]Argonne National Laboratory, [3]National Institute of Standards and Technology, [4]University of Delaware
Correspondence:
*Lupingyu@uchicago.edu

This work was supported by the National Science Foundation (NSF), the Air Force Office of Scientific Research, and the NSF Materials Research Science and Engineering Centers (The University of Chicago). The works described here were also partially supported by Solarmer Energy, Inc. Use of the Advanced Photon Source at Argonne National Laboratory was supported by the U. S. Department of Energy, Office of Science under Contract No. DE-AC02-06CH11357.

8-ID-E • XSD • Materials science, polymer science, physics • Grazing incidence small-angle scattering, x-ray photon correlation spectroscopy, intensity fluctuation spectroscopy, grazing incidence diffraction • 7.35-7.35 keV, 12-12 keV • On-site • Accepting general users •

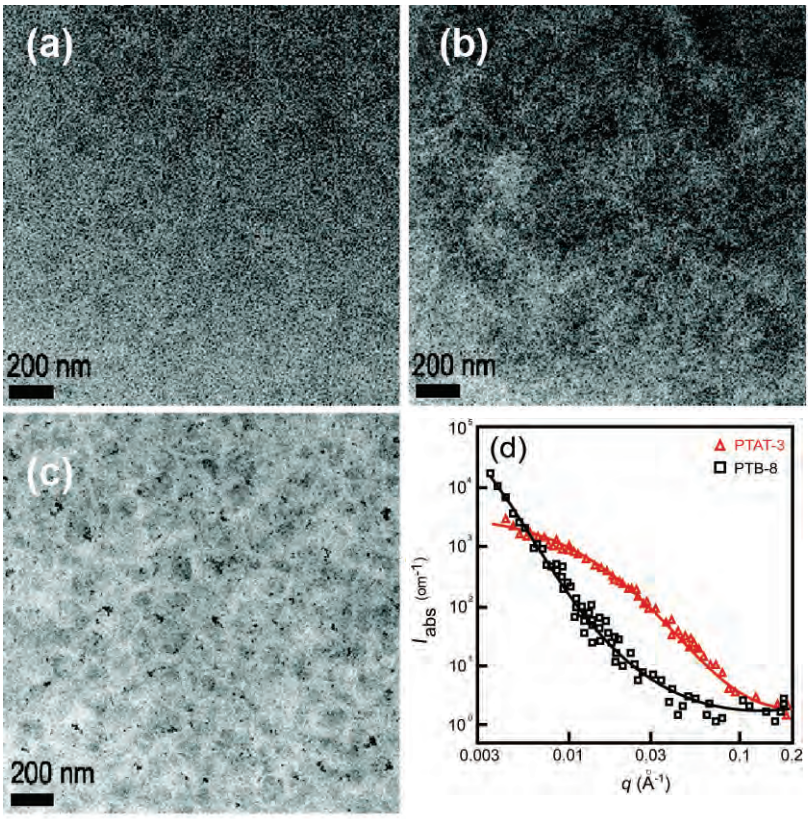

Fig. 1. Transmission electron microscopy images of polymer/PC61BM blend films. (a) PTAT-3/PC61BM from CF/DIO (98/2, v/v); (b) PTAT-4/PC61BM from CF/DIO (98/2, v/v); (c) PTB-8/PC61BM from CB/DIO (98/2, v/v), the scale bar is 200 nm. (d) SANS profiles for as-spun thin films of PTAT-3/PC61BM and PTB-8/PC61BM. Both figures: Feng He et al., J. Am. Chem. Soc. **133**, 3284 (2011), ©2011 American Chemical Society.

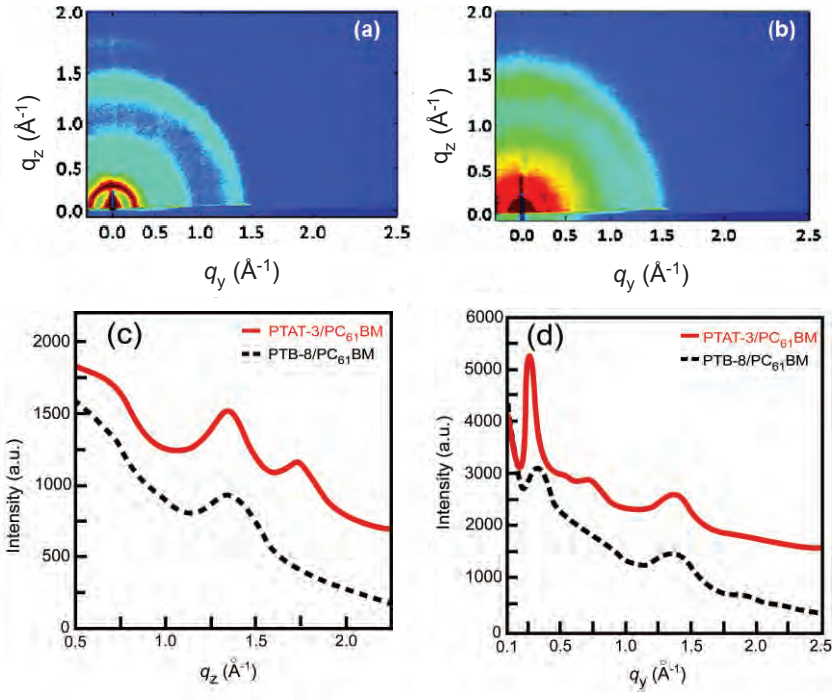

Fig. 2. Two-dimensional GIWAXS patterns of the blend films of PTAT-3/PC61BM (1:1, w/w) (a) and PTB-8/PC61BM (1:1, w/w) (b). (c) Out-of-plane linecuts of GIWAXS of PTAT-3/PC61BM and PTB-8/PC61BM films. (d) In-plane linecuts of GIWAXS of PTAT-3/PC61BM and PTB-8/PC61BM films. Note: GIWAXS profiles have been shifted vertically for clarity.

A CLOSER LOOK AT STRUCTURAL CHANGES IN DYE-SENSITIZED SOLAR CELLS

One limiting factor that plays against the widespread use of solar-panel-based photovoltaics is the problem of obtaining cost-effective materials for commercially viable systems that can sustainably meet the modern demand for energy. Most solar panels available today use solid-state, silicon-based solar cells. But during the last decade, a new technology using dye-sensitized solar cells (DSSCs) has proven to be more efficient and less costly. By most estimates, DSSCs will be capable of reaching grid parity — a break-even point of economic efficiency compared to electricity generated from conventional fossil fuels and distributed on the power grid. But in order to achieve workable DSSCs, scientists and engineers must understand the structural functioning of these promising materials at the molecular level. Researchers utilizing the XSD 11-ID-D beamline at the APS have captured the transient structural changes in the excitation state of one DSSC. Knowledge like this will move us closer to new sources of economical and renewable energy. >>>

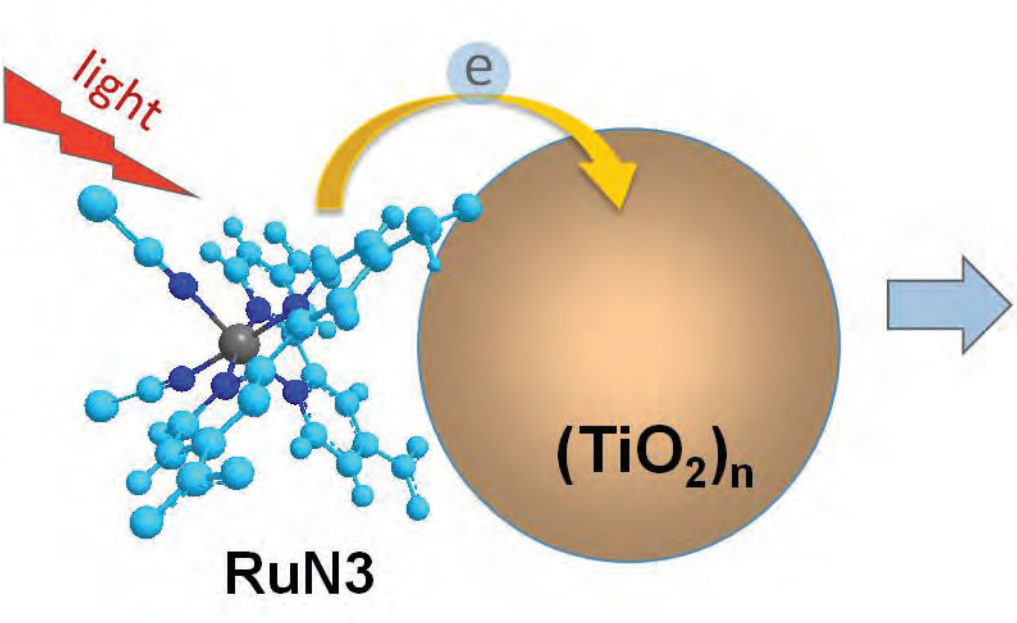

Fig. 1. Schematic of photoinduced interfacial electron transfer from RuN3 to TiO_2 nanoparticle, mimicking dye-sensitized solar cell.

The DSSCs under study in this research consist of a ruthenium (Ru)-based dye, or sensitizer, adsorbed to a thin nanocrystalline titanium dioxide (TiO_2) film to form the working electrode. Photons injected into the dye cause the transfer of an electron from the dye RuN3 to the conduction band of TiO_2 resulting in a very short burst of excitation and a charge-separated state at the interface of the dye and the anatase TiO_2 substrate. (Fig. 1). Information on the transient electronic and geometric structures of this short-lived state in DSSCs has previously been inferred using theoretical calculations, but directly visualizing the molecular structures at the atomic scale has not been possible due to the limitations of conventional measurements such as optical transient absorption (OTA).

An international team of researchers from Argonne, Southern Federal University, Lund University, The University of Chicago, and Northwestern University has captured the transient structural changes in the excitation state of this interfacial system using x-ray transient absorption spectroscopy (XTA) at the 11-ID-D beamline. The results of the experimental XTA measurements were further elucidated with the aid of other probes of the spectra produced in the reaction and using a relatively new data analysis approach.

In this experiment, the dye sensitizer was a complex of the transition metal RuN3 (Ru^{II} $(dcbpy)_2(NCS)_2$ in which dcbpy is 4,4′-dicarboxy-2,2′-bipyridine. A laser pump pulse focused on the dye sensitizer triggered a metal-to-ligand-charge-transfer (MLCT) causing one electron to be injected into the TiO_2 substrate. After a time delay of 50 ps, an x-ray probe pulse was applied, and x-ray absorption spectroscopy used to capture the short-term structural changes of the interfacial system. Since the duration of XTA measurements has an upper limit of 80 ps, only the transient excitation phase of the interfacial system was visualized, not the injection dynamics of the MLCT state, which occurs on a sub-ps-to-ps time scale depending on sample environment. The researchers' own OTA measurements indicate that the electron injection from photoexcited-dye into the TiO_2 nanoparticle lattice happens within several ps under the same sample condition as in the XTA measurement.

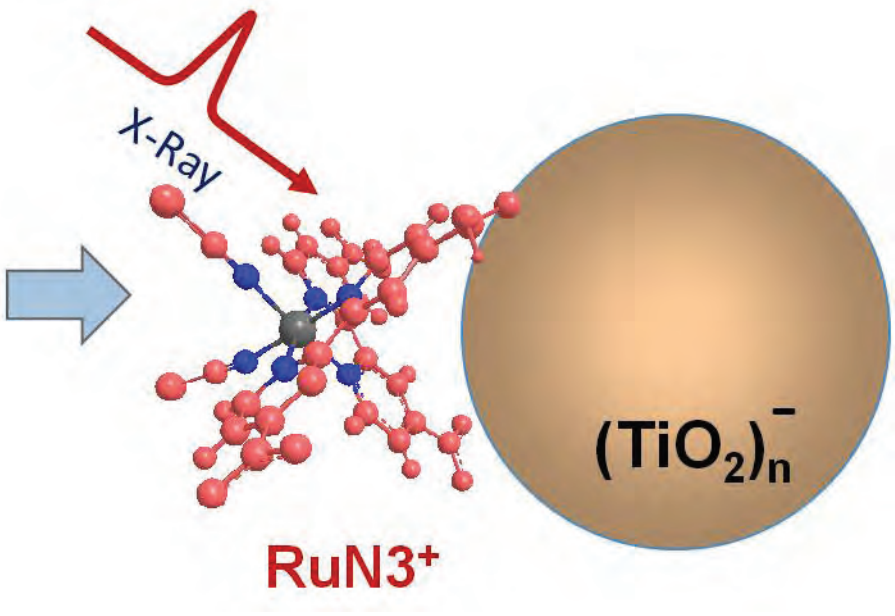

Two types of ligand bonds were observed during the two phases: the laser-off or ground state, and the laser-on or charge-separated state, Ru-NCS and Ru-dcbpy. The research team compared its monitoring of structural changes with a multidimensional interpolation analysis to fit the experimental spectra to the theoretical calculations. This analysis was used to determine the relative distances of the two ligands during the ground state and the charge-separated state. In the excitation state, the Ru-NCS bond length was shortened from 2.05 Å to 1.99 Å, while the Ru-dcbpy bond length remained nearly constant. The different bond-length response between different ligands was attributed to two important factors governing metal to ligand bonding, steric hindrance and bond-order.

Using the pump-probe approach of XTA spectroscopy to visualize interfacial, heterogeneous systems and to clarify the behavior of these complex systems at atomic-scale resolution will allow researchers to improve the selection of ligands and eventually control the chemical reaction pathways of this new generation solar cells, bringing us closer to deploying economically feasible renewable energy. *— Elise LeQuire*

See: Xiaoyi Zhang[1]*, Grigory Smolentsev[2,3], Jianchang Guo[1,4,‡], Klaus Attenkofer[1], Chuck Kurtz[1], Guy Jennings[1], Jenny V. Lockard[1], Andrew B. Stickrath[1], and Lin X. Chen[1,5]**, "Visualizing Interfacial Charge Transfer in Ru-Dye-Sensitized TiO_2 Nanoparticles Using X-ray Transient Absorption Spectroscopy," J. Phys. Chem. Lett. **2**, 628 (2011). DOI:10.1021/jz200122r

Author affiliations: [1]Argonne National Laboratory, [2]Southern Federal University, [3]Lund University, [4]The University of Chicago, [5]Northwestern University

‡Present address: Oak Ridge National Laboratory

Correspondence:

*xyzhang@aps.anl.gov

**lchen@anl.gov

This work and use of the Advanced Photon Source weres supported by the U.S. Department of Energy Office of Science under contract No.DE-AC02-06CH11357.

11-ID-D • XSD • Chemistry • X-ray absorption fine structure, general diffraction, time-resolved x-ray absorption fine structure • 4-40 keV • On-site • Accepting general users •

UNDERSTANDING DEFECT INTERACTIONS IN MULTICRYSTALLINE SOLAR CELL MATERIALS

Commercial solar cells contain large numbers of microscopic defects, most of which arise during various stages of the manufacturing process. These defects have been the focus of intense research for many years because they can lower the conversion efficiency of photons into electrical energy in the regions where they appear. Unfortunately, the characterization techniques used to gauge *in situ* solar cell defects have met with only limited success, in part due to the challenges presented by defect topology, which spans spatial dimensions over several orders of magnitude. In this study, researchers combined several separate techniques to identify the properties of defects. They compared defects with small impacts on solar cell performance to defects that had large performance impacts. Essential to revealing nanoscale defect structure and composition were the x-ray fluorescence (XRF) measurements performed at the Argonne Center for Nanoscale Materials, utilizing the CNM/XSD beamline 26-ID-C at the APS. Exploiting the power of x-ray fluorescence microscopy, the researchers linked degraded solar power conversion efficiency to a class of defects called dislocations co-located with contaminating elements, most notably copper and iron. The appearance of those elements was missing from defects that did not degrade conversion.

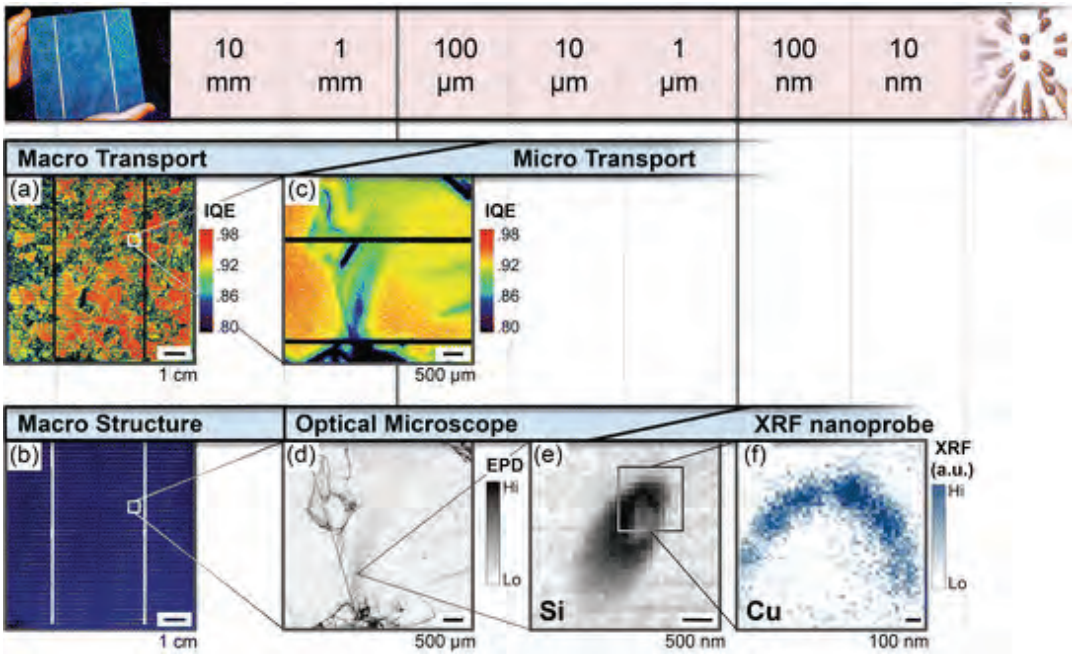

Previous research had indicated that while some subsets of dislocations, which are abrupt discontinuities in the repeating crystal structure, are not particularly harmful to overall cell efficiency, other dislocation defects do contribute to lower conversion efficiencies in solar cells. Therefore, a goal of photovoltaic manufacturers is not necessarily the elimination of all defects (which might prove impractical), but instead the reduction and control of those that degrade performance. The researchers set out to identify properties unique to both benign and harmful solar cell defects.

An outstanding feature of this research is the continuum of characterization performed over several orders of magnitude (Fig. 1). Using a technique called laser-beam-induced current (LBIC), a 10-cm × 10-cm solar cell was mapped at 50-μm resolution with regards to its current collection efficiency. Regions of the solar cell that were found to be underperforming vis-à-vis their collection efficiency were mapped with LBIC to the higher resolution of 12.5 μm. The solar cell was polished, and the contacts and emitter removed. The cell was then exposed to a chemical etch (Secco) for 1 min in order to reveal defects associated with crystalline dislocations and grain boundaries.

< Fig. 1. Multimodal hierarchical material characterization of solar cell materials: (a) Internal quantum efficiency (IQE) map of fill waver. (b) Optical microscope image — no imaging of high- vs. low-performing areas possible. (c) IQE map of selected area, with micron-scale resolution. (d) Visible light microscope image of etched sample. High recombination activity is present at defects. (e) X-ray fluorescence microscopy with a hard x-ray nano-beam is used to map the elemental distribution near dislocation etch pits. Due to its small escape depth, the silicon signal includes topographical information. (f) A high-resolution map of the copper distribution shows that copper had accumulated around the defect area. ©The Royal Society of Chemistry 2011.

Higher-resolution optical images of 0.7 μm (700 nm) were obtained over a selected area of about 25 mm^2. Utilizing an automated process, these high-resolution optical images were used to precisely locate individual defects, especially dislocations. The density of dislocations could then be calculated. In multicrystalline silicon solar cells, some of the dislocations remain relatively inactive electronically, while in other instances the dislocation is associated with the "recombination" of electrons and holes.

Combining the LBIC and optical data, a high-resolution map of electrical output versus dislocation density was derived. From this combined data set an important relationship between defect type and electrical performance emerged: electrical performance was poor in regions where recombination-active dislocations were the dominant defect type, while electrical performance appeared unaffected in areas dominated by pristine (i.e., non-recombinant) dislocations.

The highest-resolution measurements obtained in the experiment were performed on selected regions via XRF microscopy, which is capable of revealing the quantity and distribution of elements within a sample with a high degree of sensitivity. 10-keV x-rays were focused using a Fresnel zone plate to a beam spot with a width of around 80 nm. This focused beam was scanned across the cell surface in increments as low as 25 nm. The XRF data demonstrated that highly recombinant dislocations — those most associated with poor electrical performance within the solar cell — were decorated with elevated levels of particular metals, most notably iron and copper. By contrast, the non-recombinant dislocations, which did not degrade performance, had metal concentrations, if any, below the sensitivity threshold of the XRF measurements.

This research sets the stage for a systematic exploration of the interaction of metal atoms with defects and the mechanisms that lead to the degradation of electrical performance in these nanoscale regions. It characterizes structure/function relationships of the electronic properties of a commercial-grade solar cell over six orders of magnitude, from the centimeter-scale down to structures appearing at the nanoscale level. Furthermore, the characterization techniques applied to solar cells in this research should be useful in characterizing similar efficiency-robbing nanoscale defects in a variety of other materials utilized in technologies such as next-generation nanoscale electronic components, thin-film photovoltaic cells (both organic and inorganic), electric batteries, and thermoelectric devices. *— Philip Koth*

See: M. I. Bertoni[1]*, D. P. Fenning[1], M. Rinio[2], V. Rose[3], M. Holt[3], J. Maser[3], and T. Buonassisi[1], "Nanoprobe X-ray fluorescence characterization of defects in large-area solar cells," Energ. Environ. Sci. **4**, 4252 (2011). DOI:10.1039/c1ee02083h
Author affiliations: [1]Massachusetts Institute of Technology, [2]Fraunhofer ISE, Laboratory and Servicecenter [3]Argonne National Laboratory
Correspondence: *mbertoni@mit.edu

This work was supported by the U.S. Department of Energy (DOE) under Contract No. DEFG36-09GO19001, and a generous gift from the Chesonis Family Foundation. D.P. Fenning acknowledges the support of a National Science Foundation Graduate Research Fellowship. Use of the Advanced Photon Source at Argonne National Laboratory was supported by the U.S. DOE Office of Science under Contract DE-AC02-815 06CH1137.

26-ID-C • CNM/XSD • Physics, materials science • Microfluorescence (hard x-ray), microdiffraction, tomography • 8-12 keV • On-site • Accepting general users •

PROBING THE INVISIBLE IN A HIGH-CAPACITY ELECTRODE MATERIAL FOR LITHIUM-ION BATTERIES

Rechargeable lithium-ion (Li-ion) batteries are currently evolving from applications in handheld electronic devices to use in electric vehicles. Acceptance of all-electric vehicles, in addition to the high cost of the batteries, has been limited by the relatively short range of the vehicle before the necessary recharge. Conventional lithium-ion systems are currently limited by their intercalation chemistry: the electrochemical reaction leading to energy storage is limited to insertion of one Li per redox-active metal ion. With help from studies carried out at an APS beamline, researchers have shown that it is possible to improve energy capacity and storage densities required for more-efficient Li-ion batteries using a mixed-anion nanocomposite system involving both intercalation and conversion reactions. >>

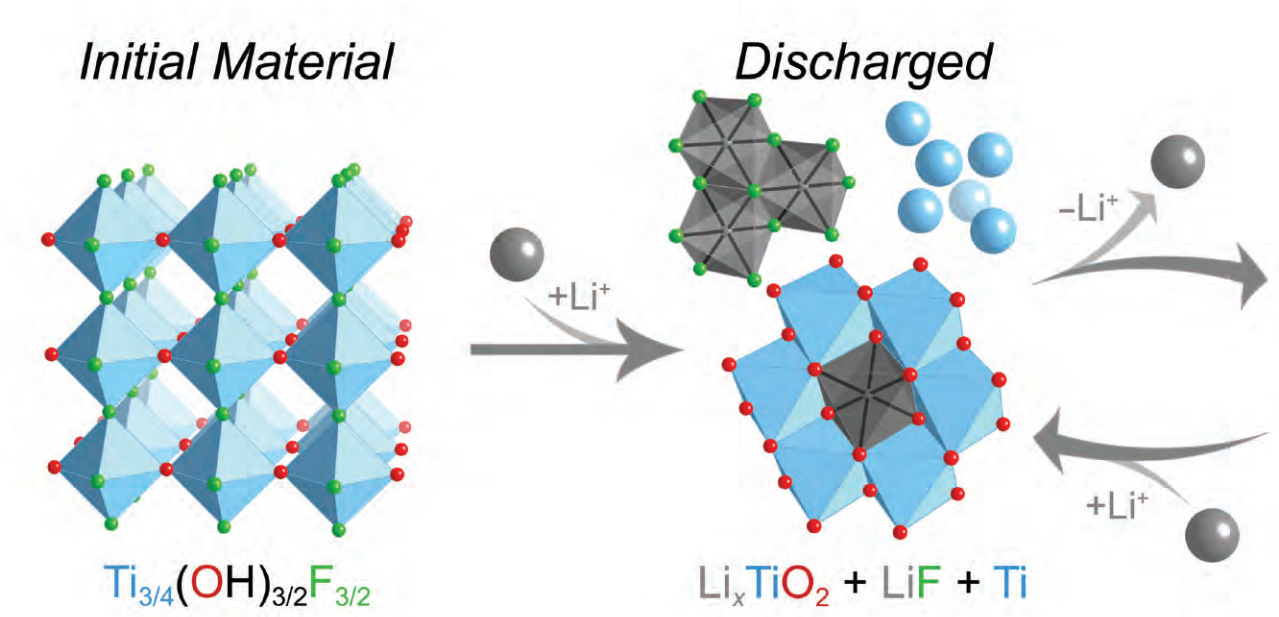

Fig. 1. Lithium storage mechanisms in a titanium hydroxyfluoride material.

The research team, from Argonne National Laboratory and the Université Bordeaux (ICMCB-CNRS) used pair distribution function (PDF) analysis of high-energy x-ray scattering data obtained at the XSD 11-ID-B beamline, together with information from nuclear magnetic resonance (NMR) and x-ray photoelectron spectroscopy (XPS).These complementary approaches allowed the researchers to characterize the electrochemical reaction of Li with a synthetic composite of titanium hydroxyfluoride in

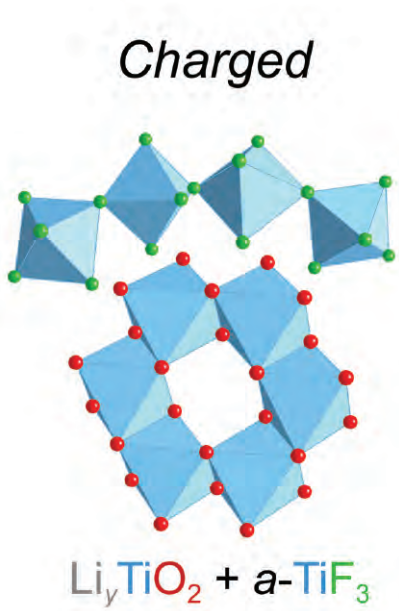

successive cycles of discharge/ charge. The high-energy x-rays penetrated the surface of the composite to reveal the crystalline structure of the interior. The surface architecture of the outer surface was characterized using XPS. NMR spectroscopy further explored the bulk lithium environment revealing two species of ionic Li from Li_xTiO_2 and LiF phases present in both discharge/ charge states. The chemical composition of the outer shell was investigated using low-energy XPS.

The nanoscale titanium hydroxyfluoride in this trial was created by modifying the cubic form of $TiOF_2$ in a microwave-assisted process that has recently been established. Hydroxide ions (OH) were substituted for anionic dioxide (0^{2-}), creating disordered cationic vacancies in the crystalline lattice. A voltage profile of the first discharge/charge phases of the modified titanium hydroxyfluoride showed two plateaus of capacity upon initial discharge, a small plateau at 1.3V and a larger one at 0.8V. These plateaus were absent upon subsequent charge cycles, suggesting an irreversible reaction. The first, small plateau likely indicated a transition from a cubic to a rhombohedral structure, a phenomenon that has been documented in titanium oxyfluoride systems.

Pair distribution function analysis of the high-energy x-ray data showed that the most dramatic structural changes occurred during the initial discharge of Li as the material underwent irreversible partitioning of the fluoro and oxo ions in the hydroxyfluoride, as suggested by the second, larger plateau.

The combined data showed that after initial discharge, the composite consisted of a nanostructured cubic rock-salt structure (Li_yTiO_2) core surrounded by a layer of metallic titanium, (TiO), and lithium fluoride (LiF). Upon subsequent charging, the Ti was reoxidized, forming an amorphous shell of TiF_3 via a conversion reaction, while crystalline Li_xTi0_2 was involved in an insertion reaction. These parallel intercalation and conversion processes allow insertion of more than one Li per Ti (Fig. 1).

This study confirms the utility of PDF analysis of high-energy x-ray data combined with NMR and XFS probes to elucidate the complex core/shell architecture and electrochemistry of a composite nanoscale material. The researchers note that diffraction studies using low-energy (CuKα) radiation should be interpreted with caution when examining transition metal systems. If an amorphous structure is suspected, a complementary PDF analysis of high-energy x-ray data should be performed.

Mixed-anion nanocomposite systems will allow an increase in the number of electrons that can be inserted into electrode materials, thus boosting energy density and storage capacity of the systems. *— Elise LeQuire*

See: Damien Dambournet[1*‡], Karena W. Chapman[1**], Peter J. Chupas[1], Rex E. Gerald[1], Nicolas Penin[2], Christine Labrugère[2], Alain Demourgues[2], Alain Tressaud[2], and Khalil Amine[1], "Dual Lithium Insertion and Conversion Mechanisms in a Titanium-Based Mixed-Anion Nanocomposite," J. Am. Chem. Soc. **133**, 13240 (2011). DOI:10.1021/ja204284h
Author affiliations: [1]Argonne National Laboratory, [2]Université Bordeaux
‡Present address: University of Pierre and Marie Curie
Correspondence: *damien_dambournet@yahoo.fr, damien.dambournet @upmc.fr, **chapmank@aps.anl.gov

This work was funded, in part, by the U.S. Department of Energy (DOE), FreedomCAR and Vehicle Technologies Office. Work done at Argonne and use of the Advanced Photon Source were supported by the U.S. DOE Office of Science under Contract No. DE-AC02-06CH11357. The researchers acknowledge support from the French Centre National de la Recherche Scientifique.

11-ID-B • XSD • Chemistry, environmental science, materials science • Pair distribution function • 58-60 keV, 90-91 keV • On-site • Accepting general users •

BUILDING A BETTER BATTERY

The lithium-rich compound material $Li_{1.2}Co_{0.4}Mn_{0.4}O_2$ is a puzzle that holds key insights into the development of more powerful and robust batteries for electric cars. Using a suite of advanced techniques, including the XSD 20-BM-B beamline at the APS, the researchers pieced together both the long-range and local structure of this compound, devising a model that could explain how such materials operate on the electrochemical level—and how to use them to build a better battery.

Argonne is at the cutting edge of the effort to create advanced battery technologies, focusing especially on the lithium-ion (Li-ion) battery, which promises more energy and longer life than the nickel-metal hydride battery currently used in electric and hybrid vehicles. For instance, the new Chevy Volt, the first mass-produced plug-in hybrid electric car, is powered by a battery whose chemistry is based in part on important breakthroughs developed by scientists at Argonne. Like all batteries, Li-ion batteries work by moving electric charge (in this case, lithium ions) between an anode and cathode. But vital properties—such as the amount of electricity a battery can deliver before recharging is necessary and how many times it can be recharged before its microstructure breaks down under the repeated cycling stress—can vary greatly depending on the composition of the cathode and anode. Most research has focused on compounds using transition metals such as cobalt and manganese, but the precise structural formulation of the compounds and what might make one work better than another have largely been a matter of trial and error and speculation. The new Argonne work is an important step toward resolving the confusion.

The researchers in this study, from Argonne and the Frederick Seitz Materials Research Laboratory at the University of Illinois examined the layered lithium oxide $Li_{1.2}Co_{0.4}Mn_{0.4}O_2$, which is a model compound for many of the advanced battery materials currently under development for electric vehicles. The experimenters subjected samples to a variety of techniques including x-ray diffraction (XRD), scanning-transmission electron microscopy (STEM), and x-ray absorption spectroscopy (XAS). The combination of methods yielded a more comprehensive picture than previously achieved.

When examined by XRD, $Li_{1.2}Co_{0.4}Mn_{0.4}O_2$ revealed an average long-range crystal structure similar to that of layered $LiCoO_2$. STEM results, however, revealed the presence of lithium atoms, in sites typically occupied by cobalt and manganese atoms, ordered in a manner similar to that in layered Li_2MnO_3. But the STEM data could not establish the structural relationship between the ordered lithium atoms and the neighboring cobalt and manganese atoms. The XAS experiments conducted at 20-BM, on the other hand, were successful in distinguishing the local atomic environments around the cobalt and manganese (Fig. 1). The research team determined that while the crystalline structure of the $Li_{1.2}Co_{0.4}Mn_{0.4}O_2$ compound is largely homogeneous over the long range, the local structure contains Li_2MnO_3 and $LiCoO_2$ nanoclusters. These local clusters might present connectivity over long distances as a dendritic network. Having continuous regions allows for each unit cell to "talk" to the next unit cell over very long distances. This connectivity enhances the transport of lithium ions and hence, the electrochemical performance of the material for battery applications.

The researchers' broad-based approach of bringing together a wide palette of experimental methods, rather than relying on a single technique, is an important step towards the custom design of battery materials based on results from advanced diagnostic techniques. In the past, most advances in battery materials development arose from intuitive experimentation. These researchers want to complement this intuitive Edisonian approach with a rigorous basic approach to tailoring new materials.

The next step is to observe the structural changes that occur in these lithium-rich compounds as they are cycled through various voltage windows, which is critical for determining battery life and durability. Tools and techniques like those available at the APS can provide unique insights to develop structure-property correlations, which are very important to predict long-term battery performance.

The work lays a solid foundation for the design and development of new compounds that are tailored with desired properties for specific applications to meet the need for transformational materials with high capacities, high power, and stable crystal struc-

20-BM-B • XSD • Chemistry, environmental science, geoscience, materials science • Micro x-ray absorption fine structure, microfluorescence (hard x-ray), x-ray absorption fine structure • 2.7-25 keV, 2.7-30 keV, 2.7-35 keV • On-site • Accepting general users •

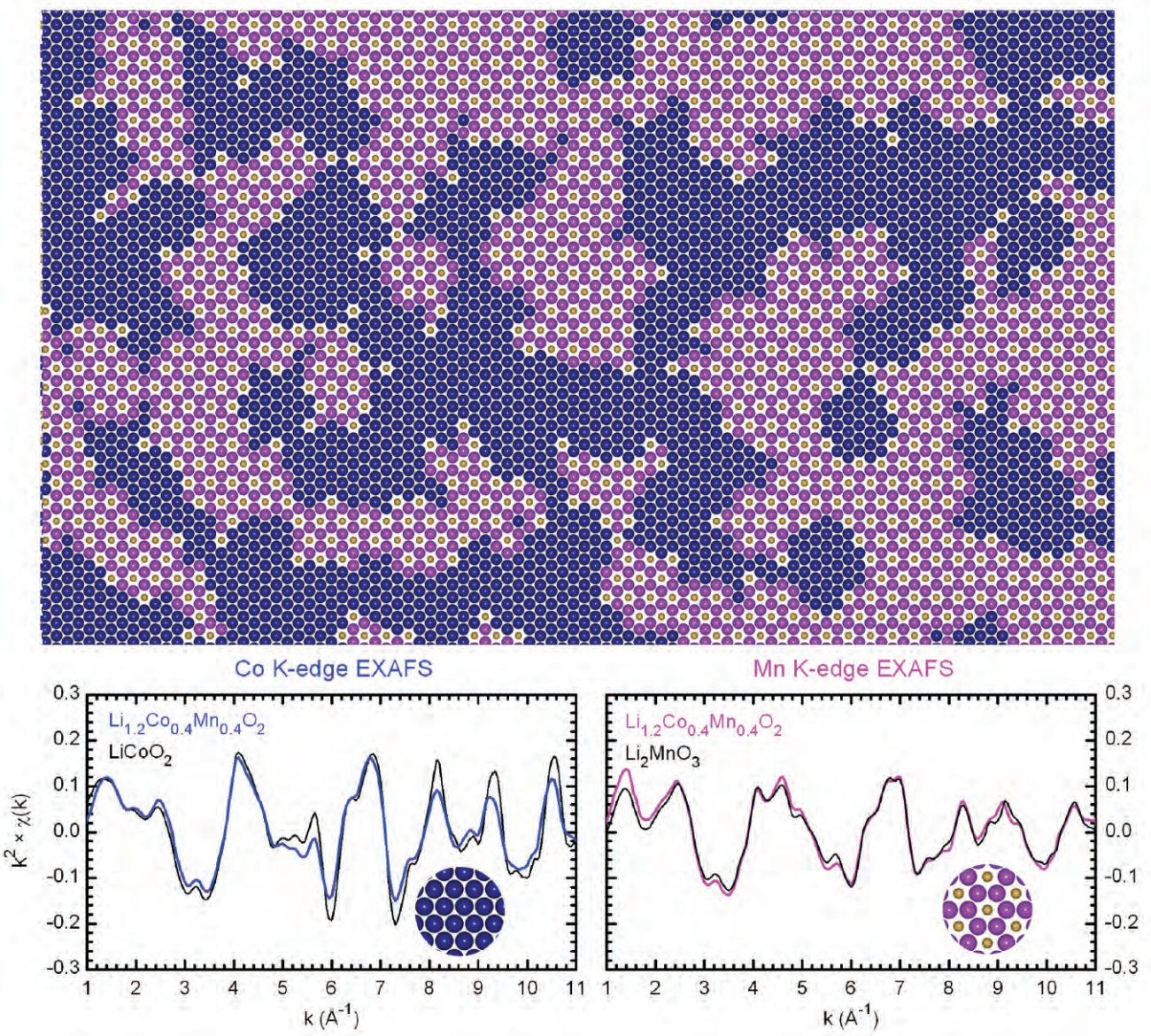

Fig. 1. (Top panel) Schematic arrangement of lithium (yellow), cobalt (blue), and manganese (magenta) atoms in the transition metal plane of the layered $Li_{1.2}Co_{0.4}Mn_{0.4}O_2$ structure. Well connected areas with $LiCoO_2$, where only cobalt is present, and Li_2MnO_3, where manganese atoms surround lithium atoms in a hexagonal pattern, are observed. Each of these areas gives rise to a distinctly different extended x-ray absorption fine structure (EXAFS) spectrum (bottom panel) that is characteristic of the local chemical environment.

tures for the successful commercialization of lithium-ion batteries for a myriad of demanding applications.

— Mark Wolverton

See: J. Bareño[1], M. Balasubramanian[1]*, S.H. Kang[1], J.G. Wen[2], C.H. Lei[2], S.V. Pol[1], I. Petrov[1], and D.P. Abraham[1]**, "Long-Range and Local Structure in the Layered Oxide $Li_{1.2}Co_{0.4}Mn_{0.4}O_2$," Chem. Mater. **23**(8), 2039 (2011). DOI:10.1021/cm200250a

Author affiliations: [1]Argonne National Laboratory, [2]University of Illinois – Urbana-Champaign

Correspondence: *mali@aps.anl.gov
**abraham@anl.gov

Support from the U.S. Department of Energy's (DOE's) Vehicle Technologies Program, and specifically from Dave Howell. Sector 20 at the APS and research at the facility are supported by the DOE, a Major Resources Support grant from the Natural Sciences and Engineering Research Council of Canada, the University of Washington, Simon Fraser University, and the APS. Use of the Advanced Photon Source was supported by the U.S. DOE Office of Science under Contract DE-AC02-815 06CH1137.

IMAGING CHEMICAL AND MICRO-/NANO-STRUCTURAL FEATURES OF ENERGY MATERIALS IN 3-D

Concerns about the diminishing availability of our petroleum reserves and the effects of greenhouse gases on the Earth's climate have spurred intense efforts to develop cleaner alternative energy technologies such as solid oxide fuel cells (SOFCs), batteries for electric and hybrid-electric vehicles, and supercapacitors. These efforts have, in turn, sparked interest in the reduction-oxidation (redox) cycling of nickel-based oxides in SOFC anodes, lithium-ion battery cathodes, and nickel oxide supercapacitors. Monitoring redox cycling of such materials (ideally during system operation) requires the ability to image and characterize changes at the chemical and morphological levels. Currently, there are no standard nondestructive analytical techniques that enable the three-dimensional (3-D) chemical imaging of complex and large architectures. X-ray absorption near-edge structure (XANES) nanotomography is being developed to fulfill that need. Now, full-field XANES nanotomography has been demonstrated at sub-30-nm spatial resolution by researchers utilizing beamlines at two U.S. Department of Energy Office of Science synchrotron light sources, including the APS. >>>

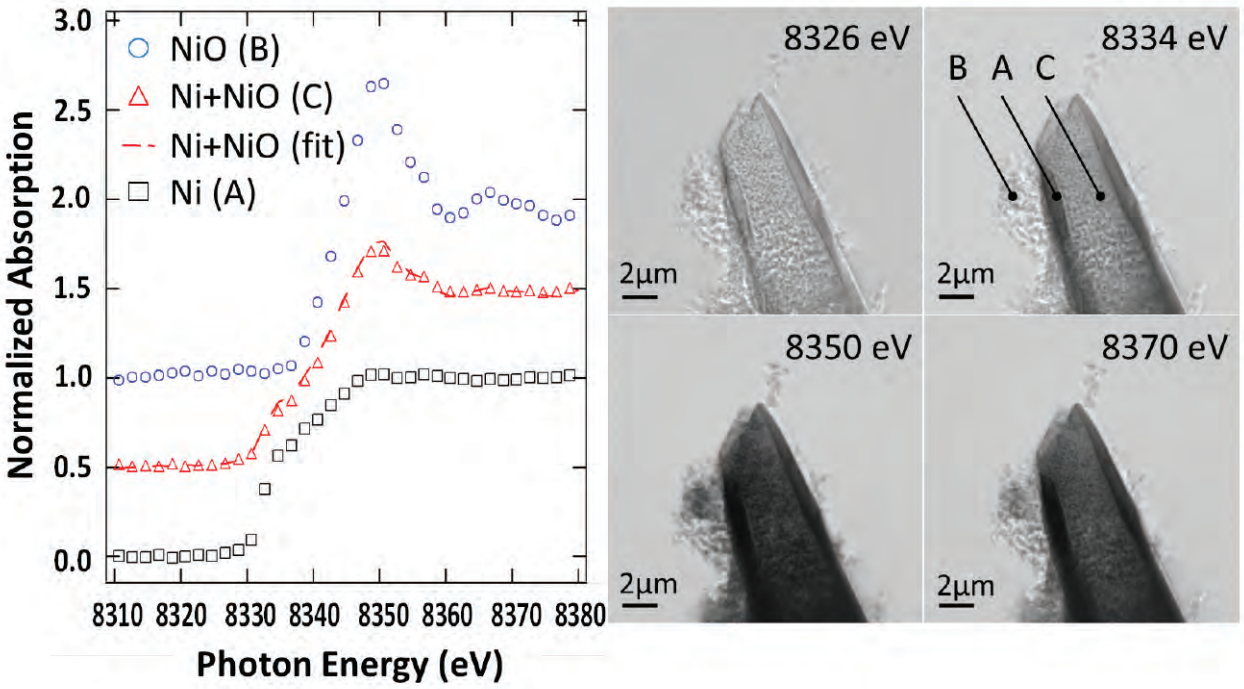

Fig. 1. Left: The distinction between Ni oxidation states is enabled by image subtraction at the energy levels associated with the primary features in the spectra. A linear combination of the Ni and NiO spectra, shown as the red dashed line, reproduces the spectrum for the region of overlapping Ni-NiO and corroborates the spectra obtained. Center: Transmission images were taken at x-ray energies of 8326 eV, 8334 eV, 8350 eV, and 8370 eV. Representative regions of each material (Ni (A), NiO (B), and overlapping Ni-NiO (C)) are indicated in the 8334-eV panel. Facing page: A region of interest highlighted in red in the upper-right image is tomographically reconstructed and segmented to identify the Ni and NiO phases. Images from Nelson et al., Appl. Phys. Lett. **98**, 173109 (2011).

XANES nanotomography combines XANES spectroscopy with full-field transmission x-ray microscopy (TXM). The researchers in this study, from the University of Connecticut, Brookhaven National Laboratory, SLAC National Accelerator Laboratory, and Argonne have demonstrated the 3-D chemical mapping and microstructural characterization capabilities of full-field XANES nanotomography by determining the near-edge characteristics of Ni foil and NiO powder samples that were prepared as a means of simulating the materials that are present in SOFC and battery electrodes. Full-field XANES spectroscopy combined with 3-D nanotomography imaging with the TXM system were performed at the XSD 32-ID-B,C beamline at the APS and at Stanford Synchrotron Radiation Lightsource (SSRL) beamline BL6-2c.

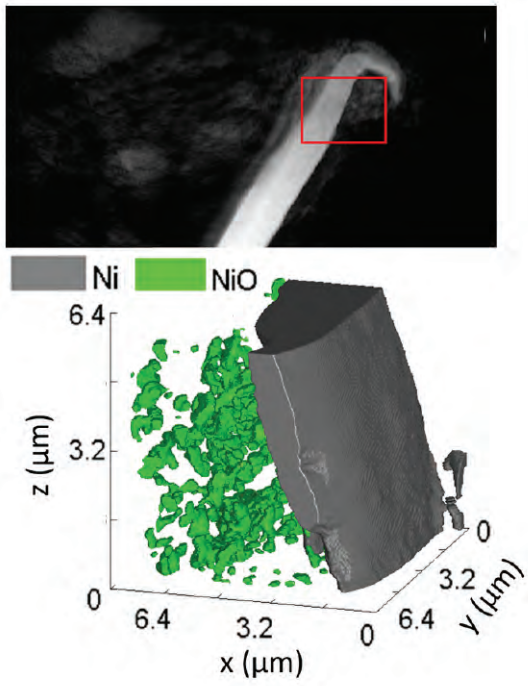

Full-field XANES nanotomography begins with XANES spectroscopy measurements in order to identify energy levels corresponding to key features in the observed transmission-based near-edge spectra to guide subsequent nanotomography measurements. This reduces the time needed for nanotomography by limiting the number of energy points to the minimum necessary to discriminate different chemical phases present in the sample. The near-edge spectra from the Ni and NiO samples, obtained at the APS by the researchers compared well with results in the literature. These spectra were also corroborated by reproducing the spectrum of the overlapping Ni-NiO region using a linear combination of the Ni and NiO results (Fig. 1). The calibration performed on the foil and powder samples showed a common peak in the absorption spectra at 8350 eV, which served as a reference point for comparing the spectra and distinguishing between the oxidation states of the Ni foil and NiO powder. Additional features in the spectra were identified where changes in the absorption characteristics of each material relative to the common peak enabled separation of the phases present in the sample. Regions of Ni foil, NiO powder, and overlapping Ni-NiO were particularly distinct at 8334 eV and 8370 eV. Determining the distinct features in the XANES spectra enabled targeted tomographic scans at the energies of interest, which were carried out at SSRL. Tomographic image reconstruction and processing techniques were applied to the full-field XANES images to achieve three-dimensional mapping of Ni-NiO phases within the entire imaged volume (Fig. 1). The resulting digitized structures enabled quantification of phase sizes, interfacial areas, and phase contiguity associated with the microstructural effects of redox cycling.

32-ID-B,C • XSD • Materials science, life sciences, geoscience • Phase contrast imaging, radiography, transmission x-ray microscopy, tomography • 7-40 keV • On-site • Accepting general users

The nondestructive nature of XANES nanotomography measurements allows for sample preservation and can facilitate *in situ* observation of battery and SOFC electrodes in controlled oxidizing or reducing environments and under operational conditions such as applied current loads. Such measurements could realize the direct three-dimensional observation of nickel oxidation and structural modifications due to lithium deintercalation phenomena. Thus the research demonstrated full-field XANES nanotomography as a technique that enables investigation of microstructural and chemical evolution in energy materials. — *Vic Comello*

See: George J. Nelson[1], William M. Harris[1], John R. Izzo, Jr.[1], Kyle N. Grew[1], Wilson K.S. Chiu[1]*, Yong S. Chu[2], Jaemock Yi[3], Joy C. Andrews[4], Yijin Liu[4], and Piero Pianetta[4], "Three-Dimensional Mapping of Nickel Oxidation States Using Full Field X-ray Absorption Near Edge Structure Nanotomography," Appl. Phys. Lett. **98**, 173109 (2011). DOI:10.1063/1.3574774

Author affiliations: [1]University of Connecticut, [2]Brookhaven National Laboratory, [3]Argonne National Laboratory, [4]SLAC National Accelerator Laboratory

Correspondence:
*wchiu@engr.uconn.edu

Financial support from an Energy Frontier Research Center on Science Based Nano-Structure Design and Synthesis of Heterogeneous Functional Materials for Energy Systems (HeteroFoaM Center) funded by the U.S. Department of Energy (DOE) Office of Science (Award No. DE-SC0001061), the National Science Foundation (Award Nos. CBET-0828612 and CBET-1134052), and the ASEE National Defense Science and Engineering Graduate Fellowship program. Use of the Advanced Photon Source at Argonne National Laboratory was supported by the DOE Office of Science under Contract No. DE-AC02-06CH11357.

A NEW, SUPER-DENSE ALUMINUM EMERGES

A new, never-before seen type of aluminum — one with a super-dense structure — has been discovered by an international team of researchers employing a single ultrashort laser pulse focused inside sapphire. This superdense form of aluminum (just over 40% denser than conventional solid aluminum) was theoretically predicted more than 30 years ago, but its existence remained unsubstantiated until this experimental research was conducted. Formed at pressures in the megabar range (millions of atmospheres), and at temperatures exceeding 100,000K (greater than 180,000° F), the superdense material was found to exist in an unusual lattice ordering: body-centered cubic aluminum (bcc-Al). The high temperatures and pressures were attained using a relatively simple table-top laser system. The new material was analyzed thanks to the penetrating capability of the x-rays from HP-CAT beamline 16-BM-D at the APS. Discovery of the bcc-Al crystalline phase should help planetary scientists and astronomers gain a better understanding of the interiors of celestial bodies because the high pressures and temperatures used to produce this superdense form of aluminum match those found within the interiors of many planets and stars.

In order to create the conditions necessary to form superdense aluminum, the research team used very short (around 150-fs-duration) pulses of light produced by an ultrafast, titanium-sapphire laser system. The laser pulses were focused by a lens to depths of 20 to 60 μm beneath the surface of a sapphire crystal; sapphire consists of a rhombohedral crystalline type of alpha aluminum oxide (α-Al_2O_3), commonly called corundum. The focused laser pulse released a total energy of 100 nJ within a submicron volume, resulting in an energy density of several megajoules per cubic centimeter.

This enormously powerful, laser-induced energy state caused a tiny region within the sapphire crystal to superheat and form hot plasma. Subsequently, the superheated plasma formed a strong shock wave that traveled outward from its initial volume, producing a compressed shell of material. This process — a brief, concentrated laser pulse ionizing a microscopic region of sapphire, followed by an expanding shockwave — produced an inner void within the sapphire, surrounded by a compressed shell of material. Repeated firings of the laser produced an array of voids near the sapphire's surface, with each void surrounded by a shell. The dimensions of the voids and shells were measured using both transmission electron microscopy and scanning electron microscopy. The radii measured for the voids averaged around 180 nm, which was also the approximate thickness of their surrounding compressed shells.

The shock wave of the expanding plasma reached pressures of over 100 Mbar (equivalent to ~10 TPa, around one hundred million times standard atmospheric pressure), which turned a microscopic region of the surrounding sapphire into an amorphous (unordered) phase. For a very brief increment of time, the extreme pressure and temperature environment produced by the microexplosion — an environment akin to conditions deep within the interiors of many planets — created "warm dense matter," a state of hot solid density plasma (Fig.1). The laser-induced microexplosions spatially separated the ionized constituents (aluminum and oxygen) of the sapphire crystal because the two ions of different mass traveled at different speeds during the superheated explosion. This segregation of aluminum and oxygen atoms, along with the extremely high temperature and pressure, synthesized and trapped nanocrystals of superdense bcc-Al within the confines of the otherwise amorphous, shock-compressed shells.

The sapphire crystal was probed and analyzed at the HP-CAT beamline using micro x-ray diffraction, a structural analysis technique that allows the examination of very small (sub-micron) sample areas using a beam of highly-intense, monochromatic (single wavelength) x-rays. The x-ray diffraction patterns matched those predicted from theory for superdense bcc-Al.

This research demonstrates that a tabletop laser setup can attain the high temperatures and pressures needed to synthesize nanoscale amounts of materials exhibiting high-density phases. While this particular set of experiments centered on the creation of aluminum in the high-density bcc phase, the basic techniques could be applicable in the production of a wide array of new, high-density materials for experimental study. Moreover, ultrafast lasers – such as the one used in this experiment – are capable of high repetition rates in the range of millions of cycles per second; this high repetition rate opens up the tantalizing possibility of creating useful quantities of exotic, high-density materials utilizing a com-

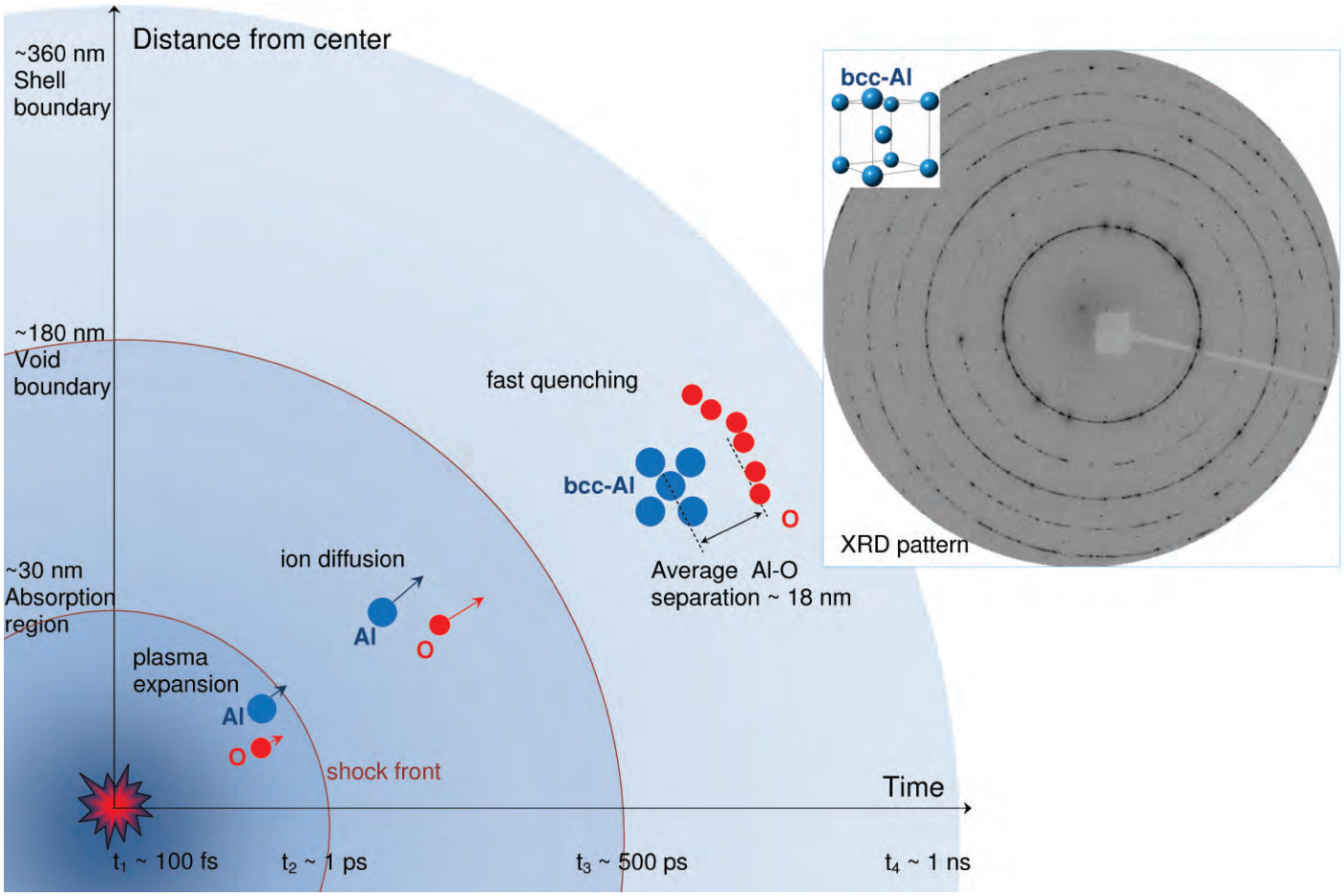

Fig. 1. The synthesis of materials from the separation of elements in the plasma state. The illustration depicts the transformations within space and time in the region of ionized sapphire affected by a microexplosion, which leads to a physical separation of aluminum (Al) and oxygen (O) ions, and subsequent quenching of the bcc-Al. The horizontal axis represents time and the vertical axis represents distance from the center of the microexplosion. Insert: This micro-x-ray diffraction image was taken in the center of the compressed shockwave region, which depicts evidence of bcc-Al formation within the laser-modified areas.

mercially-available, tabletop laser.

Looking ahead, the progenitors of this research are hopeful that innovative products based upon superdense materials – such as the superdense aluminum created in this experiment – will eventually be produced inexpensively and in large quantities. These new materials might well exhibit unusual mechanical, electric, and magnetic properties.

— William A. Atkins and Philip E. Koth

See: Arturas Vailionis[1,2], Eugene G. Gamaly[3], Vygantas Mizeikis[4], Wenge Yang[5], Andrei V. Rode[3], and Saulius Juodkazis[6]*, "Evidence of superdense aluminium synthesized by ultrafast microexplosion," Nat. Comm. **2**, 445 (23 August 2011). DOI:10.1038/ncomms1449.

Author affiliations: [1]Stanford University, [2]SLAC National Accelerator Laboratory, [3]The Australian National University, [4]Shizuoka University, [5]Carnegie Institution of Washington, [6]Swinburne University of Technology

Correspondence:
*Sjuodkazis@swin.edu.au, sauliusjuodkazis@gmail.com

This work was supported by the Australian Research Council through the Discovery program. HP-CAT is supported by the Carnegie Institution of Washington, the Carnegie-Department of Energy (DOE) Alliance Center, the University of Nevada at Las Vegas, and Lawrence Livermore National Laboratory, through funding from the DOE National Nuclear Security Administration, the DOE Office of Science, and the U.S. National Science Foundation. Use of the Advanced Photon Source was supported by the U.S. DOE Office of Science under Contract DE-AC02-06CH11357.

16-BM-D • HP-CAT • Materials science, geoscience, chemistry, physics • Powder angular dispersive x-ray diffraction, x-ray absorption near-edge structure, single-crystal diffraction, high-pressure diamond anvil cell • 6-70 keV • On-site • Accepting general users •

How Blisters Cause Stress

In water-cooled nuclear reactors, coolant travels to and from the reactor core at high pressure in tubes made of zirconium alloyed with a few percent of other metals. These alloys only weakly absorb neutrons and are generally resistant to corrosion, but over time, absorption of hydrogen from the cooling water into the metal can lead to formation of zirconium hydride "blisters" that can dangerously weaken the tubes. Working at XSD beamline 1-ID-B,C,E at the APS, a research team has for the first time characterized both the relative abundance and lattice structure of metal and hydride components across such a blister (Fig.1). The findings should help engineers to more accurately understand the failure risk of reactor pressure tubes.

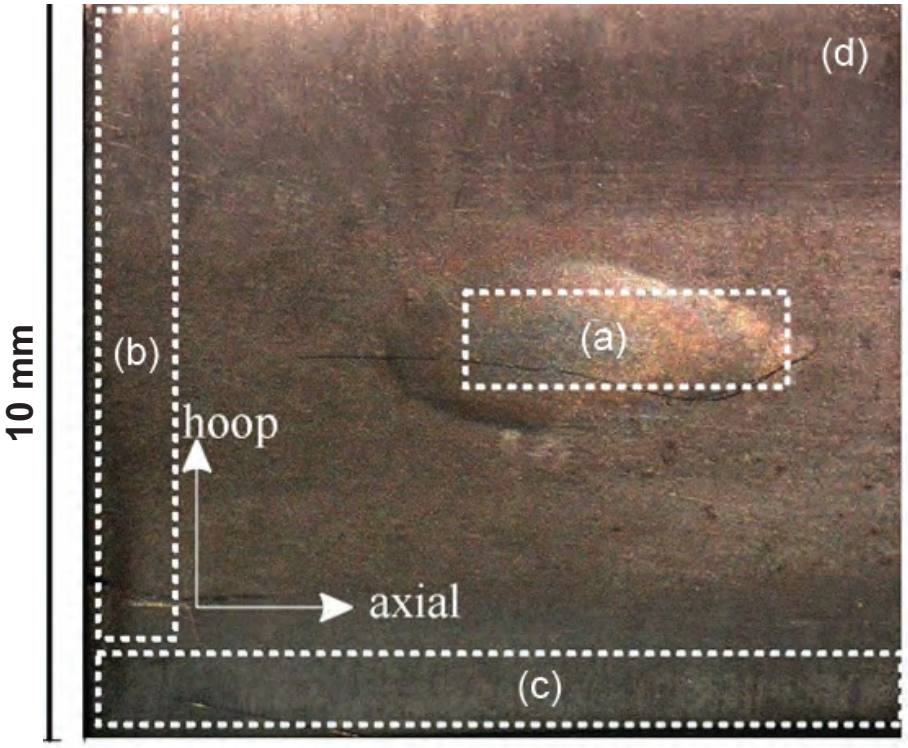

Fig. 1. Photograph of hydride blister, measuring roughly 5 mm by 2 mm, in a sample of zirconium alloyed with 2.5% niobium. (a), (b), (c), and (d) indicate specimen sectioning.

Research into the growth and properties of hydride blisters became urgent after the 1983 failure of a pressure tube in a CANDU reactor in Pickering, Ontario. At typical operating temperatures of a few hundred degrees Celsius, hydrogen dissolves into zirconium and migrates through it, but will precipitate out in the form of hydride in colder parts of a tube. Zirconium hydride formation is accompanied by a roughly 17% increase in lattice volume. The resulting stress on the tube, exacerbated by the brittleness of the hydride compared to the metal, can lead to cracks that are the starting point for potential larger scale failure. However, theoretical studies of hydride blister formation are only partly in agreement with experimental measurements of induced stresses, and little has been known until now about the precise structure of the blisters.

The researchers, from Laboratorio de Fisica de Neutrones y Reactores CAB-CNEA (Argentina), CAE-CNEA (Argentina), and Argonne used x-ray diffraction studies with a 300 x 300 μm beam to map out the presence of zirconium and zirconium hydride grains of different crystal phases across a blister a few millimeters wide (Fig. 2). They created the blister by applying an aluminum "cold finger" for 1650 h to a sample of zirconium alloy held at 320° C. The test sample, containing 2.5% niobium, was cut from a commercially available pressure tube and infused with hydrogen at high temperature.

Many models have predicted that the blisters should have a 100%

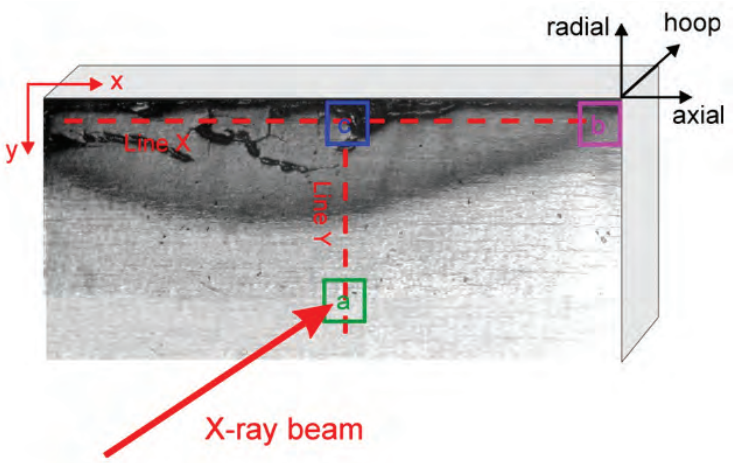

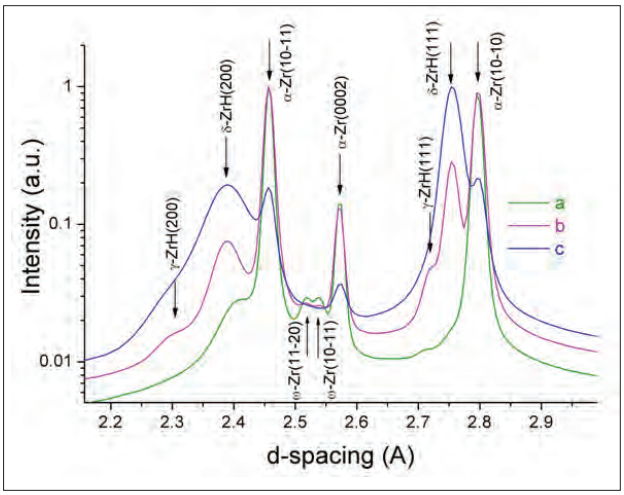

Fig. 2. Top: Photomicrograph of a blister in cross-section, showing the formation of cracks at the surface. The small colored squares indicate the size of the x-ray beam. Bottom: Average diffractograms obtained at locations a, b, and c in top figure. Figures on this and preceding page from M.A. Vicente Alvarez et al., Acta Mater. **59** 2210 (2011). ©2011 Acta Materialia Inc. Published by Elsevier Ltd. All rights reserved.

hydride composition at their centers, but the researchers found that the hydride concentration (mostly in the form of the δ-ZrH crystallographic phase) rose only to 80% by volume, the remaining material being unconverted zirconium, mostly in the α-Zr phase. The less than complete transformation of metal to hydride is consistent with measurements showing that the stress caused by the blisters is somewhat smaller than models have predicted. The high intensity of the x-ray beam also made possible detection of small but mechanically significant quantities of metal and hydride grains in other crystallographic phases.

The researchers were also able to use the diffraction studies to determine the "texture" of the metal and hydride components – that is, whether the grains are aligned randomly or are oriented preferentially in some direction or another. They found that the metal grains had a significant texture and that the hydride texture generally tracks the metal texture, consistent with a precise relationship between the hydride and matrix crystals. Some differences in texture were seen, however, most likely because metal grains that are stretched in a certain way or have a specific alignment are more likely to convert into hydride.

The unprecedented level of detail revealed by this new study would be very hard to obtain by other experimental means, the researchers say, but has great significance in understanding how hydride blisters form and what kind of stress pattern they induce. Such knowledge can lead to better predictions of the risk of failure and improvements in the materials and fabrication techniques used for reactor pressure tubes.

— David Lindley

See: M.A. Vicente Alvarez[1]*, J.R. Santisteban[1], G. Domizzi[2], and J. Almer[3], "Phase and texture analysis of a hydride blister in a Zr-2.5%Nb tube by synchrotron X-ray diffraction," Acta Mater. **59**, 2210 (2011). DOI:10.1016/j.actamat.2010.12.024

Author affiliations: [1]Laboratorio de Fisica de Neutrones y Reactores CAB-CNEA, [2]CAE-CNEA, [3]Argonne National Laboratory

Correspondence: *m.a.vicente@cab.cnea.gov.ar

This research was funded by a Pan-American Collaboration Program funded by CONICET, Argentina under Res 1161/07, with corresponding funding from NSERC and the National Science Foundation for the Canadian and American partners. Use of the Advanced Photon Source at Argonne National Laboratory was supported by the the U.S. Department of Energy Office of Science under Contract No. DE-AC02-06CH11357.

1-ID-B,C,E • XSD • Materials science, physics, chemistry • High-energy x-ray diffraction, radiography, small-angle x-ray scattering, fluorescence spectroscopy, pair distribution function • 50-90 keV, 50-150 keV • On-site • Accepting general users •

How Sea Urchins Keep Their Teeth Sharp

Sea urchin teeth are remarkable structures that remain sharp and without gaps despite constant wear. Although the teeth are composed mostly of calcite, a carbonate mineral and the most stable polymorph of calcium carbonate, sea urchins grind holes in limestone, a rock that is also made of calcite. How do they manage this trick? They have teeth with a complex internal structure that is coordinated across size ranges from nanometers to centimeters. To make sense of the structures and mechanisms involved, researchers studied sea urchin teeth using a variety of imaging methods including hard x-ray tomography at XSD beamline 2-BM-A,B at the APS. They found that sea urchin teeth grow continuously and the tip wears down as it grinds, allowing new surfaces to be uncovered as old ones wear out. The teeth stay sharp and maintain their overall shape by controlling where and how they fracture: at soft organic layers, interspersed with the hard calcite mineral. A similar strategy using layered materials could allow man-made tools to retain their sharpness and shape during use.

The research team studied in detail the structure of the tooth of the California purple sea urchin *Strongylocentrotus purpuratus*, using high-resolution x-ray photoelectron emission spectromicroscopy (X-PEEM), scanning electron microscopy (SEM), SEM energy dispersive x-ray (SEM-EDX) analysis, electron probe microanalysis (EPMA), nanoindentation, and hard x-ray microtomography.

As a sea urchin tooth grows, single-crystalline plates and fibers are cemented together at the forming end by a polycrystalline calcite matrix. The tooth function depends on this arrangement of the plates, fibers, and matrix. The researchers found that softer fault layers between plates and fibers become the site of fractures, which allows the tooth to retain its shape even while surface layers break off.

The researchers from the University of Wisconsin; the University of California, Berkeley; Argonne; the Weizmann Institute of Science; and Lawrence Berkeley National Laboratory analyzed the structure and strength of the teeth to see how and where a tooth breaks and self-sharpens.Each tooth has a T-shaped cross-section, with the vertical stroke of the T called the “keel” and the horizontal piece called the “flange.” Using SEM imaging at the University of California, Berkeley, Electron Microscopy Lab and the Irving and Cherna Moskowitz Center for Nano and Bio-Nano Imaging at the Weizmann Institute of Science, they found that the top of the flange is convex and contains plates, while the back has concave curves leading to the keel.

Although most of the tooth is made of calcite, some parts of the tooth contain unusually high levels of magnesium. In some areas, magnesium replaces almost half of the calcium atoms in calcite. Using EDX analysis at the University of Wisconsin-Madison, as well as backscatter electron SEM, they found that the stone area (the hardest part of the tooth, which emerges at the tip) has higher magnesium content than the rest of the tooth.

High-resolution X-PEEM elemental mapping carried out at the Berkeley Advanced Light Source allowed them to map a cross-section of the tooth for areas of high-magnesium content, and showed for the first time that the Mg-rich stone part which will become the tooth tip is bounded by plates.

Microindentation studies, also done at the Weizman Institute, showed that the structure controls how cracks propagate through the tool. When the indenter tip dimpled the surface, cracks spread radially. But as soon as they encountered the organic layers at the surface of a plate or a fiber, the crack deflected, often by as much as 90°.

The researchers noted holes within the polycrystalline matrix. Suspecting that these play a role in where the teeth break, they investigated the teeth using hard-x-ray tomography with a resolution of 1 μm at beamline 2-BM-A,B (Fig. 1). They found holes that had never been revealed before, which were abundant all around the stone part, but not in the stone part. These are channels in which the cells forming the tooth live, and must be absent from the stone part and the grinding tip, so these won’t break as the tooth grinds.

— Yvonne Carts-Powell

See: Christopher E. Killian[1,2], Rebecca A. Metzler[1], Yutao Gong[1], Tyler H. Churchill[1], Ian C. Olson[1], Vasily Trubetskoy[1], Matthew B. Christensen[1], John H. Fournelle[1], Francesco De Carlo[3], Sidney Cohen[4], Julia Mahamid[4], Andreas Scholl[5], Anthony Young[5], Andrew Doran[5], Fred H. Wilt[2], Susan N. Coppersmith[1], and Pupa U. P. A. Gilbert[1]*, “Self-Sharpening Mechanism of the Sea Urchin Tooth,” Adv. Funct. Mater. **21**, 682 (2011).

Author affiliations: [1]University of Wisconsin, [2]University of California, Berkeley, [3]Argonne National Laboratory, [4]Weizmann Institute of Science, [5]Lawrence Berkeley National Laboratory

Correspondence:

*pupa@physics.wisc.edu

This work was supported by U.S. Department of Energy (DOE) award DE-FG02-07ER15899, National Science Foundation award CHE-0613972, and UW-Hamel Awards to P. Gilbert. Use of the Advanced Photon Source was supported by the U.S. DOE Office of Science under Contract DE-AC02-06CH11357.

> A sea urchin, *Strongylocentrotus purpuratus*, © Laura Francis, source: BioLib.cz, http://www.biolib.cz/en/image/id26466/

> Frame from a movie of the three-dimensional x-ray microtomographic reconstruction of the sea urchin tooth cross-section, obtained at APS beamline 2-BM-A,B. The *S. purpuratus* tooth sample was mounted vertically and rotated around a vertical axis. A segment approximately 1-mm high was illuminated by x-rays of photon energy 20 keV. The sample was rotated in 0.12° steps and a total of 1,500 projection images were collected.
Two movies can be viewed at http://onlinelibrary.wiley.com/store/10.1002/adfm.201001546/asset/supinfo/adfm_201001546_sm_Movie1.mov?v=1&s=894ced6c19cbcdd675f38299ecad1047b05b3ccc

and

http://onlinelibrary.wiley.com/store/10.1002/adfm.201001546/asset/supinfo/adfm_201001546_sm_Movie2.mov?v=1&s=6743a584972e659fa603f4ef3a2fa222fe069177.
From supplementary material to C.E. Killian et al., Adv. Funct. Mater. **21**, 682 (2011).

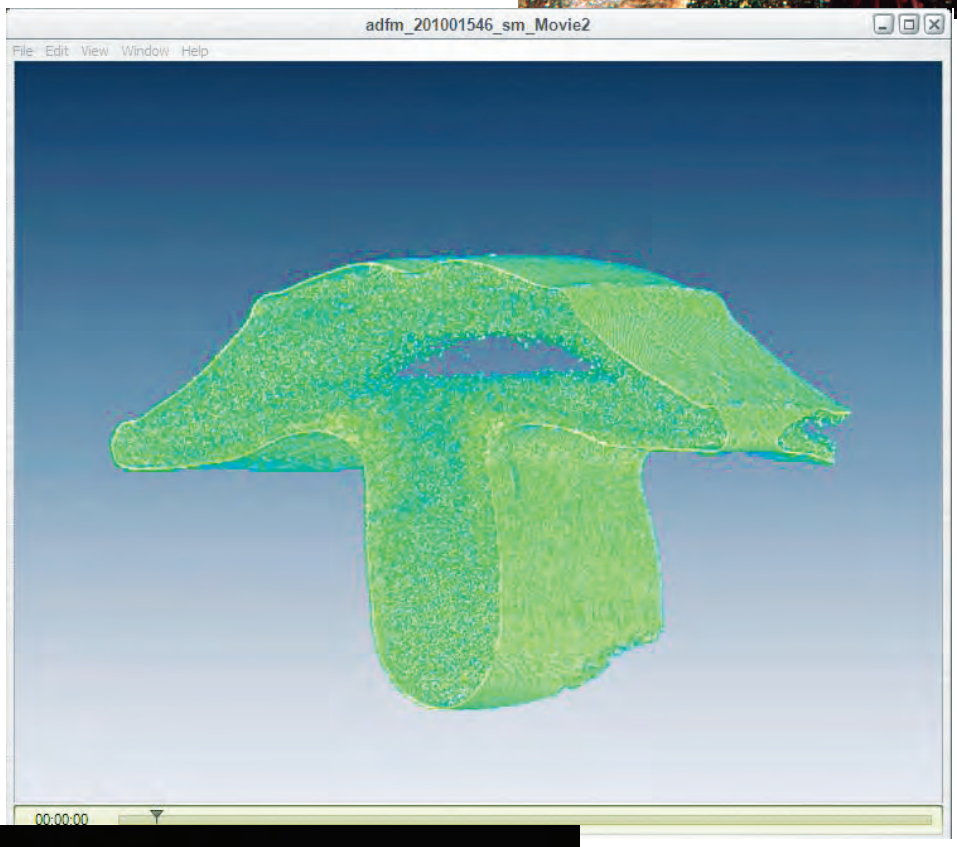

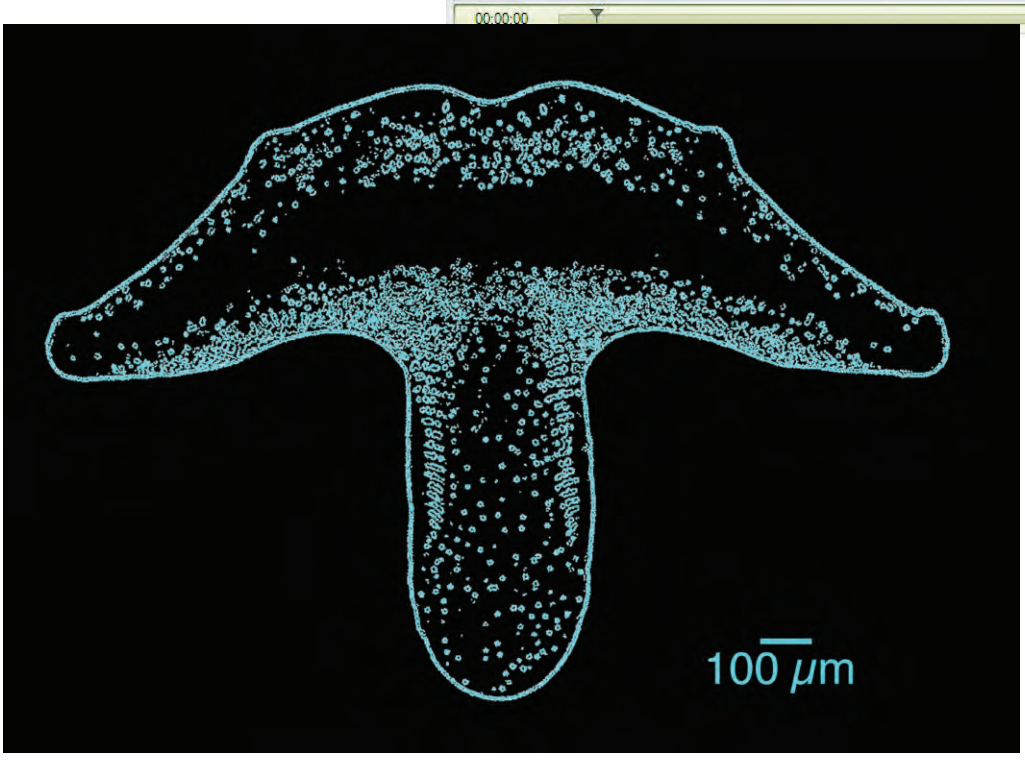

< Fig. 1. A sea urchin tooth cross-section extracted from the full three-dimensional reconstruction of the tooth from microtomography at APS beamline 2-BM. The cyan pixels indicate the locations of abrupt density variation, that is, the profile of holes in the tooth. Notice that there are no holes in the central stone part, where fracture and porosity must be prevented, while they occur everywhere else in the tooth. From C.E. Killian et al., Adv. Funct. Mater. **21**, 682 (2011). ©2011 WILEY-VCH Verlag GmbH & Co. KGaA, Weinheim

2-BM-A,B • XSD • Life sciences, physics • General diffraction, microdiffraction, phase contrast imaging, tomography • 5-30 keV, 10-33 keV • On-site • Accepting general users •

ART SCENE INVESTIGATION: PICASSO GOES NANOTECH

Volker Rose [XSD-MIC] inside the control room. Right, tools of the trade, and our Picasso sample.

From the Art Institute of Chicago's blog, "ARTicle."

August 01, 2011

If I say "ring" you might first think of Frodo. Or maybe Wagner if you're an opera lover. But you'll find neither Hobbits nor Valkyries at the ring-shaped Argonne National Laboratory just outside Chicago. What you will find is Art Institute conservation scientists, as we visited the Lab this month on a mission to bring Picasso to the ring.

Let me qualify that: we brought minuscule samples of Picasso paintings from the Art Institute to the Advanced Photon Source. At this top-notch facility, scientists rip electrons from atoms and make them spin furiously around the circumference of the experiment hall—which is large enough to encircle a baseball stadium. These enraged electrons (always charged with that negative attitude!) give off enormous amounts of energy, which the scientists can bend and direct to do wonderful things.

We used the energy from this process to penetrate every single grain of white pigment that Picasso used with nanometric resolution (that is, splitting human hair eighty thousand times to get down to a nanometer) in order to determine where it came from. Was it from a wrinkled tube from one of the artist's storied houses, produced on the banks of the river Seine in chi-chi Paris? Or did it come from a drippy can of mass-market produced house paint? Could the paint possibly have been made in the U.S.? By looking at infinitesimal contaminants in these zinc oxide pigment particles we hope we will be able to answer these questions and advance our Picasso-related detective work.

Often conservators are surprised to find themselves in facilities such as these. But at Argonne, scientists riding around on tricycles (the facility's favored mode of transportation) were probably just as surprised to find us. These scientists were encountering Picasso in unexpected places: posted in a note with our project title on our experimental station's door and attached with a drop of nail polish (an ironic fate for a known womanizer!) on a small pin!

Outside, at night (yes, because when you are awarded time for an experiment, you work 24/7 for 5 days: science cannot wait), dragonflies sparkle amidst the grass in the calm, bucolic setting. Inside, it sparkles too…we are brimming with the excitement of discovery. And that is how Picasso, a trailblazer in both life and death, went nanotech at Argonne on a hot day in July 2011.

— Francesca Casadio, Andrew W. Mellon Senior Conservation Scientist, Art Institute of Chicago

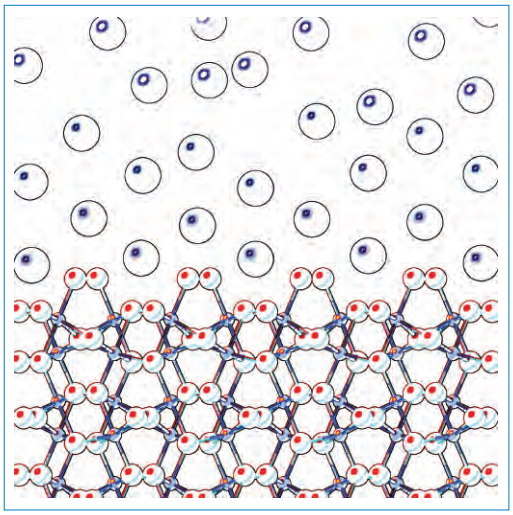

Soft Materials & Liquids

THE FIRST OBSERVATION OF RAPID ORDERING IN A SUPERCOOLED LIQUID METAL

Metallic glasses — unlike pure metals and most alloys — do not possess crystalline long-range order, but they *do* have short-range order (SRO). Scientists are still debating (and trying to measure) exactly how and when SRO develops as a liquid cools and solidifies without crystallizing. When a liquid is cooled below its freezing point without solidifying, it is said to be supercooled, a state that must be achieved in order to form a glass. This ability has been known since the 1700s, but the concept is still not fully understood today. To better understand the nature of atomic-scale ordering in supercooled metallic liquids, particularly those that can form glasses, scientists working at the XSD 6-ID-D beamline at the APS studied liquid copper-zirconium (Cu-Zr) alloys using beamline electrostatic levitation (BESL). For the first time, chemical and topological ordering was observed to occur rapidly and simultaneously in supercooled liquid $Cu_{46}Zr_{54}$ at temperatures well above that where a glass forms. This study provides scientists with a better understanding of structural and chemical ordering prior to the glass transition in liquid metals and enhances our knowledge of how supercooled liquids are stabilized (i.e., resist crystallization), which may aid in the development of new metallic glass alloys for a wide range of applications. >>>

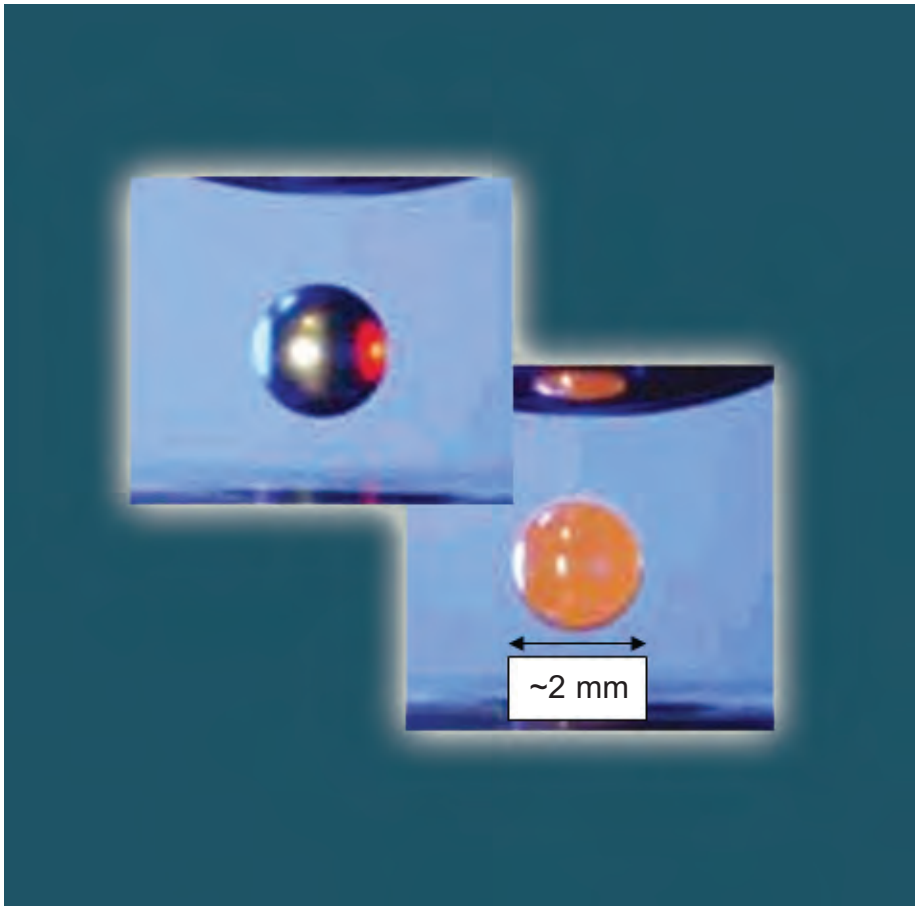

Fig. 1. Images of metal samples levitated in the ESL being melted by a laser beam.

When Cu-Zr alloys are cooled from the liquid state at a sufficiently rapid rate, the atoms are unable to arrange themselves into a crystalline state. Rather, their motion gradually slows down until they freeze in place, remaining disordered in a way that is somewhat similar to the arrangement of atoms in normal window glass. Metallic glasses (also called glassy metals or amorphous alloys) possess a unique combination of properties. Some of these properties resemble those of normal metals (high strength and elastic limit); others are like those of ceramics (hard, but often brittle); and some properties even resemble those of polymers (molding and shaping ability). Metallic glasses are already being deployed in a variety of applications, including, but not limited to, biomedical implants, magnetic cores (such as in transformers), springs, and micro-electro-mechanical systems devices.

The researchers in this experiment – representing Washington University, the University of Massachusetts, the NASA Marshall Space Flight Center, Iowa State University, Argonne, and Oak Ridge National Laboratory – placed a modified electrostatic levitator from NASA's Marshall Space Flight Center in the 6-ID-D beamline to study struc-

tural changes in the liquid Cu-Zr alloys as they cooled. They floated a small, nearly-spherical (approximately 2.5-mm-diameter) sample under high vacuum, suspended by a computer-controlled electrostatic field, and heated it from room temperature to 300° C (572° F) above its melting temperature utilizing a high-power diode laser beam. (Fig. 1.) The x-rays generated by the APS were diffracted by the liquid Cu-Zr sample, allowing the researchers to study how the arrangement of atoms in the supercooled liquid changed as it cooled (Fig. 2).

In the past, many researchers believed that metallic glasses with large physical dimensions — bulk metallic glasses — could form only for combinations of two or more metals with very different sizes and chemical characteristics. It is now well known that binary alloys such as copper-zirconium (Cu-Zr) can also form bulk glasses. In addition, Cu-Zr alloys can form glasses over a wide range of compositions. This fact and other chemical properties make CU-Zr an ideal system to study in BESL.

The results of this study suggest that the atoms of $Cu_{46}Zr_{54}$ become more ordered well before they finally slow down to form a glass. This relatively rapid chemical and topological ordering is distinctly different from the gradual ordering that is typically observed with supercooling in metallic liquids. Although chemical ordering has already been observed for metallic glasses, and has been predicted by theoretical calculations for Cu-Zr, this is the first experimental observation of its kind for a supercooled metallic liquid.

— William Arthur Atkins

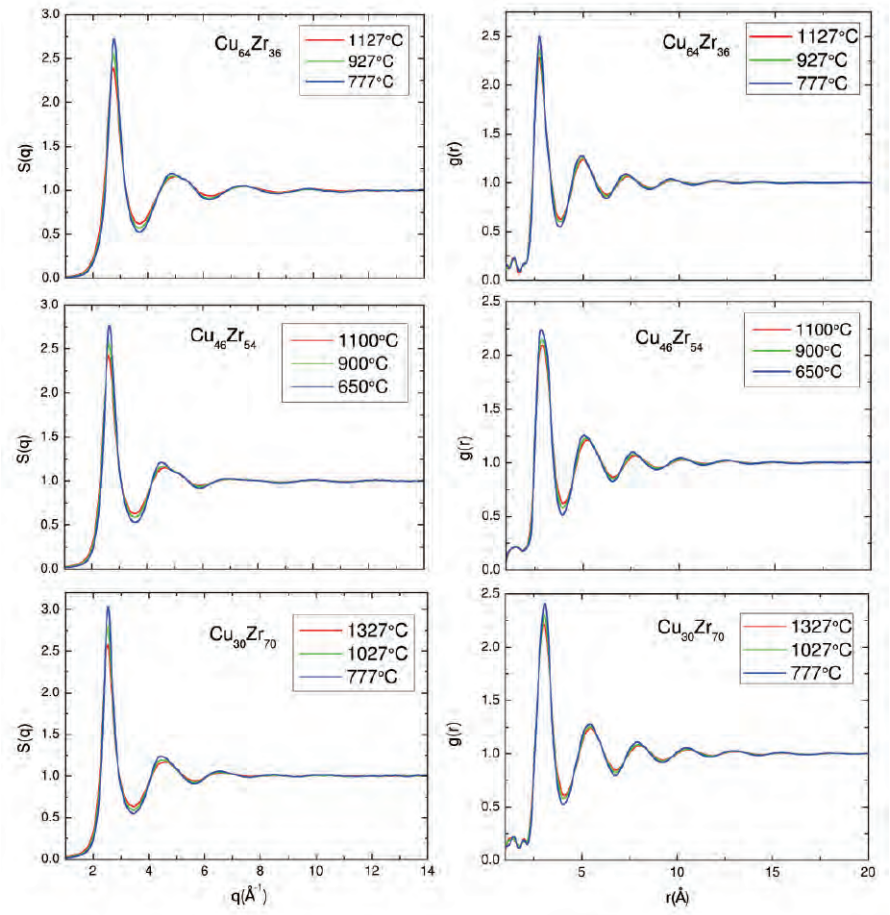

Fig. 2. Total static structure factors (left-hand side) and pair distribution functions (right-hand side), with changing temperature, for $Cu_{100-x}Zr_x$ liquids with x = 36 (top), 54 (middle), and 70 (bottom). From V. Wessels et al., Phys. Rev. B **83,** 094116 (2011). ©2011 American Physical Society.

See: V. Wessels[1,6]*, A.K. Gangopadhyay[1], K.K. Sahu[1,6], R.W. Hyers[2], S.M. Canepari[2], J.R. Rogers[3], M.J. Kramer[4], A. I. Goldman[4], D. Robinson[4,5], J. W. Lee[7], J. R. Morris[7], and K. F. Kelton[1], "Rapid chemical and topological ordering in supercooled liquid $Cu_{46}Zr_{54}$," Phys. Rev. B **83**, 094116 (2011). DOI:10.1103/PhysRevB.83.094116

Author affiliations: [1]Washington University, [2]University of Massachusetts, [3]NASA Marshall Space Flight Center, [4]Ames Laboratory, [5]Argonne National Laboratory, [6]ETH Zurich, [7]Oak Ridge National Laboratory

Correspondence: *victor.wessels@mat.ethz.ch

The work at Washington University was partially supported by the U.S. National Science Foundation under Grants No. DMR-0606065 and No. DMR-0856199 and by NASA under Contracts No. NNX07AK27G and No. NNX10AU19G. The work of J.R.M. was sponsored by the Laboratory Directed Research and Development Program of Oak Ridge National Laboratory, managed by UT-Battelle, LLC, for the U.S. Department of Energy (DOE). J.W.L.'s research was performed at the Oak Ridge National Laboratory, Materials Science and Technology Division and sponsored by the Republic of Korea, Ministry of Knowledge Economy, Visiting Scientists Program, under IAN:16B642601, with the U.S. DOE. Simon Fraser University, and the APS. Use of the Advanced Photon Source was supported by the U.S. DOE Office of Science under Contract DE-AC02-06CH11357.

6-ID-D • XSD • Physics, materials science • Magnetic x-ray scattering, high-energy x-ray diffraction, powder diffraction, pair distribution function • 27-52 keV, 50-100 keV, 67-130 keV • On-site • Accepting general users •

WHAT HAPPENS WHEN BUBBLES BURST?

The phenomenon of bubble formation, and in particular their bursting, is a critical part of countless processes in physics, biology, chemistry, geology, oceanography — anywhere liquid and air interface with each other. When a bubble bursts, the gas contained within is released and liquid jets are created, scattering aerosol droplets. But the formation of jets upon bursting of very small bubbles, such as those less than 100 μm in radius, has remained unconfirmed because of the difficulty of experimentally visualizing the process at such scales. Now a team of researchers from Pohang University of Science and Technology and Argonne has used ultrafast x-ray and optical imaging at the APS to directly visualize the bursting of very small bubbles. Their work demonstrates that jet formation occurs only with bubbles larger than a critical size limit that is dependent upon the specific liquid properties. Their work provides clues about the behavior of aerosols in various natural processes, such as the emission of gases from the ocean into the atmosphere, and has potential practical applications in areas including glass manufacturing and biotechnology.

Working at the XSD 32-ID-B,C undulator beamline of the APS, the experimenters used a drop-impact setup to create the bursting and control the size of the bubbles in five low-viscosity liquids: water, ethanol, dodecane, tridecane, and decalin. The bursting phenomena were first observed under ultrafast optical microscopy, followed by ultrafast x-ray phase-contrast imaging. The latter method allowed the process to be observed with extremely high time and spatial resolution, avoiding reflection and scattering effects that can occur with visible light imaging and offering precise visualization of the liquid-air interface because of the penetrating APS x-ray beam.

In the drop-impact technique, a drop of the test liquid is allowed to fall freely from a height onto a solid surface. Upon impact, a small bubble is created inside the drop, which quickly rises and bursts upon reaching the air-liquid interface.

The team found that jetting from the bursting bubble is the result of capillary waves converging at the interface, described by the Ohnesorge number (Oh), the ratio of the viscosity and surface forces that dampen the propagation of the capillary waves. The experimenters suggest that above a certain critical Oh number, jetting does not occur because capillary waves are suppressed by viscous stresses.

Drawing a parallel between jetting in bubble bursting and the pinching-off process in liquid coalescence, the researchers note that the Oh number determines the minimum bubble radius in a given liquid, below which jetting does not occur. In the five liquids studied, that minimum radius was approximately 4, 26, 34, 48, and 54 μm in water, ethanol, dodecane, decalin, and tridecane, respectively.

Various bubble sizes were observed under ultrafast optical imaging (Fig. 1) and a phase diagram for jetting constructed in which the critical Oh number was found to be 0.052±0.005, matching the experimental data. (The absence of jetting in water could not be observed directly because bubbles of such small radius [4 μm] cannot be created by the drop-impact technique.)

The experiments confirm that jetting does not always occur when bubbles burst, and that the presence of jetting is indeed dependent on the size of the bubbles involved (Fig. 2). Generally speaking, jets will not form from bursting bubbles below a certain critical size, dependent on the particular liquid. Aside from the insights the work can provide into the behavior of aerosols in various natural processes, particularly in the emission of gases from the ocean into the atmosphere, it also has potential application in many practical scenarios. Whether one wishes to control the "fizziness" of soft drinks or reduce jetting in various manufacturing processes that involve an air-liquid interface, the present work demonstrates that jetting can be controlled by changing properties of the liquids involved. Altering the liquid's viscosity, surface tension, or density can ensure that bubbles formed in the liquid remain small enough to reduce or eliminate jetting. Whether they're metaphorical or real, there are some bubbles that should not be burst.

— Mark Wolverton

See: Ji San Lee[1], Byung Mook Weon[1]*, Su Ji Park[1], Jung Ho Je[1]**, Kamel Fezzaa[2], and Wah-Keat Lee[2], "Size limits the formation of liquid jets during bubble bursting," Nat. Commun. **2**, 367 (21 June 2011). DOI:10.1038/ncomms1369

Author affiliations: [1]Pohang University of Science and Technology, [2]Argonne National Laboratory

Correspondence:
*bmweon@postech.ac.kr,
**jhje@postech.ac.kr

This research was supported by the Creative Research Initiatives (Functional X-ray Imaging) of MEST/NRF. Use of the Advanced Photon Source at Argonne National Laboratory was supported by the U. S. Department of Energy Office of Science under Contract No. DE-AC02-06CH11357.

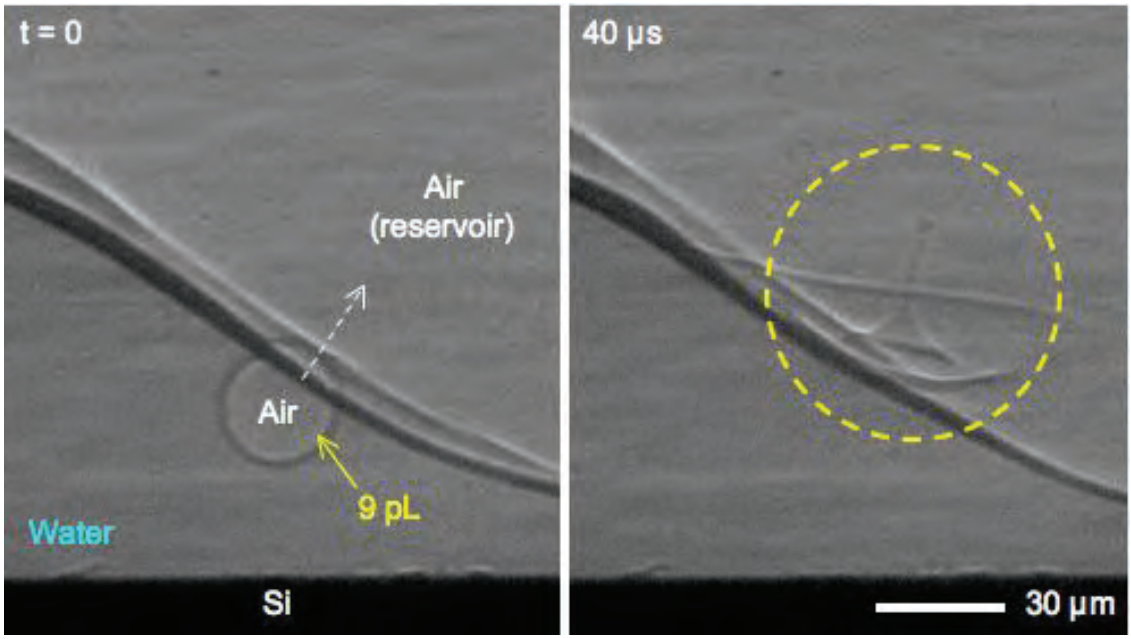

Fig. 1. The moment of the jet formation from a bursting bubble in water, which is visualized by ultrafast x-ray imaging at the XSD 32-ID-B,C undulator beamline.

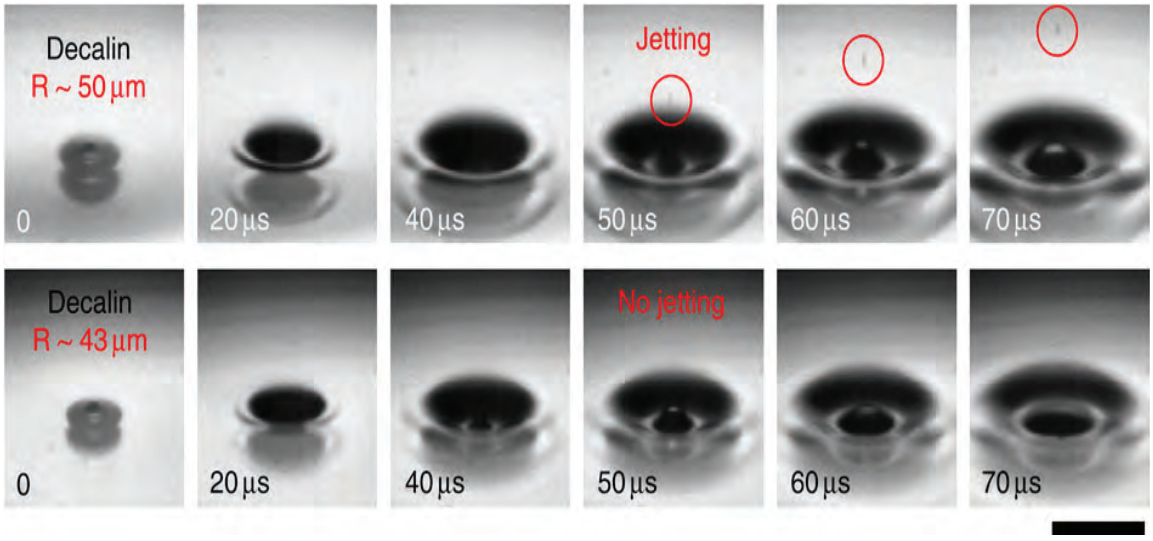

Fig. 2. Bubble bursting from small bubbles (R<100 µm) in a typical drop-impact experiment. A liquid drop that freely falls from a height onto a solid surface robustly forms a single small bubble after impact. Once a trapped bubble reaches the fluctuated liquid free surface, it rapidly bursts. The critical size differs with the liquid. Ultrafast optical images of jetting (upper, R~50 µm) and the absence of jetting (lower, R~43 µm) in decalin. Scale bar, 150 µm. The jet formation is characterized by the emission of aerosol droplets into the atmosphere (marked as circles). Ethanol, dodecane and tridecane show a similar size limitation for jetting, but water always shows jetting. From Ji San Lee et al., Nat. Commun. **2** (2011).

A Quicktime movie showing x-ray imaging of jetting in water can be viewed at http://www.nature.com/ncomms/journal/v2/n6/extref/ncomms1369-s5.mov

32-ID-B,C • XSD • Materials science, life sciences, geoscience • Phase contrast imaging, radiography, transmission x-ray microscopy, tomography • 7-40 keV • On-site • Accepting general users

DISORDERED WATER ON MINERAL SURFACES

The interaction of water with minerals is one of the most important processes in environmental and geological systems. Mineral-water reactions control the composition of rivers, lakes, and the oceans, affect where and how fast contaminants migrate in the environment, influence how microorganisms carry out metabolism, and are key steps in the formation and destruction of rocks near the Earth's surface. To better understand how water and minerals interact, scientists have probed the nanoscopic region where water molecules and minerals meet. In this particular research, the arrangement and disorder of the first few molecular layers of water residing on surfaces of the minerals hematite (Fe_2O_3) and corundum (Al_2O_3) were precisely determined. The highly intense and monochromatic x-rays at the APS were essential to the successful probing of the boundary between mineral surfaces and water, which shows the variety of water dynamics among the different crystal faces of hematite and corundum, and that this relates to differences in their chemical reactivity. The research, which suggests that mineral surfaces in general will show either strong or weak ordering of water and that mineral surface adsorption of heavy metals like arsenic and lead is affected by the properties of water near the surface, will improve our understanding of how minerals sequester toxic materials in the natural world, and could lead to technological applications for optimizing engineered systems, such as in water treatment facilities.

Previous investigations by this researcher from Washington University and colleagues had determined that near most crystal faces of hematite and corundum, such as the (012) and (110) surfaces, water takes on a regular arrangement with a high degree of ordering (left side of Fig. 1). However, the ordering of water on the most common face of these minerals, (001), had not been previously determined with high precision in the presence of liquid water. The (001) surfaces have previously been suggested to display chemical behavior different from other common surfaces of hematite and corundum, including little surface charge development over a wide pH range. This implied that water may behave differently near these surfaces.

Specular x-ray reflectivity was utilized to investigate the structure and disorder of water near these mineral surfaces. This technique involves measuring the intensity of a beam of x-rays bounced off a sample surface as a function of incident angle. The vast majority of those x-rays scatter off the surface in random directions. However, a very small fraction, sometimes less than one out of a billion x-ray photons, is reflected like light bouncing off a mirror. A high-intensity x-ray source is required for these experiments because the percentage of reflected x-ray photons is so low. The bright and monochromatic x-ray beams produced by the APS allow specular reflectivity measurements to be performed in a rapid and efficient manner that is impossible in an ordinary laboratory setting, and difficult at most other synchrotron light sources.

Corundum was studied at DND-CAT beamline 5-ID-B,C,D; data on hematite was obtained at XSD beamline 33-ID-D,E. The x-ray data collected on the mineral samples were used to deduce information about the positions and degree of disorder of the first few molecular layers of water wetting their surfaces. In contrast to what was observed for other surfaces of hematite and corundum (left side of Fig. 1), water adjacent to the (001) surfaces of hematite and corundum shows very weak ordering and becomes fully disordered like bulk water closer to the surface (right side, Fig. 1). This weak water ordering is attributable to two properties of these surfaces. First, atoms on other surfaces of these minerals take on an undulating form, analogous to a corrugated metal roof. Water molecules adsorbed to those surfaces follow this undulating form. This "corrugated pattern" limits the lateral (side-to-side) motion of water molecules, keeping them in fixed locations. In contrast, atoms on the (001) face form an atomically flat surface and nearby water molecules can move more freely, and are hence more disordered. Second, reactive sites on other surfaces have a charge even when the net charge of the surface is neutral (i.e., the number of positive and negative sites are perfectly balanced). Because water molecules are dipoles, with positively and negatively charged ends, they orient themselves near these sites, which help hold them in place. In contrast, reactive sites on the (001) surface have no charge over a wide pH range. Water molecules near (001) surfaces are free to rotate and move about, and show greater disorder.

This research has several significant consequences. First, it demonstrates that water dynamics vary among the different crystal faces of hematite and corundum and that this relates to differences in their chemical

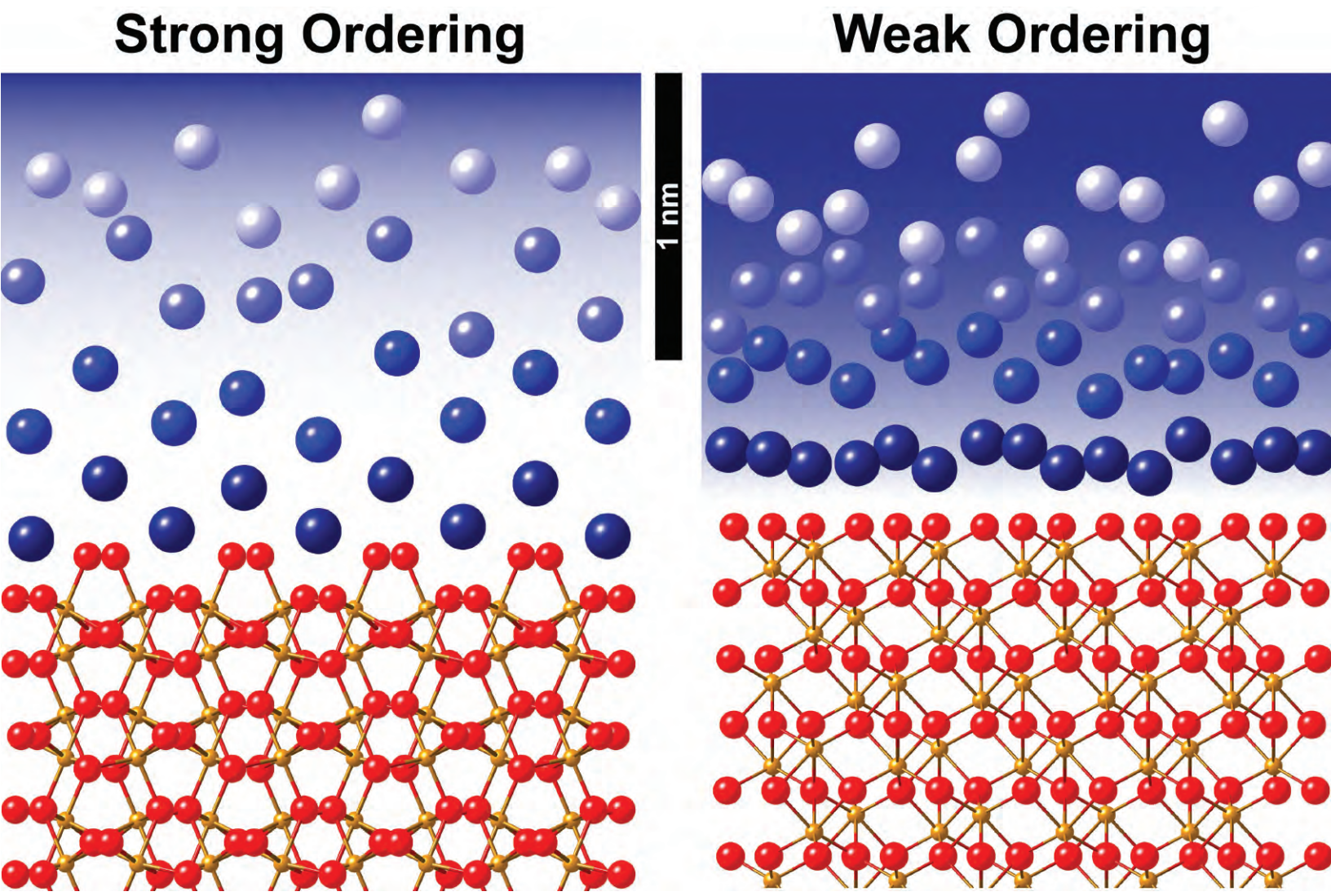

Fig. 1. Many mineral surfaces, such as the (012) surfaces of iron and aluminum oxides (left side of figure), which consist of iron or aluminum (small gold spheres) and oxygen atoms (red spheres), induce strong local ordering of water molecules (blue spheres), with the transition to disordered bulk water occurring 2 to 3 nm from the surface. The (001) surfaces of iron and aluminum oxide, however, induce only weak local ordering of water (right side of figure) and the transition to bulk-like water occurs much closer to the mineral surface.

reactivity. Additionally, at a fundamental level it suggests that mineral surfaces in general will show either strong or weak ordering of water. But these findings go beyond the interaction of water and minerals. Mineral surfaces adsorb heavy metals like arsenic and lead and this adsorption is affected by the properties of water near the surface. This work will thus improve the understanding of how minerals sequester toxic materials in the natural world, and might also find technological applications for optimizing engineered systems, such as in water treatment facilities. — *Philip Koth*

See: Jeffery G. Catalano, "Weak Interfacial Water Ordering on Isostructural Hematite and Corundum (0 0 1) Surfaces," Geochim. Cosmochim. Acta **75** 2062 (2011). DOI:10.1016/j.gca.2011.01.025

Author affiliation: Washington University
Correspondence: catalano@wustl.edu

This work was supported by Washington University and the National Science Foundation through Grant EAR-0818354 (J.G.C.). DND-CAT is supported by E.I. DuPont de Nemours & Co., The Dow Chemical Company and Northwestern University. Use of the Advanced Photon Source at Argonne National Laboratory was supported by the U. S. Department of Energy Office of Science under Contract No. DE-AC02-06CH11357.

5-ID-B,C,D • DND-CAT • Materials science, polymer science • Powder diffraction, x-ray standing waves, x-ray optics development/techniques, small-angle x-ray scattering, surface diffraction, x-ray reflectivity, wide-angle x-ray scattering • 5-20 keV • On-site • Accepting general users

33-ID-D,E • XSD • Materials science, physics, chemistry • Anomalous and resonant scattering (hard x-ray), diffuse x-ray scattering, general diffraction, surface diffraction, x-ray reflectivity, x-ray standing waves • 4-40 keV, 6-21 keV • On-site • Accepting general users •

SUB-MOLECULAR ORGANIZATION IN DE VRIES SMECTIC PHASES

Over a century ago it was recognized that certain materials form a unique phase of matter between that of liquids and crystals, commonly referred to as the liquid-crystal (LC) phase. A variety of molecular types exhibit liquid-crystal behavior, including rod-shaped molecules referred to as calamitic. The liquid-crystal phases that calamitic molecules exhibit are temperature dependent: at high temperatures, the molecules form a liquid, while at sufficiently low temperatures they become crystalline. In between these high and low temperatures, calamitic molecules exhibit various liquid-crystal phases, including smectic phases. In the various smectic phases, calamitic molecules form layers where they tend to point lengthwise in a certain direction. The object of this particular research entailed investigating the de Vries smectic phases, which are only formed by special types of calamitic molecules. Investigators utilizing an APS beamline have produced the first x-ray images directly measuring the orientation of specially-chosen calamitic molecules in two different de Vries smectic phases, thus advancing the overall understanding of these phases, which will undoubtedly find important technological applications, such as in ultrafast LC displays.

There are several distinct types of smectic phases, each representing different degrees of molecular positional ordering and relative orientation. In the smectic A (SmA) phase, the molecules on average are aligned lengthwise in a direction perpendicular to the plane they form. The situation is analogous to books on a bookshelf, with most books standing straight up, while others point slightly off vertical. On average, their orientation is vertical. In contrast, molecules in the smectic C (SmC) phase are, on average, tilted with respect to the perpendicular direction at an angle α. In any given phase, the average molecular direction defines the director.

Typically, the transition from the SmA to the SmC phase occurs at temperature T_{AC} when the molecular orientation begins to transition from perpendicular to an angle $\alpha(T)$. The transition is accompanied by a reduction (or shrinkage) in the thickness *d* of the smectic layers due to the tilt of the molecules. Layer thickness in the SmC phase is typically reduced by up to ~11%.

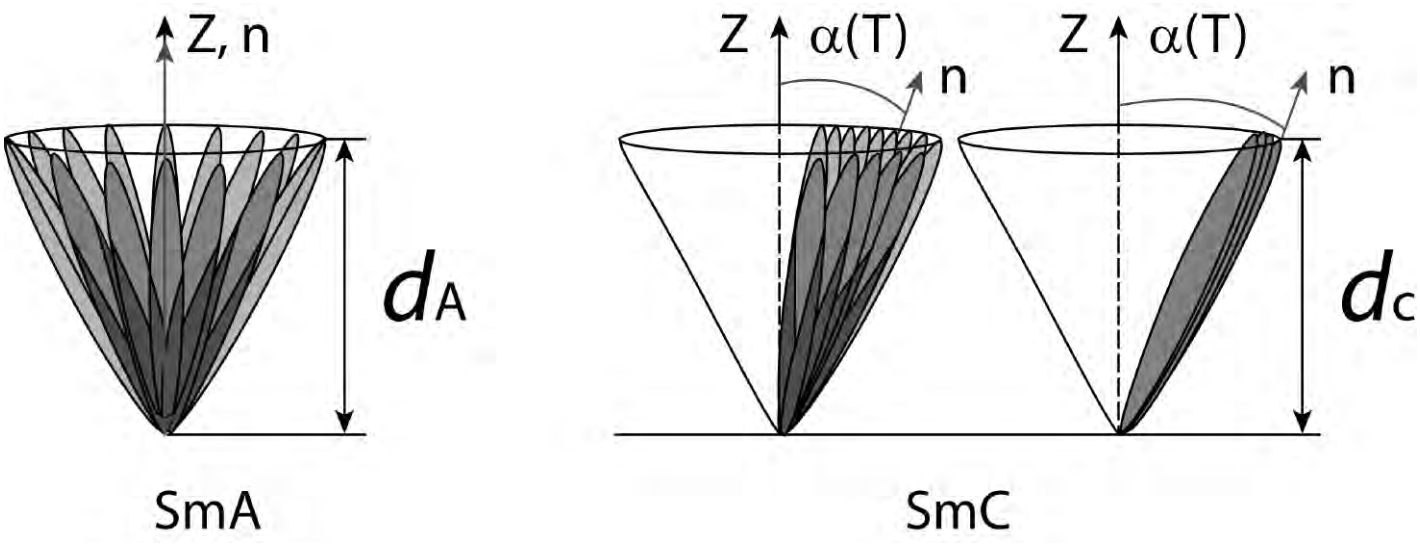

Fig. 1. Schematic representation of molecules on the surface of a cone in the SmA and SmC phases. "n" represents the director, "z" the direction perpendicular to smectic layers. Figures this page and next from HyungGuen Yoon et al., Phys. Rev. Lett **106,** 087801 (2011).

In contrast to the typical smectic behavior, molecules in the de Vries smectic phases experience a maximum layer reduction of only around one percent, about 10 times smaller than expected. The special behavior seen in the de Vries phases has been explained via the diffuse cone model.

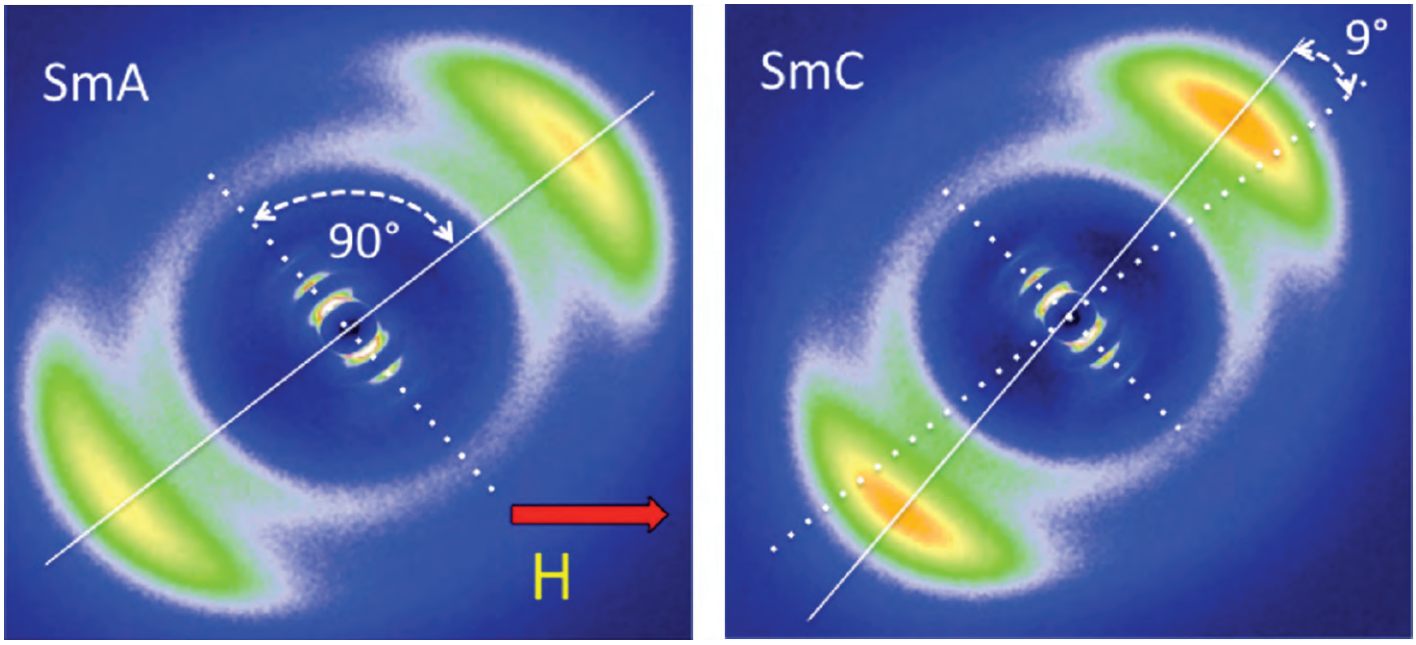

Fig. 2. Representative diffraction patterns in the SmA phase at 57.2 C and the SmC phase at 55.7 C, of mesogen C4 illustrating a change in molecular tilt from 0° in the SmA phase to 9° in the SmC phase. The dotted line passing through the large angles peaks of the SmC phase represents their orientation in the SmA phase.

In this model, calamitic molecules are constrained to statistically lie on the surface of an imaginary cone (Fig. 1). In the SmA phase, the rod-shaped molecules are distributed randomly over the surface of the cone, with each molecule making an angle α with the central axis of the cone. The director is parallel to the cone's axis since that is the average molecular orientation. At the transition temperature T_{AC}, the molecules begin to favor a single azimuthal direction upon the cone's surface. As temperature continues to lower, the director eventually transitions from being coaxial with the cone's axis, to lying on one side of the cone's surface at angle α.

To uncover details of the de Vries behavior, the researchers from Kent State University, COMSATS Institute of Information Technology, and Queen's University chose a recently synthesized molecule composed of several subunits: a rigid, central molecule (5-phenylpyrimidine), joined with two flexible molecules on either end; one a hydrocarbon (alkyloxy), and the other a siloxane/hydrocarbon (organosiloxane) combination. A homologous series of calamitic molecules was synthesized by attaching additional hydrocarbon subunits to the alkyloxy end segment, creating progressively longer molecules. The two homologs chosen were C4 and C9 (designating the fourth and ninth homologs, respectively).

The C4 and C9 homologs were placed in separate quartz capillaries for x-ray analysis. X-ray measurements were performed using the spectrometer at the XSD 6-ID-B,C beamline at the APS. Two-dimensional (2-D) x-ray diffraction patterns were generated for both samples. The 2-D diffraction patterns directly revealed molecular orientations in the SmA and SmC phases. Figure 2 shows a 9° tilt (i.e., α = 9°) in the SmC phase for C4, at approximately 12.8° C below T_{AC}. Significantly, the siloxane and hydrocarbon segments were shown to be oriented parallel to the director in both the SmA and SmC phases. However, further analysis (not yet published) has shown that the siloxane and hydrocarbon segments tilted at different angles, and the molecules progressively developed a hockey-stick shape in the SmC phase.

This research significantly advances the overall understanding of the de Vries smectic phases. The collected x-ray data provides the first direct evidence of the director tilt in de Vries smectics, as well as revealing the individual orientations of the siloxane and hydrocarbon end segments. Due to their very small layer shrinkage in the SmC phase, ferroelectric analogs of de Vries molecules will undoubtedly find important technological applications, such as in ultrafast LC displays.

— Philip Koth

See: HyungGuen Yoon[1], Dena M. Agra-Kooijman[1], Khurshid Ayub[2], Robert P. Lemieux[3], and Satyendra Kumar[1]*, "Direct Observation of Diffuse Cone Behavior in de Vries Smectic-A and –C Phases of Organosiloxane Mesogens," Phys. Rev. Lett. **106**, 087801 (2011). DOI:10.1103/PhysRevLett.106.087801

Author affiliations: [1]Kent State University, [2]COMSATS Institute of Information Technology, [3]Queen's University

Correspondence: *skumar@kent.edu

This work was supported by the U.S. Department of Energy (DOE) Office of Science grant DE-SC0001412. Use of the Advanced Photon Source at Argonne National Laboratory was supported by the U. S. DOE Office of Science under Contract No. DE-AC02-06CH11357.

6-ID-B,C • XSD • Physics, materials science • Magnetic x-ray scattering, anomalous and resonant scattering (hard x-ray), general diffraction, grazing incidence diffraction, surface diffraction (UHV) • 3.2-38 keV • On-site • Accepting general users •

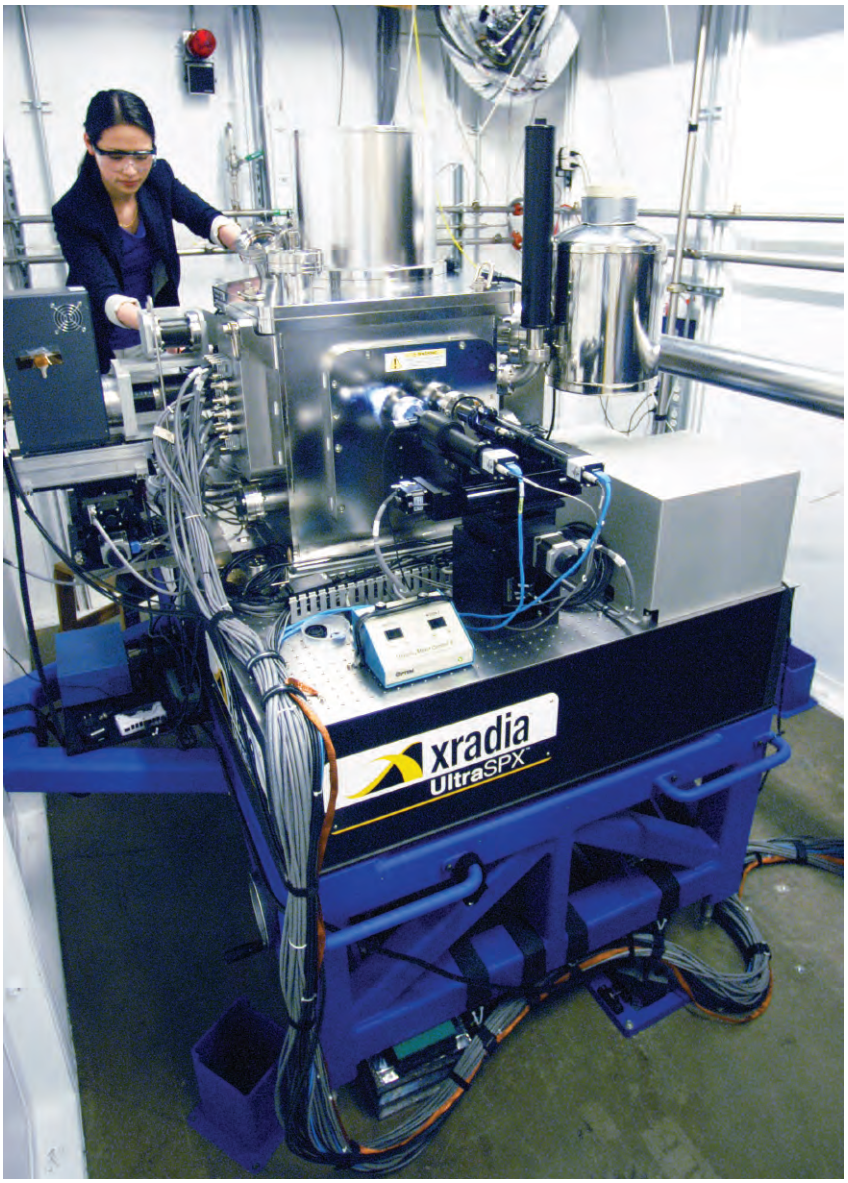

APS postdoc S. Chen (XSD-MIC) working at the x-ray Bionanoprobe at LS-CAT beamline 21-ID-D. Northwestern University, the APS, and Xradia, Inc., collaborated on the design, construction, commissioning, and operation of the Bionanoprobe. The instrument is capable of two- and three-dimensional imaging of cryogenically cooled biological samples. It has an energy range of 5 to 20 keV, with mapping resolution of δ <30 nm and spectroscopy resolution of δ <50 nm. The Bionanoprobe features an in-vacuum cryo system and fast tomography through a combination of differential phase and x-ray fluorescence mapping using dose fractionation.

Correspondence: Keith Brister, k-brister@northwestern.edu

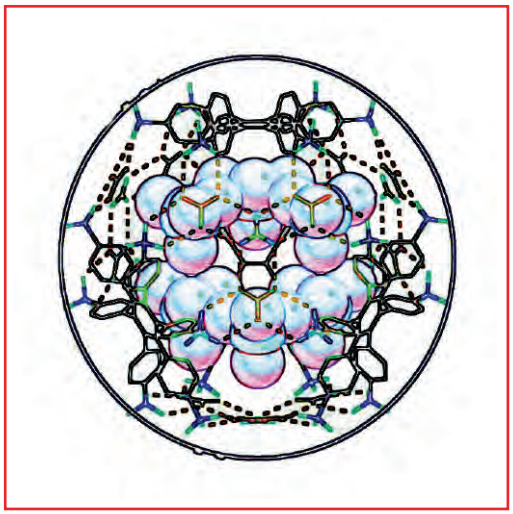

Chemical Science

Molecular Cages for More Control over Chemical Reactivity and Reaction Products

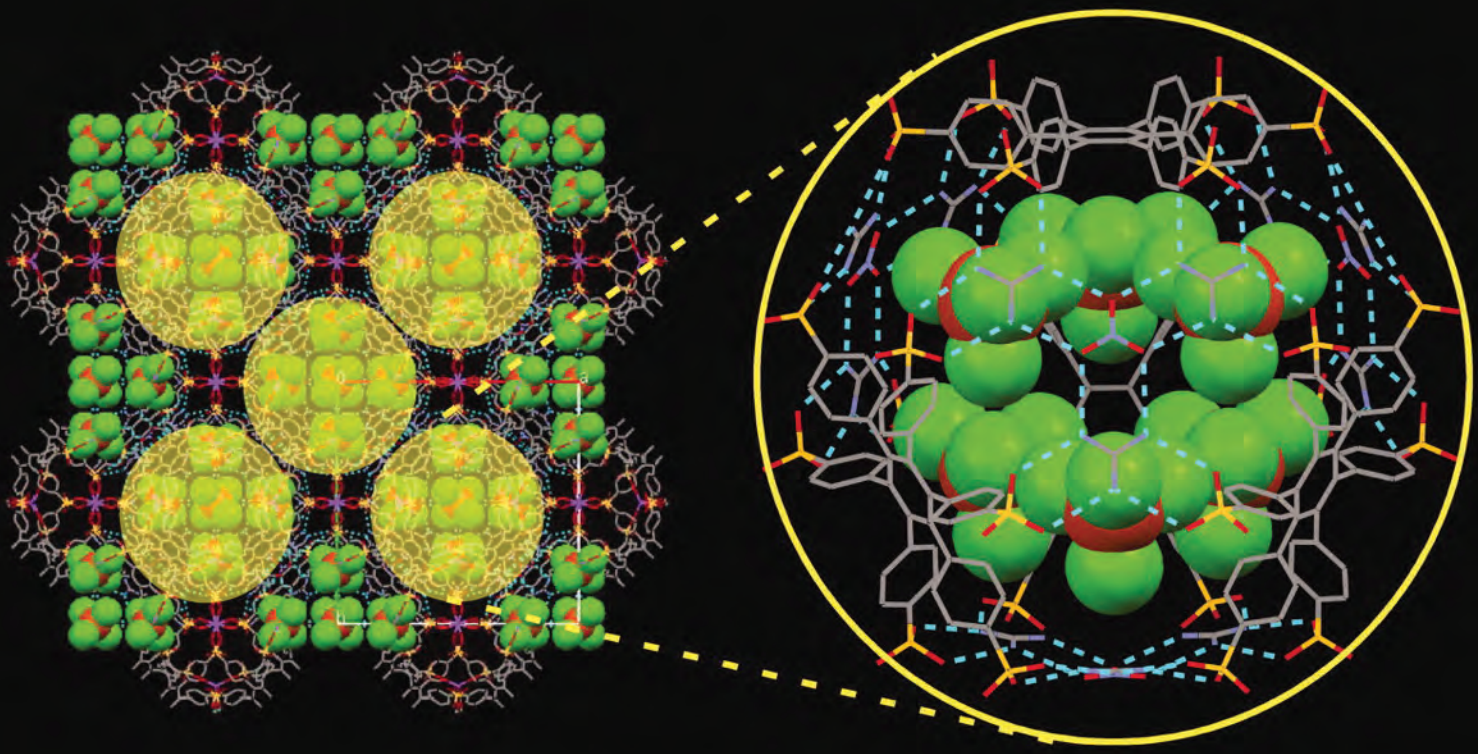

Fig. 1. Left: The q-TO framework of compound 9, in which each q-TO encapsulates six $[FeCl_4]^{1-}$ ions, as determined by single-crystal x-ray diffraction. The yellow shading denotes the position of individual q-TOs. Right: An expanded view of a single q-TO in compound 9, for which all the $[FeCl_4]^{1-}$ ions are encapsulated within the q-TO. The $[FeCl_4]^{1-}$ ions are depicted as space-filling (green, chloride; orange, iron) and the q-TO framework as wire-frame (yellow, sulfur; blue, nitrogen; gray, carbon; red, oxygen). Hydrogen atoms have been omitted for clarity. The blue dashed lines represent the N-H···O hydrogen bonds. From Yuzhou Liu et al., Science **333**, 436 (July 2011).

Coaxing molecular components to self-assemble into supramolecular cages capable of confining other molecules remains a daunting challenge for chemists, but evidently not for nature. Virus capsids — the outer shells of viruses — are composed of many protein subunits that assemble into well-defined polyhedra that function as supramolecular cages for ribonucleic acid (RNA) or deoxyribonucleic acid (DNA) molecules. Even enzymes contain molecular-sized and shaped pockets that are capable of binding substrates and catalyzing unique chemical reactions. Man-made supramolecular cages could prove capable of confining and therefore controlling chemical processes, stabilizing reactive molecules, achieving chiral separations, and, as with enzymes, promoting catalytic reactions. So as not to be outdone by nature, researchers at New York University and the University of Milano-Bicocca guided the self-assembly of supramolecular cages built from 20 ions of 3 distinct species held together by 72 hydrogen bonds.

The cages are constructed from two kinds of hexagonal molecular tiles, a tris(guanidinium)nitrate $[G_3NO_3]^{2+}$ cluster and hexa(4-sulfonatophenyl) benzene ($HSPB^{6-}$), joined at their edges through complementary and metrically matched N-H•••O-S hydrogen bonds to form quasi-truncated octahedrons (q-TOs) (see Fig. 1). The researchers showed that (1) the q-TOs have an interior volume of 2200 $Å^3$, (2) serve as building blocks of a body-centered cubic zeolite-like framework, (3) and can encapsulate a wide range of differently charged species, including organic molecules, transition metal complexes, and "ship-in-a-bottle" nanoclusters that are not readily formed outside a confined environment. These demonstrations involved the application of several analytical capabilities, including synchrotron-based x-ray diffraction experiments, which were performed on the ChemMat CARS 15-ID-B,C,D beamline at the APS and at the European Synchrotron Radiation Facility.

The q-TOs spontaneously self-assemble from water-based solutions of dimethylformamide containing guanidinium chloride, sodium nitrate, and hexaphenylbenzenehexasulfonic acid, yielding colorless block-shaped crystals that exhibit well-defined square and hexagonal facets. The q-TOs form a body-centered lattice interconnected by sodium bridges, creating a framework topology and tiling pattern that resemble those found in sodalite and zeolite A. The framework is stable up to 160°C, reflecting an uncharacteristic robustness of the hydrogen-bonded assembly in the solid state.

The q-TOs and the framework exhibit a remarkable ability to encapsulate and tolerate an assortment of molecular species with wide-ranging shapes, sizes, substituents, and electrical charges. Surprisingly, the negatively charged framework even encapsulates negatively charged metal ion complexes. The strict conservation of the q-TO framework structure across such a wide range of molecules demonstrates that framework assembly is not guided by confined-molecule templating.

Encapsulation of metal clusters in the q-TOs suggests a route to well-defined semiconductor quantum dots having highly uniform and regulated sizes, which offers an alternative to more conventional approaches relying on pores. The assembly of the q-TO framework can be reversed under mild conditions by dissolving the crystals in water to release the confined molecules, so the framework can provide a facile route to releasing stable "ship-in-a-bottle" products. It also is reasonable to suppose that the same design principles can be extended to $[G_3NO_3]^{2+}$ and suitable tetrasulfonate molecules to produce other polyhedra, such as the truncated cuboctahedron and truncated icosidodecahedron, and their corresponding frameworks. — *Vic Comello*

See: Yuzhou Liu[1], Chunhua Hu[1], Angiolina Comotti[2], and Michael D. Ward[1]*, "Supramolecular Archimedean Cages Assembled with 72 Hydrogen Bonds," Science **333**, 436 (2011). DOI: 10.1126/science.1204369
Author affiliations: [1]New York University, [2]University of Milano-Bicocca
Correspondence: *mdw3@nyu.edu

This work was supported by the National Science Foundation, primarily by DMR-0906576 and partially by CRIF/CHE-0840277, and the Materials Research Science and Engineering Center Program under award DMR-0820341. A.C. financial support was from the Cariplo Foundation and ESRF (Grenoble). Y.L. financial support was provided by New York University through a Doctoral Dissertation Fellowship. ChemMatCARS is principally supported by the National Science Foundation/Department of Energy under grant number NSF/CHE-0822838. Use of the Advanced Photon Source at Argonne National Laboratory was supported by the U.S. Department of Energy Office of Science under Contract No. DE-AC02-06CH11357.

15-ID-B,C,D • ChemMatCARS • Materials science, chemistry • Single-crystal diffraction, anomalous and resonant scattering (hard x-ray), wide-angle x-ray scattering, microdiffraction, liquid surface diffraction, small-angle x-ray scattering, ultra-small-angle x-ray scattering, high-pressure diamond anvil cell • 6-32 keV, 10-60 keV • On-site • Accepting general users •

A FICKLE MOLECULE CAUGHT IN THE ACT

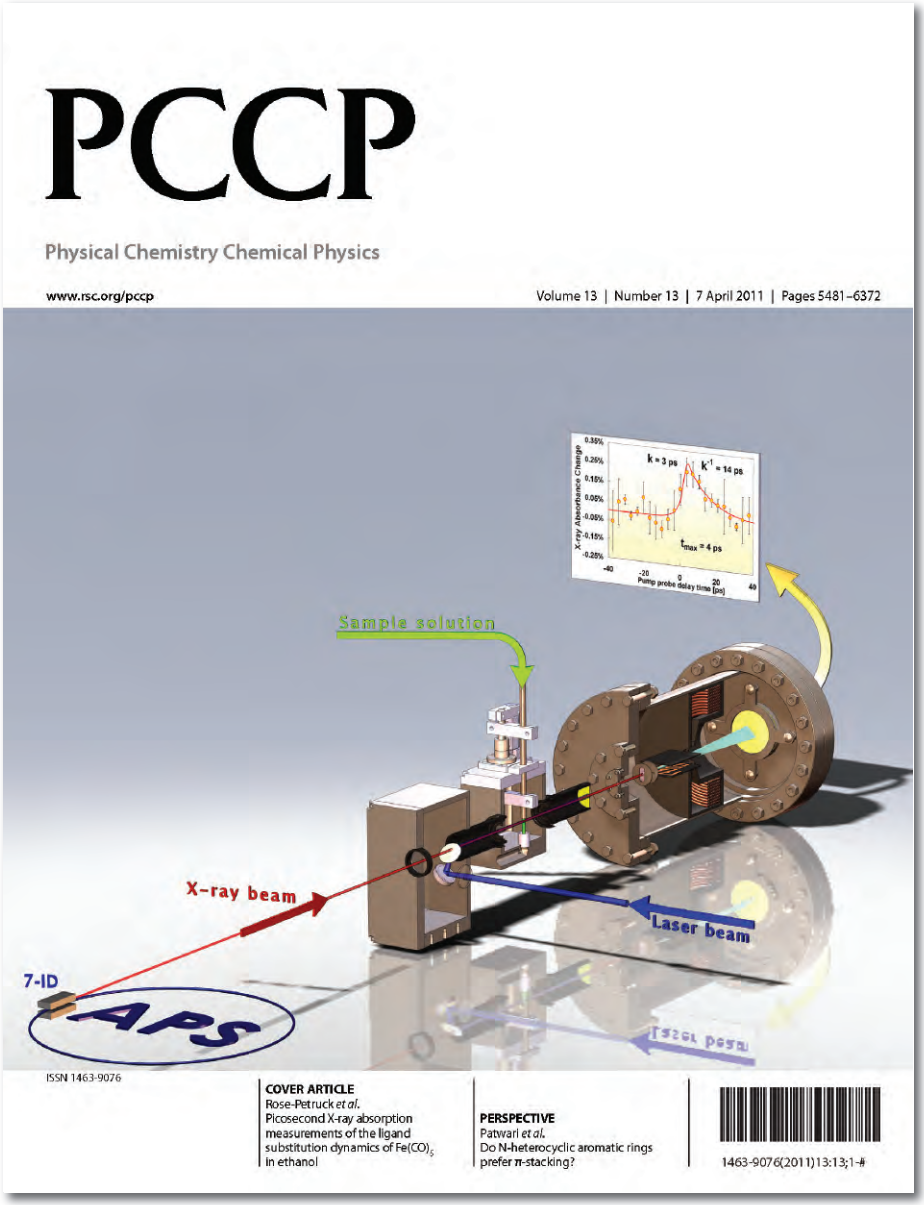

Fig. 1. As featured on the cover of *Physical Chemistry Chemical Physics*: The novel experimental apparatus at beamline 7-ID-C of the APS permits picosecond x-ray measurements of the ligand substitution dynamics of iron pentacarbonyl in ethanol solvent. Cover image from Brian Ahr et al., Phys. Chem. Chem. Phys. **13,** 5590 (2011). ©the Owner Societies 2011.

Surround a transition metal atom with carbon monoxide groups to make a metal carbonyl compound and you will have one fickle structure. "Fickle" is the word for substitution of any one of those carbonyls for a range of other chemical groups. It is this ease with which the ligands can be swapped out that makes this group of compounds so useful in organometallic syntheses and materials chemistry; they can also act as a source of "oxygenated carbon" for converting simpler organic molecules into more complex carbonyl compounds as a critical step in the production of some pharmaceuticals and agrochemicals. Now, ultrafast x-ray absorption near edge spectroscopy studies carried out at the APS have laid bare how organometallic molecules important to chemists the world over recruits the help of a solvent molecule to allow it to quickly expel a "carbon monoxide" group and replace it with another chemical group, revealing useful clues to countless reaction mechanisms in organometallic chemistry and enzyme processes as well as the underlying cause of carbon monoxide poisoning.

Fickle carbonyl-metal bonds are even present in biological systems; for instance, hydrogenase enzymes contain carbonyl bound to iron. The ease with which carbon monoxide attaches to iron is what makes the gas so toxic because it can displace oxygen from the iron center in the hemoglobin molecule in the blood.

The carbonyl-metal bonds have been endlessly studied in solution and in the gas phase with various analytical techniques, revealing much information about the reactions they can undergo. What was missing was a clear perspective on the actual substitution process on the picosecond timescale at which the carbonyls are removed and the substitute ligand added.

Researchers from Brown University, Providence College, and Argonne used a newly developed experimental apparatus at XSD beamline 7-ID-B,C,D of the APS to carry out ultrafast x-ray absorption near edge spectroscopy on an excited form of iron pentacarbonyl in ethanol solvent. The new technology allowed them to observe changes in the molecular structure that occur in just a few picoseconds.

In theory, the pentacarbonyl iron molecule forms a stable trigonal bipyramidal structure. The iron atom is at the heart of this structure, with each carbonyl sitting at an apex. In earlier research, these researchers had shown that in aromatic or alcoholic solvents, a large proportion of these bipyramids are each distorted by the presence of a single solvent molecule latching onto the structure, the effect being to change the symmetry from D_{3h}, a dihedral symmetry, to the C_{2v}, approximately a pyramid with a four-cornered base.

Exactly how solvent distorts the symmetry depends on which solvent is being used, and the effect of this distortion can be critical to the subsequent behavior of the metal carbonyl compound. This finding also hints at how ligand substitution in a solvent might occur without the carbonyl ligand first being lost, and then the substitute ligand diffusing toward this semi-clad entity and filling the gap. Indeed, if the substitution process can occur on the picosecond timescale, then it would seem that the solvent may play a more critical role and act as a mediator so that the carbonyl can be lost from the structure simultaneously with the acceptance of the new ligand, without breaking any bonding rules. In other words, a concerted substitution reaction occurs.

The team's new instrument at 7-ID uses an x-ray streak camera detector to observe the ligand substitution taking place in pentacarbonyl iron dissolved in ethanol and excited by short bursts of laser light (Fig. 1). Their measurements indicate that the loss of the carbonyl group takes less than a picosecond to occur, which has been estimated from the instrument resolution-limited rise of the corresponding x-ray absorption signals. The resolution of the data is limited only by the response time of the camera, rather than the relatively long flux time of the synchrotron x-rays. The researchers suggest that the same setup could be used more generally on other beamlines. *— David Bradley*

See: Brian Ahr[1], Matthieu Chollet[2], Bernhard Adams[2], Elizabeth M. Lunny[3], Christopher M. Laperle[3], and Christoph Rose-Petruck[1]*, "Picosecond X-ray absorption measurements of the ligand substitution dynamics of $Fe(CO)_5$ in ethanol," Phys. Chem. Chem. Phys. **13,** 5590 (2011). DOI:10.1039/c0cp01856b

Author affiliations: [1]Brown University, [2]Argonne National Laboratory, [3]Providence College
*Correspondence:**crosepet@brown.edu

C.R.-P. acknowledges support from the U.S. Department of Energy (DOE) under Grant No. DE-FG02-08ER15937. E.M.L. acknowledges support from the National Science Foundation under EPSCoR grant #0554548. Use of the Advanced Photon Source was supported by the DOE Office of Science under Contract No. DE-AC02-06CH11357.

7-ID-B,C,D • XSD • Materials science, atomic physics, chemistry • Time-resolved x-ray scattering, time-resolved x-ray absorption fine structure, phase contrast imaging • 6-21 keV • On-site • Accepting general users •

A FLICK OF THE SWITCH: MOLECULAR MAGNETS UNDER PRESSURE

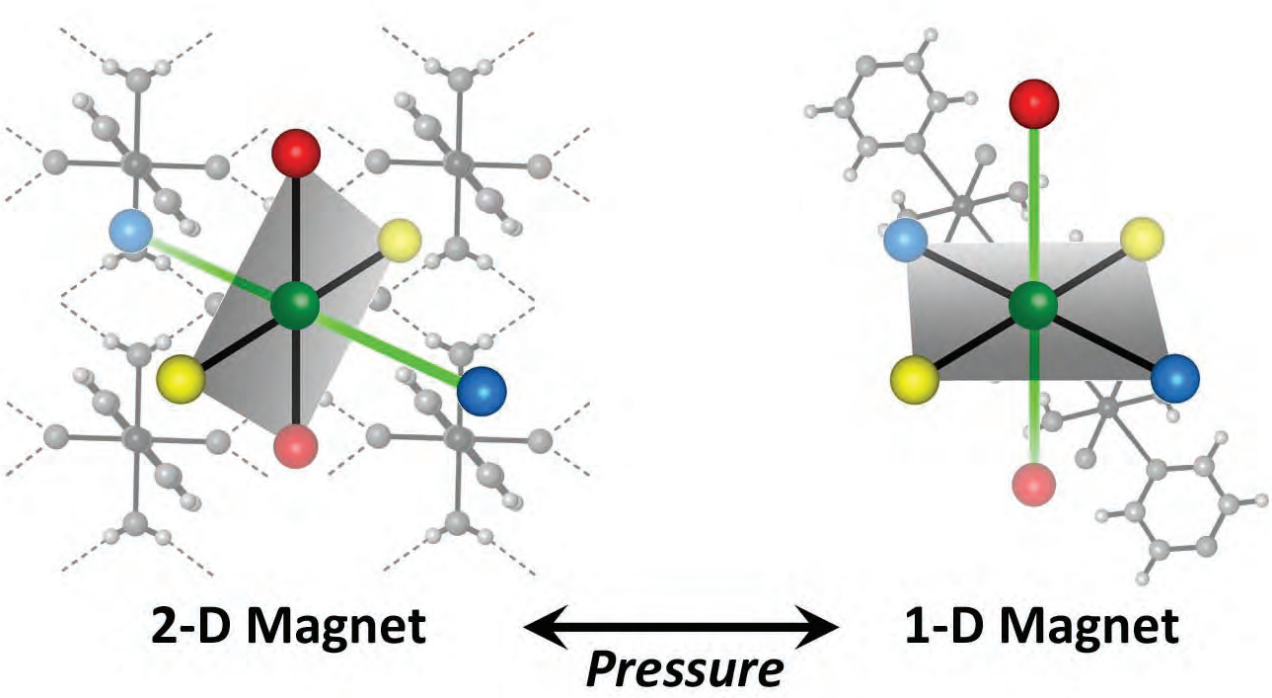

Fig. 1. Pressure-induced magnetic switching effect. The colored images represent the direction of the magnetic orbitals (gray plane) with dark green balls for the copper (Cu) centers, blue balls for nitrogen (N), red balls for oxygen (O) in water (H_2O), yellow for fluoride (F); and the bright green lines for the elongated JT-axis.

1-BM-B,C • XSD • Chemistry, materials science, physics • Powder diffraction, high-pressure diamond anvil cell • 8-22 keV • On-site • Accepting general users •

Molecular materials represent the forefront of modern materials discovery efforts, where their modular structures, comprised of molecular building blocks, can be rationally designed to include useful properties such as magnetism or porosity. However, it has been difficult in the past to predict the behavior of these materials when pressure is applied. Due to such difficulties, scientists from Argonne and Eastern Washington University have focused their efforts on optimizing high-pressure experimentation at XSD beamline 1-BM-B,C at the APS for this broad family of modern materials. In doing so, they observed that high pressures predictably induce a switching effect in a molecular magnet based on Jahn-Teller effect active metal centers (those that undergo geometrical distortions to remove electronic degeneracy and lower the overall energy of the material). This discovery of large pressure-induced changes represents a major advance in our knowledge of molecular-based magnetic materials and could yield many important technological applications, such as using magnetic switches for data storage, as well as in the displays of next-generation advanced magnetoelectronic devices such as laptops, mobile devices, and many other consumer products.

In the past, the scientific community has overlooked the study of molecular materials under applied pressures. Such studies are important because these materials move toward real-world applications that may require materials to be subjected to significantly high applied pressures, such as pelletization. Indeed, molecular materials are expected to be much softer than traditional solid-state materials, and as such, it is critical to develop a thorough understanding of the potential structural and functional perturbations that pressure may induce.

Following on from their pioneering work investigating the high-pressure behavior of porous molecular materials, the researchers in this study turned their attention to materials with interesting magnetic properties. Specifically, they targeted materials based on Jahn-Teller effect active metal centers because their magnetic orbitals are arranged relative to an elongated Jahn-Teller axis (which allows their magnetic properties to be modified through pressure-induced structural perturbations).

For this experiment the scientists used magnetic materials made of pyrazine- (pyz-) bridged linear chains of copper (Cu) ions, fluoride (F), and water (H_2O) - $CuF_2(H_2O)_2(pyz)$. Under ambient conditions, the chains align along the direction of the Jahn-Teller effect axis, with elongated nitrogen-copper-nitrogen (N-Cu-N) bonds. The magnetic orbital is directed along the Cu-L bonds (where L stands for a particular ligand of differing field strength) of the $CuO2F_2$ plane. The chains are linked perpendicularly with strong two-dimensional hydrogen bonds (OH-F).

Each copper ion, which contains an unpaired electron, is positioned at one of the corners of a molecular cube. Their magnetic spins are disordered at normal temperatures but begin to align in opposite directions when temperatures are dropped, bringing about the state of antiferromagnetism. The scientists used high-pressure equipment and highly focused x-ray beams from the 1-BM-B,C beamline. The devices allowed the scientists to observe a series of structural transitions as pressure is increasingly exerted onto the material. These rearrangements abruptly reorient the magnetic spins of the material (thus re-stabilizing itself at one of the possible Jahn-Teller orientations), and, in the process, creating a reversible magnetic switch effect.

The team discovered that as increasing pressure is exerted on the materials, a sudden reorientation of their spins occurs. These structural transitions occur at 0.9 GPa (the first transition) and at 3.1 GPa (the second transition). This corresponds to a reorientation of the Jahn-Teller-elongated axis from the original N-Cu-N bond to the O-Cu-O bond (after the first transition), and to the F-Cu-F bond (after the second transition). The magnetic orbital reorients, correspondingly, from the CuF_2O_2, to the CuF_2N_2, and then to the CuN_2O_2. This action creates a reversible magnetic switch effect because the Jahn-Teller active metal centers are coordinated with different ligands (Fig. 1). The switching occurs when pressure is released, causing the magnetic orbital to make a reversible and predictable switch from two-dimensional to one-dimensional coupling.

Their results expand scientific knowledge about the way molecular-based materials function. Specifically, it provides scientists with a much better theoretical understanding of how to induce changes in such materials at relatively low pressures, at least when compared to traditional solid-state materials such as metal oxides. Consequently, this study is a key step in learning the diverse potential of molecular materials and applying this knowledge for a large number of applications. *— William Arthur Atkins*

See: Gregory J. Halder[1]*, Karena W. Chapman[1], John A. Schlueter[2], and Jamie L. Manson[2], "Pressure-Induced Sequential Orbital Reorientation in a Magnetic Framework Material," Angew. Chem. Int. Ed. **50**, 419 (2011). DOI:10.1002/anie.201003380
Author affiliations: [1]Argonne National Laboratory, [2]Eastern Washington University
Correspondence: *halder@aps.anl.gov

Work performed at Argonne and use of the Advanced Photon Source were supported by the U.S. Department of Energy (DOE) Office of Science under Contract No. DE-AC02-06CH11357. Part of the pressure cell preparation used the GSECARS facility Sector 13, APS. GSECARS is supported by the National Science Foundation-Earth Sciences (EAR-0622171) and DOE-Geosciences (DE-FG02-94ER14466).

RINGING THE HEMOGLOBIN BELL

Knowing the structure of a molecule is an important part of understanding it, but quite often it's even more important to know how the molecule moves — the vibrational dynamics that drive and control its interactions with other molecules in chemical reactions. That's particularly true of proteins, the enormously complex molecular structures found at the heart of important life processes such as cell signaling, ion transport, and other functions. But most of the available techniques for studying the vibrational properties of a protein run into some vexing limitations, especially when probing the lower frequencies at which the proteins actually do their job. A team of researchers has found a way around that problem by using the APS to investigate the iron-based heme molecules at the reactive core of a multitude of proteins, such as hemoglobin. Their work provides new information about the vibrational dynamics of hemes. >>>

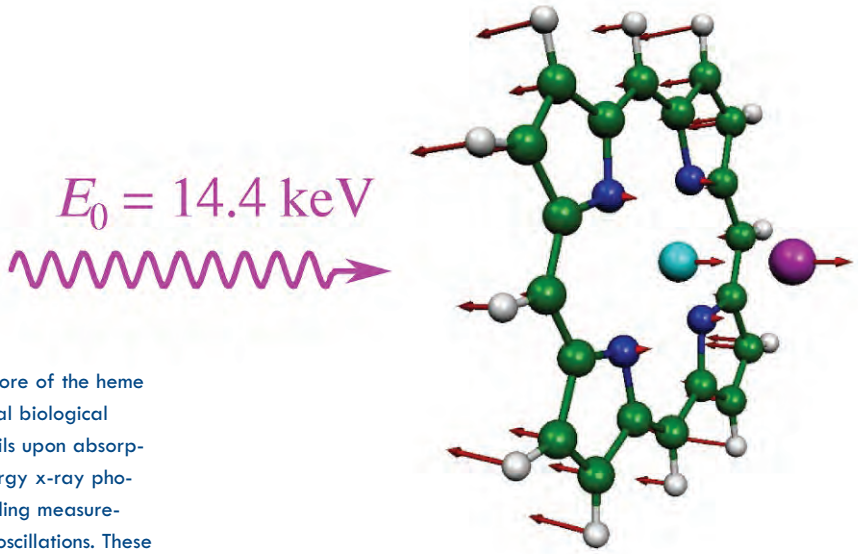

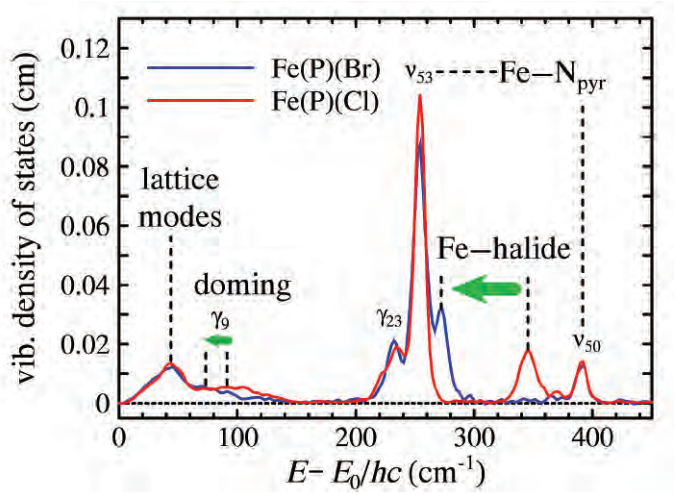

Fig. 1. Top: Iron is the reactive core of the heme molecule responsible for essential biological processes. The ^{57}Fe nucleus recoils upon absorption of precisely tuned high-energy x-ray photons available at the APS, enabling measurement of the resulting molecular oscillations. These include the heme "doming" motion shown here, which controls the reaction of oxygen with heme-containing proteins, such as hemoglobin. Below: Measured (NRVS) and predicted (DFT) iron VDOS are compared for sextet and quartet states of Fe(P)(Br) and Fe(P)(Cl).

The experimenters from Northeastern University and Argonne employed a new technique called nuclear resonance vibrational spectroscopy (NRVS) at the XSD 3-ID-B,C,D beamline at the APS. One way to use vibrational motions — particularly at high frequencies — is as a structural probe, looking at vibrations of individual bonds, which tells how strong that bond is. The research team had conducted previous work in the far infrared portion of the spectrum using another synchrotron x-ray facility, but found those efforts came up short in part because biological molecules always have to be put in water, and there's a lot of competing signal from the water.

At the APS, the researchers could use NRVS to try another strategy. What originally brought them to the APS was extending their investigations to lower frequencies where vibrational motions not only are probes but actually participate in and drive the reactions that these molecules are involved in. The NRVS technique allows the ultimate in probe selectivity while avoiding vibrational interference from other sources. One can zoom in on the iron, specifically looking at one atom out of thousands of surrounding atoms, surgically targeting those vibrations.

The team examined the spectrum of ^{57}Fe vibrations in several different halide complexes of iron porphyrin molecules that mimic the heme group found in hemoglobin. In particular, they focused on a doming vibration of the heme complex that is believed to play a vital role in controlling reactions in hemoglobin such as oxygen binding.

With just the static structures, they could only speculate. What they really wanted was to arrive at something quantitative on how easy it is to excite and what the modes actually look like. X-ray photons carry a great deal of momentum and one can tune them to target specifically toward iron. In effect, the x-ray photons "ring the bell" of the molecular structure and set it into oscillation, while allowing the vibrational spectra to be identified and studied.

Using the iron porphine molecule Fe(P) as a basis for vibrational density-of-states measurement, the team used density functional theory calculations to obtain the spectra of increasingly complex heme molecules (Fig. 1).

The most common biological version of the molecule protoporphyrin IX, the actual form found in hemoglobin, is less symmetric because of these side chains sticking off the edge, so the spectra look much more complicated. The researchers spent a great deal of time so that they could really understand precisely what the vibrations were, and then they developed some mathematical analysis to find those vibrations in the more complicated molecule.

The research team plans to both continue the present work and to expand the experimental technique to other proteins. Most of their work involved these heme groups, and has yielded a detailed understanding of how to interpret the heme molecules. The next step is to extend that to look at more complicated proteins, beginning to branch out to proteins with multiple metal sites that bind iron directly to amino acid side chains without involving heme. The low frequencies available at the APS are what is really giving the researchers a unique window. *— Mark Wolverton*

Note: Beamline 3-ID, where the experiments were conducted, has pioneered the applications of nuclear resonance techniques.Current plans include improving the energy resolution further such that collective motions of groups of atoms in the molecule can also be reliably characterized.

See: Alexander Barabanschikov[1], Alexander Demidov[1], Minoru Kubo[1], Paul M. Champion[1], J. Timothy Sage[1]*, Jiyong Zhao[2], Wolfgang Sturhahn[2], and E. Ercan Alp[2], "Spectroscopic identification of reactive porphyrin motions," J. Chem. Phys. **135**, 015101 (7 July 2011). DOI:10.1063/1.3598473
Author affiliations: [1]Northeastern University, [2]Argonne National Laboratory
Correspondence: *jtsage@neu.edu

Financial support for this work came from the National Science Foundation (CHE-1026369 and MCB-0744738) and the National Institutes of Health (DK35090). Use of the Advanced Photon Source at Argonne National Laboratory was supported by the DOE Office of Science under Contract No. DE-AC02-06CH11357.

This work was featured on the cover of J. Chem. Phys. **135** (2011). ©2011 American Institute of Physics.

3-ID-B,C,D • XSD • Physics • High-pressure diamond anvil cell, inelastic x-ray scattering, nuclear resonant scattering • 7-27 keV, 14.41-14.42 keV • On-site • Accepting general users

Jun Qian (left) and Lahsen Assoufid (both XSD-OPT) at the new APS slope measuring profiler, which is located in the XSD Metrology Lab in the APS experiment hall. Optical metrology is essential for both x-ray optics quality control and for advancing x-ray optics. Development of advanced metrology instruments and techniques remains a continuing effort at the APS. The new slope measuring profiler can measure beamline mirrors with less than 100-nrad rms slope error. The data acquisition is based on the Argonne-developed Experimental Physics and Industrial Control System and was evolved in collaboration with the AES Beamline Controls Group. Preliminary testing began in mid-December 2011. A repeatability of 60-nrad rms was obtained on a 350-mm flat mirror with a slope error of about 0.200 $\approx$rad, thus meeting the goal of 100-nrad rms of the first phase of the project. The new system began routine operation in March 2012.

Correspondence: Lahsen Assoufid, assoufid@aps.anl.gov

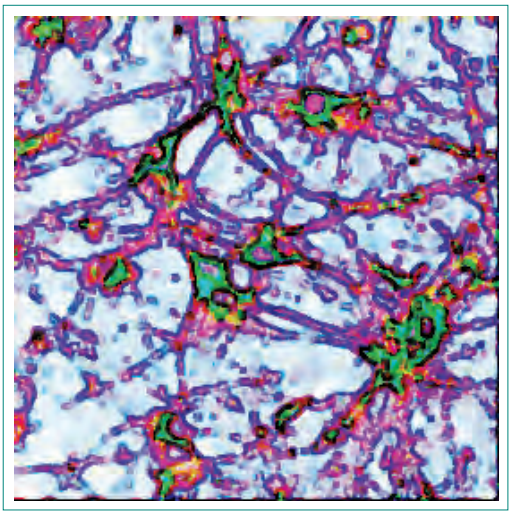

Life Science

BRAIN IRON AS AN EARLY PREDICTOR OF ALZHEIMER'S DISEASE

Early and correct diagnosis of Alzheimer's disease (AD) is important for reasons that go beyond treatment. These include more time to make critical life decisions, planning for future care, and maximizing the safety of the person with Alzheimer's disease and their family. New scientific information relevant to this pernicious disease has been obtained by researchers utilizing the APS and the National Synchrotron Light Source (NSLS) at Brookhaven National Laboratory. This work points to the use of elevated brain iron content, already observed in late-stage AD, as a potential tool for early diagnosis. Since the disease is usually diagnosed only in later stages after cognitive symptoms appear and treatment may not be effective, a method for early detection would be a major breakthrough in fighting this debilitating neurological illness. >>>

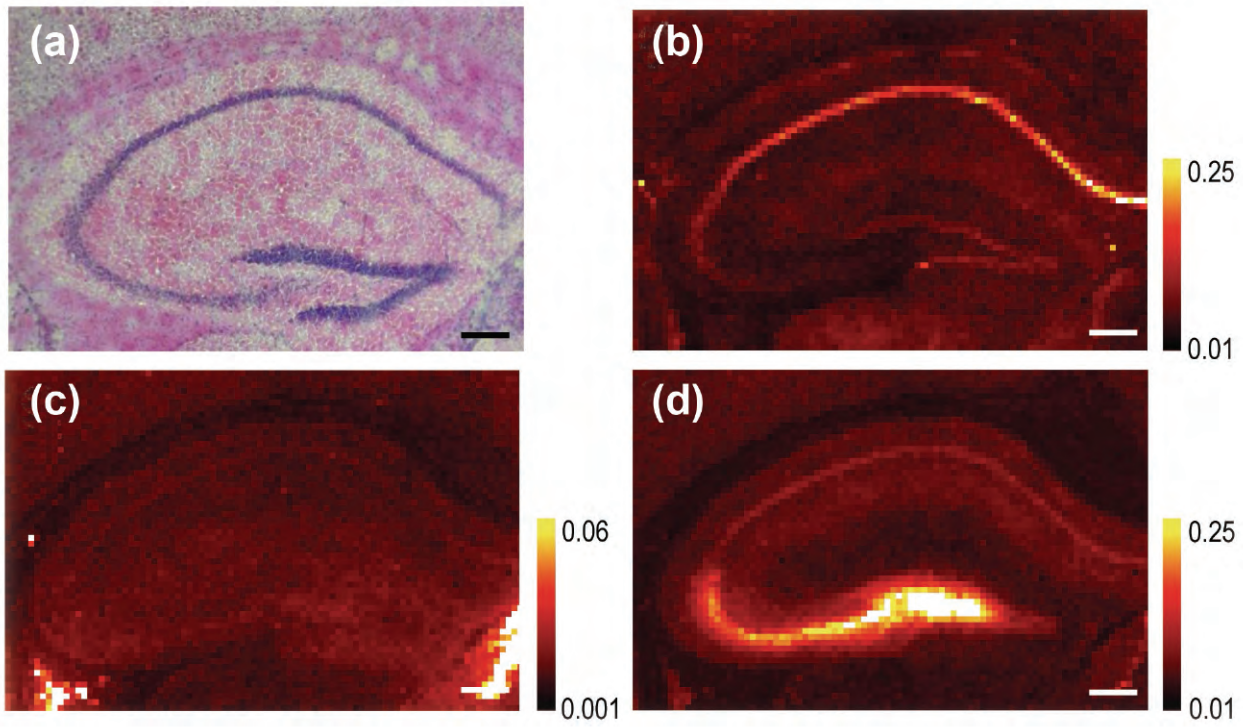

Fig. 1. (a) Light micrograph of a stained hippocampal brain section from a mouse. XFM images: iron (b), copper (c), and zinc (d) in the same tissue section. Units are mM. Scale bar = 300 μm.

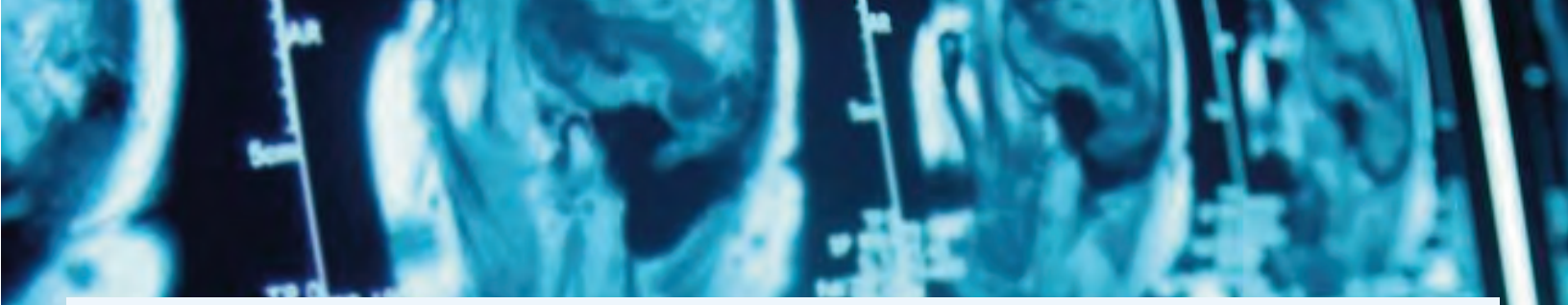

It has been long known that the formation of amyloid plaques in brain tissue is associated with AD. Plaques may form for years before the patient actually suffers neurological symptoms. So, much recent research has focused on finding a way to detect the disease in its very early stages when treatment would be most effective.

One line of research has centered on the observation that the brains of patients in late stages of the disease showed elevated levels of metal ions such as iron, copper, and zinc. Measuring metal concentrations in cerebrospinal fluid or using magnetic resonance imaging would be an attractive technique for early diagnosis because it is non-invasive. Until recently, however, not much was known about how metal ions were distributed in plaque and non-plaque tissues during various stages of the disease.

Now, thanks to the efforts of the researchers from Stony Brook University, Brookhaven, the University of Chicago, the Illinois Institute of Technology, and Argonne, new light has been shed on the relationship between metal content, plaque formation, and Alzheimer's disease.

The scientists used a model system of amyloid plaque formation in mice to investigate how iron was distributed in the brain cortex and hippocampus over time. The cortex is the center of higher brain functions such as thought and reasoning, while the hippocampus is important for long-term memory storage. Malfunction of both of these brain regions is associated with AD, though the hippocampus appears to be the first and most drastically affected.

The x-ray fluorescence microscopy (XFM) technique employed at the APS and the NSLS allowed the researchers to determine how iron content changes as the diseased brain ages. Their results show that iron content is significantly higher in the cortex early in the disease and that it corresponds with the onset of plaque formation; interestingly, the iron was not found within the plaques.

Given these findings, it is clear that quantifying brain iron content could be a powerful early indicator of AD and has great potential as a diagnostic tool.

Eight years ago, these researchers used XFM to analyze the plaques of end-stage human Alzheimer's disease and found the plaques to be loaded with iron, copper, and zinc. They wanted to know whether metal ions were involved in plaque formation and/or brain cell toxicity. To do this, they needed the mouse model to study metal accumulation in AD plaques over the course of the disease. Interestingly, they found that the mouse plaques never accumulated metal, except for a small amount of zinc in the late stages. These mice also exhibited very little brain cell death. This was in stark contrast to humans, where the plaques take up a lot of metal and brain cell death is significant.

Having the right tools and techniques was critical to moving the work forward. Access to synchrotron light sources such as the APS and NSLS, where XFM could be employed, was instrumental in this work because there is really no other way besides XFM to simultaneously image all of the physiological metals (calcium, iron, copper, and zinc) in the brain. The team was able to use the NSLS to study the plaques, but needed the high brightness and small beams at the Bio-CAT 18-ID-D beamline at the APS to efficiently image the large cortex and hippocampus regions.

The team's work leads them to question whether metals in the plaques are a sign of metal ion imbalance in Alzheimer's disease, causing brain cell toxicity. Perhaps the "metallated" plaques are even toxic themselves. Understanding this mechanism is our direction for the future. *— Mona Mort*

See: Andreana C. Leskovjan[1,2], Ariane Kretlow[2‡], Antonio Lanzirotti[3], Raul Barrea[4], Stefan Vogt[5], and Lisa M. Miller[1,2*], "Increased brain iron coincides with early plaque formation in a mouse model of Alzheimer's disease," NeuroImage **55**(1), 32 (1 March 2011). DOI:10.1016/j.neuroimage.2010.11.073
Author affiliations: [1]Stony Brook University, [2]Brookhaven National Laboratory, [3]The University of Chicago, [4]Illinois Institute of Technology, [5]Argonne National Laboratory. ‡Present address: BfR-Federal Institute for Risk Assessment
Correspondence: *lmiller@bnl.gov

This work was funded by National Institutes of Health Grant R01-GM66873. Bio-CAT is a National Institutes of Health-supported Research Center RR-08630. Use of the Advanced Photon Source at Argonne National Laboratory was supported by the U.S. Department of Energy Office of Science under Contract No. DE-AC02-06CH11357.

18-ID-D • Bio-CAT • Life sciences • Fiber diffraction, microdiffraction, microfluorescence (hard x-ray), small-angle x-ray scattering, time-resolved x-ray scattering, micro x-ray absorption fine structure • 3.5-35 keV • On-site • Accepting general users •

TRACKING COPPER IN THE BRAIN

While it might at first seem counterintuitive, metals, which we commonly think of as non-biological materials, are actually prevalent and important ingredients for cells. For instance, cells often utilize the movement of metals for signaling processes, as in the well-studied cases of alkali and alkaline Earth metals like potassium, sodium, and calcium. But a similar role had not been established for vital transition metals like copper and iron, which have been studied for their non-dynamic functions in relation to certain enzymes. Now a research team that carried out experimentation at the XSD 2-ID-E beamline at the APS reports new methods for watching the movement of these transition elements, as well as interesting information about the way copper, specifically, moves around. Their results indicate that the way copper is stored and organized within cells has an important connection to the functioning of neurons in the brain. This work also reveals a causal connection between copper and established intracellular signal transduction pathways. Taken together, these new findings point to a better understanding of intracellular copper as being of great use in studies of the brain.

Copper is of particular interest since the brain needs much higher levels of copper than other parts of the body. Also, abnormal copper stores are connected to a variety of neurodegenerative ailments, including Alzheimer's disease. To study — and visually observe — copper atoms, the team of researchers, who represent the University of California, Berkeley; the Howard Hughes Medical Institute; and Argonne developed a bright, fluorescent sensor called Coppersensor-3 (CS3). Tests on CS3 revealed a high selectivity for copper ions, even in the presence of competing metals. It also provides a robust fluorescence enhancement, enabling the observation of copper in live mammalian cells under a fluorescent microscope.

The team used CS3 with live hippocampal cultured neurons. They observed unadulterated cells and cells treated with potassium chloride to "activate" them by inducing depolarization. In the activated cells, pools of copper began to move around.

In order to confirm this unexpected movement, the researchers employed a second technique, x-ray fluorescence microscopy (XRFM), at the 2-ID-E beamline, which boasts a spatial resolution of 200 nm, fine enough to examine elemental distribution inside a single cell. X-ray fluorescence microscopy must be used on static, fixed cells, so the team examined a series of samples of the hippocampal neurons, each sample a static snapshot of the copper movement process previously observed. This technique monitored 15 elements simultaneously, and it also showed large movement of the copper.

The two sets of observations (Fig. 1) reveal copper movement in conjunction with information transfer from one cell to the other – characteristic of cells undergoing some kind of learning or memory task. Not only did the copper move, but cellular uptake and release was quite rapid. The copper also seemed to move in conjunction with calcium release, an element previously known to redistribute throughout cells for signaling purposes. Studying this relationship could open the door to new information about potential cross talk or co-dependence of these elements.

Adding such copper movement to the fact of the brain's high copper demand and growing connections between copper and neurodegenerative diseases suggest that understanding copper will be of particular importance to understanding the brain.

— Karen Fox

See: Sheel C. Dodani[1], Dylan W. Domaille[1], Christine I. Nam[1], Evan W. Miller[1], Lydia A. Finney[2], Stefan Vogt[2], and Christopher J. Chang[1], "Calcium-dependent copper redistributions in neuronal cells revealed by a fluorescent copper sensor and X-ray fluorescence microscopy," Proc. Nat. Acad. Sci. **108**(15), 5980 (April 12, 2011). DOI:10.1073/pnas.1009932108

Author affiliations: [1]University of California, Berkeley, [2]Argonne National Laboratory

Correspondence:

*chrischang@berkeley.edu

The first three authors contributed equally to this work, which was supported by the Packard and Sloan Foundations; the University of California, Berkeley Hellman Faculty Fund; Amgen; Astra Zeneca; Novartis; and the National Institutes of Health (GM 79465). C.J.C. is an Investigator with the Howard Hughes Medical Institute. D.W.D. and E.W.M. were partially supported by a Chemical Biology Training Grant from the National Institutes of Health (T32 GM066698) and E.W.M. acknowledges a Stauffer graduate fellowship. Use of the Advanced Photon Source was supported by the U.S. Department of Energy Office of Science under Contract No. DE-AC02-06CH11357.

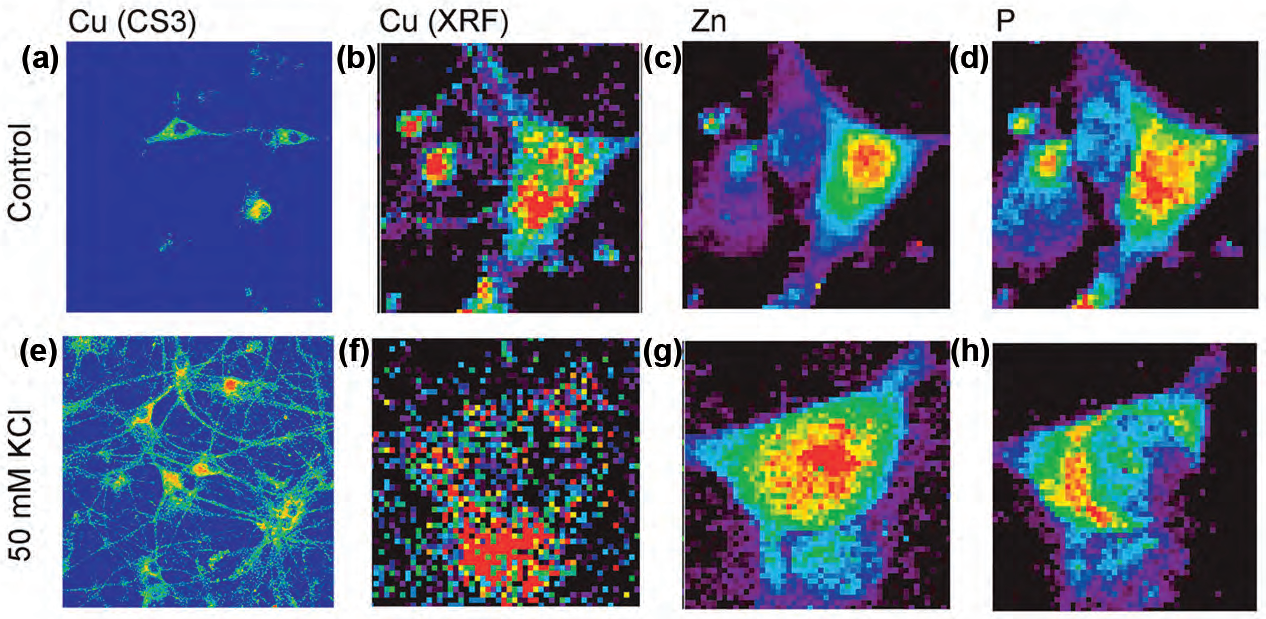

Fig. 1. Molecular imaging of Cu distributions in resting and depolarized rat hippocampal neurons with CS3 and XRFM. (a) Live primary rat hippocampal neurons treated with extracellular solution (ECS) buffer for 2 min and then stained with 2-μM CS3 for 10 min. (b–d) Rat hippocampal neurons treated with ECS buffer for 2 min, fixed with 4% PFA and imaged by XRFM. Images shown are for (b) Cu, (c) Zn, and (d) P channels. (e) Live primary rat hippocampal neurons treated with 50-mM KCl in ECS buffer for 2 min and then stained with 2 μM CS3 for 10 min. (F–H) Rat hippocampal neurons treated with 50-mM KCl in ECS buffer for 2 min and then fixed with 4% PFA and imaged by XRFM. Images shown are for (f) Cu, (g) Zn, and (h) P channels. From Sheel C. Dodani et al., Proc. Nat. Acad. Sci. **108**, 5980 (2011).

2-ID-E • XSD • Life sciences, environmental science, materials science • Microfluorescence (hard x-ray) • 7-10.5 keV, 11-17 keV • On-site • Accepting general users •

How Plutonium Hijacks the Body's

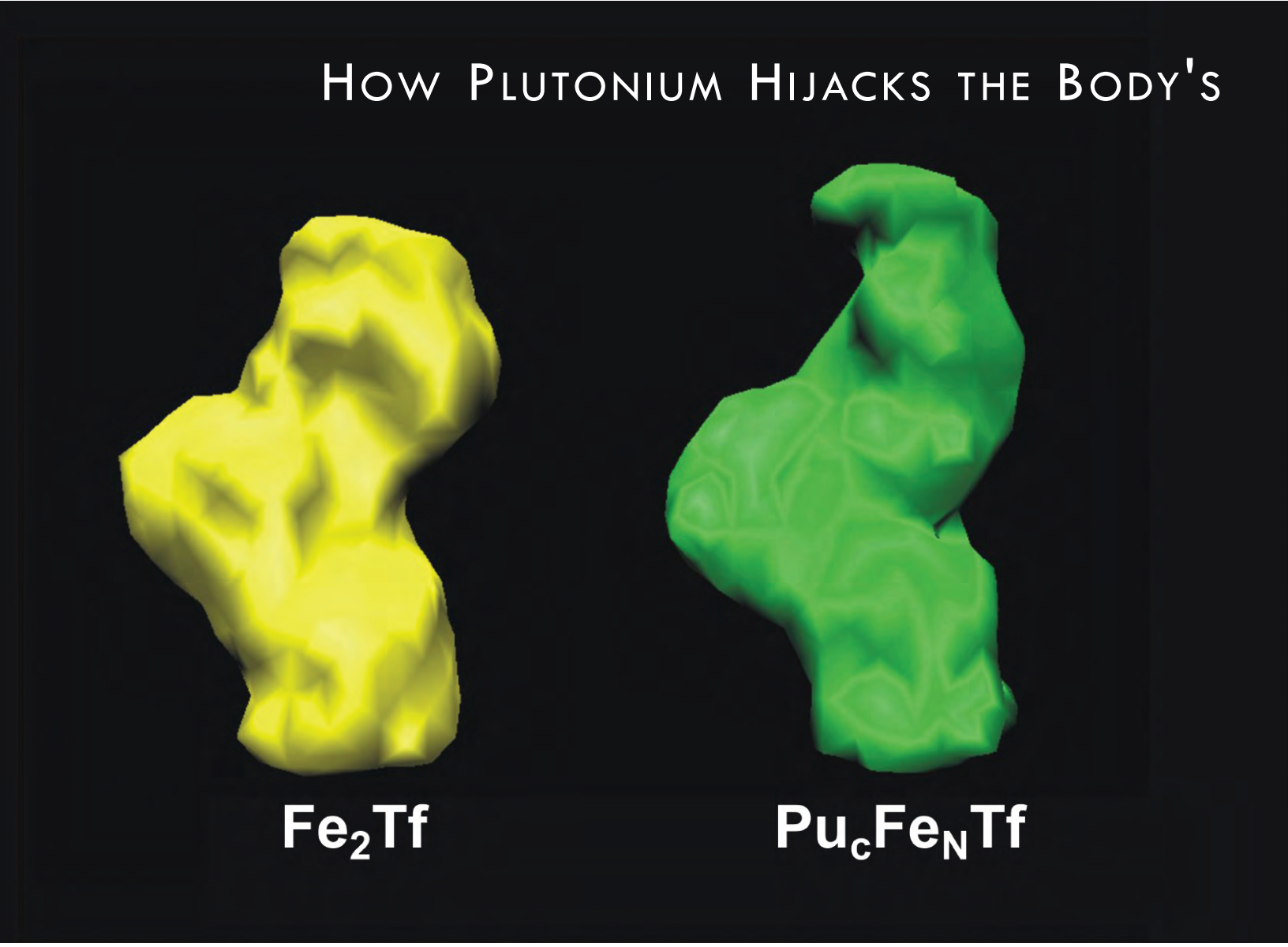

The radioactive element plutonium has no known natural biological function and is highly toxic. In spite of these obvious drawbacks, the human body retains it in tissue when ingested. Researchers utilized beamline XSD 12-ID-B to assist with small-angle x-ray scattering (SAXS, Fig. 1), as well as receptor binding assays and synchrotron x-ray fluorescence microscopy (XSD beamline 2-ID-D) to investigate how plutonium is accumulated in the body. Their research could pave the way to a clearer understanding of how treatments might be developed to allow the body to clear this lethal heavy metal.

The researchers from Argonne. The University of Chicago, and Northwestern University demonstrated that rat adrenal gland cells (PC12 cells) accumulate plutonium that has hijacked a biochemical pathway usually used by the body for transporting the essential element iron. Upon ingestion, plutonium ions can hide in the iron transport protein serum transferrin. An important clue about how this occurs was also revealed, in that there are two forms of the plutonium-transferrin complex, but only one of these is active.

The low-resolution model based on the small-angle scattering data reveals that only when plutonium binds to the so-called C-terminal lobe of the transferrin protein at the same time that iron is bound to the N-terminal lobe does the protein adopt a three-dimensional structure that enables plutonium uptake into cells. However, if iron is not present in the N-lobe or plutonium binds to the N-lobe, the protein has the wrong shape and is essentially deactivated.

Plutonium can enter the body following accidental release from a nuclear facility, environmental contamination, or nuclear or radiological attack. The radioactive metal localizes in the liver and bones and can remain there for decades. The conundrum facing biochemists hoping to understand the interaction of plutonium with proteins and cells is that this metal bears little resemblance to the natural metals present in our bodies in trace quantities that are essential for life.

Plutonium is, for instance, a potent reducing and oxidizing metal depending on its oxidation state, unlike many biological metals. It has four oxidation states — III, IV, V, and VI — that are putatively relevant to biology, although most researchers suspect that pluto-

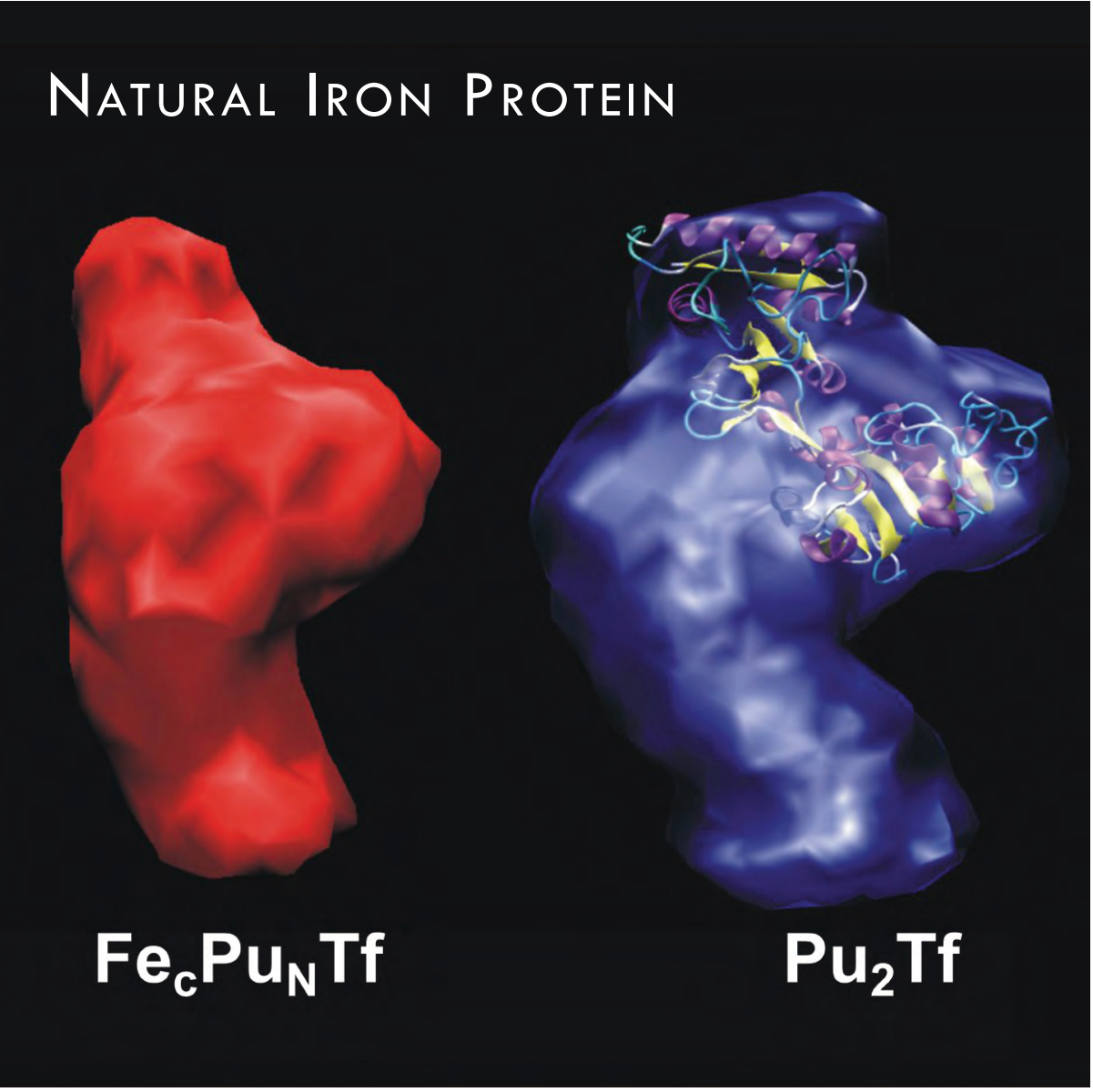

Fig. 1. Structural models of bovine serum transferrins derived from SAXS data show that Pu_CFe_NTf adopts a closed conformation.

nium(IV) is the most significant. But there are a few characteristics shared by plutonium and the essential transition metal iron. This means that plutonium can, under certain conditions, hijack iron's place in some proteins such as ferritin and transferrin. This might underpin its ability to be uploaded into cells and remain there undisturbed, silently causing damage to biological molecules and tissues through the emission of radiation.

The team points out that in healthy individuals, transferrin is usually not fully loaded with iron, as there are balances to maintain in the transport system. This leaves open the possibility of plutonium exposure quickly filling the vacant spaces. If the transferrin is partially loaded with iron in the N-lobe, then the conditions conspire to allow transportation of plutonium into one's cells. It might thus be possible to disrupt this biochemical pathway with drugs taken before or as soon as possible after exposure to plutonium. The drugs could be targeted to the transferrin protein and inhibit the processes that allow it to bind to the cell membranes or release its metallic payload. A second compound or group of compounds could then be used to mop up, or chelate, the plutonium ions as they float free in the body and allow them to be excreted before they do too much harm. *— David Bradley*

See: Mark P. Jensen[1]*, Drew Gorman-Lewis[1‡], Baikuntha Aryal[1,2], Tatjana Paunesku[3], Stefan Vogt[1], Paul G. Rickert[1], Soenke Seifert[1], Barry Lai[1], Gayle E. Woloschak[3], and L. Soderholm[1], "An iron-dependent and transferrin-mediated cellular uptake pathway for plutonium" Nat. Chem. Biol. **7**, 560 (August 2011).

DOI:10.1038/nchembio.594
Author affiliations: [1]Argonne National Laboratory, [2]The University of Chicago, [3]Northwestern University
‡Present address: University of Washington
Correspondence: *mjensen@anl.gov

The work at Argonne National Laboratory, including the use of the Advanced Photon Source, was supported by the U.S. Department of Energy Office of Science under contract no. DE-AC02-06CH11357.

2-ID-D • XSD • Life sciences, materials science, environmental science • Microfluorescence (hard x-ray), microdiffraction, small x-ray absorbtion fine structure • 5-30 keV • On-site • Accepting general users

12-ID-B • XSD • Chemistry, materials science, life sciences, geoscience, polymer science • Small-angle x-ray scattering, grazing incidence small-angle scattering, wide-angle x-ray scattering • 7.9-14 keV • On-site • Accepting general users •

AN UNDERSTANDING OF ELASTIN'S PROPERTIES SPRINGS FORTH

It's not stretching the truth to say that flexibility is an important and desirable human physiological trait. We owe our flexibility to a protein called elastin, which derives its properties from a building-block molecule called tropoelastin. Tropoelastin behaves as an ideal elastomer because it loses no energy between stretch and relaxation. Understanding the structure and function of tropoelastin is already helping to pave the way for the development of synthetical materials that can reproduce nature's elastic properties. Researchers using the APS have identified how tropoelastin molecules form a "head-to-tail" assembly, which helps explain how these molecules work together to confer elastic properties in tissues throughout the body.

Elastin is the natural elastic material in our bodies that allows us to stretch and flex skin, expand and contract our lungs, and respond to surges of blood pressure. Elastin is made by connecting lots of tropoelastin molecules, so if we study tropoelastin, we learn about the assembly of the body's elastic tissue.

Over the course of a lifetime, the human heart beats about 2 billion times, and the lungs expand and contract with every breath. Elastin makes this possible and as the name suggests, allows tissues to expand and contract throughout the body.

The tropoelastin building blocks that form elastin are laid down mainly in utero and during early childhood. While elastin is a highly ordered molecule, the actual tropoelastin subunits are somewhat disordered, a characteristic that helps allow elasticity within the elastin molecule. Still, the structure of tropoelastin must be ordered enough to be able to provide a functional and usable building block which displays a defined three-dimensional solution shape.

To identify the structure of tropoelastin, the researchers utilized small-angle x-ray scattering, along with neutron scattering, to visualize the shape of tropoelastin in solution. They used several facilities in addition to the APS, including the European Synchrotron Radiation Facility in Grenoble, France; and the ISIS Neutron Source and Diamond Light Source at the Harwell Oxford campus, United Kingdom.

The researchers, from the Wellcome Trust Centre for Cell-Matrix Research, the University of Texas Medical Branch, Cardiff University, the University of Sydney, Diamond Light Source Ltd., ISIS Science and Technology Facilities Council, and the Illinois Institute of Technology constructed regions of tropoelastin that were of different lengths and were able to identify distinct regions of the tropoelastin molecule. Synchrotron measurements of tropoelastin encoded by exons 2–18 were conducted at the Bio-CAT beamline 18-ID-D at the APS. In this way, the researchers determined the structure of tropoelastin, and identified a curved, spring-like molecule with a "foot" region that helps attach the molecule to cells (Fig. 1).

To investigate the spring-like properties of tropoelastin, they also used atomic force microscopy to perform stretching experiments on the individual tropoelastin molecule. These experiments showed that the molecule could extend to eight times its length and then return to its original form without losing its properties, indicating that this molecule is a near perfect spring.

Elastin is lost as we get older, and through damage and disease. Sophisticated elastic and biologically interactive constructs are a reality, and are incredibly useful for tissue repair. Replacing the body's elastic components is now becoming possible thanks to this exciting tissue engineering opportunity with these sophisticated elastic constructs.

The beauty of this tiny, elastic assembly unit is amazing. It is a coiled spring, connected to a specialized interactive appendage. Nature solved the problem of elasticity by making a little protein spring. *— Emma Hitt*

18-ID-D • Bio-CAT • Life Sciences • Fiber diffraction, microdiffraction, microfluorescence (hard x-ray), small-angle x-ray scattering, time-resolved x-ray scattering, micro x-ray absorption fine structure • 3.5-35 keV • On-site • Accepting general users •

See: Clair Baldock[1], Andres F. Oberhauser[2], Liang Ma[2], Donna Lammie[3], Veronique Siegler[3], Suzanne M. Mithieux[4], Yidong Tu[4], John Yuen Ho Chow[4], Farhana Suleman[1], Marc Malfois[5], Sarah Rogers[6], Liang Guo[7], Thomas C. Irving[8], Tim J. Wess[3], and Anthony S. Weiss[1]*, "Shape of tropoelastin, the highly extensible protein that controls human tissue elasticity," Proc. Nat. Acad. Sci. USA **108**(11), 4322 (March 15, 2011). DOI:10.1073/pnas.1014280108

Author affiliations: [1]University of Manchester; [2]University of Texas Medical Branch; [3]Cardiff University; [4]University of Sydney; [5]Diamond Light Source Ltd.; [6]ISIS Science and Technology Facilities Council; [7]Illinois Institute of Technology

Correspondence:

*anthony.weiss@sydney.edu.au

A.S.W. acknowledges funding support from the Australian Research Council, National Health and Medical Research Council, National Heart Research Fund, University of Sydney, and the Australian Institute of Nuclear Science and Engineering. The AFM study was funded by the John Sealy Memorial Endowment Fund for Biomedical Research and in part by National Institutes of Health (NIH) Grant R01DK073394. Bio-CAT is a NIH-supported Research Center RR-08630. Use of the Advanced Photon Source at Argonne National Laboratory was supported by the U.S. Department of Energy Office of Science under Contract No. DE-AC02-06CH11357.

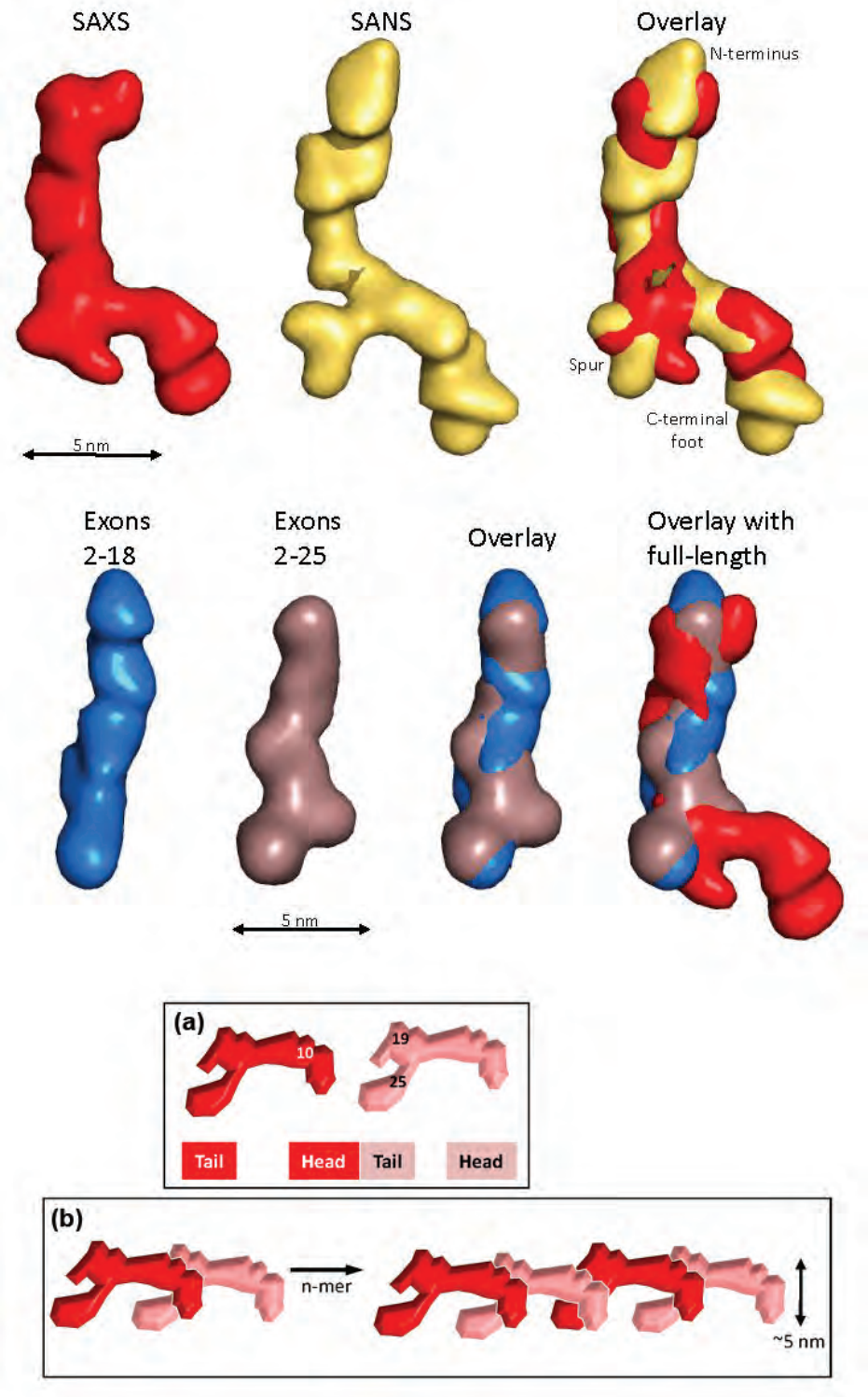

Fig. 1. Top: *Ab initio* shapes of full-length tropoelastin calculated from solution small-angle x-ray scattering (SAXS) or small-angle neutron scattering (SANS) data. The filtered average shapes of 20 SAXS (red) and small-angle neutron scattering (yellow) simulations are shown as a surface representation. An overlay of the models from the two scattering methods is also shown. The proposed locations of the N-terminus, the spur region containing exons 20-24 and the C-terminus are indicated. Scale bar is 5 nm. Middle: SAXS analysis of overlapping fragments of human tropoelastin. *Ab initio* models were calculated from SAXS data for tropoelastin constructs 2-18 (blue), 2-25 (brown) and full-length (red). An overlay of the two N-terminal fragments shows a conserved linear region. Scale bar is 5 nm. Bottom: Head-to-tail model for elastin assembly. (a) Juxtaposed domains 19 and 25 on one tropoelastin molecule and domain 10 on an adjacent monomer would allow the formation of a three-way desmosine cross-link found *in vivo*. (b) Tandem assembly of tropoelastin monomers displaying *n*-mer propagation as an outcome of covalently bonded molecules.

How Dinosaurs Put Proteins into Long-Term Storage

How does one prove that the protein isolated from a 68-million-year-old dinosaur bone is not a contamination from the intervening millenia or from the lab? This is the task of a research team who say they have isolated peptides of the common structural protein, collagen, from bones of *Tyrannosaurus rex* and *Brachylophosauraus canadensis*. In their current work, the researchers used x-ray diffraction data collected at the Bio-CAT 18-ID-D beamline at the APS to generate a model of collagen structure on which to overlay the location of the putative dinosaur peptides. The results provide support for a model in which the dinosaur peptides were protected from degradation due to their location within the collagen fibril. This is important evidence supporting the ancient origin of the peptides and the mechanism by which they were preserved. In addition, this new knowledge of collagen structure could be used in the design of highly stable collagenous scaffolds to promote bone and tissue regeneration in humans. >>>

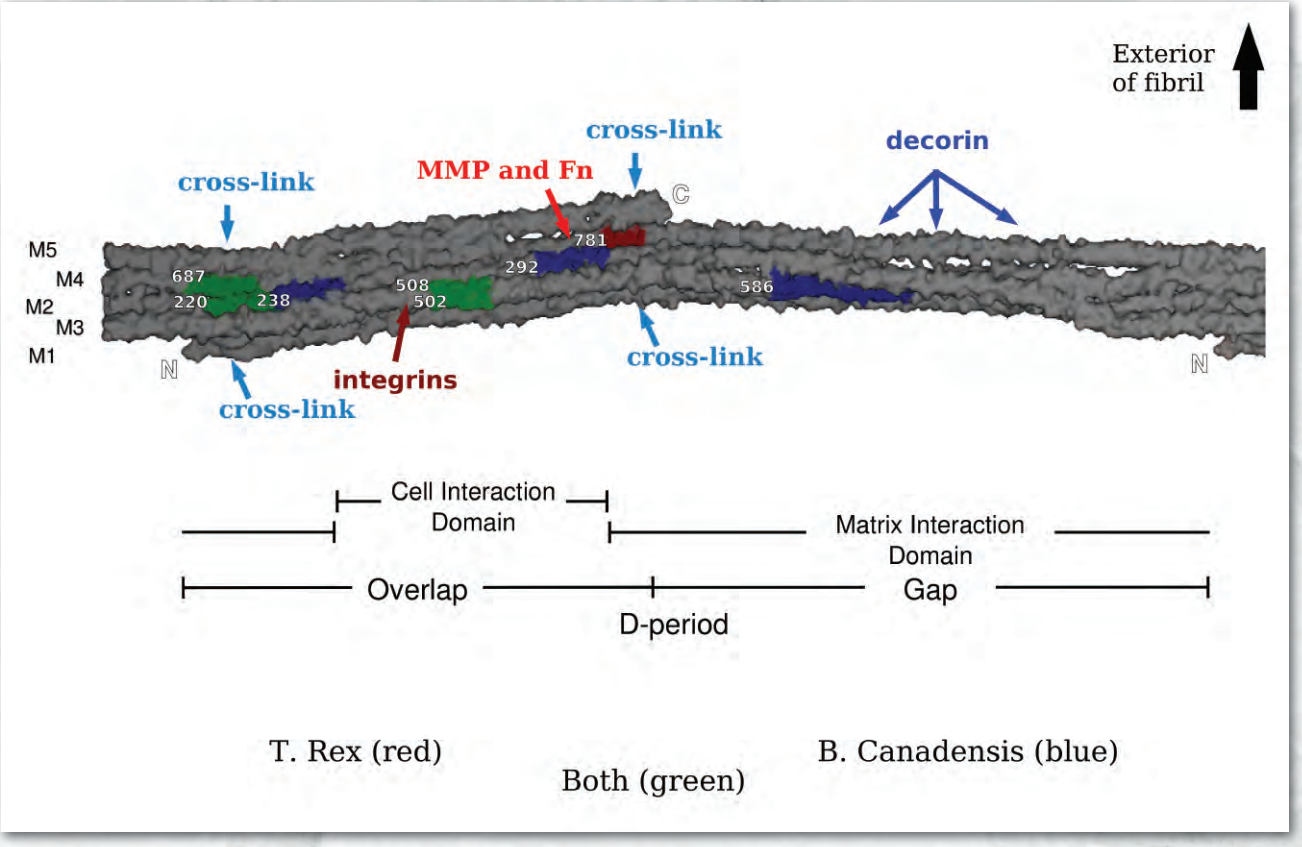

Fig. 1. X-ray diffraction model of the rat collagen microfibril showing the location of sites for fibronectin (Fn), decorin, and integrin binding, matrix metalloproteinase (MMP) cleavage, and the location of putative cell and matrix interaction domains. Dinosaur peptide locations are shown in red, green, and blue. Image originally published in San Antonio et al., PLoS ONE **6**(6), e20381 June 2011.

Although the team had previously presented multiple lines of evidence supporting the veracity of the find, the fact that the age of the peptides far exceeds any previous predictions of how long a protein could resist degradation has generated controversy.

Collagen is a common structural protein found in animals. It makes up about 25% of the human body and is a major component of tendons, ligaments, skin, and bone. Collagen literally holds the body together and its high tensile strength is attributed to its fibrillar structure. Recent evidence has shown that the collagen fibril is made up of microfibrillar units. Three polypeptides wind into a triple helical structure to form a collagen molecule. Five collagen molecules twist around each other to make microfibrils which then pack next to each other to form larger characteristic collagen fibrils. The amino acid sequence of collagen is highly conserved, so it is possible to compare peptides from diverse and ancient species.

To explain the remarkable durability of dinosaur collagen, the researchers from Orthovita, Inc.; North Carolina State University; Montana State University; the University of Pennsylvania; the Beth Israel Deaconess Medical Center and Harvard Medical School; the Harvard-Massachusetts Institute of Technology Division of Health Sciences and Technology;The University of Manchester; The University of York; and the Illinois Institute of Technology hypothesized that areas of the protein deeply within the complex fibrillar structure might be preferentially protected from degradation.

To test this, they set out to create a model on which to map specific amino acid sequences along and within the collagen fibril to see where their dinosaur peptides matched up. This was achieved by using x-ray diffraction data from the rat tendon collagen I microfibril and fibril *in situ*, collected at the Bio-CAT beamline, to construct a model showing the orientation of the molecules of the triple helix within the microfibril (Fig. 1).

The approach the team took over the last decade has been to study the structure of collagen in its context, as fibrils located within intact tissue samples. By far their most important work has been in developing the x-ray diffraction techniques and facilities at Bio-CAT to allow them to understand collagen structure *in situ*. Without this understanding, they would not have been able to perform the analysis undertaken in this recent work.

Using this approach, the team was able identify the location of collagen sequences that are known to interact with other molecules and those which would be expected to be protected in the interior of the fibrillar structure. Sequencing and mapping of 11 dinosaur peptides that represented 8 sequences revealed that the dinosaur sequences were from regions of the protein that were partly protected by molecular packing. This localization could be responsible for protecting the peptides over the millenia.

Further comparison of the sequences to human collagen provided other clues to how these particular peptides might have been preserved. First, there were very few acidic residues found in five of the sequences, meaning their hydrophobic nature would limit their solubility and availability for degradation. Also, few of the peptides represented regions of collagen containing sites targeted by breakdown enzymes and none of them were from the most unstable region of the protein. These features provide hard biochemical evidence for why these particular peptides endured for such a long time.

Does this work satisfy the skeptics? Not yet, but having a new mechanism for how ancient proteins might be preserved is a dinosaur-sized step in the right direction. *— Sandy Field*

See: James D. San Antonio[1]*, Mary H. Schweitzer[2,3], Shane T. Jensen[4], Raghu Kalluri[5,6], Michael Buckley[7,8], and Joseph P. R. O. Orgel[9]**, "Dinosaur Peptides Suggest Mechanisms of Protein Survival," PLoS ONE **6**(6), e20381 (June 2011). DOI:10.1371/journal.pone.0020381

Author affiliations: [1]Orthovita, Inc.; [2]North Carolina State University; [3]Montana State University; [4]The University of Pennsylvania; [5]Beth Israel Deaconess Medical Center and Harvard Medical School; [6]Harvard-Massachusetts Institute of Technology Division of Health Sciences and Technology; [7]The University of Manchester; [8]The University of York; [9]Illinois Institute of Technology

Correspondence:
*jsanantonio@orthovita.com,
**orgel@iit.edu

This research was funded by National Institutes of Health (NIH) RR 08630 and a National Science Foundation (NSF) Career Award 0644015 to JPROO; NIH DK 55001 grant to RK; and grants from NSF and The David and Lucile Packard Foundation to MHS. Bio-CAT is a NIH-supported Research Center RR-08630. Use of the Advanced Photon Source at Argonne National Laboratory was supported by the U. S. Department of Energy Office of Science under Contract No. DE-AC02-06CH11357.

See also: "Twisted structure preserved dinosaur proteins," by Ed Yong, *nature news*, http://www.nature.com/news/2011/110614/full/news.2011.369.html

18-ID-D • Bio-CAT • Life Sciences • Fiber diffraction, microdiffraction, microfluorescence (hard x-ray), small-angle x-ray scattering, time-resolved x-ray scattering, micro x-ray absorption fine structure • 3.5-35 keV • On-site • Accepting general users •

On July 14, 2011, distinguished representatives of Eli Lilly and Company and Argonne celebrated the completion of Lilly's $2 million upgrade to the company's research-guided LRL-CAT beamline located at Sector 31 of the APS. The LRL-CAT upgrade enables unattended automatic operation of the beamline for extended periods. Previously, LRL-CAT beamline scientists worked in shifts on nights and weekends to maintain throughput. They now monitor and, if necessary, operate the facility from remote locations using the Internet. Lilly scientists are now able to get the data they need, as quickly as possible, in order to make informed decisions on the development of future Lilly medicines. The cost of the upgrade was funded by Lilly and supports Lilly Research Laboratories' objective of producing more "timely shots in goal," in other words, getting medicines approved and available as quickly as possible to the patients who are waiting. The facility currently examines more than 10,000 protein crystals per year and supports nearly half of Lilly's research portfolio. Participants in the LRL-CAT dedication were (l. to r.): John Koss, Consultant Scientist-Automation, Lilly; Stephen Burley, Distinguished Lilly Scholar, Lilly; Dennis Mills, Deputy Associate Laboratory Director, X-ray Science, Advanced Photon Source; Brian Stephenson, Associate Laboratory Director, Photon Sciences, and Director, Advanced Photon Source; Horst Hemmerle, Senior Director, Translational Science, Quantitative and Structural Biology, Lilly; Jan Lundberg, Executive Vice President, Science and Technology, and President, Lilly Research Laboratories, Lilly; Karin Briner, Vice President, Translational Science and Technologies, Lilly; David Lewis, Senior Research Scientist, Lilly; Eric Isaacs, Director, Argonne National Laboratory; Sonal Sojitra, Senior Biologist, Lilly; Stephen Wasserman, Director, Quantitative and Structural Biology, Lilly; and Laura Morisco, Senior Associate, Projects, Lilly.

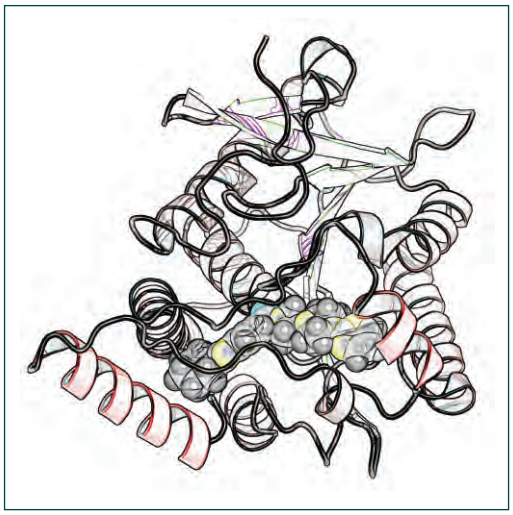

Structural Biology

Structural Clues to Preventing Strep-Related Toxic Shock

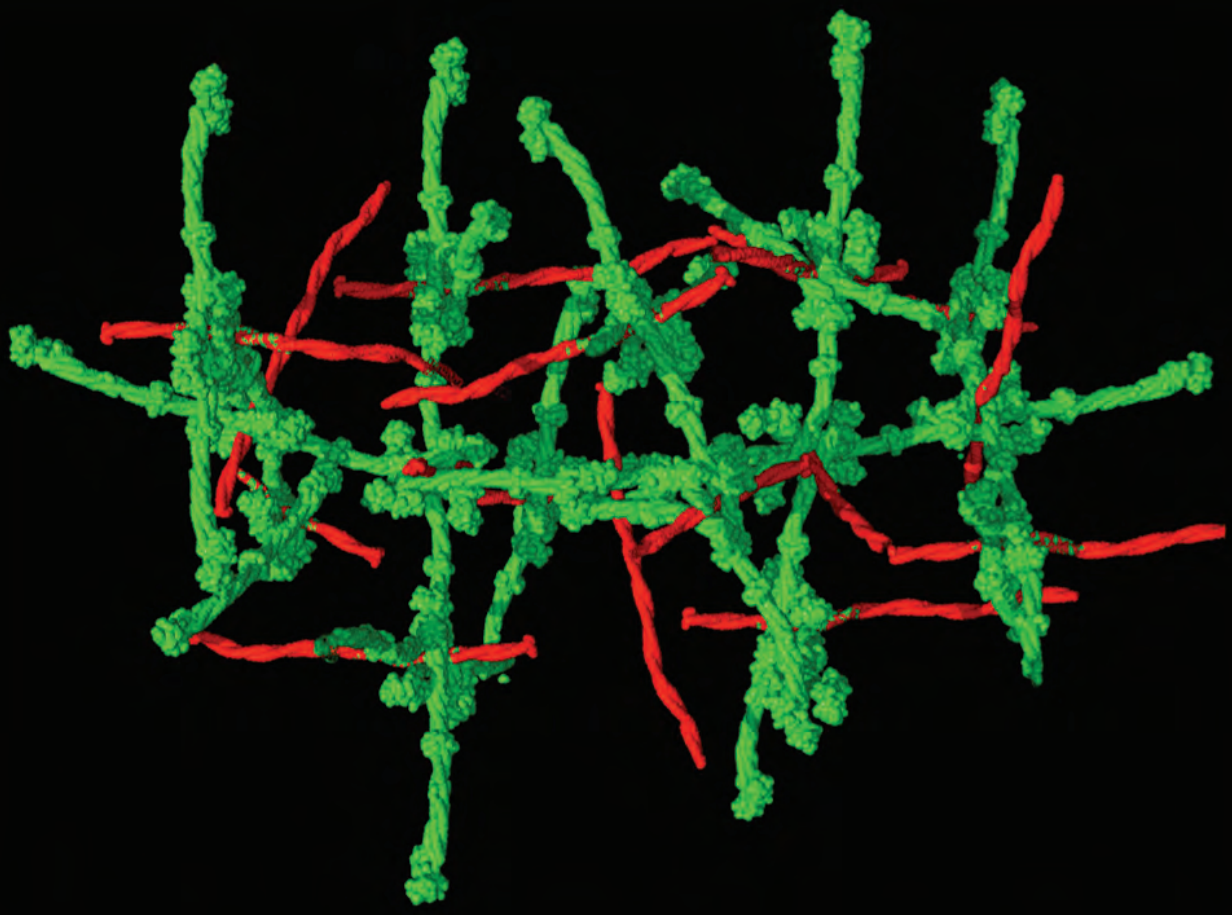

Group A *Streptococcus*, a class of bacteria that causes mild-to-severe and even fatal infections, releases the protein M1, which can cause toxic-shock-like vascular leakage and tissue injury. These events are triggered by the formation of a complex between M1 and a clotting factor in the blood called fibrinogen. The complex in turn triggers the activation of neutrophils, a type of white blood cell that is a key player in the immune response. Researchers utilizing the GM/CA-CAT beamline 23-ID-B at the APS have determined the crystal structure of the complex that forms between streptococcal M1 and human fibrinogen. They found that a single molecule of M1 linked together four fibrinogen molecules into the pattern of a cross. This pattern helped explain the way in which the complex helps activates neutrophils. Finding out more about this structure may help us better understand the pathology underlying streptococcal toxic shock syndrome (STSS).

Streptococcal toxic shock syndrome is a major health concern, with a mortality rate of 30-60%. STSS is marked by a massive inflammatory response, and a major factor in causing this response is known to be the M1 protein of group A *Streptococcus* and its interaction with the human blood clotting protein fibrinogen. It is known that the M1–fibrinogen complex binds proteins called β_2 integrins on neutrophils and triggers the release of heparin-binding protein (HBP), a potent dilator of blood vessels and a strong indicator of sepsis and circulatory failure in patients. But it was unknown why the particular interaction between M1 and fibrinogen led to a massive inflammatory response and activation of neutrophils. This was especially puzzling as neither M1 nor fibrinogen in the absence of the other was capable of activating neutrophils.

This study aimed to help answer that question. Carryng out x-ray crystallography studies at beamline 23-ID-B, the researchers from the University of California, San Diego; The Scripps Research Institute; and The University of Queensland found that the M1 protein organized fibrinogen into a specific structure, with four molecules of fibrinogen arranged in cross-like fashion around a single molecule of the M1 protein (Fig. 1). This structure supports the formation of a supramolecular network, which is distinct in appearance from a blood clot, but has the same properties present in a blood clot that could elicit an inflammatory response.

< Fig. 1. The pathological network formed by streptococcal M1 protein (red) and host fibrinogen (green).

According to the researchers, the level of fibrinogen density that is induced by the M1–fibrinogen network is likely to be a critical factor for neutrophil activation. They established this by disrupting the M1–fibrinogen network into fibers or sparse networks, which in turn resulted in loss of neutrophil activation. The cross-like structure of M1-fibrinogen presents high densities of integrin-binding sites just like a blood clot, indicating that integrin clustering and avidity are conserved mechanisms for neutrophil activation.

From these findings, it is possible to speculate that STSS may be treatable by inhibiting the formation of the complex between the M1 protein and fibrinogen. Preventing the formation of this complex would likely prevent the uncontrolled inflammatory response that arises from the complex formed by these two molecules. *— Emma Hitt*

See: Pauline Macheboeuf[1‡], Cosmo Buffalo[1], Chi-yu Fu[2], Annelies S. Zinkernagel[1 ‡‡], Jason N. Cole[1,3], John E. Johnson[2], VictorNizet[1], and Partho Ghosh[1*], "Streptococcal M1 protein constructs a pathological host fibrinogen network," Nature **472**, 64 (7 April 2011). DOI:10.1038/nature09967

Author affiliations: [1]University of California, San Diego, [2]The Scripps Research Institute; [3]The University of Queensland. ‡Present addresses: Université Joseph Fourier-EMBL-CNRS, ‡‡University Zurich
Correspondence: *pghosh@ucsd.edu

This work was supported by National Institutes of Health R21 AI071167 (P.G.), T32 GM007240 (C.B.), R01 AI077780 (V.N.), R01 GM54076 (J.E.J.), and a fellowship (J.N.C.) from the National Health and Medical Research Council of Australia (514639). GM/CA-CAT has been funded in whole or in part with Federal funds from the National Cancer Institute (Y1-CO-1020) and the National Institute of General Medical Sciences (Y1-GM-1104). Use of the Advanced Photon Source was supported by the U.S. Department of Energy Office of Science under contract no. DEAC02-06CH11357.

23-ID-B • GM/CA-CAT • Life sciences • Large unit cell crystallography, macromolecular crystallography, microbeam, multi-wavelength anomalous dispersion, single-wavelength anomalous dispersion, subatomic (<0.85 Å) resolution • 3.5-20 keV • On-site, remote • Accepting general users •

DIGGING DEEPER FOR CLUES TO HELP PREVENT CANCER

Ribonucleotide reductase (RR) is an enzyme with a critical role in DNA synthesis and repair. Due to its importance in helping to preserve the balance of genetic material, it has become a target for development of anti-cancer drugs. One intriguing feature about RR is how its overall activity is controlled. The molecule that inhibits its activity, dATP, binds more strongly to RR than its activator (ATP), despite being present at lower levels in the cell. Utilizing the BioCARS 14-ID-B beamline, the GM/CA-CAT 23-ID-D beamline, and the NE-CAT 24-ID-C and 24-ID-E beamlines at the APS, researchers have described the first report of structures of human RR in complex with its various substrates. The most important finding of their study was the structural explanation as to the increased binding affinity of the inhibitory dATP. They found that this inhibitor digs deeper into a pocket in the enzyme's activity site because one functional region of its structure is chemically different from that of ATP. This difference is thought to lead to conformational changes in the enzyme that keep it in an inactive state. Understanding the results of this study will be important in guiding future research in the development of RR inhibitors as anti-cancer agents.

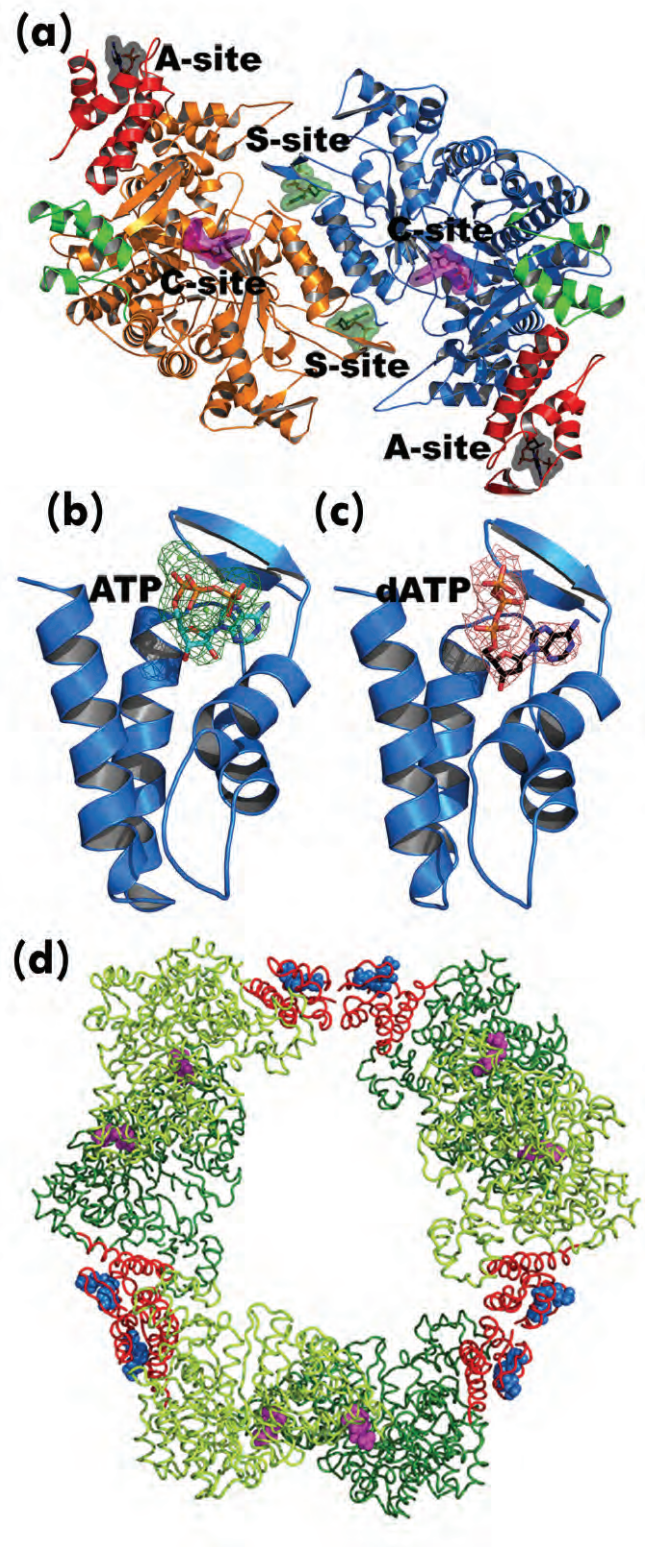

Fig. 1. (a) Ribbon diagram of the hRRM1 dimer. Chains A and B are colored yellow and cyan, respectively. The four-helix-ATP cones of both subunits are shown in red. TTP (green), GDP (magenta), and ATP/dATP (grey) bound at the S-, C- and A-sites, respectively, are represented as transparent surfaces. (b) The four-helix-ATP cone with ATP-bound. $2F_o$-F_c electron density for ATP (carbon, oxygen and nitrogen atoms are colored yellow, red and blue, respectively) contoured at 1σ is shown in green wire mesh. (c) The four-helix-ATP cone with dATP-bound. $2F_o$-F_c electron density for dATP (carbon, oxygen and nitrogen atoms are colored black, red and blue, respectively) contoured at 1σ is shown in red wire mesh. (d) Hexameric packing of RR1 based on the x-ray crystal structure of the ScRR1 hexamer. Ribbon diagrams of the hexamer packing arrangement. ScRR1 monomers are colored in forest green and limon. All the four-helix ATP-binding cones are colored in red. The blue ball is dATP molecule in four-helix ATP-binding cones.

DNA, the molecule that carries the genetic information in cells and passes it along from one generation to the next, is made up of units called deoxynucleotides that form the building blocks for its synthesis and repair. Ribonucleotide reductase is crucial because it is involved in the only pathway that can produce deoxynucleotides from scratch, using individual precursor molecules. Cells need enough deoxynucleotides to ensure accurate cell function, but too many can lead to mutations and tumor formation. Because of this critical role in DNA synthesis, RR is a target for development of anti-cancer treatments, and RR inhibitors are produced as drugs to block its activity. These drugs interfere with tumor cell growth by blocking deoxynucleotide formation, and reducing DNA synthesis and cell replication.

Allosteric mechanisms can be used to control enzyme activity. They involve a change in enzyme shape and function when substrates bind at a region other than the active site. This type of mechanism is used to control the overall activity of RR, depending on whether an ATP or a dATP binds to the allosteric activity site. Although dATP is present in the cell at lower levels than ATP, it can bind more strongly at this site. The reason for this was previously unknown, but this study aimed to investigate this.

Based on their studies at the APS, the researchers from the University of Tennessee, Case Western Reserve University, Karolinska Institutet, and the Harvard Medical School reported for the first time the x-ray crystallographic structure of human RR1 in complex with various substrates. The most important finding in the study was in the area of how the enzyme's activity is regulated. Human RR was described in complex with both dATP and ATP in the region that contains the allosteric activity site in a structural cleft. Comparing the binding sites on the dATP inhibitor and the ATP activator, they discovered an important chemical difference in structure that provided a clue as to their different binding affinities. In dATP, a specific chemical group is missing, allowing it to bind deeper into the enzyme's cleft. It is proposed that this deep binding of the inhibitor to RR leads to conformational changes in the enzyme that involve formation of a 6-subunit structure, or hexamer (Fig.1). This prevents stimulation of its active site, keeping it inactive.

Although some of the finer details behind the regulation of RR remain to be determined, this study has provided a first glimpse into the structural basis for its control. It has also provided the first report of the structure of human RR and the first dATP-bound hexamer structure providing the molecular basis for the reduction of its activity. The results of this study will help to guide future research in developing RR inhibitors with anti-cancer properties.

— Nicola Parry

See: James Wesley Fairman[1], Sanath Ranjan Wijerathna[2,] Md. Faiz Ahmad[2], Hai Xu[2‡], Ryo Nakano[2], Shalini Jha[2] Jay Prendergast[2] R. Martin Welin[3] Susanne Flodin[3], Annette Roos[3], Pär Nordlund[3], Zongli Li[4], Thomas Walz[4], and Chris Godfrey Dealwis[2*], "Structural basis for allosteric regulation of human ribonucleotide reductase by nucleotide-induced oligomerization," Nat. Struct. Mol. Biol. **18**(3), 316 (March 2011). DOI:10.1038/nsmb.2007

Author affiliations: [1]University of Tennessee, [2]Case Western Reserve University, [3]Karolinska Institutet, [4]Harvard Medical School, ‡Present address: Trevigen

Correspondence:
*chris.dealwis@case.edu

This research was supported by U.S. National Institutes of Health (NIH) grants 2R01CA100827-04A1 and 3R01CA100827-07S1 (to C.G.D.), and grants from the Swedish Research Council and Swedish Cancer Society (to P.N.). The Structural Genomics Consortium is a registered charity (number 1097737) that receives funds from the Canadian Institutes for Health Research, the Canadian Foundation for Innovation, Genome Canada through the Ontario Genomics Institute, GlaxoSmithKline, Karolinska Institutet, the Knut and Alice Wallenberg Foundation, the Ontario Innovation Trust, the Ontario Ministry for Research and Innovation, Merck, the Novartis Research Foundation, the Swedish Agency for Innovation Systems, the Swedish Foundation for Strategic Research, and the Wellcome Trust. T.W. is funded by the Howard Hughes Medical Institute. BioCARS is supported by grants from the National Center for Research Resources (grant 5P41RR007707) and the National Institute of General Medical Sciences (grant 8P41GM103543) from the National Institutes of Health. GM/CA-CAT has been funded in whole or in part with Federal funds from the National Cancer Institute (Y1-CO-1020) and the National Institute of General Medical Sciences (Y1-GM-1104). NE-CAT is supported by grants from the National Center for Research Resources (5P41RR015301-10) and the National Institute of General Medical Sciences (8 P41 GM103403-10) from the NIH.

14-ID-B • BioCARS • Life sciences • Time-resolved crystallography, time-resolved x-ray scattering, Laue crystallography, wide-angle x-ray scattering, biohazards at the BSL2/3 level, macromolecular crystallography • 7-20 keV • On-site • Accepting general users •

23-ID-D • GM/CA-CAT • Life sciences • Macromolecular crystallography, microbeam, large unit cell crystallography, subatomic (<0.85 Å) resolution, multi-wavelength anomalous dispersion, single-wavelength anomalous dispersion • 5-20 keV • On-site, remote • Accepting general users •

24-ID-C • NE-CAT • Life sciences • Macromolecular crystallography, microdiffraction, single-wavelength anomalous dispersion, single-crystal diffraction, microbeam • 6.5-23 keV • On-site • Accepting general users •

24-ID-E • NE-CAT • Life sciences • Macromolecular crystallography, microbeam, microdiffraction, single-wavelength anomalous dispersion, single-crystal diffraction • 12.68 keV • On-site •

TAKING THE BITE OUT OF MALARIA

Malaria is a global tropical disease caused by protozoan *Plasmodium* parasites, and transmitted by *Anopheles* mosquitoes. Researchers utilized the IMCA-CAT beamline 17-ID-B at the APS to investigate the crystal structure of serpin-2 (SRPN2) from the African malaria mosquito *Anopheles gambiae s.s.* (Fig. 1), the first serpin fold from a dipteran insect. They determined that despite serpin fold similarities between SRPN2 and other serpins, some differences do exist. In contrast with the fold of most other serpins, SRPN2 adopted a different conformation of the N-terminal hinge of the reactive loop center (RCL), the region of the protein that acts as "bait" during the reaction with its target protease. This change in conformation allows the RCL to partially insert into a β-sheet in the protein's central serpin fold region, reducing the accessibility of the "bait" region to the protease target. Understanding the results of this study will therefore be important in guiding future research in the identification of novel insecticide targets for malaria control. >>>

Fig. 1. The African malaria mosquito, *Anopheles gambiae s.s.* is the major vector of malaria in sub-Saharan Africa. The immunomodulatory protein, SRPN2, from this species is crucial for the female mosquito's survival. The crystal structure of SRPN2 will help researchers to develop small inhibitors of SRPN2 that may be used as future insecticides to combat malaria. Photo credit: D. Mayes, K-State Communications and Marketing, and K. Michel, Division of Biology, Kansas State University.

Fig. 2. The overall structure of SRPN2. The A-sheet is colored red, B-sheet blue, C-sheet in tan, α-helices are shown in green and the RCL is colored cyan. PDB: 3PZF. From C. An et al., Proiteins **9**, 1999 (2011).

Malaria is one of the most serious public health problems in the world. It is especially widespread in many tropical and subtropical countries, causing one million deaths and 300 million clinical cases annually. The condition is caused by protozoan parasites from the genus *Plasmodium* that are transmitted to people exclusively by infected mosquitoes. Although treatment and preventative measures are important to control this disease, drug resistance is becoming an increasingly significant problem. It is therefore important to not only reevaluate current insecticide targets, but to explore novel ones, in the hope of developing new insecticides to help combat malaria.

Serpins comprise a group of proteins (serine protease inhibitors) in various eukaryotes that function to inhibit protease enzymes. In mosquitoes, they regulate key innate immune reactions against certain stages of the malaria parasite. Serpins act as "suicide inhibitors," forming a stable complex with their target protease. They associate with the protease via a "bait" reside, in their reactive center loop (RCL) (the region that is split by the target protease), that mimics the enzyme's normal substrate. Melanin also plays a major role in the innate immune system of mosquitoes, which produce it to damage and encase invading bacteria and other parasites. Serpin-2 (SRPN2) is an important regulator of melanization, and it has been shown that its removal from the mosquito's body results in tumor formation, death of some malaria parasites, and shortening of the mosquito's lifespan.

Utilizing IMCA-CAT beamline 17-ID-B at the APS, the researchers from Kansas State University, the University of Kansas, and IMCA-CAT were able to evaluate the crystal structure of SRPN2 from the African malaria mosquito, *Anopheles gambiae* (Fig. 2), the first serpin fold from a dipteran insect. Although the researchers discovered that SRPN2 adopts a fold similar to that in other serpins, composed of three central β-sheets surrounded by nine alpha helices, one major difference was found. This was in the conformation of the N-terminal hinge region of the RCL. In the case of SRPN2, this enables the RCL to partially insert into, and interact with, one of the β–sheets of its central serpin fold. This partial insertion of the hinge region can reduce the activity of the serpin as it moves the RCL towards the main body of the protein. This therefore reduces the accessibility of the "bait" region to the protease target.

The study has revealed the first serpin fold, in its native conformation, from a dipteran insect, although there is still a lot to learn about the partial hinge insertion in the SRPN2 molecule. Understanding this process at the molecular level, however, will help to determine whether this represents a new regulatory mechanism of serpin function, and whether SRPN2 is a useful insecticide target. If so, this understanding would also help guide future research in the development of these compounds for malaria control.

— Nicola Parry

See: Chunju An[1], Scott Lovell[2], Michael R. Kanost[1], Kevin P. Battaile[3], and Kristin Michel[1]*, "Crystal structure of native *Anopheles gambiae* Serpin-2, a negative regulator of melanization in mosquitoes," Proteins **9**(6), 1999 (2011). DOI:10.1002/prot.23002

Author affiliations: [1]Kansas State University; [2]University of Kansas; [3]IMCA-CAT, Hauptman-Woodward Medical Research Institute
Correspondence: *kmichel@ksu.edu

Grant sponsor: US Department of Energy, Office of Science, Office of Basic Energy Sciences; Grant number: DE-AC02-06CH11357; Grant sponsor: NIH; Grant number: P20 RR-17708; Grant sponsor: Hauptman-Woodward Medical Research Institute. Use of the Advanced Photon Source was supported by the U.S. Department of Energy Office of Science under contract no. DEAC02-06CH11357.

17-ID-B • IMCA-CAT • Life sciences • Macromolecular crystallography, multi-wavelength anomalous dispersion, microbeam, single-wavelength anomalous dispersion • 6-20 keV • On-site, remote, mail-in • Accepting general users •

WINNING THE ARMS RACE AGAINST HIV DEFENSE MECHANISMS

Viruses that rapidly evolve, such as the human immunodeficiency virus (HIV) that causes Acquired Immune Deficiency Syndrome (AIDS), are very good at getting around a host's immune defenses. The viruses create their own defense systems against the host's attempts to thwart them. Then, when the host finds ways to disable the latest viral defense system, the process continues and an arms race ensues. Because HIV has proven to be a superpower in this arms race, much research effort has been put into understanding and then finding ways to circumvent the defenses that HIV puts into play when it invades the host. Thanks to the efforts of two research groups and the help of x-ray beamlines at the APS and the Stanford Synchrotron Radiation Lightsource, our understanding of how to penetrate the HIV defense system has made several leaps forward.

The Wilson/Burton research team (from The Scripps Research Institute, the Ragon Institute, the University of Washington, the University of Oxford, Cornell University, Progenics Pharmaceuticals, the National Institutes of Health, Imperial College London, the Japan Science and Technology Agency, the Academic Medical Center Amsterdam, and the International AIDS Vaccine Initiative) collected data at the GM/CA-CAT beamline 23-ID-B and the Stanford Synchrotron Radiation Lightsource beamlines 11-1 and 12-2. The Kwong research team (from the National Institutes of Health, the University of Washington, the Scripps Research Institute, Duke University, Tumaini University, the Kilimanjaro Reproductive Health Programme, the Ragon Institute, the International AIDS Vaccine Initiative, and the University of Maryland) collected data from SER-CAT beamlines 22-BM-D and 22-ID-D and GM/CA-CAT beamline 23-ID-B, all at the APS.

Both research groups focused on the HIV viral envelope protein, which is capable of fending off a host's antibodies that aim to neutralize the virus and to prevent it from damaging the cell. In HIV, the envelope protein is coated with glycan that prevents the host's antibodies from recognizing it. But the diligent efforts of the research teams, which studied different antibodies, have proven that this is not always the case. Despite the presence of the glycan shield, a select few of the host's antibodies are capable of penetrating the shield, recognizing the HIV surface protein, and binding — the first steps in the neutralization process. Not only that, but the particulars of this antibody recognition process make it a good target for designing vaccines against HIV.

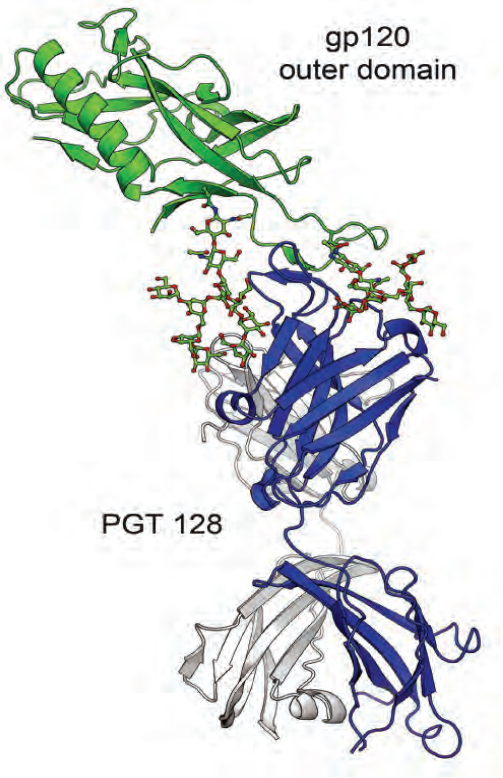

Fig. 1. The PGT 128 antibody (silver grey and blue) recognizes HIV's gp120 outer domain (green) by binding to two glycans (ball-and-stick representation) and a short segment of the V3 loop.

The Wilson/Burton team focused on a part of the HIV envelope protein gp120, which had been thought to be resistant to antibodies because of protection from the dense glycan shield. But recent work called into question the limits of that protection when it was discovered that several PGT broadly neutralizing antibodies interacted directly with the HIV glycan coat and gained access to the protein surface. The Wilson/Burton researchers used crystal structures and electron microscopy data from PGT 128 bound to antigens and glycan binding data to identify the antibody recognition site. The team was able to show that the antibody could penetrate the glycan shield and then bind at three sites — two glycans and a segment of the gp120 V3 loop — in such a way that gave it both high binding affinity and strong specificity (Fig. 1). The team also found that the high neutralization potency of two PGT antibodies could be due to the cross-linking of envelope proteins on the viral surface, which accelerates viral inactivation.

The Kwong team focused on variable regions 1 and 2 (V1/V2) of the HIV gp120 envelope. These variable regions of the protein are key players in HIV evasion of antibody neutralization and are themselves densely covered with glycan. Recent data showed that the human antibody PG9 could interact with V1/V2 and neutralize most circulating strains of HIV-1. By using structural data of V1/V2 in complex with PG9, the researchers showed how PG9 recognition proceeds from molecular interactions, over half of which involve glycan. By studying related antibodies CH04 and PGT145, both V1/V2-directed, the team found that the antibodies likely accomplished similar glycan penetration by using extended anionic loops (Fig. 2). The data suggest a general mechanism for antibody recognition of highly-glycosolated antigens, such as HIV. In the case of PG9, the researchers found that the viral weak spot, the point at which an anti-

body may initiate neutralization, consists of two glycans and a strand. This is the same motif recognized by PGT 128.

The research teams built their work upon recent evidence that, contrary to what had been previously surmised, antibodies could get through the HIV glycan coat. Though HIV is well armed with its glycan shield for evading antibodies, biochemical mechanisms exist by which human antibodies can penetrate this coat. Although the penetration mechanisms appear to be biochemically simple, the immunological mechanisms for their creation may not be easy to recreate. The new atomic-level information will certainly boost structure-based efforts to create vaccines against HIV. The arms race between HIV and humans now ratchets to the next stage. — *Mona Mort*

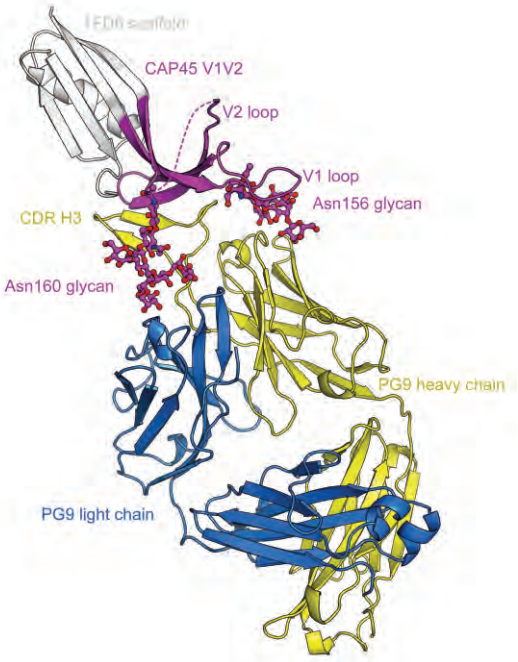

Fig. 2. The PG9 antibody (blue and yellow) inserts an extended loop past protective glycans (ball-and-stick representation) to recognize a strand of the V1/V2 sheet (purple). A heterologous scaffold (grey) substitutes for the rest of HIV-1.

See: Jason S. McLellan[1], Marie Pancera[1], Chris Carrico[2], Jason Gorman[1], Jean-Philippe Julien[3], Reza Khayat[3], Robert Louder[1], Robert Pejchal[3], Mallika Sastry[1], Kaifan Dai[1], Sijy O'Dell[1], Nikita Patel[1], Syed Shahzad-ul-Hussan[1], Yongping Yang[1], Baoshan Zhang[1], Tongqing Zhou[1], Jiang Zhu[1], Jeffrey C. Boyington[1], Gwo-Yu Chuang[1], Devan Diwanji[3], Ivelin Georgiev[1], Young Do Kwon[1], Doyung Lee[1], Mark K. Louder[1], Stephanie Moquin[1], Stephen D. Schmidt[1], Zhi-Yong Yang[1], Mattia Bonsignori[4], John A. Crump[5,6], Saidi H. Kapiga[7], Noel E. Sam[6,9], Barton F. Haynes[4], Dennis R. Burton[1,8], Wayne C. Koff[9], Laura M.Walker[1], Sanjay Phogat[9], Richard Wyatt[3], Jared Orwenyo[10], Lai-XiWang[10], James Arthos[1], Carole A. Bewley[1], John R. Mascola[1], Gary J. Nabel[1], William R. Schief[2,3], Andrew B. Ward[3], Ian A. Wilson[3], and Peter D. Kwong[1]*, "Structure of HIV-1 gp120 V1/V2 domain with broadly neutralizing antibody PG9," Nature **480**, 336 (15 December 2011). DOI:10.1038/nature10696

Author affiliations: [1]National Institutes of Health, [2]University of Washington, [3]The Scripps Research Institute, [4]The Duke Human Vaccine Institute, [5]Duke University Medical Center, [6]Tumaini University, [7]Kilimanjaro Reproductive Health Programme [8]Ragon Institute of MGH, MIT, and Harvard, [9]International AIDS Vaccine Initiative (IAVI), [10]University of Maryland School of Medicine
Correspondence: *pdkwong@nih.gov

Support for this work was provided by the Intramural Research Program of the National Institutes of Health (NIH), by the International AIDS Vaccine Initiative, by the Ragon Institute, by the Canadian Institute of Health Research, and by grants from the NIH. SER-CAT at the APS is operated by the University of Georgia.

and

Robert Pejchal[1], Katie J. Doores[1,2], Laura M. Walker[1], Reza Khayat[1], Po-Ssu Huang[3], Sheng-Kai Wang[1], Robyn L. Stanfield[1], Jean-Philippe Julien[1], Alejandra Ramos[1], Max Crispin[4], Rafael Depetris[5], Umesh Katpally[6], Andre Marozsan[6], Albert Cupo[6], Sebastien Maloveste[7], Yan Liu[8], Ryan McBride[1], Yukishige Ito[9], Rogier W. Sanders[5,10], Cassandra Ogohara[3], James C. Paulson[1], Ten Feizi[8], Christopher N. Scanlan[4], Chi-Huey Wong[1], John P. Moore[5], William C. Olson[6], Andrew B. Ward[1], Pascal Poignard[1,11], William R. Schief[1,3], Dennis R. Burton[1,2]*, and Ian A. Wilson[1]**, "A Potent and Broad Neutralizing Antibody Recognizes and Penetrates the HIV Glycan Shield," Science **334**, 1097 (25 November 2011). DOI:10.1126/science.1213256

Author affiliations: [1]The Scripps Research Institute; [2]Ragon Institute of MGH, MIT, and Harvard; [3]University of Washington; [4]University of Oxford; [5]Weill Medical College of Cornell University; [6]Progenics Pharmaceuticals; [7]National Institutes of Health; [8]Imperial College London; [9]Japan Science and Technology Agency; [10]Academic Medical Center; [11]International AIDS Vaccine Initiative
Correspondence: *burton@scripps.edu, **wilson@scripps.edu

Work was supported by the International AIDS Vaccine Initiative Neutralizing Antibody Center, National Institutes of Health (NIH) grant AI84817 (I.A.W.), National Institute of Allergy and Infectious Diseases grant AI33292 (D.R.B.), NIH/National Research Service Award fellowship AI74372 (R.P.), Canadian Institutes of Health Research fellowship FRN HFE-224662 (J.-P.J.), HIV Vaccine Research and Design grant AI082362 (W.C.O., J.P.M., and I.A.W.), UK Research Councils' Basic Technology Initiative "Glycoarrays" grant GRS/79268, Engineering and Physical Sciences Research Council Translational Grant EP/G037604/1, National Cancer Institute (NCI) Alliance of Glycobiologists for Detection of Cancer and Cancer Risk grant U01 CA128416, and the Ragon Institute. SER-CAT supporting institutions may be found at www.ser-cat.org/members.html. GM/CA CAT is funded in whole or in part with Federal funds from the NCI (Y1-CO-1020) and the National Institute of General Medical Sciences (Y1-GM-1104). Use of the Advanced Photon Source supported by the U.S. Department of Energy Office of Science under contract no. DEAC02-06CH113

22-BM-D • SER-CAT • Life sciences • Macromolecular crystallography • 8-20 keV • On-site, remote • Accepting general users •

22-ID-D • SER-CAT • Life sciences • Macromolecular crystallography • Multi-wavelength anomalous dispersion • microbeam • 6-20 keV • On-site, remote • Accepting general users •

23-ID-B • GM/CA-CAT • Life sciences • Macromolecular crystallography, microbeam, large unit cell crystallography, subatomic (<0.85 Å) resolution, multi-wavelength anomalous dispersion, single-wavelength anomalous dispersion • 3.5-20 keV • On-site, remote • Accepting general users •

LEARNING TO CONTROL THE HEPATITIS C VIRUS

The hepatitis C virus (HCV), a worldwide health problem with relatively inefficient treatment options, is a focus of considerable medical research. Its RNA polymerase enzyme, non-structural protein 5B (NS5B), is among the most targeted enzymes for control of the virus. Researchers from Bristol-Myers Squibb utilized the IMCA-CAT beamlines 17-BM-B and 17-ID-B, and SER-CAT beamlines 22-BM-D and 22-ID-D at the APS to investigate the genotype selective activity of some examples of piperazine-based NS5B inhibitors against two different HCV strains, 1a and 1b. They determined the crystal structures of a potent form of the inhibitor combined with NS5B proteins from both strains (Fig.1). Their study showed that although the conformation of the inhibitor in both cases was similar, there was a single amino acid change between the genotypes, located close to the binding site of the inhibitor, and suggested that this could account for the potency differences. Understanding the results of this study will be important in guiding future research in the development of potent piperazine-based NS5B inhibitors for HCV control. >>>

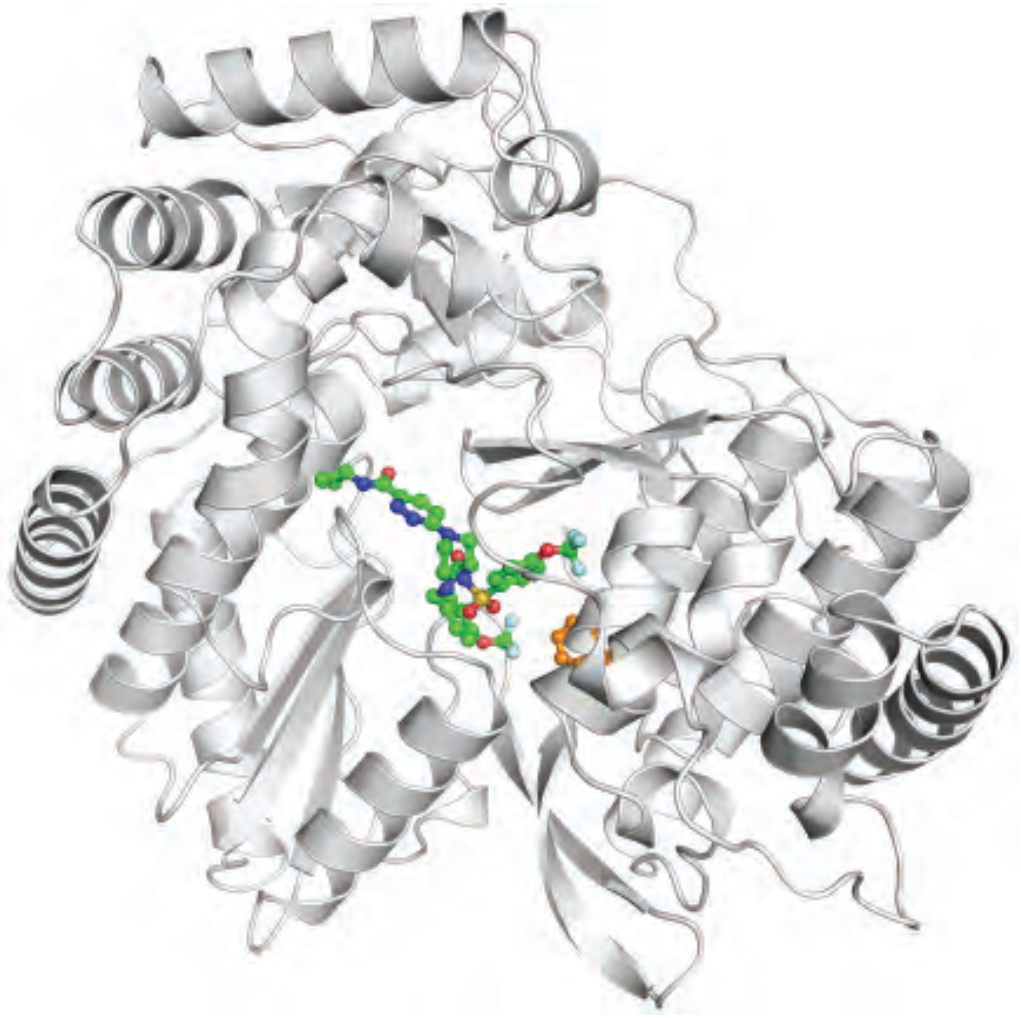

Fig. 1. Crystal structure of compound 5 (green carbon atoms), a potent form of the inhibitor, bound to NS5B 1a: The orange carbon atoms represent the location of the single amino acid difference. In the case of NS5B 1a, the amino acid phenylalanine occupies this position. NS5B genotype 1b, on the other hand, contains a tyrosine residue at this position.

Hepatitis C virus (HCV) infection is a major cause of acute and chronic hepatitis globally, and although the prevalence of HCV infection varies throughout the world, it affects over 170 million people. The virus causes liver disease, which in 15-20% of cases can lead to chronic hepatitis, cirrhosis and liver failure, and even liver cancer in some patients. First characterized in the late 1980s, HCV belongs to the flavivirus family of viruses, and its genome contains a single strand of RNA. The virus comprises 6 major genotypes with over 50 subtypes, and the existence of these numerous "strains," combined with its ability to mutate rapidly, make it difficult for the immune system to combat it.

Consequently, it has so far proven difficult to target the virus with single intervention therapies. The current standard of care for patients with chronic HCV infection is a dual combination therapy, but less than 50% of genotype 1 patients respond to the treatment. However, novel drug development strategies are constantly being pursued for treatment of this viral pandemic.

One particular area of focus has been the search for inhibitors of nonstructural protein 5B (NS5B). This is an RNA-dependent RNA polymerase, a protein that is required by the virus for its replication, and for progression through its life cycle. Unsurprisingly, it is therefore one of the main potential targets for anti-HCV drugs, and recent evaluation of NS5B inhibitors in clinical trials has produced encouraging results.

Previous studies of the piperazine class of HCV NS5B inhibitors have shown that some have different levels of activity against different HCV genotypes. This study aimed to further investigate this variation in potency. Utilizing the IMCA-CAT and SER-CAT x-ray beamlines at the APS, the researchers obtained co-crystal structures consisting of potent examples of the inhibitor in complex with the NS5B protein of two different HCV genotypes, 1a and 1b. The structure of the inhibitor was similar in both cases, but a single amino acid difference was present between genotypes 1a and 1b, at a location close to the binding site of the inhibitor (Fig. 1). The researchers proposed that this sequence change could account for the potency differences. Because the binding site is only available for interactions following displacement of the C-terminus, they suggested that the amino acid change could regulate the displacement, or change the structural preferences of the C-terminus after it dissociates from the binding site.

Although specific interactions remain to be determined between the inhibitors and the protein to explain the variable potency against different HCV genotypes, this study has provided possible explanations for the difference. Understanding this process at the molecular level may not only reveal the mechanism for the selective activity of potent piperazine-based NS5B inhibitors against different HCV genotypes, but it will also help guide future research in the development of these compounds for HCV control.

— Nicola Parry

See: Robert G. Gentles*, Steven Sheriff, Brett R. Beno, Changhong Wan, Kevin Kish, Min Ding, Xiaofan Zheng, Louis Chupak, Michael A. Poss, Mark R. Witmer, Paul Morin, Ying-Kai Wang, Karen Rigat, Julie Lemm, Stacey Voss, Mengping Liu, Lenore Pelosi, Susan B. Roberts, Min Gao, and John F. Kadow, "Investigation of the mode of binding of a novel series of N-benzyl-4-heteroaryl-1-(phenylsulfonyl) piperazine-2-carboxamides to the hepatitis C virus polymerase," Bioorg. Med. Chem. Lett. **21**, 2212 (2011). DOI:10.1016/j.bmcl.2011.03.011

Author affiliation: Bristol-Myers Squibb
Correspondence:
*robert.gentles@bms.com

Use of the IMCA-CAT beamline at the Advanced Photon Source was supported by the companies of the Industrial Macromolecular Crystallography Association through a contract with Hauptman-Woodward Medical Research Institute. Institutions supporting SER-CAT may be found at www.ser-cat.org/members.html. Use of the Advanced Photon Source was supported by the U.S. Department of Energy Office of Science under Contract No. DEAC02-06CH113.

17-BM-B • IMCA-CAT • Life sciences • Macromolecular crystallography, multi-wavelength anomalous dispersion, microbeam, single-wavelength anomalous dispersion • 7.5-14 keV • On-site, remote, mail-in • Accepting general users •

17-ID-B • IMCA-CAT • Life sciences • Macromolecular crystallography, multi-wavelength anomalous dispersion, microbeam, single-wavelength anomalous dispersion • 6-20 keV • On-site, remote, mail-in • Accepting general users •

22-BM-D • SER-CAT • Life sciences • Macromolecular crystallography • 8-20 keV • On-site, remote • Accepting general users •j

22-ID-D • SER-CAT • Life sciences • Macromolecular crystallography, multi-wavelength anomalous dispersion, microbeam • 6-20 keV • On-site, remote • Accepting general users •/

CLUES TO IMPROVING PAIN CONTROL

Cannabinoids are well known for their analgesic effects, and there is increasing evidence that they produce a reduction in sensitivity to pain via interactions with both cell membrane cannabinoid receptors 1 (CB1) and 2 (CB2). Recent studies have suggested that the enzyme monoglyceride lipase (MGL) may represent a target for the treatment of pain. MGL is the main enzyme in the brain that breaks down 2-arachidonoyl glycerol, a ligand for both CB1 and CB2. It is through this action that MGL plays a key role in the regulation of endocannabinoid molecular signaling of pain. Utilizing the IMCA-CAT 17-ID-B beamline at the APS, researchers have described a new crystal structure of a mutant form of MGL complexed with an inhibitor, the second structure of this enzyme to be reported in complex with a ligand. They discovered a novel structure of the regulatory lid-domain, as well as the mechanism of binding of a pharmaceutically important reversible inhibitor. Understanding the results of this study will be important in guiding future research in the development of MGL inhibitors as pharmacologic agents for the treatment of pain. >>>

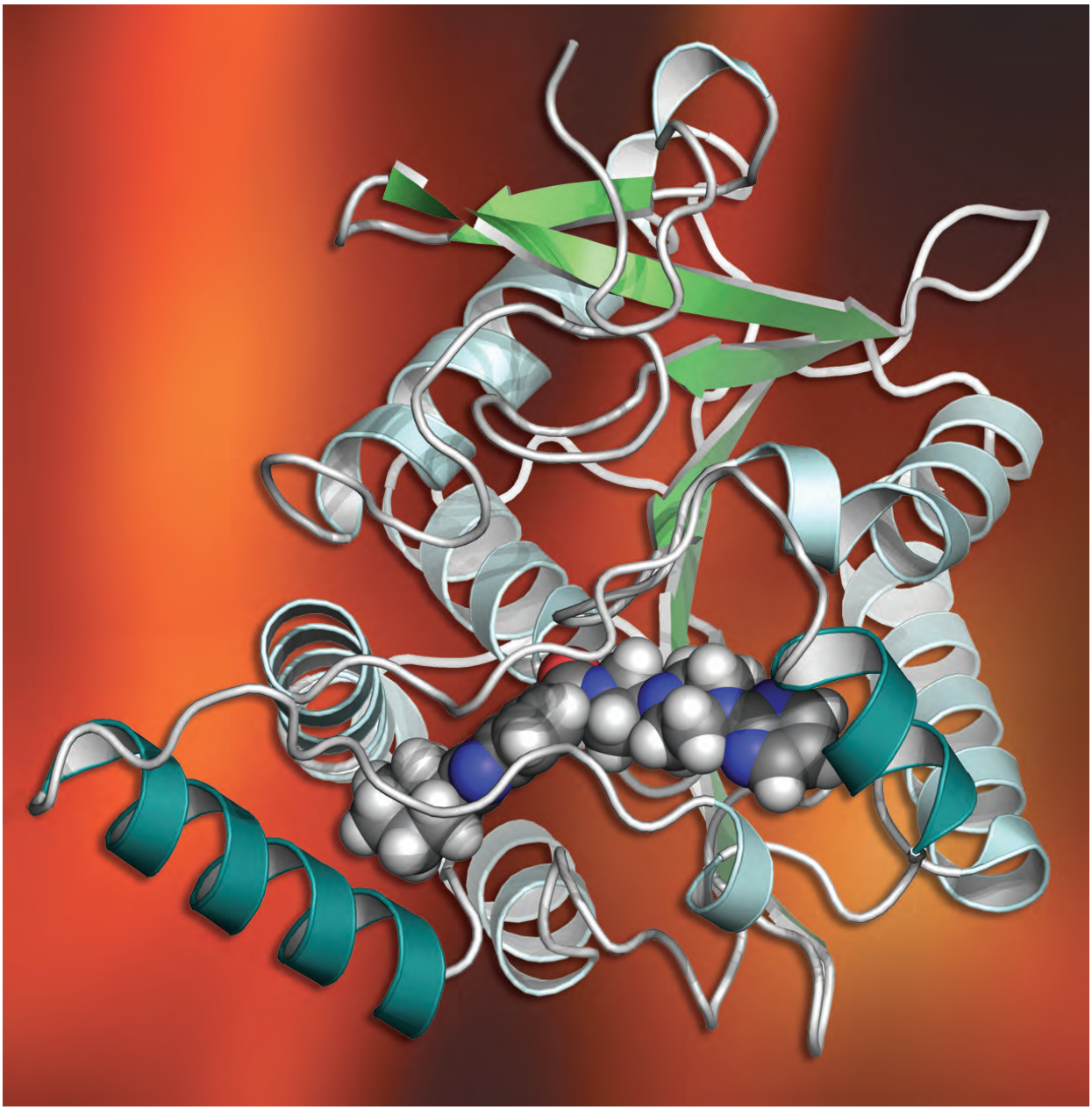

The earliest known use of cannabis-derived products for medicinal purposes dates back at least 3,000 years. Since then, many cultures throughout the world have been using cannabis-derived products to treat various ailments, and they came into use in Western medicine in the nineteenth century. Although controversial, the analgesic effects of cannabis are well known, and various clinically related products are available for safe and efficacious therapy for different diseases.

The main active component of cannabis is the cannabinoid Δ^9-tetrahydrocannabinol (THC), and this exerts its effects by activating two G-protein coupled receptors in the body, CB1 and CB2. CB1 is found throughout the central nervous system, while CB2 is especially common in peripheral tissues. There is now increasing evidence that cannabinoids produce antinociception (reduced sensitivity to pain) via interactions with the two receptors, both within and outside the central nervous system.

Endocannabinoids are cannabinoid compounds that are produced naturally in the body, and 2-arachidonoylglycerol (2-AG) is one such compound that is involved in various physiological processes in the brain. It acts as a lipid transmitter and its regulation is thought to be of great therapeutic potential. Monoglyceride lipase, a member of the α/β hydrolase family of enzymes, plays a major role in the metabolism of 2-AG.

Researchers engineered a soluble, crystallizable form of MGL by direct mutagenesis, and used the IMCA-CAT beamline at the APS to evaluate the protein's three-dimensional conformation (Fig. 1). They described a new crystal structure of this mutant form of MGL in complex with a potent inhibitor, and found it to very similar to the typical α/β-hydrolase fold (the enzyme's characteristic catalytic domain), comprising 8 β-sheets surrounded by 8 α-helices. According to the researchers, in spite of some similarities with previously reported conformations of MGL, evaluation of this novel structure of the enzyme also revealed a ligand-induced closed conformation of the regulatory lid-domain (an α helical region of the enzyme that controls substrate entrance to the active site). In this closed conformation, a region of the lid-domain covered the ligand, a bound inhibitor, almost completely burying it within the enzyme's active site. Evaluation of the structure lacking the inhibitor demonstrated that the closed conformation could accommodate the native compound 2-AG. It was also found that during its catalytic reaction, the change from the open to closed conformation of MGL is associated with electrostatic alterations that result in its detachment from the cell membrane upon completion of the cycle.

Although the reason for this detachment remains to be determined, this study has provided further insight into the various conformations of MGL, and additionally outlines a successful approach for transformation of membrane-associated proteins into a monomeric and soluble form. It also provided information about the binding mechanism of a reversible inhibitor with pharmaceutical potential. This will help to guide future research in development of MGL inhibitors with antinociceptive or other favorable properties.

— Nicola Parry

< Fig. 1. Structure of MGL in the closed conformation bound to a nanomolar inhibitor. MGL adopts a typical α/β-hydrolase fold comprising 8 β-sheets (lime-green), 6 canonical α-helices (cyan) and an additional lid-domain (teal). The inhibitor (sphere representation) is located in the elongated active-site, which is capped by loops connecting the lid-domain helices. The lid domain is present in the closed conformation, sealing access to the active site.

See: Céline Schalk-Hihi*, Carsten Schubert**, Richard Alexander, Shariff Bayoumy, Jose C. Clemente, Ingrid Deckman, Renee L. DesJarlais, Keli C. Dzordzorme, Christopher M. Flores, Bruce Grasberger, James K. Kranz, Frank Lewandowski, Li Liu, Hongchang Ma, Diane Maguire, Mark J. Macielag, Mark E. McDonnell, Tara Mezzasalma Haarlander, Robyn Miller, Cindy Milligan, Charles Reynolds, and Lawrence C. Kuo, "Crystal structure of a soluble form of human monoglyceride lipase in complex with an inhibitor at 1.35 Å resolution," Prot. Sci. **20**(4), 670 (2011). DOI:10.1002/pro.596

Author affiliation: Johnson & Johnson Pharmaceutical Research and Development

Correspondence:

*cschalkh@its.jnj.com,
**cschuber@its.jnj.com

Use of the IMCA-CAT beamline at the APS was supported by the companies of the Industrial Macromolecular Crystallography Association through a contract with Hauptman-Woodward Medical Research Institute. Use of the Advanced Photon Source at Argonne National Laboratory was supported by the U.S. Department of Energy Office of Science under Contract No. DE-AC02-06CH11357.

17-ID-B • IMCA-CAT • Life sciences • Macromolecular crystallography, multi-wavelength anomalous dispersion, microbeam, single-wavelength anomalous dispersion • 6-20 keV • On-site, remote, mail-in • Accepting general users •

WINGS OF THE PROTEIN: NEW ROLES FOR FANCY SHAPES

In the intricate and complex terrain of cellular biochemistry, shape means a lot. Slight changes in the three-dimensional structure of a molecule can make or break its ability to function properly. This law holds throughout the rich variety of biochemical processes and is especially critical to regulating how and when DNA is read and turned into a cell's building blocks. It is not surprising, then, that biochemists and molecular biologists have long searched for more and more detail about how molecular complexes are able to get it right when gleaning information from a bewilderingly large number of genes. Certain proteins that activate stretches of DNA and help control the timing of RNA and protein production from a cell's genome are especially important in this whole scenario. If the molecules that control gene expression are mutated and do not function properly, a disease state usually follows. Two research groups — the Lei team from the University of Michigan and Stanford University schools of medicine, and the Couture team from the University of Ottawa, the Ottawa Hospital Research Institute, and Northwestern University — collected data at the LS-CAT beamline 21-ID-G at the APS and used these data to greatly advance our knowledge of DNA-binding proteins. Their work provides critically needed details that can be used to understand how cells remain healthy.

The research teams focused on proteins important to a process called histone methylation, which is associated with regulation of gene expression in cells containing a nucleus (eukaryotes). In particular, the groups studied the protein Ash2L, a core component of the MLL family of histone methyltransferases. The importance of Ash2L was indicated by its known, but not clearly understood, role in histone methylation and because its structure is conserved across species. In working on Ash2L, the research teams, though each studied a different aspect of the protein's behavior, set out to answer two main questions: Does Ash2L bind directly to DNA, and what are the effects of Ash2L mutations on gene expression. In answering these questions, the researchers came up with much needed and surprising details about Ash2L's function in the cell. The data provided by the researchers dovetail nicely to give a new understanding of the importance of Ash2L in gene expression.

The Lei team set out to characterize the amino-terminal end of the Ash2L molecule known as the plant homeodomain (PHD) finger, and came up with some surprising results. By

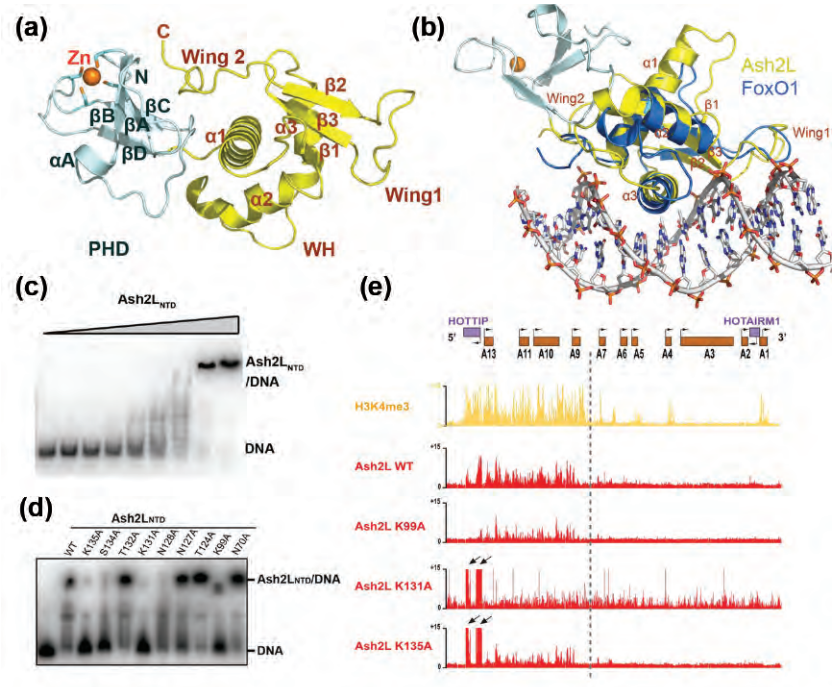

Fig. 1. (a). The structure of Ash2L N-terminus with two sub-domains: PHD and WH domain. (b). The structure of Ash2L WH domain resembles FOXO1, the DNA-binding motif. (c). Ash2L N-terminal domain has double-stranded DNA binding activity. (d). The single mutations of Ash2L on proposed DNA-binding interface can disrupt Ash2L-DNA interaction. (e). Ash2L mutations have defects on chromosome occupancy.

21-ID-G • LS-CAT • Life sciences • Macromolecular crystallography • 12.7 keV • On-site, remote, mail-in • Accepting general users •

obtaining the crystal structure of the N-terminal domain of Ash2L, they found an atypical PHD finger that lacks histone tail-binding activity. The structure revealed a previously unrecognized winged-helix motif located next to the PHD finger on the C-terminal end (Fig. 1). The researchers combined their structural data with biochemical and cellular analyses to show how the winged-helix motif of Ash2L binds DNA — specifically, how Ash2L targets the *Homeobox* (*HOX*) locus, a region important to regulating development. Given the presence of Ash2L in all MLL complexes, the researchers used the data to propose an important role of Ash2L: to provide non-specific DNA binding that helps stabilize other specific binding mechanisms to an area of active gene expression. The team produced mutations of Ash2L's wing motif that also suggested the protein's role in marking chromosome domain boundaries.

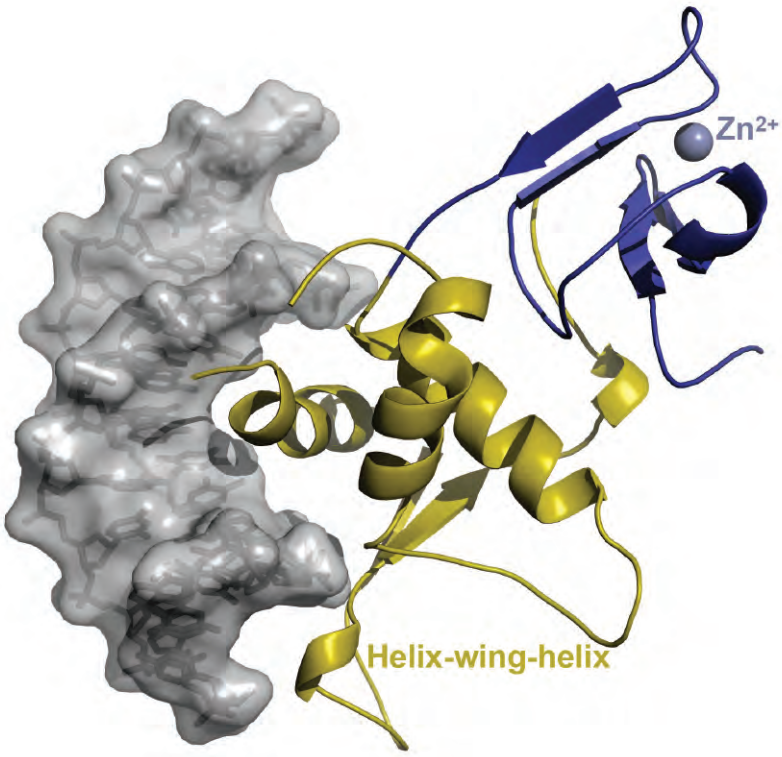

Fig. 2. Crystal structure of Ash2L: Cartoon representation of Ash2L PHD (dark blue) and helix-wing-helix (dark yellow) domains in which Ash2L is modeled in complex with a DNA fragment corresponding to the β-globin promoter region. The surface of the DNA fragment is rendered in grey.

The Couture team focused on how Ash2L is involved in regulating expression of β-globin genes. Decreased levels of Ash2L had previously been shown to decrease β-globin transcription and additional data had suggested that Ash2L is important in linking transcription factors to histone methylation. The researchers wanted to uncover details about the mechanisms underlying these processes. To this end, the team studied the crystal structure of Ash2L and combined their structural data with experimental results that give an excellent picture of how Ash2L affects β-globin production. A region of the Ash2L molecule known as the forkhead-like helix-wing-helix (HWH) domain — the same as the winged-helix domain described by the Lei group, but named differently — binds directly to DNA and is critical for stable association with the histone site HS2 and activation of β-globin transcription (Fig. 2). The characteristics of this AshL2 association and its link to gene activation led the researchers to propose that this mechanism could be applied to understanding regulation of other genes. Since Ash2L is also known as a trithorax protein, these data suggest such a regulatory role for the Ash2L HWH domain in regulating *HOX* gene loci during embryonic development.

The efforts of the two research teams have provided critical and fascinating details about how wing motifs of the protein Ash2L play important roles in DNA binding that lead to gene expression. Most important is that their work suggests general processes for the all-important cellular activity of gene regulation. Powered by both the specific details and general mechanisms proposed in these studies, further work on gene regulation takes flight. *— Mona Mort*

See: Yong Chen[1], Bingbing Wan[1], Kevin C. Wang[2], Fang Cao[1], Yuting Yang[1], Angeline Protacio[2], Yali Dou[1], Howard Y. Chang[2], and Ming Lei[1]*, "Crystal structure of the N-terminal region of human Ash2L shows a winged-helix motif involved in DNA binding," EMBO Rep. **12**(8), 797 (2011). DOI:10.1038/embor.2011.101
Author affiliations: [1]University of Michigan Medical School, [2]Stanford University School of Medicine
Correspondence:
*leim@umich.edu

M.L. acknowledges generous financial support from the National Institutes of Health (RO1 GM083015) and the American Cancer Society. M.L. and H.Y.C. are Howard Hughes Medical Institute Early Career Scientists.

and

Sabina Sarvan[1], Vanja Avdic[1], Véronique Tremblay[1], Chandra-Prakash Chaturvedi[2], Pamela Zhang[1], Sylvain Lanouette[1], Alexandre Blais[1,2], Joseph S Brunzelle[3], Marjorie Brand[2], and Jean-François Couture[1]*, "Crystal structure of the trithorax group protein ASH2L reveals a forkhead-like DNA binding domain," Nat. Struct. Mol. Biol. **18**(7), 857 (7 July 2011). DOI:10.1038/nsmb.2093
Author affiliations: [1]University of Ottawa, [2]Ottawa Hospital Research Institute, [3]Northwestern University
Correspondence:
*jean-francois.couture@uOttawa.ca

This work was supported by Canadian Institutes of Health Research (CIHR) grants to J.-F. C. (191666) and M.B. (MOP-89834). J.-F. C. holds a Canada Research Chair in Structural Biology and Epigenetics. P.Z. is sponsored by a Natural Sciences and Engineering Research Council of Canada (NSERC) fellowship. C.-P. C. is supported by a CIHR/Thalassemia Foundation of Canada postdoctoral fellowship. Use of LS-CAT supported by the Michigan Economic Development Corporation and the Michigan Technology Tri-Corridor for the support of this research program (Grant 085P1000817).

Use of the Advanced Photon Source at Argonne National Laboratory was supported by the U. S. Department of Energy Office of Science under Contract No. DE-AC02-06CH11357.

CONVERTING CHEMICAL SIGNALS TO THOUGHTS

Researchers working to understand how chemical signals in the brain are converted into learning and memory have started to tease out some of the details of this suitably complex process. The molecules that relay chemical signals between neuronal cells of the brain during tasks of cognitive function interact with their cellular receptors in a highly specialized and tightly regulated manner. Reduced signaling of one of these molecules, glutamate, has been identified in a number of diseases including Alzheimer's, schizophrenia, attention deficit/hyperactivity disorder, narcolepsy, autism, and Parkinson's. Drugs have been developed that can enhance glutamate signaling and, although they have shown promise in improving cognitive function in preliminary studies, they have proven to be of limited efficacy or to cause adverse effects. In work completed by researchers at IMCA-CAT beamline 17-ID-B and LRL-CAT beamline 31-ID-D of the APS, the structure and function of two new compounds that modulate glutamate receptor signaling have been studied. This work provides new insights that will be important in the development of effective treatments for diseases in which impaired glutamate receptor signaling causes problems with cognitive function. >>>

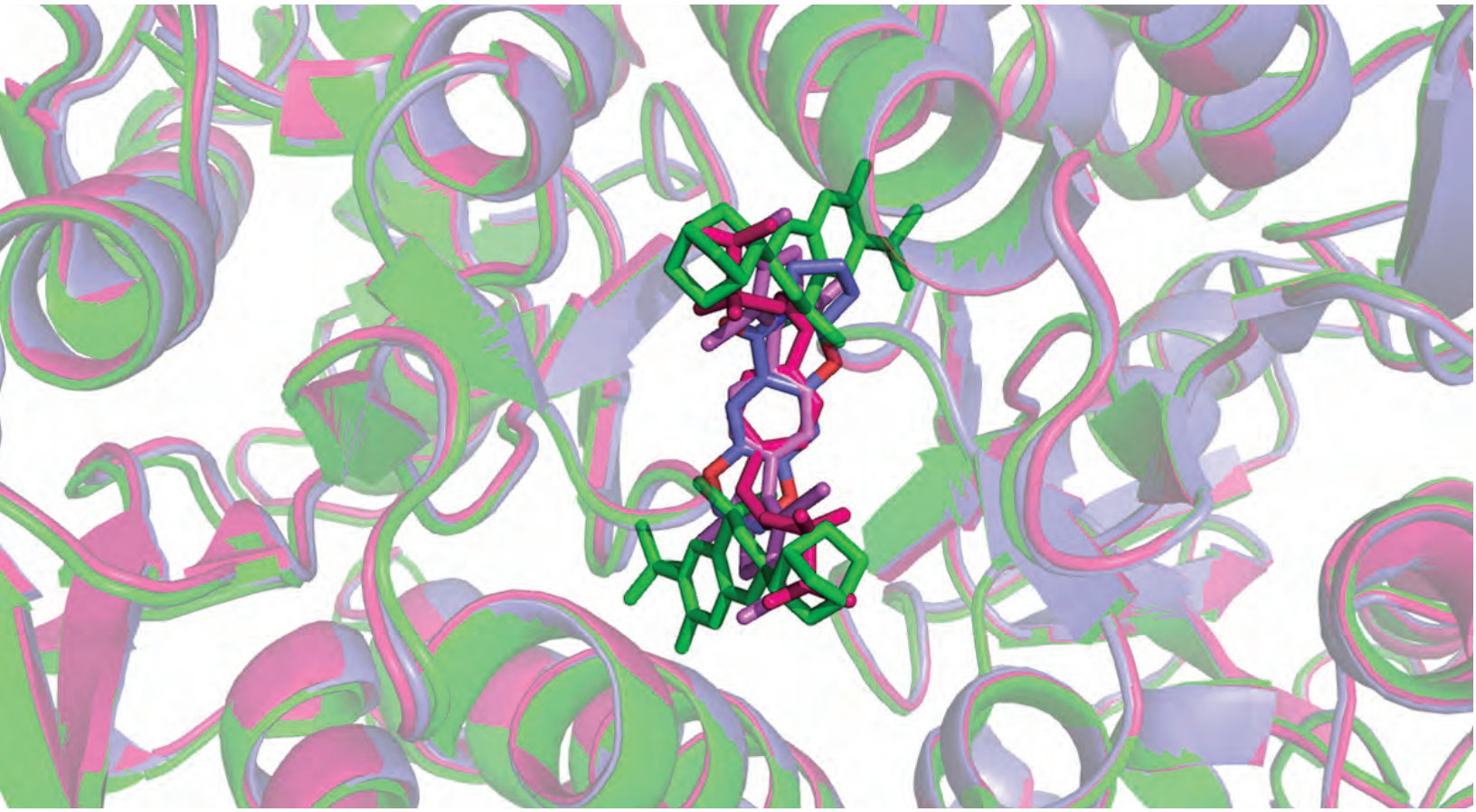

Fig. 1. Computer modeling of overlapping structures of CTZ (green), CX614 (purple), Compound A (dark pink), and Compound B (light pink) binding to the glutamate receptor. Image provided by Jonathan Harms, Doctoral Candidate, Colorado State University.

At the junctions between neuronal cells in the brain, glutamate molecules released by one cell transmit signals to the next cell through complex interactions with receptors that recognize glutamate and relay the message. The strength of the signal is modulated by the level of exposure to glutamate and can be deactivated after brief exposure for the next round of activation. Longer exposure can cause desensitization wherein the receptor must recover before it can be activated again. Current drugs are known to enhance glutamate receptor signaling by modulating this receptor deactivation or desensitization process. Structural studies of two classes of drugs, represented by cyclothiazide (CTZ) and CX614, have shown that these drugs affect glutamate receptor desensitization and deactivation, respectively.

New drug screening and optimization efforts have yielded two new modulators of glutamate receptor signaling. In order to better understand the details of how the two compounds act, the researchers from Colorado State University, Eli Lilly and Company, and the Morehouse School of Medicine built on previous structural information to evaluate the action of these compounds on glutamate receptor signaling and compare their findings to those for CTZ and CX614. Their first approach involved experiments in cells that express one of two forms of the glutamate receptor on their cell membrane to test whether the compounds modulated the action of glutamate when it was added. They found that both compounds enhanced the activity of the receptors on the cells, but one of the compounds had a preference for a specific form of the receptor, referred to as the "flip" variant. Due to the fact that glutamate signaling diseases could be caused by different errors in the way the receptor works, this information could allow physicians to tailor treatments to the individual needs of their patients.

Next, structural studies showed that both compounds bind to the receptor at the same site as CTZ and CX614 but, although their binding sites overlap with those of both CTZ and CX614, they also bind to unique areas of the receptor (Fig. 1). Interestingly, the crystal structures showed that the compounds shared molecular interactions with CX614 that had been hypothesized to account for its effects on receptor deactivation. The structural data is consistent with functional assays that showed that both compounds are more potent and effective than CTZ and CX614, both block desensitization of the receptor, and both slow deactivation of the receptor but in different ways. One compound preferentially slows deactivation of the "flop" form of the receptor while the other preferentially slows deactivation of the flip variant.

With this promising data in hand, the group will continue to focus on learning the structural and functional characteristics of glutamate receptor modulators as a pathway to finding new, more effective compounds that may be turned into drugs. With new and exciting compounds being discovered or synthesized every year by pharmaceutical companies, there is no shortage of hope that this pipeline will produce powerful new treatments for cognitive impairment. *— Sandy Field*

See: David E. Timm[2], Morris Benveniste[3], Autumn M. Weeks[1], Eric S. Nisenbaum[2], and Kathryn M. Partin[1], "Structural and Functional Analysis of Two New Positive Allosteric Modulators of GluA2 Desensitization and Deactivation," Mol. Pharmacol. **80**(2), 267 (2011). DOI:10.1124/mo1.110.070243

Author affiliations: [1]Colorado State University, [2]Eli Lilly and Company, [3]Morehouse School of Medicine
Correspondence: *kathy.partin@colostate.edu

This work was supported by the National Institutes of Health (NIH) National Institute of Mental Health [2801-MH064700-06A2]; and the NIH National Institute of Neurological Disorders and Stroke [S11-NS065883]. Use of the IMCA-CAT beamline 17-ID at the Advanced Photon Source was supported by the companies of the Industrial Macromolecular Crystallography Association through a contract with Hauptman-Woodward Medical Research Institute.Use of the Advanced Photon Source at Argonne National Laboratory was supported by the U. S. Department of Energy Office of Science under Contract No. DE-AC02-06CH11357.

17-ID-B • IMCA-CAT • Life sciences • Macromolecular crystallography, multi-wavelength anomalous dispersion, microbeam, single-wavelength anomalous dispersion • 6-20 keV • On-site, remote, mail-in • Accepting general users •

31-ID-D • LRL-CAT • Life sciences • Macromolecular crystallography, single-wavelength anomalous dispersion, single-crystal diffraction • 4.7-28 keV • Mail-in • Accepting general users •

SENDING A MESSAGE: HOW RECEPTORS TALK TO G PROTEINS

The mechanism by which cells respond to stimuli and trigger hormonal responses, as well as the senses of sight, smell, and taste, has for the first time been brought into focus by researchers from Stanford University, the University of Copenhagen, the University of Michigan, the University of Wisconsin, Vrije Universiteit Brussel, and Trinity College utilizing the GM/CA-CAT beamline 23-ID-B at the APS. This work will pave the way to new research avenues in drug discovery, cell signaling, and cellular regulation. >>>

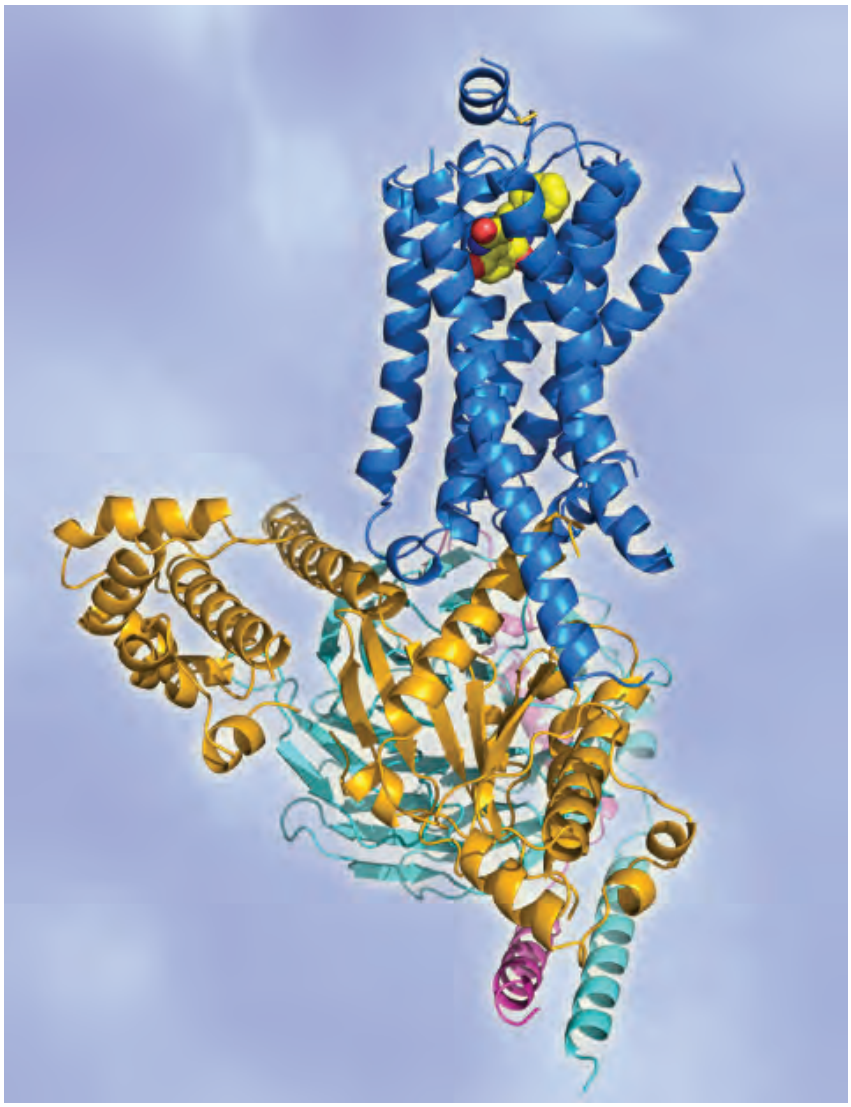

Fig. 1. The structure of the β2AR-Gs complex: The β2AR (blue) occupied by a high affinity agonist (yellow spheres) forms a complex with Gs, the stimulatory G protein for adenylyl cyclase. Gs is composed of three proteins: Gα (gold), Gβ (cyan) and Gγ (purple).

Receiving a signal, interpreting it, and responding correctly are three activities that cells must be good at in order to respond to stimuli. For responding to hormones, and for the senses of sight, smell, and taste, the activated receptors are coupled with G proteins. These G protein-coupled receptors (GPCRs) are involved in a complex set of steps in which an extracellular hormone or neurotransmitter binds to and activates a GPCR in the cell membrane. The activated receptor passes on the signal to a G-protein inside the cell, triggering reactions that ultimately create a cellular response to the stimulus.

The intricacy of this set of reactions has been appreciated—and studied—for some time. What was lacking, however, was a finely-detailed crystal structure of the GPCR as it actually signals across the membrane. The importance of acquiring this knowledge and knowing a lot more about how GPCRs function is apparent when we consider that the human genome contains over 800 GPCR genes.

The structure of protein receptors that are involved in cellular responses to stimuli is available thanks to experiments carried out at the 23-ID-B beamline at the APS, and the process of cell signaling has come into crystal clear focus (Fig. 1). This crystal structure is the first high-resolution look at transmembrane signaling by a GPCR and adds critical insight about signal transduction across the plasma membrane.

The research team studied a specific model system for GPCR signaling that has long been used by biochemists and about which much was already known. In this system, a β2 adrenergic receptor (β2AR) is bound by the outside stimulus, known as an agonist, and then activates Gs, the stimulatory G protein for adenylyl cyclase.

The researchers were able to capture the β2AR bound to the Gs protein before the latter went on to the next step in the dance, which would be binding a nucleotide. One technical challenge, and perhaps the reason that the crystal structure had been so elusive to date, was to create a stable β2AR-Gs complex in detergent solution. Once this problem was solved, the team could proceed to unveiling the crystal structure of this active-state β2AR-Gs complex (Fig. 1).

The new data allowed the research team to construct the early stages of GPCR signaling. Using their own observations, and other data collected on this model system, a mechanism for the initial stages of complex formation came into being. The data provided a pinpoint determination of exactly which changes in the molecules permitted that binding stage to carry on to completion.

Shape changes in the Gs, particularly in the nucleotide-binding pocket, prepared the protein for the next step. In the β2AR, the researchers were able to identify major changes in two areas of the molecule that fit well with understanding of how the β2AR interacts with molecules outside the cell and how the two molecules—β2AR and Gs—interact each other. The researchers note that the minibeam and the rastering capabilities of the GM/CA-CAT beamline were essential for collecting the diffraction data on these crystals.

Future research avenues for the team involve determining how the complex forms and dissociates after activation. *— Mona Mort*

See: Søren G. F. Rasmussen[1,2], Brian T. DeVree[3], Yaozhong Zou[1], Andrew C. Kruse[1], Ka Young Chung[1], Tong Sun Kobilka[1], Foon Sun Thian[1], Pil Seok Chae[4], Els Pardon[5], Diane Calinski[3], Jesper M.Mathiesen[1], Syed T. A. Shah[6], Joseph A. Lyons[7], Martin Caffrey[6], Samuel H. Gellman[4], Jan Steyaert[5],Georgios Skiniotis[7],William I. Weis[1], Roger K.Sunahara[3]**, and Brian K. Kobilka[1]*, "Crystal structure of the β_2 adrenergic receptor–Gs protein complex," Nature **477**, 549 (29 September 2011). DOI:10.1038/nature10361

Author affiliations: [1]Stanford University School of Medicine; [2]University of Copenhagen; [3]University of Michigan Medical School; [4]University of Wisconsin, Madison; [5]Vlaams Instituut voor Biotechnologie; [6]Trinity College; [7]University of Michigan

Correspondence:
*kobilka@stanford.edu,
**sunahara@umich.edu

This work supported by National Institutes of Health Grants NS028471 (B.K.K.) and GM083118 (B.K.K. and R.K.S.), GM56169 (W.I.W.), P01 GM75913 (S.H.G), and P60DK-20572 (R.K.S.), GM75915, P50GM073210 and U54GM094599 (M.C.); Science Foundation Ireland (07/IN.1/B1836) and FP7 COST Action CM0902 (M.C.); the Mathers Foundation (B.K.K. and W.I.W.); the Lundbeck Foundation (Junior Group Leader Fellowship, S.G.F.R.); the University of Michigan Biomedical Sciences Scholars Program (R.K.S.); the Fund for Scientific Research of Flanders (FWO-Vlaanderen) and the Institute for the encouragement of Scientific Research and Innovation of Brussels (ISRIB) (E.P. and J.S.); and The Danish Council for Independent Research, Medical Sciences (J.M.M.). GM/CA-CAT is funded in whole or in part with Federal funds from the NCI (Y1-CO-1020) and the National Institute of General Medical Sciences (Y1-GM-1104). Use of the Advanced Photon Source at Argonne National Laboratory was supported by the U.S. Department of Energy Office of Science under Contract No. DE-AC02-06CH11357.

See also: "Cell signalling: It's all about the structure," by Lizzie Buchen, "naturenews," 24 August, 2011. DOI:10.1038/476387a

23-ID-B • GM/CA-CAT • Life sciences • Large unit cell crystallography, macromolecular crystallography, microbeam, multi-wavelength anomalous dispersion, single-wavelength anomalous dispersion, subatomic (<0.85 Å) resolution • 3.5-20 keV • Remote • Accepting general users •

DOUBLE DUTY: BACTERIAL IMMUNITY AND DNA REPAIR

For some time now, biochemists have been unraveling the complex genetic and metabolic processes that grant immunity. A team of researchers from the University of Toronto, Argonne, and the National Institutes of Health, with the help of the SBC-CAT 19-ID-D beamline at the APS, has provided definitive evidence that a particular enzyme is involved in DNA repair. The team's work supports the argument that certain bacterial genetic elements are involved in both immunity and DNA repair. This work represents a breakthrough in terms of general understanding of these cellular processes and shines light on our understanding of how cells resist enemies and repair damage. >>>

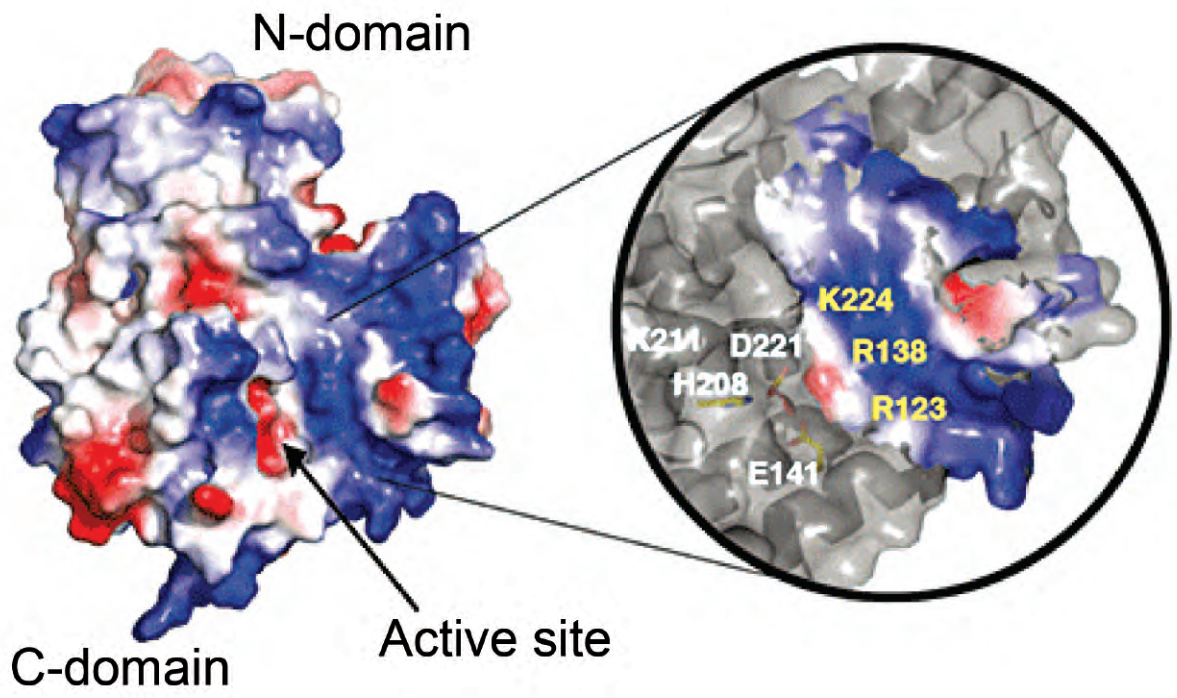

Fig. 1. Crystal structure of YgbT and the potential active site. Left: Surface charge presentation of the YgbT monomer showing the presence of several large basic patches representing potential DNA binding sites (colored in blue). Right: Close-up view of the main basic patch of YgbT located close to the potential active site (E141, H208 and D221) and showing the position of several conserved residues. From M. Babu et al. Mol. Microbiol. ***79,*** 484 (2011). © 2010 Blackwell Publishing Ltd.

All living things have their natural enemies. So it is not surprising to discover that bacteria and eukaryotes have evolved elaborate defenses against the viruses and plasmids that try to invade and destroy them. For some time now, biochemists have been unraveling the complex genetic and metabolic processes that grant immunity. Certain bacterial genetic elements, known as CRISPRs (clustered regularly interspaced short palindromic repeats), and their associated proteins (Cas) confer immunity against viruses and plasmids. That the CRISPR system is probably involved in microbial defense has been clear for some time; some of the spacers in the CRISPR genome resemble sequences from bacteriophage and plasmid genomes and can silence them. But some of the CRISPR spacers were observed to be similar to bacterial genetic sequences, leading to the hypothesis that CRISPR elements could be involved in repair or regulation of the bacterial genome. This potential dual function for the CRISPR system was intriguing, but required proof.

The research team focused on a CRISPR-associated protein called Cas1, which is found in most prokaryotes — single-celled organisms lacking a nucleus, such as bacteria. Though widespread, the actual function of Cas1 was unclear, so it seemed like a good candidate in the search for the second, DNA repair function of the CRISPR system. The team isolated the Cas1 protein of the bacterium *Escherichia coli*, called YgbT, and found it to be a nuclease — it was able to degrade DNA sequences that would be involved in DNA repair, such as Holliday junctions and replication forks.

The researchers went on to discover the potential active site of YgbT by obtaining its crystal structure and performing site-directed mutagenesis (Fig. 1). The team then used genome-wide screens to show that YgbT interacts, both physically and genetically, with key elements of the *E. coli* DNA repair system.

To further substantiate the role of YgbT in DNA repair, the researchers deleted its gene in a strain that then exhibited greater sensitivity to DNA damage, thus demonstrating the importance of YgbT to the DNA repair systems. Similar sensitivity to DNA damage was observed when the CRISPR clusters were deleted, suggesting that YgbT performs its DNA repair role by interacting with the CRISPRs. Since three Cas1 proteins from different organisms showed slightly distinct biochemical behavior and low sequence similarity, further research would investigate whether members of a group of Cas1 proteins have varying functions.

When taken together, results of the work carried out by the research team allowed them to characterize YgbT as a new, structurally distinct type of nuclease that is capable of acting on branched DNAs, as well as linear strands of DNA and RNA. YgbT appears to be a generalist in that it is capable of cleaving a broad range of branched DNAs and, because of its ability to cleave flap sequences, may represent a new group of flap endonucleases. Because of its demonstrated role in DNA repair and its association with the CRISPR-Cas system, YgbT provides strong evidence that the CRISPR-Cas system is involved in both its well-known role of anitviral immunity and its newly demonstrated role of DNA repair.

Interestingly, the DNA repair role of the CRISPR system had been proposed at one time solely on the basis of its enzyme components. But when the similarity between CRISPR spacers and viral genomes was discovered, immunity became the favored role for the CRISPR system. Now that an important DNA repair role has been discovered for a Cas protein, supporting the idea of a dual role for the CRISPR-Cas system, we may be looking at a biochemical system that evolved in concert to provide both DNA repair and defense against viruses. The present data shines much light on our understanding of how cells resist enemies and repair damage.

— Mona Mort

See: See: Mohan Babu[1], Natalia Beloglazova[1], Robert Flick[1], Chris Graham[1], Tatiana Skarina[1], Boguslaw Nocek[2], Alla Gagarinova[1], Oxana Pogoutse[1], Greg Brown[1], Andrew Binkowski[2], Sadhna Phanse[1], Andrzej Joachimiak[2], Eugene V. Koonin[3], Alexei Savchenko[1], Andrew Emili[1], Jack Greenblatt[1], Aled M. Edwards[1,2], and Alexander F. Yakunin[1]*, "A dual function of the CRISPR–Cas system in bacterial antivirus immunity and DNA repair," Mol. Microbiol. **79**, 484 (2011). DOI:10.1111/j.1365-2958.2010.07465.x

Author affiliations: [1]University of Toronto, [2]Argonne National Laboratory, [3]National Institutes of Health

Correspondence:

*a.iakounine@utoronto.ca

This work was supported by the Government of Canada through Genome Canada and the Ontario Genomics Institute (J.G., A.E. and A.F.Y.; 2009-OGI-ABC-1405), by the Canadian Institutes of Health Research Grant CIHR 82852 (to J.G. and A.E.), by the National Institutes of Health Grant GM074942 (to A.J.), and by the U.S. Department of Energy (DOE) Office of Biological and Environmental Research, under contract DE-AC02-06CH11357 (to A.J.). E.V.K. is supported by the intramural funds of the U.S. Department of Health and Human services (NIH, National Library of Medicine). The Structural Biology Center at Argonne is operated by UChicago Argonne, LLC, for the U.S. Department of Energy under contract DE-AC02-06CH11357. Use of the Advanced Photon Source at Argonne National Laboratory was supported by the DOE's Office of Science under Contract No. DE-AC02-06CH11357.

19-ID-D • SBC-CAT • Life sciences • Large unit cell crystallography, macromolecular crystallography, microbeam, multi-wavelength anomalous dispersion, single-wavelength anomalous dispersion, subatomic (<0.85 Å) resolution, ultra-low-temperature (15K) • 6.5-19.5 keV • On-site, remote, mail-in • Accepting general users •

IT TAKES A WELL-TAILORED ENZYME TO BREAK THE FLUORIDE BOND

Fluorinated compounds are widely used in industrial applications. They can be found in 20% of pharmaceuticals and up to 30% of agrochemicals. Because fluorine forms the strongest known bond to carbon, fluorinated organics are valued for being inert, hydrophobic, and in some cases, lipophobic. But these same characteristics make large-scale production and use of organofluorines open to debate about toxicity, ozone depletion, and bioaccumulation. Although the special properties of the carbon-fluorine bond have been known for some time, details are needed about how only a few selected enzymes are able to break this bond. A research team set out to map the reaction process by which defluorination occurs. The work, which relied heavily on the BioCARS 14-BM-C and SBC-CAT 19-ID-D beamlines at the APS, provides a detailed and thorough view of the reaction sequences leading to enzymatic defluorination. Armed with these details about the necessary reaction conditions, new enzymes might be constructed that would improve synthesis, biodegradation, disposal, and regulatory strategies for the growing markets of organofluorines. >>>

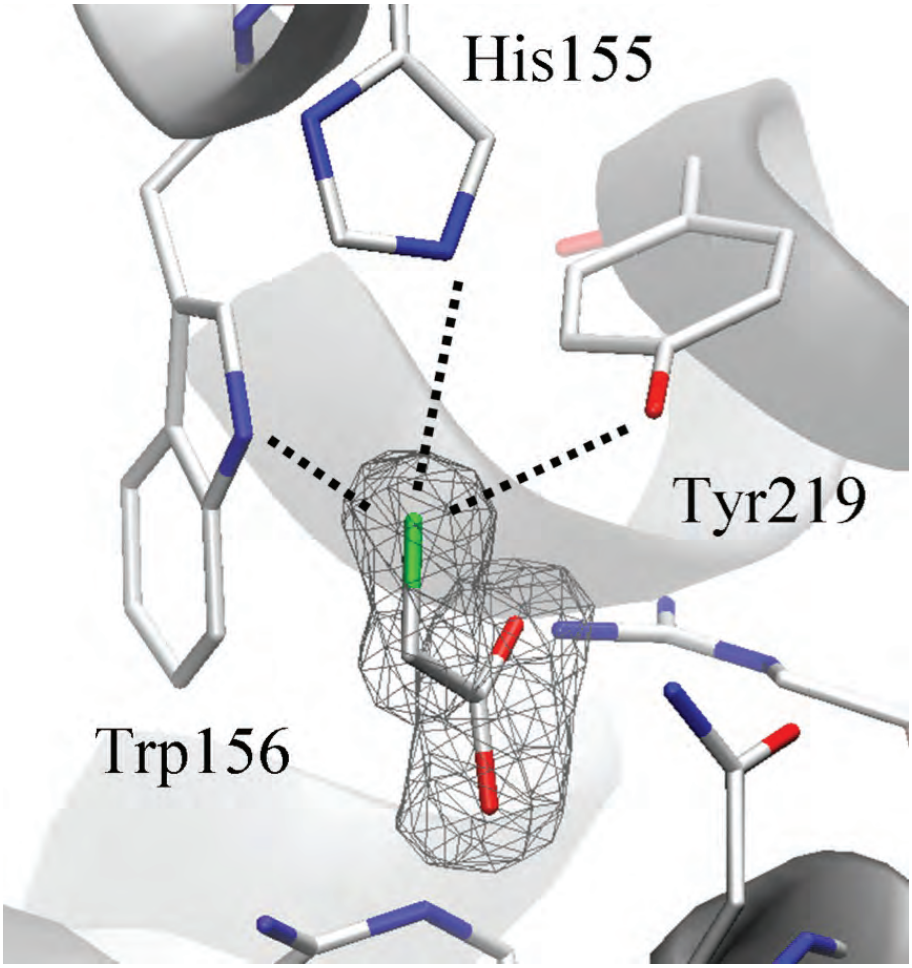

Fig. 1. Crystal structure: Michaelis complex of the fluoroacetate dehalogenase from *Rhodopseudomonas palustris*. The intact fluoroacetate substrate is trapped in the active site of the defluorinase using an inactive mutant, revealing the three important interactions between the halide pocket and the fluorine atom in green.

The carbon-fluorine bond is strong — the strongest known in natural products — because of the high electronegativity of fluorine, which polarizes and strengthens the bond. Adding to the difficulty of breaking this bond is the somewhat poor accessibility of the valence electrons in the bonded fluorine atom. Although structural insights on the enzymatic breakdown of weaker carbon-halogen bonds are already available, exactly how the strong carbon-fluorine bond is broken remains largely a mystery. The research team in this study, from the University of Toronto and the Ontario Cancer Institute concentrated on a group of enzymes called "fluoroacetate dehalogenases," which possess the rare ability of being able to hydrolyze the carbon-fluorine bond under normal physiological conditions. Previous work had pointed the way toward focusing on the spatial constraints arising from the shape of the enzyme, in particular the binding pocket.

The researchers searched through the genomes of a number of microbes and discovered several fluoroacetate dehalogenases. One of them was found in the photosynthetic bacterium *Rhodopseudomonas palustris*, already well known for its metabolic versatility and bioremediation potential. The team then obtained high-resolution crystal structures of this fluoroacetate dehalogenase as it stepped along the defluorination pathway. They were able to observe the enzyme in its free state, then bound to intermediates, and finally bound to product. By following the enzyme through these biochemical stages, the researchers could construct a mechanism by which defluorination occurred and, at the same time, collect important details about reaction conditions and spatial associations that will prove extremely useful in the future design of defluorinating enzymes.

The researchers confirmed that a halide pocket on the dehalogenase is necessary for enzymatic defluorination (Fig. 1). This pocket provides three hydrogen bonds to stabilize the fluoride ion. The enzyme's pocket also seems to be custom made for fitting the small fluoride ion in such a way that explains how this dehalogenase selectively operates on fluorinated compounds. Even though other suitable substrates would involve breaking a weaker carbon-halogen bond, the enzyme shows a marked preference for breaking the carbon-fluorine bond.

The researchers also evaluated structural intermediates of the enzyme-substrate complex to provide a step-by-step picture of how the dehalogenase performs its awesome feat of defluorination. Very detailed descriptions about how the molecules move in relation to each other are now available. By introducing mutations that enlarged the size of the halide pocket, the team was able to change the enzyme's substrate specificity such that it now preferentially operates on compounds that contain chlorine and bromine over those with fluorine. Thus, the particular spatial and molecular attributes of the pocket largely determine its preference for fluorinated compounds.

The researchers have demonstrated that an enzyme capable of defluorination can do so only after close and precise positioning of the compound containing the small fluoride ion. The beauty of this very specific reaction, though, is that the enzyme can carry out the work of breaking the strong carbon-fluorine bond without external energy input. This is in contrast to other strong bonds in nature, such as nitrogen-carbon and nitrogen-nitrogen triple bonds, where the catalytic enzymes require energy input. Biotechnologists can use this newfound knowledge about defluorinating enzymes to develop sustainable management and disposal procedures for fluorinated organic compounds.

— Mona Mort

See: Peter W. Y. Chan[1,2], Alexander F. Yakunin[1], Elizabeth A. Edwards[1], and Emil F. Pai[1,2]*, "Mapping the Reaction Coordinates of Enzymatic Defluorination," J. Am. Chem. Soc. **133**, 7461 (2011). DOI:10.1021/ja200277d

Author affiliations: [1]University of Toronto, [2]Ontario Cancer Institute/The Campbell Family Cancer Research Institute

Correspondence:
*pai@hera.med.utoronto.ca

The research was supported by the Natural Sciences and Engineering Research Council of Canada through a graduate scholarship (P.W.Y.C.) and operating grants (E.A.E. and E.F.P.) and by the Canada Research Chairs Program (E.F.P.). BioCARS is funded by the National Center for Research Resources of the National Institutes of Health (grant RR007707). Use of the Advanced Photon Source at Argonne National Laboratory was supported by the U. S. Department of Energy Office of Science under Contract No. DE-AC02-06CH11357.

14-BM-C • BioCARS • Life sciences • Macromolecular crystallography, fiber diffraction, biohazards at the BSL2/3 level, subatomic (<0.85 Å) resolution, large unit cell crystallography • 8-14.9 keV • On-site • Accepting general users •

19-ID-D • SBC-CAT • Life sciences • Large unit cell crystallography, macromolecular crystallography, microbeam, multi-wavelength anomalous dispersion, single-wavelength anomalous dispersion, subatomic (<0.85 Å) resolution, ultra-low-temperature (15K) • 6.5-19.5 keV • On-site, remote, mail-in • Accepting general users •

BACTERIA, DISEASE, AND SCAFFOLDING

Bacteria are masters at creating, and sustaining, disease in humans. Witness recent outbreaks of *E. coli* and *Salmonella* food poisoning. How certain bacterial strains are able to consistently thwart therapeutic breakthroughs is a question that has long occupied biochemists. Accumulated evidence hinted at a bacterial pathogen's ability to influence cellular scaffolding that served as the cell's route to normal biochemical pathways for processes such as cell polarity, adhesion, receptor trafficking, and protein secretion. But the actual details of how the bacteria could accomplish this feat remained elusive — until now. Thanks to the work performed by a research team aided by the SBC-CAT beamlines 19-BM-D and 19-ID-D at the APS, exciting new details have emerged about how bacteria change the cells they invade, and could lead to an understanding of how bacteria create disease, thereby opening new pathways for inventing anti-bacterial therapies. >>>

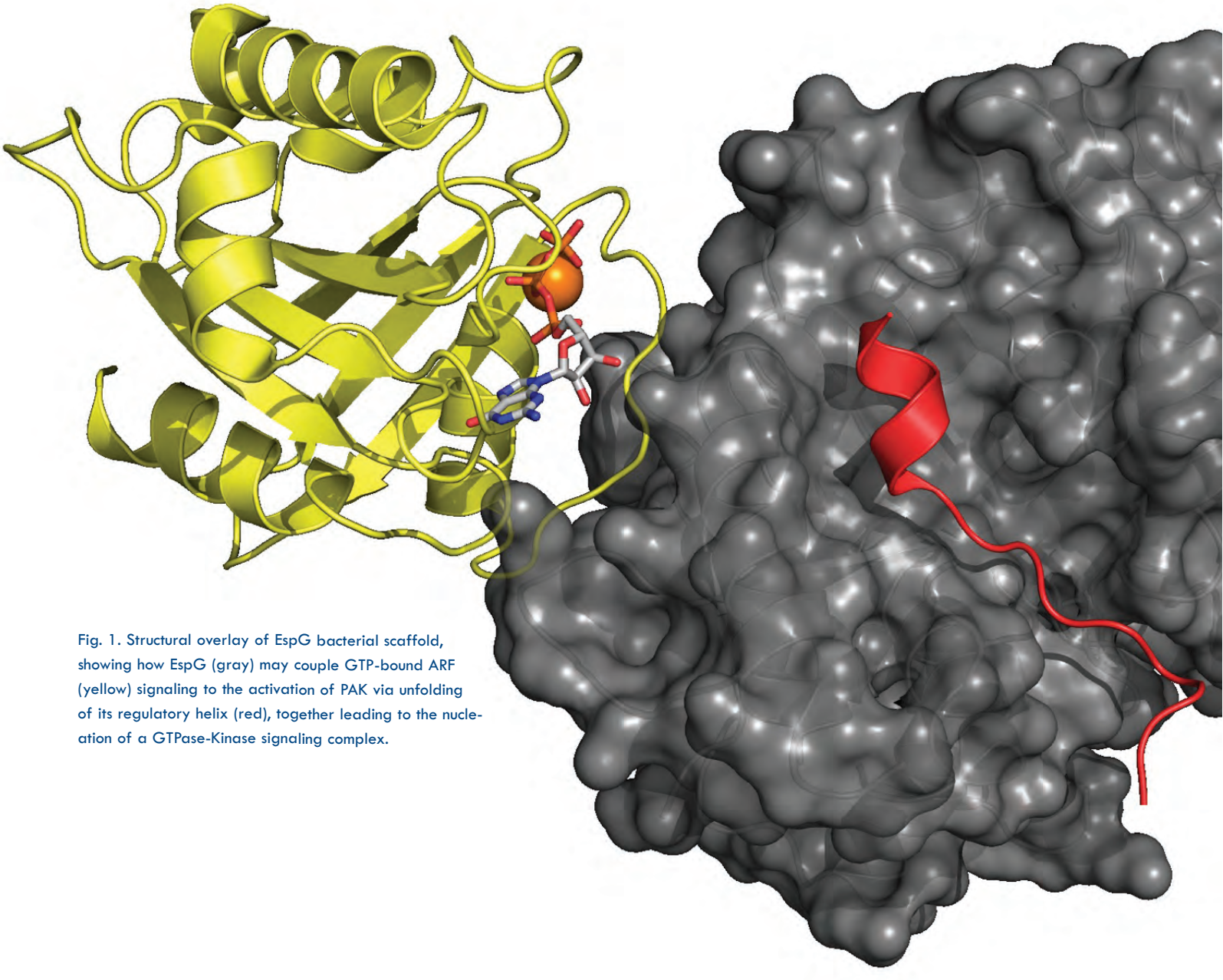

Fig. 1. Structural overlay of EspG bacterial scaffold, showing how EspG (gray) may couple GTP-bound ARF (yellow) signaling to the activation of PAK via unfolding of its regulatory helix (red), together leading to the nucleation of a GTPase-Kinase signaling complex.

To investigate how bacterial pathogens affect cellular signalling networks, the researchers from the University of Texas Southwestern Medical Center focused on an enterohaemorrhagic strain of *Escherichia coli*. In this strain of *E. coli*, the researchers identified a protein called EspG, known as an effector protein, and found that it regulated trafficking within the cell's membrane. They were also able to identify the host cell's molecules that EspG acted upon: ADP-ribosylation factor (ARF) GTPases and p21-activated kinases (PAKs). When the team looked at the crystal structure of EspG in complex with ARF6, they discovered that, by blocking GTPase Activating Protein-assisted hydrolysis, EspG was very effective at disrupting normal signalling at organelle membranes. The crystal structure of EspG in complex with a region of PAK2 revealed another new discovery: EspG has a catalytic site, previously unknown in a bacterial effector, which allows it to participate in kinase activation. Perhaps the most structurally convergent result: ARF and PAKs were found on adjacent surfaces of EspG, suggesting that EspG can act as its own "catalytic scaffold" while bypassing the cell's normal signalling scaffolding (Fig. 1).

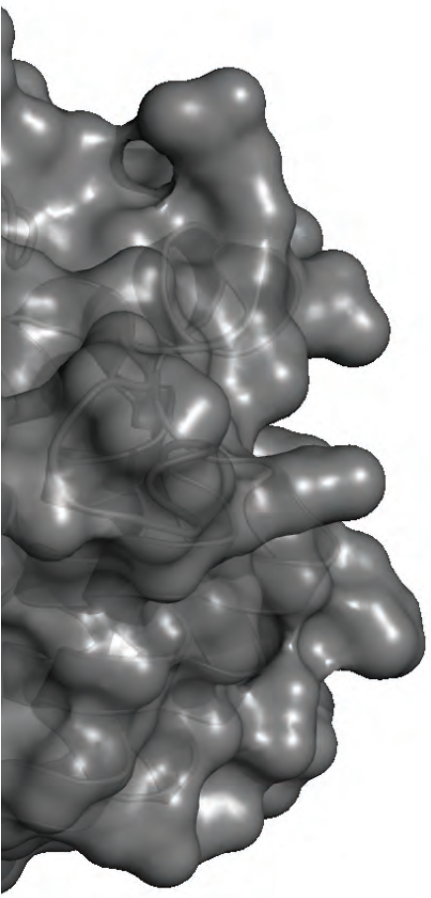

In order to get to the point where they could understand the specific role of EspG, the research team started by identifying new signalling pathways targeted by bacterial pathogens. They tagged bacterial effector proteins with Green Fluorescent protein and tracked them to host organelles. In one extracellular pathogenic *E. coli* strain, which they continued to study, they found several type III effectors that interfered with host trafficking events. In contrast, strains of intracellular pathogens, such as *Salmonella* and *Legionella*, showed very little of that type of activity. Thus, in EspG, the researchers identified a new type of bacterial signalling protein that is able to affect cargo transfers in membrane organelles. Using combined structural and cellular studies, the team described a mechanism by which bacterial pathogens can regulate membrane trafficking: EspG directly inhibits ARF guanine nucleotide turnover on host membranes and, by doing so, prevents vesicle transport. In investigating interactions between EspG and PAK, the scientists discovered catalytic machinery in EspG that appears to be unique to bacteria.

General implications arise from the research team's work on EspG, which is part of a family of type III effector proteins secreted by a diverse array of bacterial pathogens. EspG shows structural homology with VirA (from *Shigella flexneri*), suggesting that VirA may also serve as an enzyme scaffold, though it may not affect the same signalling pathways as EspG. And the presence in EspG of two unique pathogenic activities—ARF GTPase inhibition and PAK stimulation—provide little doubt that pathogenic bacteria can control signalling events and override the host cell's own signalling systems. What had been surmised about how bacteria create diseased cells by disrupting host-signalling systems is now clearly described by structural and metabolic data. Next steps will include looking for roles of EspG and related bacterial effector proteins in disrupting additional cellular processes, with an eye toward creating therapies that will thwart the ability of the bacteria to cause disease. *— Mona Mort*

See: Andrey S. Selyunin, Sarah E. Sutton, Bethany A. Weigele, L. Evan Reddick, Robert C. Orchard, Stefan M. Bresson, Diana R. Tomchick, and Neal M. Alto*, "The assembly of a GTPase–kinase signalling complex by a bacterial catalytic scaffold," Nature **469**, 107 (6 January 2011). DOI:10.1038/nature09593

Author affiliation: University of Texas Southwestern Medical Center
Correspondence:
*neal.alto@utsouthwestern.edu

This work was supported by the Welch Foundation (#I-1704) and a grant from the National Institues of Health (NIH) National Institute of Allergy and Infectious Diseases; 1RO1AI083359-01) to N.M.A. R.C.O. was supported by a NIH Molecular Microbiology training grant (5T32AI007520-12). The Structural Biology Center Argonne is operated by UChicago Argonne, LLC, for the U.S. Department of Energy (DOE) under contract DE-AC02-06CH11357. Use of the Advanced Photon Source at Argonne National Laboratory was supported by the U.S. DOE Office of Science under Contract No. DE-AC02-06CH11357.

19-BM-D • SBC-CAT • Life sciences, ultra-low-temperature (15K), multi-wavelength anomalous dispersion, single-wavelength anomalous dispersion • 6-13.5 keV • On-site, mail-in • Accepting general users •

19-ID-D • SBC-CAT • Life sciences • Large unit cell crystallography, macromolecular crystallography, microbeam, multi-wavelength anomalous dispersion, single-wavelength anomalous dispersion, subatomic (<0.85 Å) resolution, ultra-low-temperature (15K) • 6.5-19.5 keV • On-site, remote, mail-in • Accepting general users •

SPEEDY SIGNALLING IN NEURONS

Fast. That is the description applied to how information is transmitted in the nervous system. Very fast is the term especially applicable to inhibitory neurotransmission, where it takes only milliseconds for a signal to travel across the junction between two nerve cells, the synapse. The high speed at which this inhibition occurs points to a complex biochemical system whose importance has been known for over a century, but the details of which have proved difficult to pin down. Knowing more about this neuronal process is essential to understanding the mechanisms by which therapies work, such as anaesthetics, sedatives, and ivermectin, the latter of which is used to treat the disease River Blindness. By studying how ivermectin and other modulators of inhibitory neurotransmission bind to receptors, researchers from the Oregon Health and Science University, with help from the NE-CAT beamline 24-ID-C at the APS, unveiled exciting new details about this process. Their data provide essential information, especially about a previously uncharacterized binding site, that can be used in drug design and new therapies.

The researchers focused on how inhibitory neurotransmitters bind to receptors from the Cys-loop family, receptors that consist of five subunits and are found in the neuron's membrane. When the neurotransmitter binds to the receptor, the receptor changes shape. That change in shape opens up a chloride-ion channel that produces a dampening in neuronal excitability, thereby causing the inhibitory effect. There were no high-resolution structural data for this particular type of Cys-loop receptor, called an anion-selective receptor, nor was the chloride selection mechanism clear. The therapeutic importance of these chloride channels arises because they are associated with the activity of benzodiazepines, barbiturates, some anaesthetics, alcohol, strychnine, picrotoxin, and ivermectin. To learn exactly what was happening during this series of mega-fast events, the research team studied an inhibitory anion-selective Cys-loop receptor from the nematode worm *Caenorhabditis elegans*.

The researchers produced the first known three-dimensional structure of an inhibitory Cys-loop receptor, the *C. elegans* glutamate-gated chloride channel α (GluCl). The team examined the x-ray structure of GluCl in complex with ivermectin, and also with the endogenous neurotransmitter L-glutamate and the open channel blocker picrotoxin (Fig. 1). They found that ivermectin stabilizes an open-pore formation by binding in the receptor's transmembrane domain. Glutamate binding occurs in the extracellular agonist site at the receptor's subunit interfaces and picrotoxin acts by blocking the pore near its cystolic base. Because picrotoxin is an open-channel blocker, the researchers were able to use these results to support the hypothesis that the pore was in an open conformation.

The structural data on GluCl allow a detailed and clear understanding of how fast inhibitory neurotransmission works and how shape-changes in Cys-loop receptors make it possible. In particular, the data point to two shape changes when ivermectin binds to GluCl. First, the receptor changes shape locally in the region of the binding site. Second, a large-scale change in shape occurs when the receptor switches from its closed, resting state to its open, activated state. By examining the crystal structure of GluCl, the team was able to show that the ion channel is activated by ivermectin.

To understand how the ion channel selectively uses chloride, the researchers analyzed the surface electrostatics of the GluCl crystal structure. They found that none of the amino acids lining the pore has a formal charge. They also found that selectivity for chloride was probably mediated by pore constriction and a positive electrostatic potential, arising from the orientation of helical dipoles. Additional data collected by the team were used to propose general principles of ion selectivity in Cys-loop receptors.

Besides providing much insight into why inhibitory neurotransmission is so fast, the structural data provide a map of a previously undescribed protein-lipid binding site and define a biochemical scaffold that can be used for design of new pharmaceuticals. The data also allow the research team to propose a similar mode of action in other Cys-loop receptors interacting with lipids, such as neurosteroids and cholesterol. *— Mona Mort*

See: Ryan E. Hibbs[1] and Eric Gouaux[1,2]*, "Principles of activation and permeation in an anion-selective Cys-loop receptor," Nature **474**, 54 (2 June 2011).
DOI:10.1038/nature10139
Author affiliation: Oregon Health and Science University
Correspondence: *gouauxe@ohsu.edu

This work supported by a National Institutes of Health (NIH) National Research Service Award (F32NS061404) to R.E.H. E.G. is an investigator with the Howard Hughes Medical Institute. NE-CAT is supported by grants from the National Center for Research Resources (5P41RR0 15301-10) and the National Institute of General Medical Sciences (8 P41 GM103 403-10) from the NIH. Use of the APS at Argonne was supported by the U.S. DOE Office of Science under Contract No. DE-AC02-06CH11357.

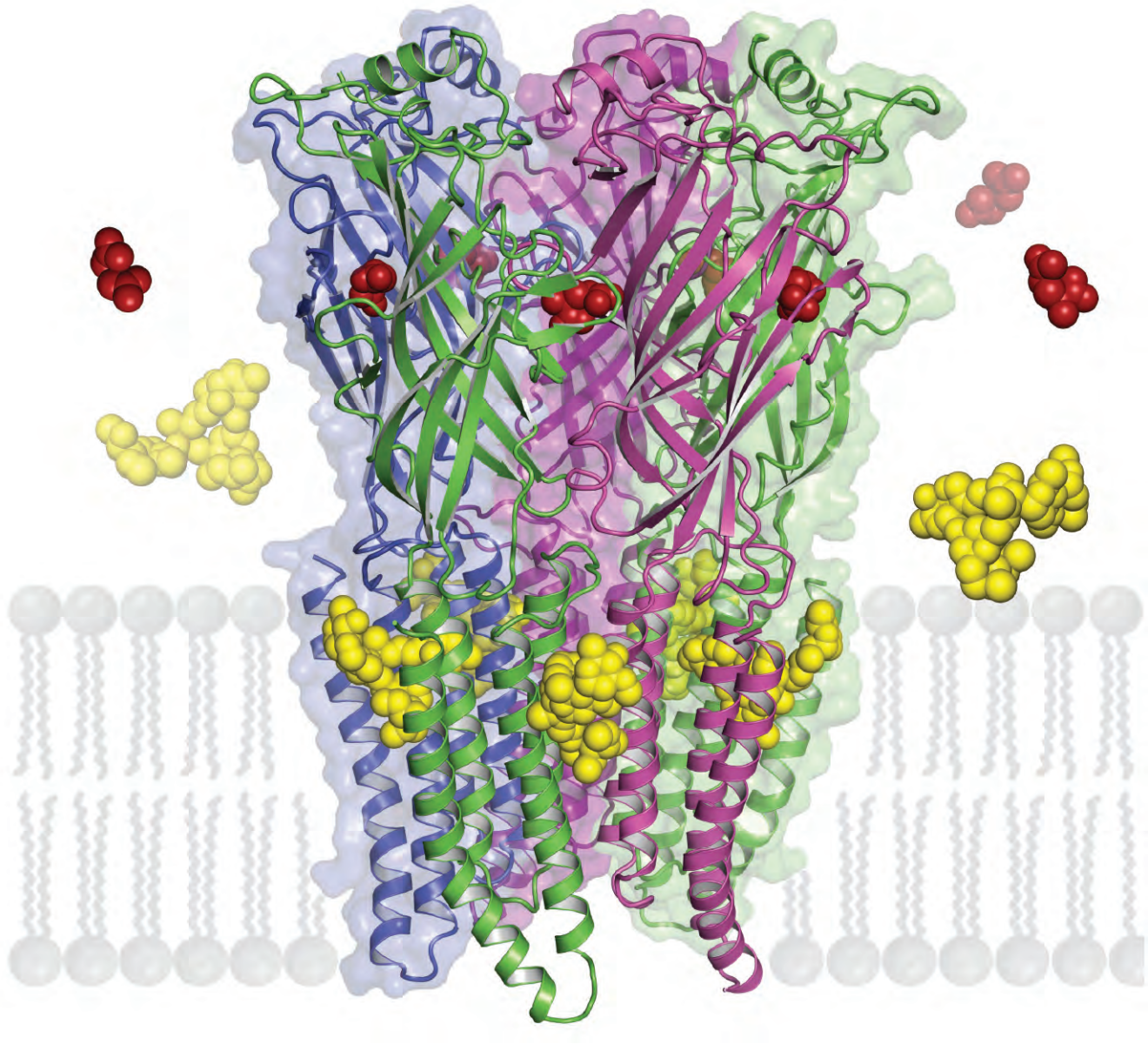

Fig. 1. The glutamate-gated chloride channel α from C. *elegans* sits in cell membranes and mediates fast inhibitory neurotransmission. This first x-ray structure of a eukaryotic pentameric ligand-gated ion channel, or "Cys-loop" receptor, provides an atomic-resolution snapshot of receptor modulation by the therapeutic compound ivermectin (yellow) and by the endogenous neurotransmitter L-glutamate (red). Figure by Ryan Hibbs.

24-ID-C • NE-CAT • Life sciences • Macromolecular crystallography, microdiffraction, single-wavelength anomalous dispersion, single-crystal diffraction, microbeam • 6.5-23 keV • On-site • Accepting general users •

WHO GOES THERE? RECOGNIZING CELLULAR ENEMIES

If a cell wants to stay healthy, it must find ways to distinguish between its own molecules and those of foreign invaders. This is especially true for invading viruses, which are notorious for finding ways to subvert a cell's defense mechanisms. It is not surprising, then, that both the cell and its pathogens have developed elaborate biochemical recognition systems for detecting its own and thwarting what is not its own. One such recognition system is specific to differentiating between the cell's RNA and that of an invading pathogenic virus. Once the viral RNA has been detected, an intricate cellular signalling cascade is set into motion, resulting in an antiviral immune defense reaction. Understanding exactly how this complex biochemical process works is critical to knowing how innate immunity aids in fighting viral infection. Important new structural data on this complex process are now available, thanks to a research team aided by three synchrotron light sources, including the LRL-CAT 31-ID-D beamline at the APS.

The research team from Rutgers University, the University of Medicine & Dentistry of New Jersey-Robert Wood Johnson Medical School, and the University of Washington focused on a biochemical system in which a gene called retinoic-acid-inducible gene-I (RIG-I, also known as DDX58) is a cytoplasmic receptor that distinguishes between viral and cellular RNA by recognizing pathogenic-associated molecular pattern (PAMP) motifs. The RIG-I gene is activated by both double-stranded and single-stranded-RNA only if those molecules are marked by certain additional strings of molecules, such as phosphates. RIG-I is an important gene—when it binds to PAMP motifs, it starts a signalling cascade that triggers the cell's own immune defenses and inflammatory responses to produce an antiviral state. Not surprisingly, then, what goes on in the RIG-I pathway is highly controlled by the cell. If the RIG-I pathway is not working properly, cellular biochemistry goes awry, possibly leading to cell death, inflammation, autoimmune diseases, and cancer.

Two specific areas of the RIG-I gene, called the helicase and repressor domains, are particularly important to its proper functioning. These domains recognize certain forms of double-stranded and single-stranded RNA. And it is this recognition that activates the next stage in the signaling process. The research team was particularly interested in discovering how the helicase and repressor domains acted together to allow RNA binding and how ATP hydrolysis led to RIG-I activation. To obtain answers to these questions, the team determined the structure of human RIG-I helicase-repressor domain in complex with double-stranded RNA and an ATP analog.

The native data set was recorded at the 31-ID-D beamline. Data from iodouridine derivative crystals were collected at the Cornell High Energy Synchrotron Source (CHESS) F1 beamline; SAXS data were collected at the CHESS beamline G1. The single-wavelength anomalous dispersion data set was collected at the National Synchrotron Light Source beamline X29. This structural data allowed the research team to see that the helicase-repressor domain forms a ring around double-stranded RNA, capping one end (Fig. 1). The team discovered a previously unknown motif of the domain, used to recognize both strands of the RNA. The team then went on to use small-angle x-ray scattering, limited proteolysis, and differential scanning fluorimetry to show that the RIG-I conformation is extended and flexible and compacts when it binds RNA.

The research team synthesized their results into a clear view of how helicase plays a role in double-stranded RNA recognition, how the repressor and helicase domains interact for RNA binding, and how full-length RIG-I is bound to double-stranded RNA. Their data also show that RIG-I changes shape when it binds RNA. The structural data obtained by the research team support a mechanism by which double-stranded RNA moves without unwinding. The data will also have a broader impact because they reveal important biochemical details that can be used to better understand RNA interference and DNA repair, which use similar helicase domains.

Taken together, the structural details provide much-needed insight into critical steps of a cell setting into motion its innate immunity, vital if the cell is to successfully battle invaders. Understanding how to keep cells healthy just got a whole lot easier.

— Mona Mort

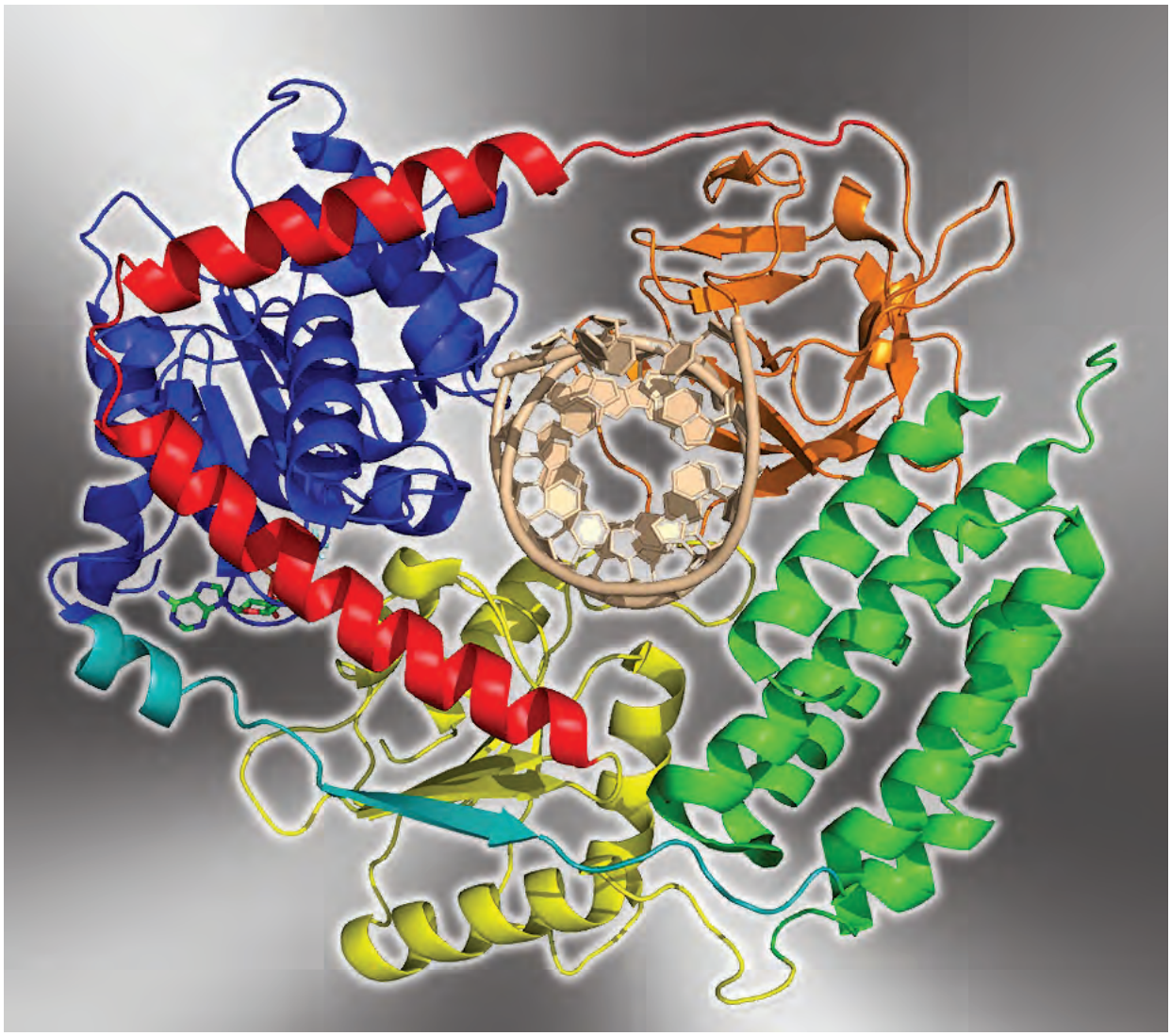

Fig. 1. Ribbon diagram of the RIG-I domains and linkers (teal and orange) surrounding strands of RNA (beige).

See: Fuguo Jiang[1], Anand Ramanathan[2]*, Matthew T. Miller[1], Guo-Qing Tang[2], Michael Gale, Jr.[3], Smita S. Patel[2]**, and Joseph Marcotrigiano[1]*, "Structural basis of RNA recognition and activation by innate immune receptor RIG-I," Nature **479**, 423 (2011). DOI:10.1038/nature10537

Author affiliations: [1]Rutgers University, [2]University of Medicine & Dentistry of New Jersey-Robert Wood Johnson Medical School, [3]University of Washington School of Medicine

Correspondence:
*jmarco@cabm.rutgers.edu,
**patelss@umdnj.edu

This work was supported by NIH grants GM55310 to S.S.P. and AI080659 to J.M. LRL-CAT is operated by Eli Lilly & Company. Use of the Advanced Photon Source at Argonne National Laboratory was supported by the U.S. Department of Energy Office of Science under Contract No. DE-AC02-06CH11357.

31-ID-D • LRL-CAT • Life sciences • Macromolecular crystallography, single-wavelength anomalous dispersion, single-crystal diffraction • 4.7-28 keV • Mail-in • Accepting general users •

DECODING THE MYSTERIES OF NON-CODING RNA

The central dogma of biology states that DNA is transcribed into messenger RNA, which is then translated into protein. Proteins, with all of their relative structural and functional complexity, have been considered to be the primary "active" molecules in biological organisms, while DNA and RNA provide information storage. Evidence has been mounting that scientists were missing a big part of the picture. Various genome projects have shown that only a small portion of the DNA of complex organisms codes for proteins, but a large percentage of DNA is nonetheless transcribed. This has led to increased understanding of the role of non-coding RNA in cells, including the fact that much of what was referred to as "junk" DNA actually codes for RNA molecules that adopt three-dimensional structures and regulate all kinds of cellular processes. Unfortunately, the chemical nature of these RNA molecules makes them challenging to crystallize for structural determinations that would provide insight into how they work. Researchers, with help from the LS-CAT beamline 21-ID-D at the APS, have developed a new protein chaperone that facilitates RNA crystallization. Their work provides structural information on the RNA of interest, the class I ligase ribozyme, and more importantly, their portable chaperone can be used to crystallize other non-coding RNAs, opening the door for greater understanding of this exciting role for RNA.

To overcome the significant challenges of crystallizing and phasing RNA molecules, the researchers developed the idea for an approach based on two concepts that have been applied to protein and RNA crystallography to facilitate the formation of crystals. First, it has been shown that antibody fragments that recognize a protein can stabilize that protein and make it more likely to form crystals. Second, an RNA-binding protein called U1A has been successfully used as a chaperone that favors the formation of crystals of RNA for structure determinations. Combining these two ideas, they decided to make an antibody fragment that recognizes an RNA molecule to see if it would act as a chaperone to facilitate its crystallization.

The first challenge for the team was to generate an antibody that recognized the ligase ribozyme with high enough affinity to act as a chaperone. Using recently developed phage display methodologies that allow the production of "synthetic" antibodies without host immunization, they first generated a set of antibodies that recognized the ribozyme. Picking the best candidate, they then increased its affinity through cycles of selection and enrichment to ensure that it had sufficient affinity to act as a chaperone. This candidate RNA/antibody complex was then tested in functional assays. This is important because if the antibody chaperone binds to the RNA but does not change its activity, that is a good indicator that the association does not change its structure. Testing confirmed that their candidate antibody did not change the activity of the ligase ribozyme and suggested that the structural integrity of the ribozyme was maintained in the complex.

The new antibody chaperone enabled the team to crystallize the ligase ribozyme/antibody complex and determine its three-dimensional structure (Fig. 1). Initial molecular replacement of the antibody portion, for which the structure was already known, also facilitated phasing of the ribozyme portion making the refinement of the structure to 3.1 Å straightforward. In addition to defining important catalytic features of the ligase ribozyme, the structure of the complex showed that the antibody recognized portions of the P7 backbone and the P5 loop of the ribozyme. Based on this success, the team was interested in whether this recognition site could be used to crystallize other RNAs.

They used isolated pieces of RNA with the same sequence as the P7 and P5 hairpin loops to determine that the antibody chaperone did not require the full structure of the ligase ribozyme for recognition and, in fact, did not need the P7 interaction either. Antibody binding could be narrowed down to just the P5 hairpin loop. Best of all, when they took that small P5 loop sequence and engineered it into another RNA sequence, their antibody chaperone bound that RNA with the same affinity as it had the ligase ribozyme, suggesting that this portable P5 loop and antibody combination can be engineered into other RNAs and used to facilitate their crystallization too. Will the researchers use their new tool to clear the bottleneck of RNA structures? That's the plan. — *Sandy Field*

See: Yelena Koldobskaya[1], Erica M Duguid[1], David M Shechner[2,3,‡], Nikolai B Suslov[1], Jingdong Ye[4], Sachdev S Sidhu[5], David P Bartel[2,3], Shohei Koide[1], Anthony A Kossiakoff[1]**, and Joseph A Piccirilli[1]*, "A portable RNA

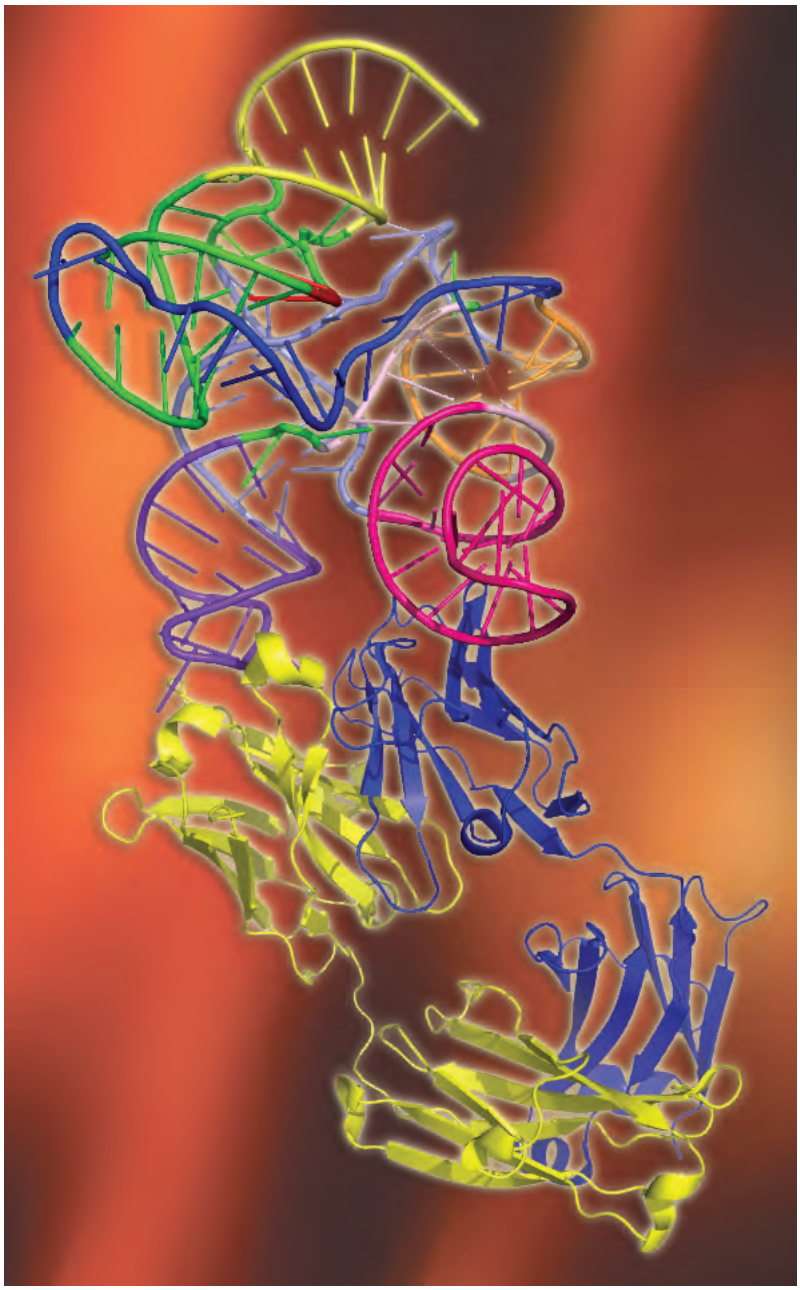

Fig. 1. Structure of the Class I ligase RNA enzyme in complex with an antibody chaperone. The antibody fragment is shown in yellow and blue, the RNA enzyme in multi-colored ribbon. The P5 and P7 loops recognized by the antibody are shown in purple and pink, respectively.

sequence whose recognition by a synthetic antibody facilitates structural determination," Nat. Struct. Mol. Biol. **18**(1), 100 (1 January 2011). DOI:10.1038/nsmb.1945

Author affiliations: [1]University of Chicago, [2]Whitehead Institute for Biomedical Research, [3]Massachusetts Institute of Technology, [4]University of Central Florida, [5]University of Toronto
‡Present address: Broad Institute and Harvard University
Correspondence:
*jpicciri@uchicago.edu,
**koss@bsd.uchicago.edu

This work was funded by the Howard Hughes Medical Institute (J.A.P.), National Institute of General Medical Sciences Medical Scientist National Research Service Award no. 5 T32 GM07281 (Y.K.), and National Institutes of Health grants R01-GM72688 and U54-GM74946 (to S.K. and A.A.K.) and R01-GM61835 (to D.P.B.). Use of LS-CAT was supported by the Michigan Economic Development Corporation and the Michigan Technology Tri-Corridor for the support of this research program (Grant 085P1000817). Use of the Advanced Photon Source was supported by the U.S. Department of Energy Office of Science under Contract No. DEAC02-06CH11357.

21-ID-D • LS-CAT • Life sciences • Macromolecular crystallography, microfluorescence (hard x-ray), nano-fluorescence imaging, nanotomography • 6.5-20 keV • On-site, remote, mail-in • Accepting general users •

IS GENE EXPRESSION REGULATED BY A TOGGLE OR A DIMMER SWITCH?

DNA methylation has emerged in recent years as an important gene regulatory mechanism involved in everything from behavior to cancer. Methylation of DNA is a reversible modification that shuts down expression of genes and is particularly important during development, when genes must be turned on or off according to what is appropriate for each tissue type, and during cell division when DNA is replicated. DNA methyltransferase 1 (DNMT1) is the major maintenance enzyme responsible for DNA methylation during semi-conservative DNA replication in human cells. A research team working at the SER-CAT 22-BM-B beamline at the APS has shown that the stability, and therefore the activity, of DNMT1 is carefully regulated by two different types of modifications that respond to cellular signals to mediate the DNA methylation process. The work highlights the elegant balance of cross-talk between positive and negative signals that regulate this important enzyme and provides information that could be used to develop therapies to target the DNMT1 pathway in diseases where DNA methylation has gone awry.

The team had shown that stability of the DNMT1 protein is regulated by protein methylation of DNMT1 on the amino acid lysine 142 (Lys142) by an enzyme called SET7. When SET7 methylates DNMT1, it is tagged for destruction, reducing methylation of the genome. However, in the course of that work, they noticed something else interesting. The amino acid right next to Lys142, serine 143 (Ser143), is in the right place to be modified by another regulatory enzyme called a protein kinase that adds a phosphate group to the amino acids serine or threonine. This led the team to wonder whether this site is actually phosphorylated and how that modification affects the methylation right next door at Lys142.

Using a peptide from DNMT1 that included the amino acids from 137-146 of human DNMT1, the team established that Ser143 is phosphorylated and identified a protein kinase called AKT1 as the enzyme that makes the modification. AKT1 is known to be involved in growth and development and was identified as an oncogene, a normal gene that is involved in the development of cancer when it is overexpressed or mutated. Biochemical assays showed that if they used a DNMT1 peptide that had been phosphorylated by AKT1, it could not also be methylated by SET7. The structural basis for this was elucidated by solution of the three-dimensional structure of SET7 with the peptide from DNMT1 and the substrate for methylation, S-adenosyl-L-methionine. The crystallographic structure that was obtained at the SER-CAT beamline showed that if DNMT1 was phosphorylated on Ser143, it would set up repulsive forces that would make it impossible for SET7 to add the methyl group to Lys142 (Fig. 1). The two modifications are mutually exclusive. These data suggested that cross-talk between AKT1 and SET7 adjusts the stability of DNMT1 to regulate methylation of the genome during the cell cycle and development.

Experiments in cultured cells supported this hypothesis by showing that when AKT1 was active and expressed in high concentration, the amount of DNMT1 increased, and when SET7 was expressed in high concentration, the amount of DNMT1 decreased. The effects of activated AKT1 were not immediate, however, and appeared to be regulated by the cell cycle, suggesting that other levels of regulation are also present. When AKT1 activity was inhibited in cells, DNMT1 levels decreased and methylation of the genome was reduced. Therefore, genome methylation is controlled in a cell cycle-dependent manner that involves methylation of DNMT1 by SET7 to cause destruction of DNMT1 and phosphorylation of DNMT1 by AKT1 to cause preservation of DNMT1 by preventing methylation.

This work has clear implications in cancer, which is characterized by unregulated cell division. Data from other groups have shown that in breast cancers that have aberrant AKT1 activation, inappropriate hypermethylation is responsible for turning off a tumor suppressor gene and consequent development of cancer. The work here suggests that this could be due to the effects of AKT1 on DNMT1 stabilization, suggesting that DNA methylation could be a therapeutic target in these cancers. *— Sandy Field*

See: Pierre-Olivier Estève[1], Yanqi Chang[2], Mala Samaranayake[1], Anup K. Upadhyay[2], John R Horton[2], George R. Feehery[1], Xiaodong Cheng[2], and Sriharsa Pradhan[1]*, "A methylation and phosphorylation switch between an adjacent lysine and serine determines human DNMT1 stability," Nat. Struct. Mol. Biol. **18**(1), 42 (1 January 2011). DOI:10.1038/nsmb.1939

Author affiliations: [1]New England Biolabs, [2]Emory University School of Medicine

Correspondence: *pradhan@neb.com

This work was supported by New England Biolabs and National Institutes of Health grants GM049245 and GM068680. X.C. is a Georgia Research Alliance Eminent Scholar. Supporting institutions for SER-CAT may be found at www.ser-cat.org/members.html. Use of the Advanced Photon Source at Argonne National Laboratory was supported by the U.S. Department of Energy Office of Science under Contract No. DE-AC02-06CH11357.

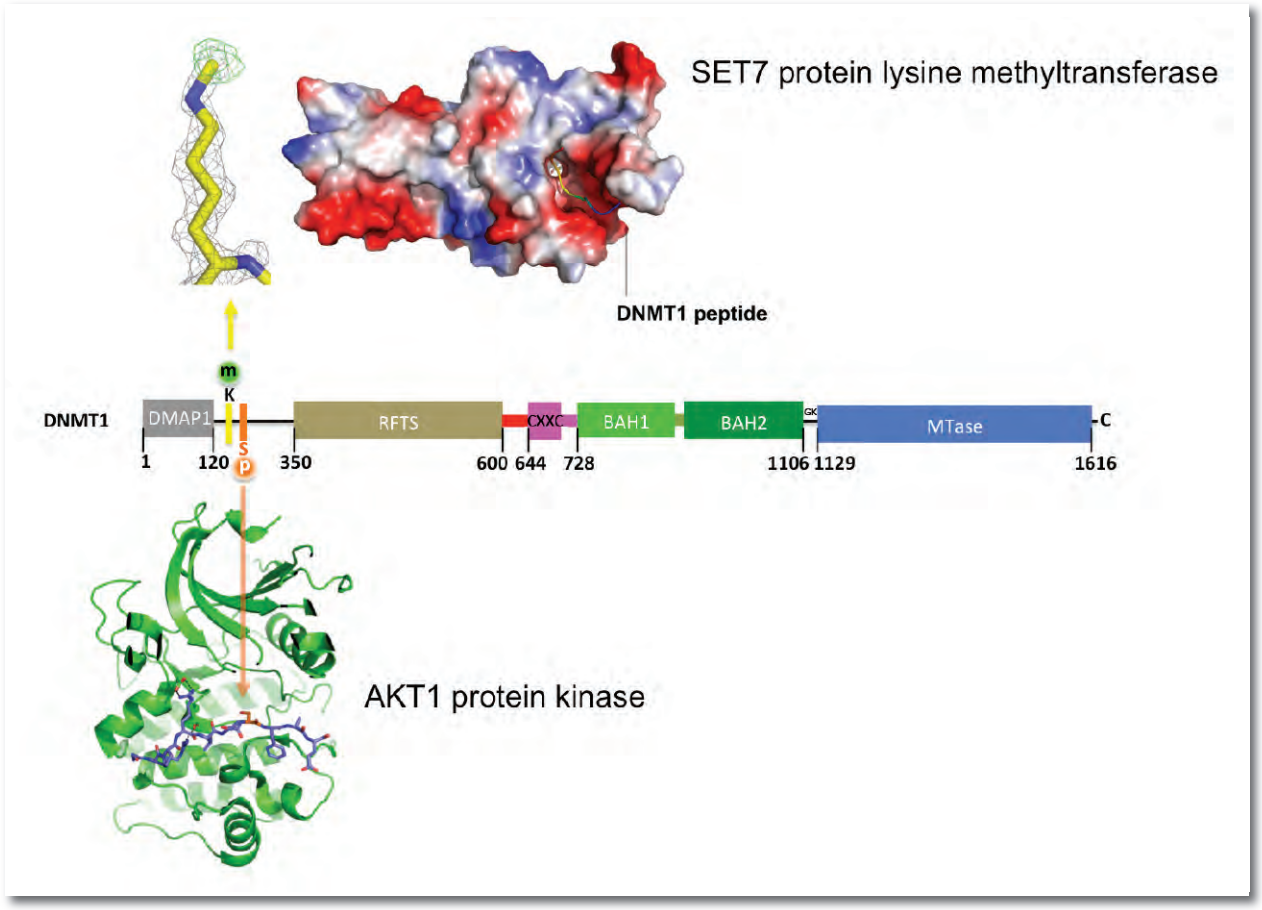

Fig. 1. Human DNA methyltransferase 1 is methylated by SET7 (top panel) and phosphorylated by AKT1 (bottom panel) between an adjacent lysine and serine (middle panel).

22-BM-B • SER-CAT • Life sciences • Macromolecular crystallography • 8-20 keV • On-site, remote • Accepting general users •

PING-PONG IN THE ACTIVE SITE OF RADICAL SAM ENZYMES

Ribosomes are giant cellular machines responsible for translating gene transcripts into protein. They are complexes of ribosomal RNA (rRNA) and proteins, and their essential nature makes them important targets for antibiotics. Chemical modification of rRNA contributes to the development of antibiotic resistance as well as to normal ribosome assembly and function. Two recently-identified bacterial enzymes add methyl group modifications to rRNA using an unusual radical mechanism. One of these enzymes, Cfr, has been shown to provide resistance against antibiotics that attack the bacterial ribosome in methicillin-resistant *Staphylcoccus aureus* (MRSA), the most common species of staphylococci to cause infections; the other, RlmN, methylates rRNA as a normal housekeeping modification. New studies by a research team utilizing two beamlines at the APS have elucidated the three-dimensional structure of the radical methylase enzyme, RlmN. Their work provides additional insight into the underlying chemical mechanism that this enzyme uses to modify rRNA, as well as an important glimpse into how essential building blocks can be modified to circumvent antibiotics that target the bacterial ribosome. >>>

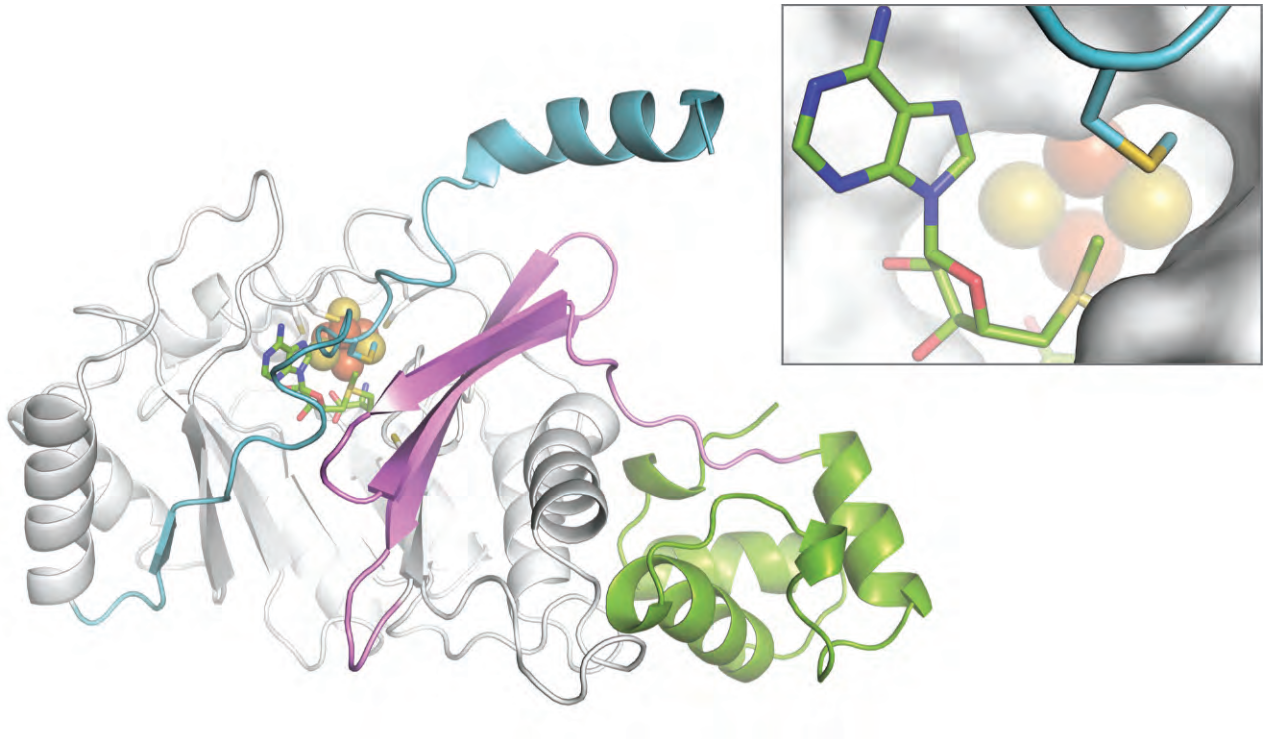

Typical enzymes that transfer a methyl group from *S*-adenosyl-L-methionine (SAM) to DNA, RNA, or protein do so by a single displacement reaction that moves the methyl group from SAM to a chemically receptive oxygen, nitrogen, or sulfur atom. RlmN and Cfr differ in that they methylate an inert carbon atom. One of the first clues into how RlmN and Cfr might accomplish this difficult transformation came from their identification as radical SAM enzymes [1]. The radical SAM enzymes use SAM to activate inert substrates, making them receptive to modification. They do this by using a SAM-bound iron-sulfur cluster to form a radical species in the active site that can remove a hydrogen atom from carbon or other substrate atoms to initiate modification of chemically challenging targets. RlmN and Cfr differ from typical radical SAM enzymes in their requirement for two SAM molecules, one for activation and another to donate a methyl group [2, 3].

RlmN and Cfr are proposed to use SAM to perform these two reactions via a "ping-pong" mechanism [3]. In this mechanism, the methyl group to be added to rRNA moves from SAM to a conserved cysteine residue, Cys^{355}, of the enzyme by a standard methylation reaction. Then a second SAM molecule is used to activate that methyl group for addition to the rRNA. To release the product, Cys^{355} forms a bond with another cysteine, Cys^{118}, located in the active site of the enzyme.

To visualize how the enzyme accommodates such a distinctive mechanism, the researchers from Northwestern University and The Pennsylvania State University carried out multiple anomalous dispersion experiments at the LS-CAT 21-ID-D and the GM/CA-CAT 23-ID-D beamlines at the APS to solve the structures of RlmN alone and in complex with SAM (Fig. 1). The structure of the RlmN/SAM complex revealed that the three-dimensional orientation of Cys^{355}, the enzyme-bound iron-sulfur cluster, SAM, and Cys^{118} in the active site of RlmN are consistent with the proposed ping-pong mechanism. Furthermore, the structure indicates that SAM-dependent methyl transfer and activation reactions occur from the same SAM binding pocket [4].

The authors point out that this observation reveals that RlmN is an example of the principle of economy in the evolution of enzyme binding sites in which a single active site evolved to facilitate two different reactions, the removal of a methyl group from SAM in the first reaction and then its activation in a second reaction. If all of this seems like so much esoteric chemical detail of interest to only a few enzyme chemists, consider the fact that this chemistry has been hijacked by bacterial pathogens to provide resistance to several key classes of our available antibiotics. Those bacteria are pretty good chemists. — *Sandy Field*

< Fig. 1. The overall structure of *Escherichia coli* RlmN in complex with SAM. The loop containing mechanistically important methylcysteine residue ($mCys^{355}$) is shown in blue. The location of $mCys^{355}$ in the active site (inset) indicates that methylation of the residue and activation by SAM occur from the same SAM binding site.

REFERENCES:

[1] F. Yan, J.M. LaMarre, R. Röhrich, J. Wiesner, H. Jomaa, A.S. Mankin, and D.G. Fujimori, "RlmN and Cfr are radical SAM enzymes involved in methylation of ribosomal RNA," J. Am. Chem. Soc. **132**(111), 3953 (2010).

[2] F. Yan and D.G. Fujimori, "RNA methylation by radical SAM enzymes RlmN and Cfr proceeds via methylene transfer and hydride shift," Proc. Nat. Acad. Sci. USA. **108**(10), 3930 (2011).

[3] T.L. Grove, J.S. Benner, M.I. Radle, J.H. Ahlum, B.J. Landgraf, C. Krebs, and S.J. Booker, "A radically different mechanism for S-adenosylmethionine-dependent methyltransferases," Science **332**(6029), 604 (2011).

[4] T.L. Grove, M.I. Radle, C. Krebs, and S.J. Booker, "Cfr and RlmN contain a single [4Fe-4S] cluster, which directs two distinct reactivities for S-adenosylmethionine: methyl transfer by S_N2 displacement and radical generation," J. Am. Chem. Soc. 133(49),19586 (December 14, 2011).

See: Amie K. Boal[1], Tyler L. Grove[2], Monica I. McLaughlin[2], Neela H. Yennawar[2], Squire J. Booker[2]*, and Amy C. Rosenzweig[1]**, "Structural Basis for Methyl Transfer by a Radical SAM Enzyme," Science **332**, 1089 (27 May 2011).
DOI:10.1126/science.1205358

Author affiliations: [1]Northwestern University, [2]The Pennsylvania State University
Correspondence: *squire@psu.edu, **amyr@northwestern.edu

This work has been supported by National Institutes of Health grants GM58518 (A.C.R.) and GM63847 (S.J.B.) and a National Research Service Award fellowship to A.K.B. LS-CAT is supported by the Michigan Economic Development Corporation and the Michigan Technology Tri-Corridor for the support of this research program (Grant 085P1000817). Use of the Advanced Photon Source at Argonne National Laboratory was supported by the U.S. Department of Energy Office of Science under Contract No. DE-AC02-06CH11357.

21-ID-D • LS-CAT • Life sciences • Macromolecular crystallography, microfluorescence (hard x-ray), nanofluorescence imaging, nanotomography • 6.5-20 keV • On-site, remote, mail-in • Accepting general users •

23-ID-D • GM/CA-CAT • Life sciences • Macromolecular crystallography, microbeam, large unit cell crystallography, subatomic (<0.85 Å) resolution, multi-wavelength anomalous dispersion, single-wavelength anomalous dispersion • 5-20 keV • On-site, remote • Accepting general users •

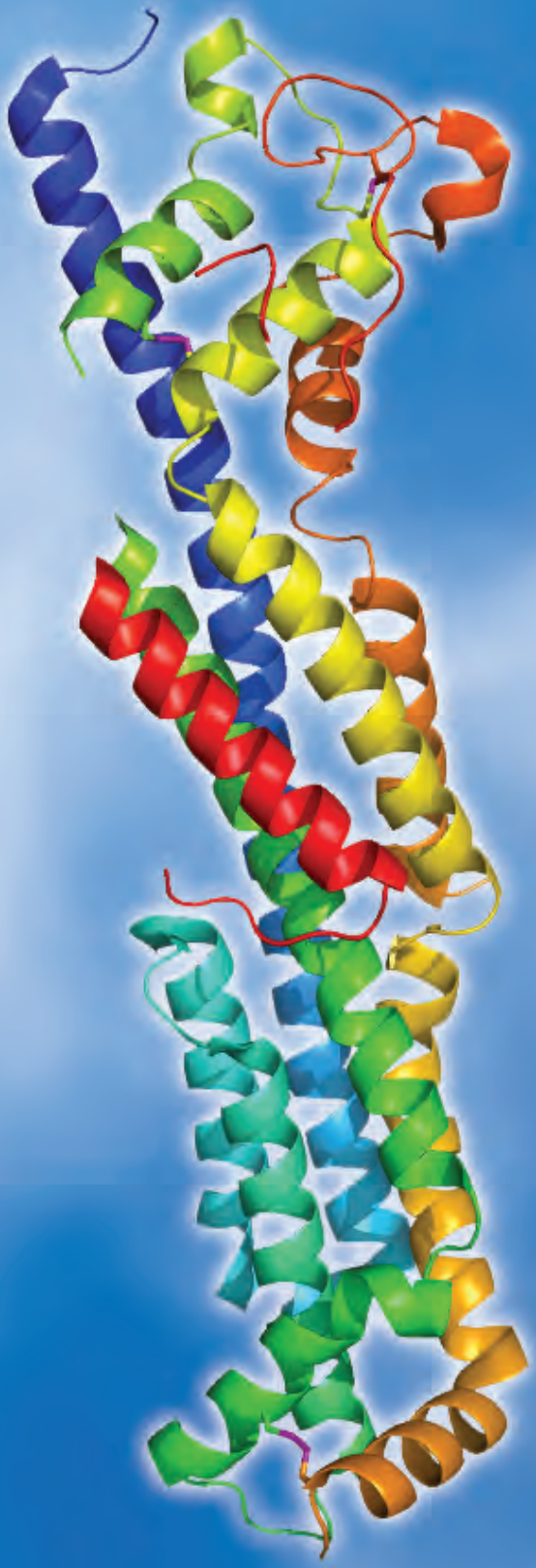

MINING THE INTRICACIES OF DEVELOPMENTAL DEFECTS

Glypicans are cell surface proteins that play a role in regulating development, and loss of their function is associated with widespread developmental abnormalities. Finding out more about these proteins may help pave the way to new therapies. With the use of x-ray crystallography, researchers working at the LRL-CAT 31-ID beamline at the APS identified the crystal structure of a region of a glypican that may be involved in the regulation of development. Specifically, they pursued information about the molecular mechanism by which glypicans regulate a signaling pathway known as the "Hedgehog" signaling pathway, which is involved in development as well as other functional aspects. The team's findings provide new insights into glypican function, and its potential role in birth defects, which may in turn lead to strategies to correct those defects.

The Dally-like Protein (Dlp) in the fruit fly *Drosophila* is a member of a family of cell surface proteins called glypicans. These cell-surface proteins play a role in regulating cell development. One end of the glypican protein is called the N-terminal globular region. The glypican protein also contains several attachment points for sugars called heparan sulfate. Recently, Dlp was shown to be important for cells to be able to respond to the developmental signaling protein Hedgehog, which stimulates cells to grow into specific tissues during development. Loss of function of the Hedgehog protein results in a range of birth defects ranging from mild to lethal depending on the type of mutation. In addition, inappropriate activation of Hedgehog signaling is associated with several cancers.

The researchers in this study, from the Johns Hopkins University School of Medicine and the Stanford University School of Medicine, were therefore interested in establishing the mechanism whereby Dlp regulates Hedgehog signals. By determining the crystal structure of the N-terminal globular region of Dlp (Fig. 1), the researchers sought to find out more about the molecular mechanism through which glypicans mediate Hedgehog signaling as well as other non-Hedgehog related functions. Of note, they found that the Dlp structure was not similar to any known structures, which is unusual, because most newly determined structures are often at least distantly related to previously determined structures, which can provide insights into their function.

The other surprising aspect of the Dlp structure was that it is formed in only a single unit (called a domain) despite being about 400 amino acids in size. The protein also had no apparent active sites or regions similar to those found in other proteins. Although the absence of similarity to known proteins provided no functional clues, these features suggested that the role of Dlp is most likely to bind other proteins, and the most likely binding partner would be Hedgehog proteins themselves. However, the researchers also showed that Dlp does not bind to Hedgehog, at least by itself. This finding then raised the question of whether partner proteins combine with Dlp to mediate their actions. Ultimately, understanding glypican function may lead to understanding its role in birth defects as well as to the development of strategies to correct those defects. Also, defining exactly how the Hedgehog signaling pathway is activated may ultimately give rise to new strategies to inhibit the inappropriate activity of this pathway in cancer. *— Emma Hitt*

< Fig. 1. A ribbon diagram of the Dally-like N-terminal domain is shown. The ribbon is colored in a rainbow gradient from the N-terminus (blue) to the C-terminus (red). Figure made with PyMol (Schrödinger, LLC).

See: Min-Sung Kim[1], Adam M. Saunders[2], Brent Y. Hamaoka[1], Philip A. Beachy[2], and Daniel J. Leahy[2]*, "Structure of the protein core of the glypican Dally-like and localization of a region important for hedgehog signaling," Proc. Nat. Acad. Sci. **108**(32), 13112 (2011). DOI:10.1073/pnas.1109877108

Author affiliations: [1]Johns Hopkins University School of Medicine, [2]Stanford University School of Medicine

Correspondence: *dleahy@jhmi.edu

This work was supported by the Howard Hughes Medical Institute (P.A.B.) and the National Institutes of Health (Grant R01HD055545 to D.J.L.). Use of the LRL-CAT beamline was provided by Eli Lilly Company, which operates the facility. Use of the Advanced Photon Source at Argonne National Laboratory was supported by the U. S. Department of Energy Office of Science under Contract No. DE-AC02-06CH11357.

31-ID • LRL-CAT • Life sciences • Macromolecular crystallography, single-wavelength anomalous dispersion, single-crystal diffraction • 4.7-28 keV • Mail-in • Accepting general users •

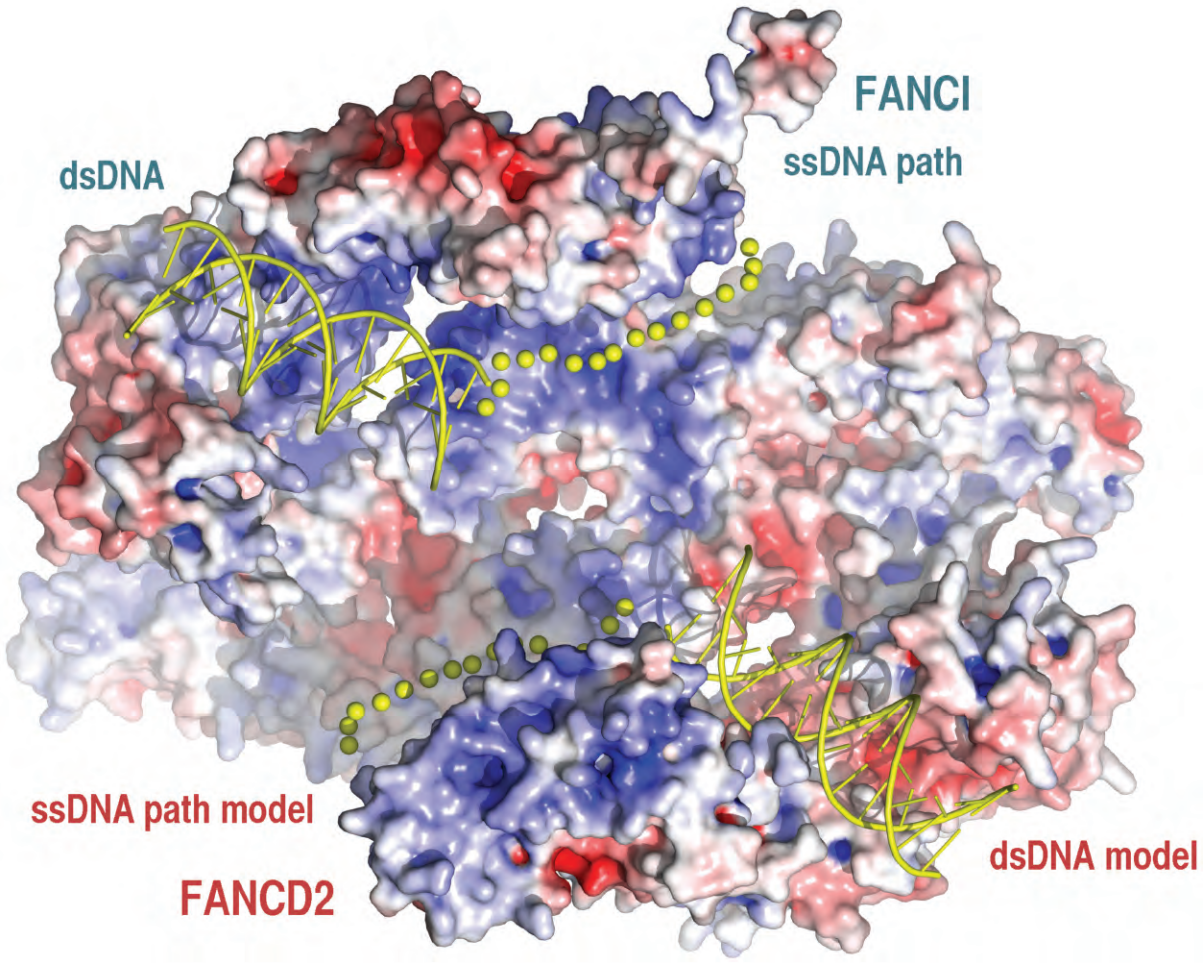

Fig. 1. Electrostatic potential of the ID molecular surface showing the dsDNA cartoon and sDNA path (yellow spheres) from the Y DNA–FANCI maps.

CLUES TO CANCER TREATMENTS IN A RARE GENETIC DISORDER

Fanconi anemia is a rare genetic disorder that leads to an increased susceptibility to cancer. Studies of this disease have revealed that proteins coded for Fanconi and Fanconi-like genes are crucial for repairing certain types of DNA damage. Conversely, when these proteins are mutated and do not function properly, DNA damage goes unrepaired and cancer can develop. Little is known about some of the proteins involved in this pathway. Utilizing x-ray crystallography at the APS and the National Synchrotron Light Source (NSLS), researchers have identified the crystal structure of two proteins, FANCI and FANCD2, involved in Fanconi's anemia and the way that they interact with each other and with DNA, revealing new information about the function of these proteins and suggesting some intriguing future directions for research. A greater understanding of these proteins and how cells repair DNA damage may lead not only to insights about how cancer develops, but also how to best treat it.

The Fanconi pathway proteins — 13 of them have been identified to date — are involved in the repair of a specific type of damage to a part of the DNA called the interstrand crosslink, which acts like a rung in the ladder of the double-stranded DNA molecule. However, little is known about the function of each of the proteins involved in the Fanconi pathway. To make matters worse, most of the proteins do not have any recognizable similarities to other proteins that would provide clues about their function.

The researchers in this study, from Memorial Sloan-Kettering Cancer Center, Cornell University, Brigham and Women's Hospital, and The Rockefeller University therefore wanted to identify the structure of two important Fanconi pathway proteins, FANCI and FANCD2, to see if they could glean insights into their function. X-ray crystallography revealed that these proteins contain structures called alpha helical solenoids. In addition, each protein has a large, positively charged groove, with one part having a semicircular cross-section of ~20 Å in width, which happens to be the same width as double-stranded DNA, suggesting an interaction between each protein and the DNA. The other end of the groove in each protein was too narrow for the double-stranded DNA to fit (Fig. 1).

With this information and further biochemical analysis, the researchers theorized that each protein and the complex of the two proteins together bind to DNA structures containing both double- and single-stranded DNA. Crystallography at the NE-CAT 24-ID-C beamline at the APS provided low-resolution data on the FANCI-DNA complex that confirmed the previous findings. Taken together, the data suggest that the FANCI-FANCD2 complex recognizes DNA structures that result from the collision of replication forks with the inter-strand crosslink, which helps explains why this complex is needed for DNA repair. A surprising finding was that the interface between FANCI and FANCD2 contained sites of "mono-ubiquitination," which indicates that the attachment of ubiquitin molecules may play a regulatory function in this process.

Since the FANCI and FANCD2 proteins function as "tumor suppressors," (i.e., cancers occur if these proteins are not functioning properly), the structural information helps explain how mutations inactivate these proteins and why some mutations are more inactivating, and thus cancer-causing, than others. Ultimately, by improving our understanding of the mechanism of DNA repair that occurs through these proteins, more insights may be gained into the biological processes that lead to cancer and how to prevent and/or treat it. For instance, a complete understanding of this pathway could elucidate points of intervention, such as areas of the pathway that could be targeted for cancer suppression by drugs. In addition, many cancers have already been found to contain proteins that are dysfunctional in this pathway and may therefore be more susceptible to certain chemotherapies that damage the crosslinks of DNA. This knowledge may improve the ability to give these chemotherapies to patients who may benefit most from them. *— Emma Hitt*

See: Woo Joo[1], Guozhou Xu[2], Nicole S. Persky[1], Agata Smogorzewska[3,4], Derek G. Rudge[1], Olga Buzovetsky[1], Stephen J. Elledge[1,3], and Nikola P. Pavletich[1]*, "Structure of the FANCI-FANCD2 Complex: Insights into the Fanconi Anemia DNA Repair Pathway," Science **333**(6040), 312 (15 July 2011). DOI:10.1126/science.1205805

Author affiliations: [1]Memorial Sloan-Kettering Cancer Center, [2]Cornell University, [3]Brigham and Women's Hospital, [4]The Rockefeller University
Correspondence: *pavletin@mskcc.org

This work was supported by the National Institues of Health and the Howard Hughes Medical Institute. NE-CAT is supported by grants from the National Center for Research Resources (5P41RR015301-10) and the National Institute of General Medical Sciences (8 P41 GM103403-10) from the National Institutes of Health. Use of the Advanced Photon Source was supported by the U.S. Department of Energy Office of Science under Contract No. DEAC02-06CH11357.

24-ID-C • NE-CAT • Life sciences • Macromolecular crystallography, microdiffraction, single-wavelength anomalous dispersion, single-crystal diffraction, microbeam • 6.5-23 keV • On-site • Accepting general users •

FREEZING TIME: NEW MOLECULAR CLUES ABOUT IMPORTANT CELL PROCESSES

Light is an important signal that controls many essential biological processes, including growth, development, and day-night circadian rhythm. Consequently, almost all organisms use photoreceptors to adapt to their ambient light environment and perceive light signals, such as in vision. Phytochromes comprise a family of photoreceptor proteins first found in green plants, and more recently discovered in most biological kingdoms, including fungi, and bacteria, in which they are called bacteriophytochromes. These act as red-light sensors in bacterial organisms, transforming red-light signals into biological signals that mediate important cellular responses to light. Researchers utilizing the APS have determined the crystal structures of three intermediates in the photoreaction of a bacteriophytochrome from the organism *Pseudomonas aeruginosa*. Understanding this process at the molecular level may not only reveal the mechanism by which a photoreceptor converts a light signal into a biological signal, but it may also provide structural guides for engineering suitable light-sensitive systems for important biomedical and biotechnological applications, such as optogenetics in neurosciences and deep-tissue imaging.

Upon light activation, bacteriophytochromes reversibly convert between the red-light-absorbing (Pr), and the far-red-light-absorbing (Pfr) forms. The researchers in this study, from The University of Chicago, working at BioCARS beamline 14-ID-B and LS-CAT beamline 21-ID-G at the APS observed that absorption of light by the bacteriophytochrome can drive a series of conformational changes that begin in the light-sensitive chromophore embedded in the photoreceptor, ultimately spreading out to the protein regions. Twisting and untwisting of the methine bridges in the chromophore were found to be important initial structural events in this light-induced reaction.

Phytochrome photoreceptors covalently incorporate a chromophore (the light-absorbing part that results in its coloration) such as biliverdin; this produces a holoprotein that reversibly photoconverts between two stable isoforms, Pr and Pfr. These represent a photoreversible switching mechanism within the organism, allowing the photoreceptors to respond to environmental light changes. In this way they transduce red and far-red light signals into discrete biological signals that go on to modulate cellular processes.

Numerous structures of bacteriophytochromes have been evaluated in their dark-adapted Pr and Pfr states; however, the conformational nature of early events in the light reaction had not previously been characterized. This study aimed to address this challenge. Utilizing bright x-rays at the BioCARS and LS-CAT beamlines, the researchers were able to detect structural changes in the photoreceptor protein during the early stages of its transition from the "dark" state to the "light" state (Fig. 1). Since these transitions occur at an ultrafast rate, the technique of temperature-scanning cryocrystallography was used to slow down the reaction to follow the evolution of the structures using static crystallographic techniques. "Cryocrystallography" involves the use of low temperatures to freeze the target protein in specific conformations. "Temperature-scanning," on the other hand, mimics time as the reaction proceeds. Their combination allows the normally ultrafast reaction to proceed slowly, one step at a time, in a more controlled manner. By effectively freezing time in this way, the researchers could perform an x-ray diffraction scan at each temperature, enabling them to observe initial conformational changes in this photoreceptor that are otherwise too transient to be captured.

The study revealed three main intermediate structures, named L1, L2, and L3. Transitions between these structures began in one area of the photoreceptor's chromophore, subsequently spreading out to involve the surrounding regions of the protein. According to the researchers, light absorption by the Pfr state of the bacteriophytochrome transformed the light signal into a structural signal via twisting and untwisting of one-carbon methine bridges in its structure.

Although there is still a lot to learn about this bacteriophytochrome, and photoreceptors in general, this research has revealed a small piece of the puzzle in the big picture. In addition, this study may inspire other scientists to apply static crystallographic techniques in dynamic studies of other interesting biological systems.

— Nicola Parry

See: Xiaojing Yang*, Zhong Ren, Jane Kuk, and Keith Moffat**, "Temperature-scan cryocrystallography reveals reaction intermediates in bacteriophytochrome," Nature **479**, 428 (17 November 2011). DOI:10.1038/nature10506

Author affiliation: The University of Chicago

Correspondence:

*xiaojingyang@uchicago.edu,

**moffat@cars.uchicago.edu

This work was supported by National Institutes of Health grant GM036452 to K.M. BioCARS is funded by the National Center for Research Resources of the National Institutes of Health (grant RR007707). Use of LS-CAT was supported by the Michigan Economic Development Corporation and the Michigan Technology Tri-Corridor for the support of this research program (Grant 085P1000817). Use of the Advanced Photon Source at Argonne National Laboratory was supported by the U. S. Department of Energy Office of Science under Contract No. DE-AC02-06CH11357.

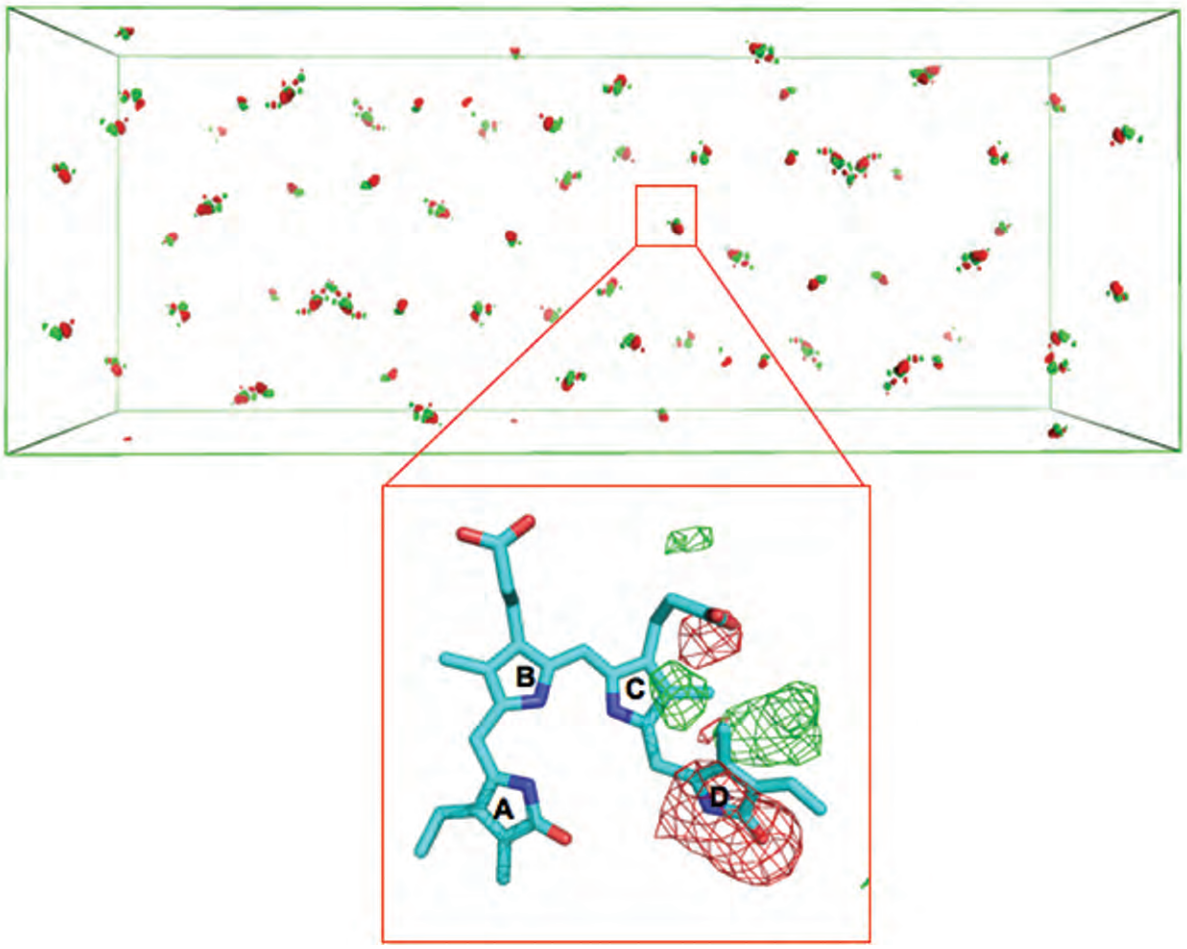

Fig. 1. Strong difference densities between the light and dark states are associated with light-sensitive chromophores (represented by the cyan structure in the zoomed-in inset) that are scattered in the entire unit cell. Positive green densities represent the formation of the light-induced structures, and negative red densities are a result of decay of the parent dark state.

14-ID-B • BioCARS • Life sciences • Time-resolved crystallography, time-resolved x-ray scattering, Laue crystallography, wide-angle x-ray scattering, biohazards at the BSL2/3 level, macromolecular crystallography • 7-20 keV • On-site • Accepting general users •

21-ID-G • LS-CAT • Life sciences • Macromolecular crystallography • 12.7 keV • On-site, remote, mail-in • Accepting general users •

THE RHYTHMS OF FLIES

Evolution is an amazing tinkerer. Again and again biologists discover evidence that nature has taken an existing gene or protein and tweaked it to come up with a diverse new function. Changes that provide value are kept and may be improved upon through future meanderings of random mutation. Mother Nature's use of this flexible biological toolkit is evident in the cryptochrome/photolyase (CRY/PL) family of proteins that regulate functions as diverse as day-night circadian rhythms, magnetosensing, and DNA repair in response to ultraviolet or blue light in all the kingdoms of life. While these proteins share a similar overall structure and are all activated by light, they recognize diverse targets and fulfill diverse functions. Now, work by researchers using the 24-ID-E NE-CAT microbeamline at the APS has revealed the molecular basis for the functional differences between CRY and PL photoreceptor family members. Their solution of the three-dimensional (3-D) structure of a CRY protein from the fruit fly *Drosophila* provides important insight into the regulation of these fundamental light-driven processes that will affect how we understand our own circadian rhythms as well.

In flies, processes that are regulated by daily rhythms of day and night, such as hatching, are dependent upon the actions of proteins that can respond to light. The CRY photoreceptor in flies regulates circadian rhythms by binding to another protein, known as timeless, or TIM, in the presence of light. This causes both proteins to be destroyed and results in gene activation. Its protein "relative," the PL photoreceptor, performs a very different function by repairing damage to DNA caused by ultraviolet radiation and requires light to perform its function. The 3-D structure of PL shows that damaged DNA is aligned into a groove in the protein that recognizes the break and catalyzes a light-activated chemical reaction to fix it. A major question has been: How do these two proteins perform their very different functions using the same general protein fold and light activation mechanism? The solution of the 2.3-Å resolution structure of CRY provides some clues as to how this works.

The 3-D structure of CRY shows that it shares the same overall features as the fruit fly PL protein with some important exceptions. Most notably, the carboxy terminal tail (CTT) region of CRY, that is not present in PL and is important for targeting the TIM protein, appears to mimic the way damaged DNA binds to the PL protein. The CTT is positioned so that it juts directly into the catalytic groove of CRY where it causes the shift of an important phenylalaine-phenylalanine-tryptophan (FFW) motif to a location that mimics the way a damaged piece of DNA is arranged in the PL (Fig. 1). In both proteins, this interaction causes changes in the conformation of the protein that affects the light-sensitive cofactor. For PL, that means the light activates the DNA repair mechanism. For CRY, further experiments performed by the team on CRY mutants with changes to the amino acids in the CTT area showed that this is the area responsible for the light sensitivity of TIM targeting.

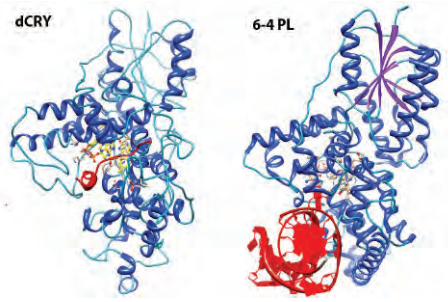

Fig. 1. Structural representations of the fruit fly cryptochrome and photolyase proteins (blue and purple ribbons) show that the C-terminal tail and damaged DNA (red in both panels) orient within a similar groove in the protein to interact with active site amino acids in light-activated reactions (yellow and beige).

These clear differences between CRY and PL were accompanied by some provocative clues about how CRY proteins could make use of subtle changes in the chemical interactions between amino acid side chains and the photo-activable cofactor used by PL proteins to perform DNA repair. These differences in the way electrons are transferred between cofactor and protein in CRY suggest that shifting the FFW motif into the active site may also facilitate photosensing or magnetosensing, providing insight into how these functions work as well. Now that the team has figured out how this subtle shift in structure has provided a new array of functions for the CRY/PL family, they plan to determine structures of CRY in light-activated states and in complex with its downstream targets.

— Sandy Field

See: Brian D. Zoltowski[1], Anand T. Vaidya[1], Deniz Top[2], Joanne Widom[1], Michael W. Young[2], and Brian R. Crane[1], "Structure of full-length *Drosophila* cryptochrome," Nature **480**, 396 (15 December 2011). DOI:10.1038/nature10618

Author affiliations: [1]Cornell University, [2]The Rockefeller University
Correspondence: *bc69@cornell.edu

This study was supported by National Institutes of Health Grant GM079679 to B.R.C. and GM054339 to M.W.Y. The NE-CAT beamlines are supported by grants from the National Center for Research Resources (5P41RR015301-10) and the National Institute of General Medical Sciences (8 P41 GM103403-10) from the National Institutes of Health. Use of the Advanced Photon Source was supported by the U.S. Department of Energy Office of Science under contract no. DEAC02-06CH11357..

24-ID-E • NE-CAT • Life sciences • Macromolecular crystallography, microbeam, microdiffraction, single-wavelength anomalous dispersion, single-crystal diffraction • 12.68 keV • On-site • Accepting general users •

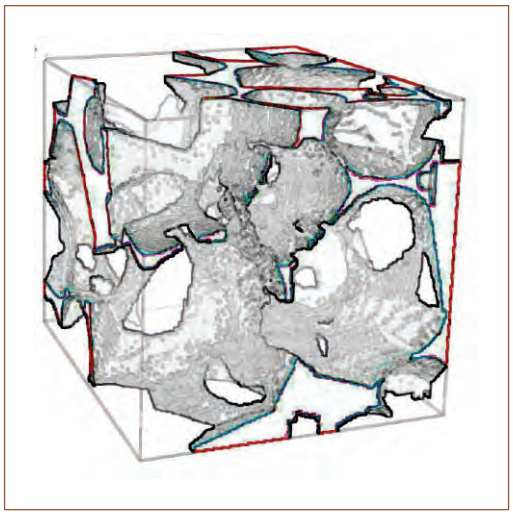

Environmental, Geological, & Planetary Science

Visualizing the Flow of Molten Rock through Seabed Mantle

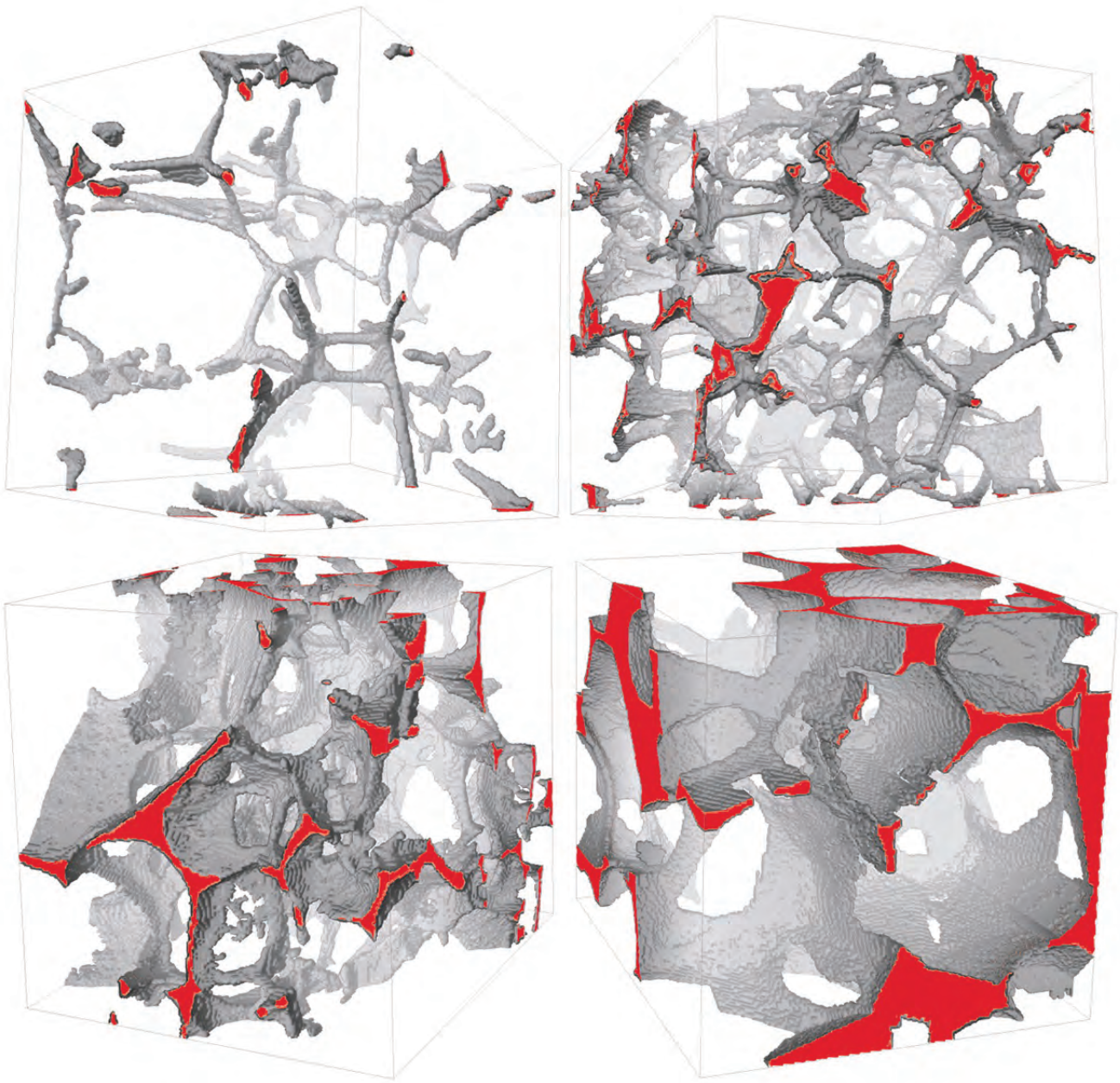

Fig. 1. X-ray microtomography images show the networks formed by molten rock in a cube of mantle material, 140 μm on a side, at four different melt fractions. Grey areas are melted material between solid olivine grains, represented by the white regions. Red indicates channels of melt slicing through the faces of the cube. (A movie of tomographic visualizations of the three-dimensional melt distribution in the olivine-basalt aggregates can be viewed at http://www.sciencemag.org/content/suppl/2011/03/29/332.6025.88.DC1/1202221s1.mov.)

New information about how most of the Earth's crust formed has been uncovered by investigators from the University of Maryland, Woods Hole Oceanographic Institution, the University of Western Australia, and Argonne who utilized the XSD 2-BM-A,B beamline at the APS to obtain unprecedented, three-dimensional x-ray images of melted rock. Their results offer a more sophisticated picture of rock porosity and a resolution of the discrepancy between permeability and melt velocity.

Where the Earth's tectonic plates drift apart at ocean floor spreading centers, mantle rock partially melts and seeps upward, solidifying to form new crust. Geologists have had difficulty reconciling estimates of the permeability of the partially molten mantle with analyses of the rate at which molten rock ascends. In microtomography experiments carried out at beamline 2-BM-A,B the research team has, for the first time, directly imaged the intricate network formed by the molten fraction within a mainly solid rock.

The Earth's upper mantle consists mostly of olivine as well as other minerals with lower melting points. Using measurements of seismic wave speeds, geophysicists estimate that 1% to 2% of the mantle beneath seafloor locations at the East Pacific Ocean ridge is in a molten state. This melt fraction implies that the permeability of these rocks is relatively low: The less permeable the mantle, the harder it is for buoyancy to drive the melted fraction upward, and the greater the amount of melt the mantle retains.

On the other hand, geochemical analyses of ocean-ridge basalts show that the relative abundances of uranium, thorium, and radium isotopes belonging to a single decay chain have not reached the long-term equilibrium values dictated by their half-lives. This contradicts the geophysical data because it implies that magma rose rapidly from great depths, which requires high permeability.

Adding to the confusion are analyses that predict thermodynamically favored arrangements of solid and melted fractions for given temperature and pressure, and for known rock compositions. These suggest melt fractions should be around 0.5% or lower.

The weak link is using the thermodynamic model to guess rock structure. Permeability depends on fine details of how the melted fraction within a rock connects together. Previous studies attempted to infer the three-dimensional network of melted material from two-dimensional images of slices through a rock, but they were ambiguous, especially at low melt fractions.

The researchers turned to x-ray studies of basalt heated to 1350 °C and compressed at a pressure of 1.5 GPa to image directly the three-dimensional network formed at different melt fractions. Because the density contrast between the solid and melted fractions was small, they used an edge-enhancement technique to obtain Fresnel fringes from the liquid-solid boundaries in their millimeter-diameter sample. Rotating the sample through 180° in 0.12° increments allowed the team to build up three-dimensional microtomographic images with submicron resolution (Fig. 1).

At four melt fractions, from 2% to 20%, the researchers see an interconnected network of melt channels running along the edges where three or more olivine grains meet, in broad agreement with thermodynamic predictions.

At higher melt fractions, however, the images show films of melted material coating the boundaries between adjacent grains, but these films are far less evident at lower melt fractions. A nicely connected network of channels controls the flow, but the structure is not as simple as models predicted. That more complex structure changes the exponent in the power law relating permeability to grain size.

To understand why mantle rocks have a melt fraction of 2% rather than the lower figure predicted, the team suggests thinking of their structure as less like a sponge and more like a snowball.

When one squeezes a sponge, it is very compliant, whereas a snowball is easy to squeeze at first but then becomes much harder as its solid particles are compacted together. In the same way, the matrix of highly compressed mantle grains resists compression so that the melt network between the grains doesn't feel so much pressure and therefore doesn't flow as fast as expected. Geologists have sometimes wondered about this kind of behavior, but the new results show that it cannot be ignored.

Although these data were collected from quenched samples, in the future, the research team hopes to image the rocks while they are heated and kept under pressure.

— David Lindley

See: Wenlu Zhu[1]*, Glenn A. Gaetani[2], Florian Fusseis[3], Laurent G.J. Montési[1], and Francesco De Carlo[4], "Microtomography of Partially Molten Rocks: Three-Dimensional Melt Distribution in Mantle Peridotite," Science **332**, 88 (2011).

Author affiliations: [1]University of Maryland, [2]Woods Hole Oceanographic Institution, [3]University of Western Australia, [4]Argonne National Laboratory
Correspondence: *wzhu@umd.edu

This work is supported by National Science Foundation (NSF) Division of Earth Sciences NSF-EAR 0753505 (W.Z. and G.A.G.) and NSF Division of Ocean Sciences NSF-OCE 0937277 (L.G.J.M.). F.F. was supported by the Western Australian State Government through the Premier's Fellowship Program and the Australian Synchrotron Research Program, funded by the Commonwealth of Australia under the Major National Research Facilities Program. Use of the Advanced Photon Source at Argonne National Laboratory was supported by the U.S. Department of Energy Office of Science under Contract No. DE-AC02-06CH11357.

2-BM-A,B • XSD • Life sciences, physics • General diffraction, microdiffraction, phase contrast imaging, tomography • 5-33 keV, 5-33 keV • On-site • Accepting general users •

Helium Makes Glass Pressure-Resistant

Geophysicists who want to understand how the properties of rocks and melts at high pressures are changed by absorption of gases often conduct laboratory tests using inert gases, which do not chemically interact with the minerals. However, a new study at the HP-CAT beamline 16-ID-B at the APS finds that silicon glass pressurized under helium behaves in an anomalous way, compressing very little even at pressures as high as 200,000 atm. The finding suggests that if helium behaves similarly in silicate melts, geophysicists may have to modify their views on a variety of processes in the Earth's interior, volcanoes, in planetary interiors, and in the evolution of the Earth's crust.

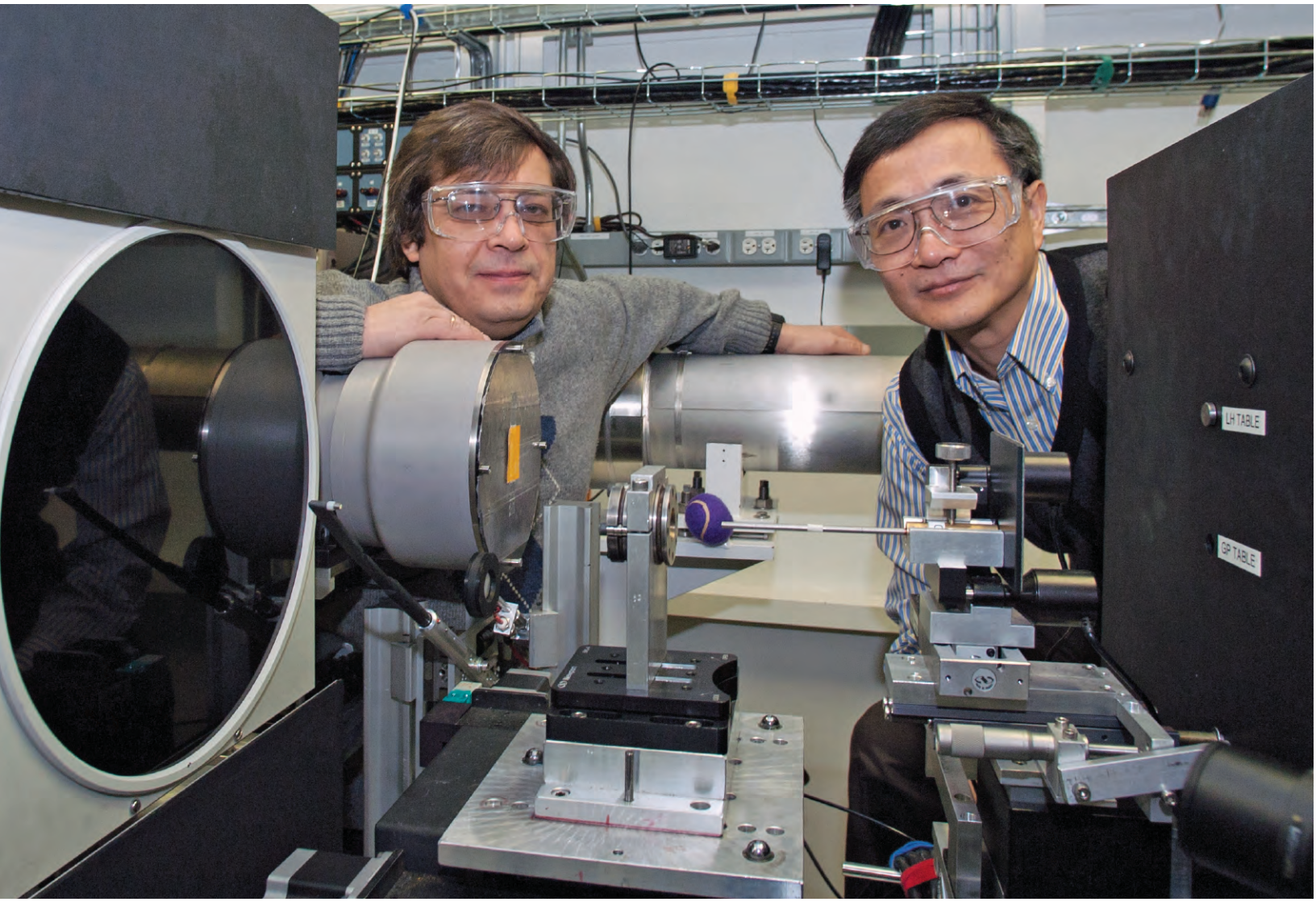

Stanislav Sinogeikin (left) and Guoyin Shen in the HP-CAT 16-ID-B research station.

Pure silicon dioxide glass has a molecular structure consisting of shared tetrahedra, in which each silicon atom sits amid four oxygen atoms. At normal pressures, the tetrahedral adopt a somewhat capacious arrangement, with rings of four to eight tetrahedral enclosing voids. Under pressure, the density of glass increases significantly, and x-ray diffraction studies suggest that the tetrahedral rings collapse and shrink. For applied pressures above about 12 GPa, or 120,000 atm, the structure changes irreversibly; it does not spring back when the pressure is removed.

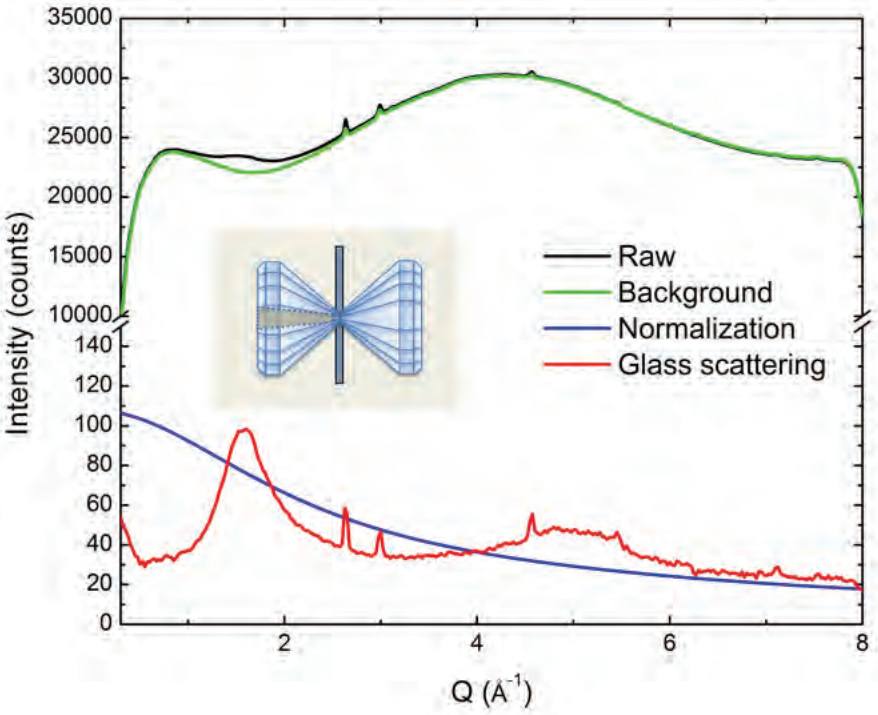

Fig. 1. X-ray diffraction data collected at 16-ID-B for SiO_2 glass at high pressure in a diamond anvil cell.

Working at the 16-ID-B beamline, researchers from the Carnegie Institution of Washington, The University of Chicago, and Uppsala University used x-ray diffraction to measure structural changes in glass samples compressed in a diamond anvil cell (Fig. 1). With no helium present, the first sharp diffraction peak shifted by a considerable amount when the pressure was raised to almost 20 GPa, in line with previous experimental results. But when helium was added to the pressurized cell, the diffraction peak shifted hardly at all. Raman spectroscopy conducted at Uppsala University likewise revealed dramatic changes in the arrangement of the tetrahedra in glass compressed in the absence of helium, but far smaller changes when helium was included.

Using structures from other silica materials as a guide, the researchers judge that a six-member tetrahedral ring in glass encloses a cavity about 0.3-nm across, just big enough to accommodate a helium atom. They suggest that helium seeps into glass at high pressures, fills the larger voids in its molecular structure, and therefore makes it relatively incompressible. Consistent with this picture is the researchers' finding that the tiny change in the x-ray diffraction pattern seen in glass compressed in the presence of helium is reversed when the pressure is released.

To test this idea, they compressed silicon dioxide glass in the presence of hydrogen and germanium dioxide glass in the presence of helium. In both cases, high pressures caused marked changes in the x-ray diffraction patterns, indicating that the molecular structures of both glasses did not withstand compression. Molecular hydrogen is too big to fit into most of the voids in the silicon dioxide glass, the researchers say, and the voids in germanium dioxide glass are somewhat smaller, and so cannot take in helium molecules.

Although these results indicate that the effect of helium on pure silicon dioxide glass is a peculiarity due to an unusual match between the size of helium atoms and the molecular structure of glass, the team suggests that it will be important to test for similar behavior in silicate melts of geophysical importance. Since helium is the second-most abundant element in the universe, after hydrogen, its influence on other materials is significant for the evolution of the solar system. If it can alter the compressibility of such materials in natural circumstances, scientists might have to rethink their understanding of magma processes in volcanoes, in planetary interiors, and in the evolution of the Earth's crust. — *David Lindley*

See: Guoyin Shen[1]*, Qiang Mei[1], Vitali B. Prakapenka[2], Peter Lazor[3], Stanislav Sinogeikin[1], Yue Meng[1], and Changyong Park[1], "Effect of helium on structure and compression behavior of SiO2 glass," Proc. Nat. Acad. Sci. USA 1**08**, 6004 (2011). DOI:10.1073/pnas.1102361108

Author affiliations: [1]Carnegie Institution of Washington, [2]The University of Chicago, [3]Uppsala University
Correspondence: *gshen@ciw.edu

This work was supported by the U.S. National Science Foundation (NSF) under EAR-0738852. HP-CAT is supported by the Carnegie Institution of Washington, the Carnegie-Department of Energy (DOE) Alliance Center, the University of Nevada at Las Vegas, and Lawrence Livermore National Laboratory, through funding from the DOE National Nuclear Security Administration, the DOE Office of Science, and the NSF. Use of the Advanced Photon Source at Argonne National Laboratory was supported by the DOE Office of Science under Contract No. DE-AC02-06CH11357.

16-ID-B • HP-CAT • Materials science, geoscience, chemistry, physics • Microdiffraction • single-crystal diffraction, high-pressure diamond anvil cell • 24-35 keV • On-site • Accepting general users •

HOW SUBSURFACE BACTERIA BREATHE AFFECTS URANIUM MOBILITY AND DISPERSAL

Uranium contamination in aquatic and terrestrial environments has resulted from power generation, nuclear weapons production, and the weathering of uranium (U)-bearing minerals. Under oxic conditions, uranium is stable as uranyl U^{VI}, which is the more soluble and mobile form in groundwater. However, when bacteria are active in subsurface environments they can reduce U^{VI} to the less-soluble U^{IV} form; stimulating indigenous microbes to reduce U^{VI} in subsurface plumes has been investigated as a remediation strategy for over 15 years. Researchers have thought that the reduced U^{IV} always formed uraninite (UO_2), the most stable and insoluble uranium mineral. However, recent discoveries suggest that bioreduced U^{IV} in natural sediments may remain as single atoms for extended periods, either complexed to bacterial or mineral surfaces or incorporated in less-stable U^{IV} minerals. Researchers carrying out experiments at the MR-CAT 10-ID-B beamline at the APS have gained a new understanding of how uranium reduction occurs so that it may be used to control the spread of uranium contamination, and how a form of reduced uranium could be used as an indicator of how bacteria breathe, providing insight into bacterial physiology. >>>

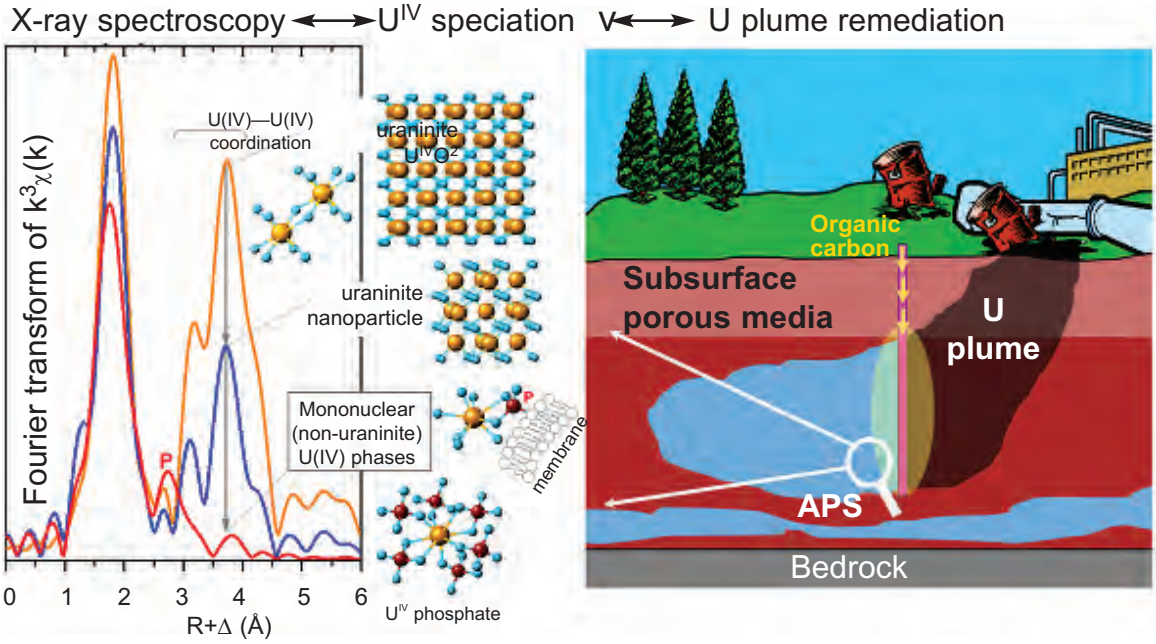

Fig. 1. Left: Fourier transform of U L_{III}-edge EXAFS data collected from U^{VI} bioreduction samples at the MR-CAT beamline 10-ID. Analysis of these data provides insight on the molecular speciaton of reduced U^{IV} (middle). This information is essential to predicting uranium plume propagation and devising effective remediation strategies.

In the absence of oxygen, bacteria oxidize carbon to gain energy, using oxidized metals, including uranium, as electron acceptors. With their different cell envelopes, cellular respiration occurs differently in gram-positive and gram-negative bacteria. Each type uses a different mechanism to transfer electrons out of the envelope to external electron receptors. Gram-negative bacteria have outer membrane reductases, allowing direct electron transfer to dissolved or solid electron receptors. In contrast, gram-positive bacteria do not have exposed electron transport proteins on their outer surface, suggesting that electron transfer may occur through soluble intermediates called electron shuttles. Both types of bacteria are found in natural environments and at contaminated field sites.

The researchers from Argonne, the Georgia Institute of Technology, the University of Notre Dame, the University of Tennessee, and Oak Ridge National Laboratory studied the reduction of carbonate-complexed U^{VI} by active gram-positive and gram-negative bacteria, and compared the results to reduction by a soluble reductant in the same medium. Using the 10-ID-B beamline at the APS for uranium L_{III}-edge x-ray absorption spectroscopy analyses (via x-ray absorption near-edge spectroscopy, XANES, and extended x-ray absorption fine structure, EXAFS), the authors determined the precise atomic coordination of U^{IV} produced biotically and abiotically in phosphate-free and phosphate-amended media.

The XANES measurements demonstrated that both types of bacteria reduce dissolved uranium U^{VI} to U^{IV}. When phosphate was not present, the researchers observed different U^{IV} reduction products for the two bacteria types from analysis of the U^{IV} EXAFS measurements. Gram-negative bacteria create uraninite; in contrast, gram-positive bacteria create a mononuclear, complexed form of U^{IV}, which may be less stable, and more easily dissolved and dispersed. These findings indicate that gram-positive and gram-negative strains use distinct mechanisms to reduce U^{VI}. Conversely, by determining the coordination environment of reduced U^{IV} atoms, the chemical conditions of their formation and the mechanism of electron transfer to U^{VI} can be inferred. With the addition of phosphate, EXAFS shows U^{VI} reduction to nonuraninite, phosphate-complexed U^{IV} species independent of microbial activity (Fig. 1). This result highlights a previously unappreciated control of phosphate on reduced U^{IV} speciation.

Besides aiding in the understanding of how uranium reduction occurs so that it may be used to control the spread of uranium contamination, the form of reduced uranium could be used as an indicator of how bacteria breathe, providing insight into bacterial physiology. Using the APS, uranium speciation could be employed as a "tag" to uncover electron transfer pathways in highly coupled biotic-abiotic redox systems such as the subsurface.

— Dana Desonie

See: Maxim I. Boyanov[1]*, Kelly E. Fletcher[2], Man Jae Kwon[1], Xue Rui[3], Edward J. O'Loughlin[1], Frank E. Lőffler[4,5], and Kenneth M. Kemner[1], "Solution and Microbial Controls on the Formation of Reduced U(IV) Species," Environ. Sci. Technol. **45**, 8336 (2011). DOI:10.1021/es2014049

Author affiliations: [1]Argonne National Laboratory, [2]Georgia Institute of Technology, [3]University of Notre Dame, [4]University of Tennessee, [5]Oak Ridge National Laboratory

Correspondence: *mboyanov@anl.gov.

Research under the Subsurface Science Focus Area program at Argonne National Laboratory was supported by the Subsurface Biogeochemical Research Program, U.S. Department of Energy (DOE) Office of Science under contract DE-AC02-06CH11357. Additional DOE funding was provided by the U.S. DOE Environmental Remediation Sciences Program (grant numbers ER63718 and ER64782). K.E.F. acknowledges support through a National Science Foundation graduate research fellowship. M.J.K. was supported by an Argonne Director's Fellowship and the KIST-Gangneung Institute (Grant 2Z03402). MR-CAT operations are supported by the DOE and the MR-CAT member institutions. Use of the Advanced Photon Source at Argonne National Laboratory was supported by the DOE Office of Science under Contract No. DE-AC02-06CH11357.

10-ID-B • Materials science, environmental science, chemistry • X-ray absorption fine structure, time-resolved x-ray absorption fine structure, micro x-ray absorption fine structure, microfluorescence (hard x-ray) • 4.3-27 keV, 4.3-32 keV, 15-90 keV • On-site • Accepting general users •

Using Ancient Zircon as a Thermometer

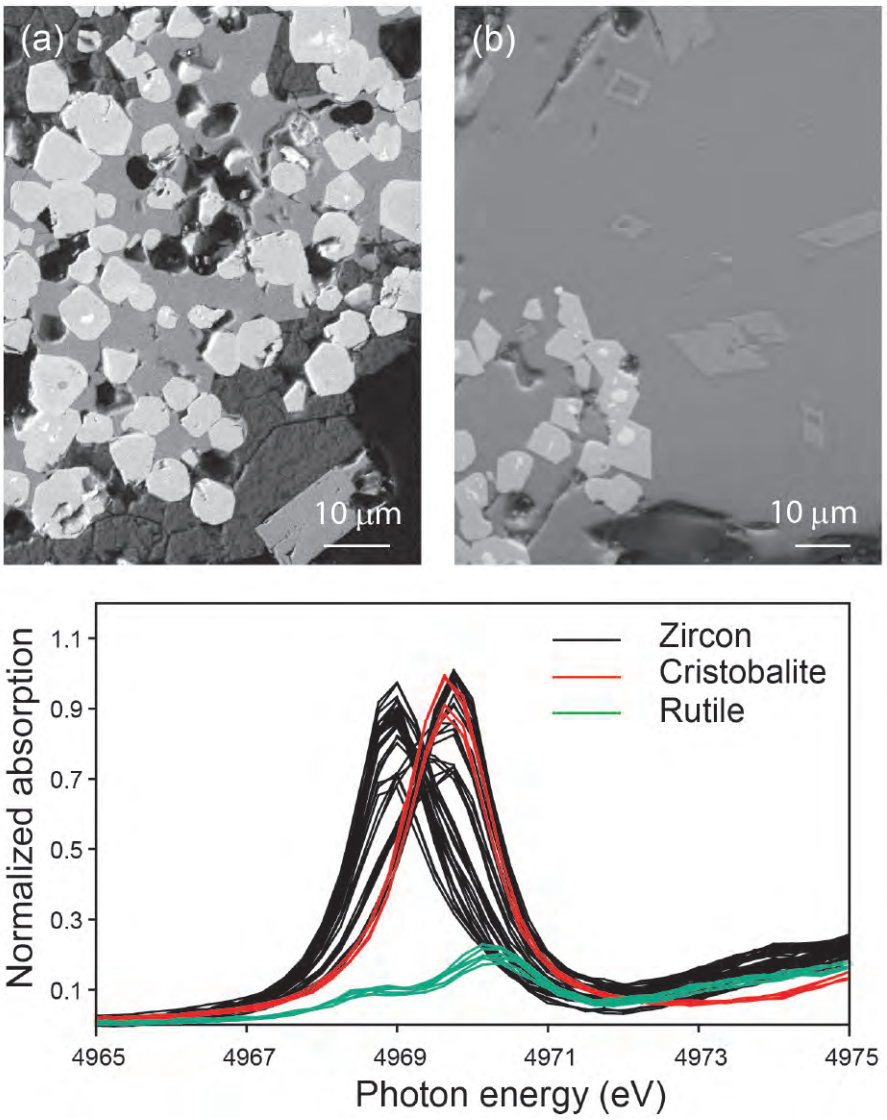

Fig. 1. Image (a) on the top left shows an electron microscopy image of a silica-saturated zircon experiment. Image (b) on the top right shows a silica-undersaturated zircon experiment. The color image on the bottom is a series of XANES spectra from zircon and other standard compounds.

The oldest known materials on Earth are sedimentary zircon grains from Western Australia that are 4.37 billion years old. Because zircon resists degradation from both radiation and chemicals, and has a physical structure that remains stable over billions of years, such grains look much like they did when they were formed. Their chemical characteristics are highly dependent on their original environment, so these ancient minerals hold clues to the temperature and pressure they experienced at their genesis. For example, knowledge of zircon composition suggests that they formed in low-temperature magmas, which in turn suggests that such granite creation processes existed very early in Earth's history. In order to improve the use of titanium concentrations in zircon as an ancient thermometer and pressure gauge — a process known as thermobarometry — a group of researchers synthesized zircon grains in a variety of environments and studied them utilizing the GSECARS 13-ID-C,D beamline at the APS to determine the crystallographic site of Ti in them. Their findings showed that Ti substitutes preferentially into the silicon tetrahedral site allowing the dominant incorporation reaction to be identified.

Zircon crystals are made of interlocking zirconia and silica crystallographic sites. When titanium is present, this too can be incorporated, but it has not been known whether the titanium substitutes for silicon or zirconium within the material. The distinction is crucial since different substitution mechanisms will result in different temperature-dependent reactions. So decoding the zircon's initial thermal conditions relies on understanding what kind of reaction drives its composition.

To study how zircon incorporates titanium, the researchers from Australian National University, Rensselaer Polytechnic Institute, the University of Bristol, Imperial College London, Curtin University, Southern Federal University, and The University of Chicago first had to produce bulk quantities of the crystals in various chemical compositions. This represents an experimental challenge, typically requiring temperatures in excess of 2000° C. Using two specialized techniques and incorporating a low-melting-point compound, the group synthesized grains of sufficient size requiring temperatures only of 1300° C. They created three different sets of crystals, each made of the elements zirconium, silicon, oxygen, and titanium, but assembled in different chemical structures.

Next, the group imaged and analyzed the internal structure of the synthesized zircon using several techniques: laser ablation inductively coupled plasma mass spectrometry (LA-ICP-MS), electron probe microanalysis (EPMA), and x-ray absorption near edge structure (XANES) spectra that were collected at beamline 13-ID-C. The first two techniques help determine the concentrations of any given element, while the XANES spectra provide a direct structural map of the grains to determine the position of the titanium.

The combined observations showed that during formation, the titanium atoms substitute on the silicon site in zircon. So those interested in thermobarometry now know to use this kind of a reaction to create guidelines on what temperatures cause what effects. The presence of this reaction also means that in addition to initial temperatures, the very presence and amount of silica within the system help determine zircon composition. Additional results from the XANES spectra show a strong influence of crystal orientation on peak intensity and energy, indicating that the crystal field itself may play an important role.

The team believes that even more environmental indicators may be gleaned from the material. They are looking at how pressure affects titanium placement and also looking at additional elements such as cerium and europium that can be incorporated into zircon crystals. These last two elements are probably directly related to how much oxygen was present during the time of zircon growth.

— Karen Fox

See: N.D. Tailby[1,2]*, A.M. Walker[3], A.J. Berry[4], J. Hermann[1], K.A. Evans[5], J.A. Mavrogenes[1], H.St.C. O'Neill[1], I.S. Rodina[6], A.V. Soldatov[6], D. Rubatto[1], and S.R. Sutton[7], "Ti site occupancy in zircon," Geochim. Cosmochim. Acta **75**, 905 (2011). DOI:10.1016/j.gca.2010.11.004

Author affiliations: [1]Australian National University, [2]Rensselaer Polytechnic Institute, [3]University of Bristol, [4]Imperial College London, [5]Curtin University, [6]Southern Federal University, [7]The University of Chicago

Correspondence: *tailbn@rpi.edu

This work was performed with support from the Australian Synchrotron Research Project (ASRP), which is funded by the Commonwealth of Australia under the Major National Research Facilities Program. This work was also supported by the NASA Astrobiology Institute. GSECARS is supported by the National Science Foundation – Earth Sciences (EAR-1128799) and U.S. Department of Energy (DOE) – Geosciences (DE-FG02-94ER14466). Use of the Advanced Photon Source at Argonne National Laboratory was supported by the U.S. DOE Office of Science under Contract No. DE-AC02-06CH11357.

13-ID-C,D • GSECARS • Geoscience, environmental science • Inelastic x-ray scattering, small x-ray absorbtion fine structure, microdiffraction, x-ray absorption fine structure, microfluorescence (hard x-ray), high-pressure diamond anvil cell, high-pressure multi-anvil press • 4-45 keV • On-site • Accepting general users •

Iron Oxide in Earth's Outer Core

Scientists speculate on the composition of the deep Earth by using a variety of types of information. These include seismological data, and phase diagrams and thermal equations-of-state that are generated from laboratory experiments. Since much of Earth's outer core may be iron with some oxygen, understanding the behavior of iron oxide under the high-pressure, high-temperature conditions found at the core is essential to understanding conditions there. Using x-ray diffraction at the GSECARS 13-ID-C,D beamline at the APS to study FeO materials exposed to simultaneous high pressures and temperatures, researchers learned that 7.7 ± 1.1 wt.% oxygen is apparently needed to be mixed with iron in the outer core in order to match the seismologically-determined density calculations of that region. >>>

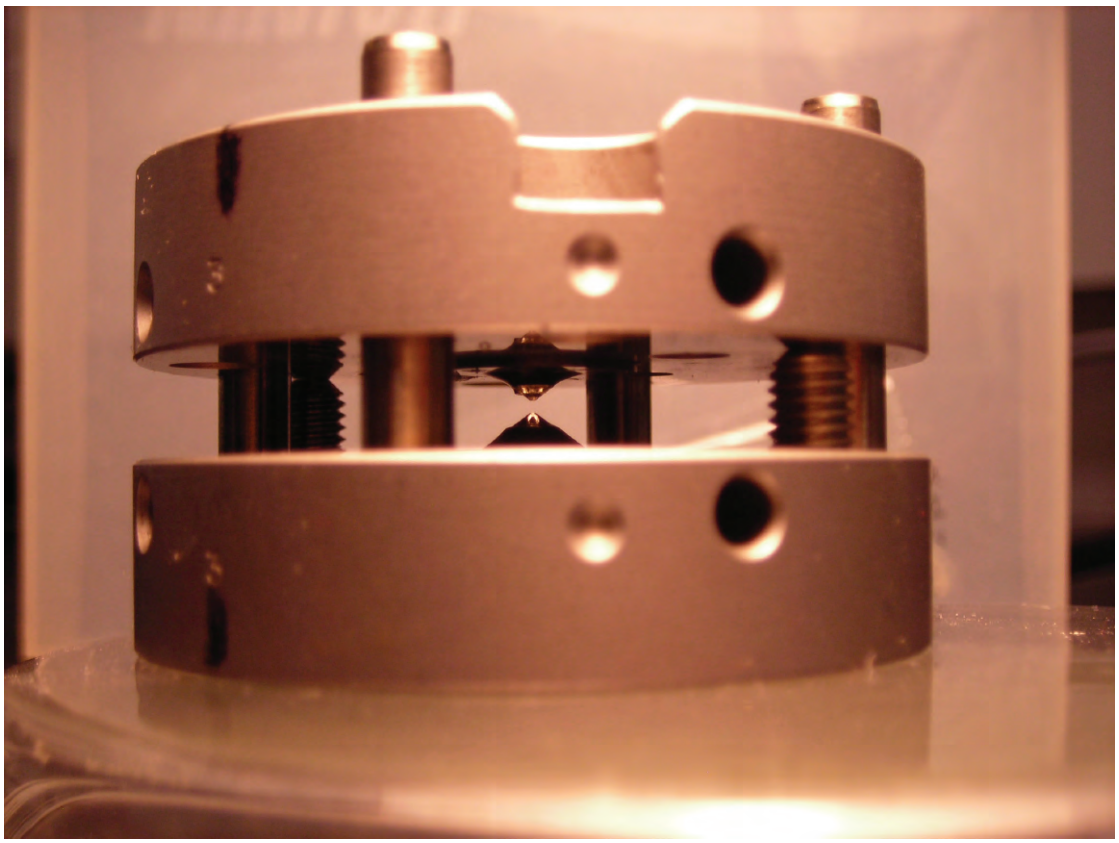

Fig. 1. This diamond anvil cell, used to generate high pressures, can fit into the palm of a human hand. Two diamonds oppose each other in the center of the cell and a tiny sample is placed in between them.

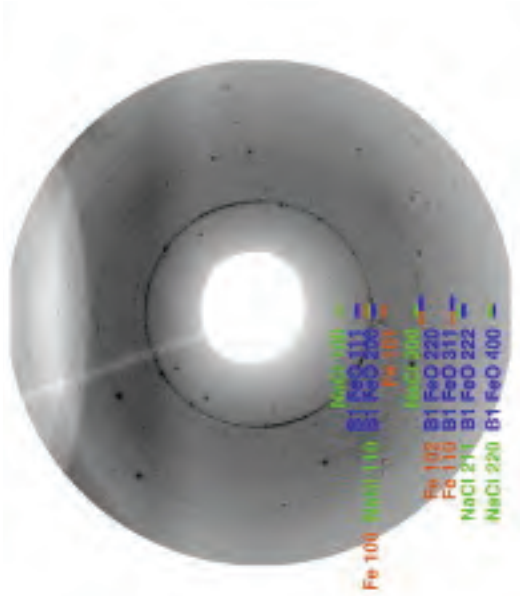

Fig. 2. Diffraction image before integration, collected at 144 GPa and 3025K.

Researchers use information collected from seismological studies to calculate the density of Earth's core, a value referred to as the Preliminary Reference Earth Model (PREM). They have also calculated the density of pure iron at outer core pressures by projecting along an adiabat, a line on a thermodynamic chart relating the pressure and temperature of a substance undergoing an adiabatic change. These two numbers do not match: the PREM is about 10.4% lower at the core-mantle boundary (CMB) than the value for the density of the region if it were made of pure iron. While 1% to 2% of this core density deficit is due to the change in the volume of iron as it melts, the rest is due to the presence of one or more elements that are lighter than iron. Although other lighter elements may be present, oxygen may be a large reason for the density deficit of the outer core.

To investigate the density deficit, researchers from the University of Maryland, the University of Bristol, and The University of Chicago created a thermal equation-of-state and phase diagram of FeO at pressures and temperatures relevant to the core-mantle boundary. The equation of state is used to determine the value of the density deficit of the outer core, to determine the amount of oxygen needed to make up the density deficit of the outer core, and to improve the understanding of the iron-iron oxide oxygen fugacity buffer at core conditions. These researchers prepared a sample that included iron and ~10 wt% oxygen that was laser heated and pressed in a diamond anvil cell (Fig. 1) to achieve temperatures and pressures consistent with the core-mantle boundary while they performed angle-dispersive x-ray diffraction experiments at the GSECARS beamline (Fig. 2).

Iron is the most common multivalent element within Earth and the oxygen fugacity of Earth's interior is dominated by the valence state of iron. The mineral wüstite, with composition $Fe_{1-x}O$, is important in the lower mantle and could also make up part of the outer core. Under these extreme pressure conditions, wüstite might be stable in a B1 (NaCl-type) or B8 (NiAs-type) crystal structure but, although both phases were seen in these experiments, only the B1 structure of FeO was shown to be stable under the P-T conditions relevant to the lower mantle and outer core.

To understand the Fe-FeO oxygen fugacity buffer at temperatures and pressures relevant to the core-mantle boundary, the research team applied the B1-FeO equation-of-state to calculations of core density under extreme pressure-temperature conditions. They determined that 7.7 ± 1.1 wt.% oxygen would remove the density deficit. Accounting for the presence of nickel in the outer core in a Ni/Fe atomic ratio of 0.0.58, 7.9 ± 1.1 wt.% oxygen is needed to match PREM at the CMB for a core of Fe-Ni-O. They concluded that B1 FeO is the stable phase of FeO in the lower mantle and core.

— Dana Desonie

See: Rebecca A. Fischer[1]*, Andrew J. Campbell[1], Gregory A. Shofner[1], Oliver T. Lord[2], Przemyslaw Dera[3], and Vitali B. Prakapenka[3], "Equation of state and phase diagram of FeO," Earth Planet. Sci. Lett. **304**, 496 (2011). DOI:10.1016/j.epsl.2011.02.025

Author affiliations: [1]University of Maryland, [2]University of Bristol, [3]The University of Chicago

Correspondence:

*rfischer@uchicago.edu

This work was supported by National Science Foundation grant EAR 0847217 to A.J.C. GSECARS is supported by the National Science Foundation - Earth Sciences (EAR-1128799) and U.S. Department of Energy (DOE) - Geosciences (DE-FG02-94ER14466). Use of the Advanced Photon Source at Argonne National Laboratory was supported by the U.S. DOE Office of Science under Contract No. DE-AC02-06CH11357.

13-ID-C,D • GSECARS • Geoscience, environmental science • Inelastic x-ray scattering, small x-ray absorbtion fine structure, microdiffraction, x-ray absorption fine structure, microfluorescence (hard x-ray), high-pressure diamond anvil cell, high-pressure multi-anvil press • 4-45 keV • On-site • Accepting general users •

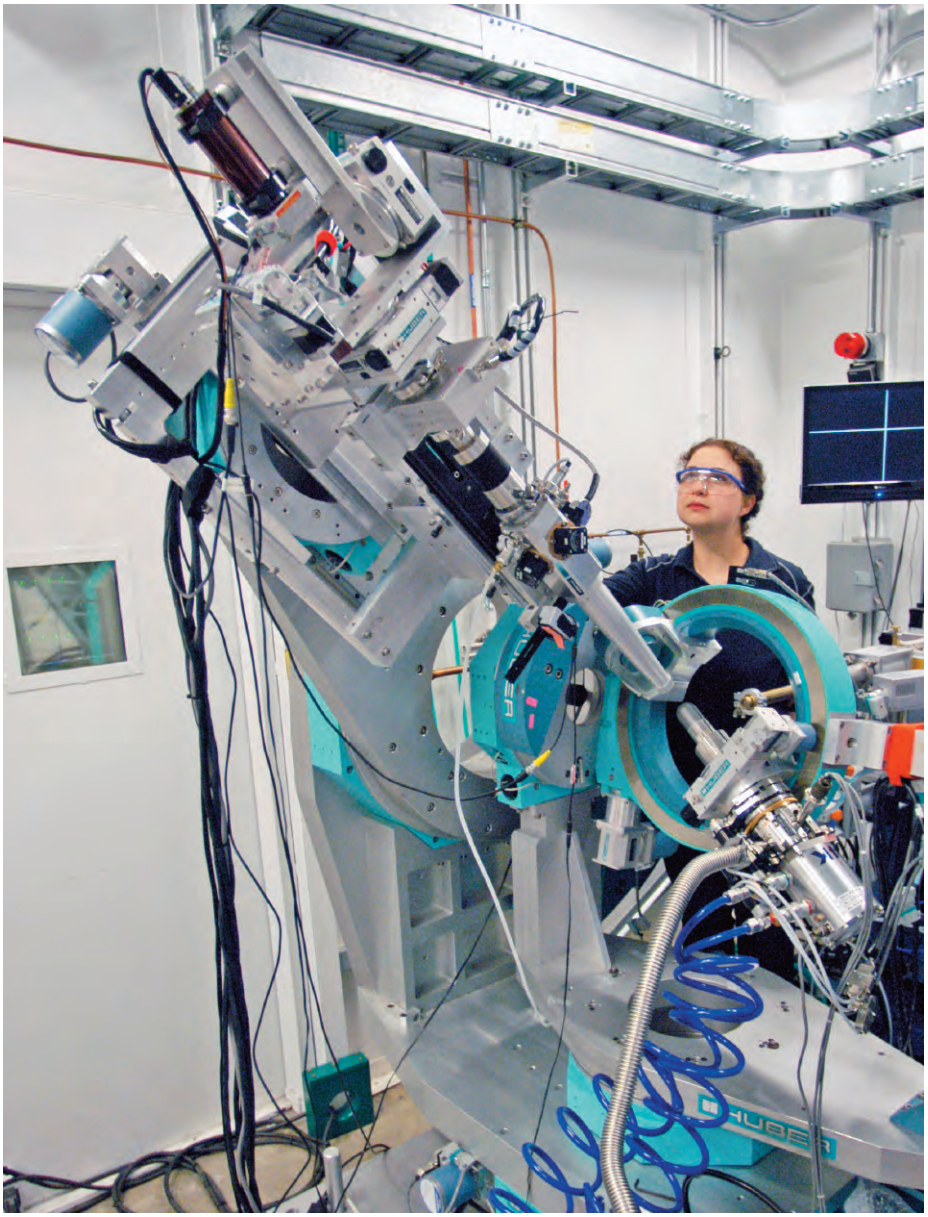

Sara Haravifard (XSD-MM and University of Chicago) with the instrument on beamline 6-ID-B at the APS used for the high-resolution, high-pressure structural measurements of the copper compound SCBO at cryogenic temperatures.

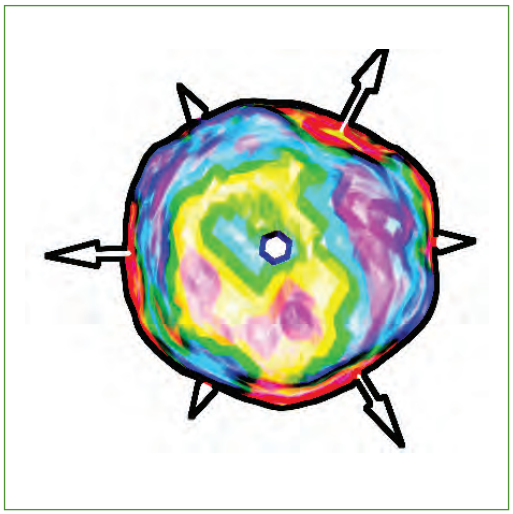

Nanoscience

3-D X-RAY MAP OF STRAIN ON A THIOL-COATED GOLD NANOCRYSTAL

Thiol-coated gold nanocrystals and polycrystalline films could potentially be used in a wide range of nanomechanical sensors, including for biomechanical applications. So an improved understanding of the factors influencing their properties at the nanoscale should lead to improvements in sensor performance. For instance, how chemically induced stress affects the shape of nanocrystals is important for the proper design and manufacture of the sensors that use them. Researchers employing the APS have deciphered the nanoscale distortions of a gold nanocrystal due to adsorption of a thiol-based self-assembled monolayer (SAMs). The researchers discovered that this chemically induced stress can be quite large, significantly altering the shape of the gold nanocrystal. Such stress was shown to be distinctly different over the curved regions of the nanocrystal as compared to its flat areas. >>>

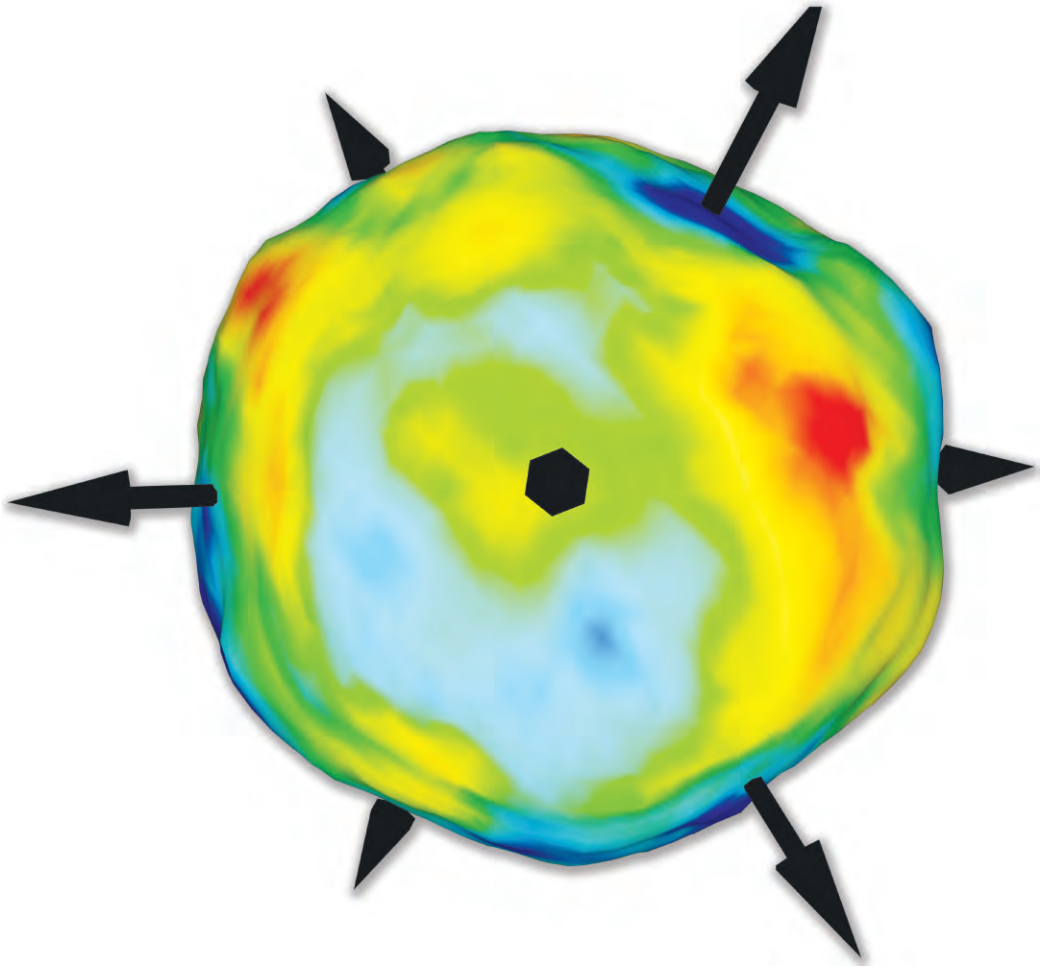

Fig. 1. Top view of the gold crystal studied at beamline 34-ID-C before dosing with thiols. The crystal has intrinsic strains (projected onto the measurement direction) shown as phases on a color scale running from -0.7 radians (blue) to +0.7 radians (red). The phases are colored onto a 15% isosurface of the density. Arrows indicate the crystal's {111} directions, which are perpendicular to its facets.

The scientists generated three-dimensional (3-D) images of a gold nanocrystal's surface by using the synchrotron-based coherent x-ray diffraction (CXD) technique that was pioneered at the APS by the London Centre for Nanotechnology. This method requires a powerful, coherent x-ray source, which was supplied by the APS facility.

The research group,including members from the London Centre for Nanotechnology and Argonne, analyzed the structural strain that occurred when single layers of propane thiol molecules, or 1-Propanethiol, C_3H_7SH (n-P mercaptan), were adsorbed into individual nanometer-sized grains of gold. (Thiol generally encompasses a range of various organosulfur compounds; that is, those organic compounds that contain sulfur.) CXD was used to analyze the shape of the metallic nanoparticles because the method is extremely sensitive to internal strains within nanocrystals.

The experiment to determine the magnitude and variety of surface strains began when the team first cleaned silicon wafers and then coated them with an evaporated layer of gold (20 nm in depth) positioned above an evaporated titanium adhesion layer (1 nm deep). The thin-film samples were then heated to approximately 1,922° F (1,050° C) for 12 h in a nitrogen gas environment. Scanning electron microscopy showed the formation of arrays of nanocrystals possessing a mean diameter of 200 nm, each separated about 1 to 2 μm from one another. Both spherical and flat surface regions were present on the nanocrystals.

A remotely operated syringe added a 5-mM solution of propane thiol dissolved in pure ethanol to the nitrogen-gas environment. Coherent x-rays of 8.92 keV from the XSD 34-ID-C beamline at the APS were focused on the sample. Three-dimensional images of the gold nanocrystals were taken at three distinct times: before they were coated with propane thiol, immediately after being coated, and 1 h after coating.

The 3-D images produced in the experiment were of a gold nanocrystal 300 nm in diameter. The images revealed that the structure of the nanocrystal changed dramatically after the adsorption of the propane thiol-based SAM molecules (Fig. 1). Upon application of the propane thiol, strain was concentrated in the gold crystal's curved areas (its corners) and away from its flat ones. Specifically, the gold crystal's flat regions contracted radially inward, while the curved ones expanded outward. A distinct pattern of differential surface strain was observed to occur across the surface along with a clear pattern of strain over 20 nm into the gold crystal's interior from its outer surface and toward its core. However, no strains penetrated to the core of the nanocrystal. The researchers concluded that the flat and curved regions of the polycrystalline gold films reacted very differently to the SAM-forming thiol molecules.

This chemically induced mechanical response is important in the design of sensors for medical applications. Nanosized sensors respond to changes in the chemical environment surrounding them and can read out the induced strains. The research provided by this study provides important insights into the chemically induced strain on gold nanocrystals due to thiol-based SAMs. These new insights will help scientists control the distortions within miniature biosensor devices, helping such sensors attain higher levels of sensitivity and reliability.

The experimental results can also be applied to biosensors that employ polycrystalline films coated with SAMs. The performance of such films is related to their grain size; that is, the density (and hence the size) of the films' nanocrystals. This performance variation can now be better understood since the chemically induced strain within such films varies with the shapes and orientations of the nanocrystals' facets, which in turn vary with respect to grain size. *— William A. Atkins*

See: Moyu Watari[1], Rachel A. McKendry[1], Manuel Vögtli[1], Gabriel Aeppli[1], Yeong-Ah Soh[2], Xiaowen Shi[1], Gang Xiong[1], Xiaojing Huang[1], Ross Harder[3], and Ian K. Robinson[1]*, "Differential stress induced by thiol adsorption on facetted nanocrystals," Nat. Mater. **10,** 862 (November 2011). DOI:10.1038/NMAT3124

Author affiliations: [1]University College London, [2]Imperial College, [2]Argonne National Laboratory
Correspondence: *i.robinson@ucl.ac.u

Work supported by the "nanosculpture" Advanced Grant from the European Research Council, a Science and Innovation Award for Nanometrology and a Nanotechnology "Grand Challenge in Healthcare" award from the UK Engineering and Physical Sciences Research Council. Use of the Advanced Photon Source at Argonne National Laboratory was supported by the U. S. Department of Energy Office of Science under Contract No. DE-AC02-06CH11357.

34-ID-C • XSD • Materials science, physics • Coherent x-ray scattering • 5-15 keV, 7-25 keV • On-site • Accepting general users •

MEASURING SPIN POLARIZATION IN A SEMI-METALLIC NANOWIRE

Spintronics constitutes a promising new avenue for improved electronic devices that exploit the spin of the electron. An essential part of developing practical spintronic devices such as racetrack memory, spin injectors, and magnetic tunnel transistors entails developing a suitable source for generating spin-polarized electrons (i.e., finding materials that emit electrons favoring the up or down spin states). In this research, carried out at XSD beamline 4-ID-C of the APS, a promising iron-silicon material doped with cobalt was synthesized with nanowire morphology, and the percentage of spin-polarized electrons it emitted was measured. The spin polarization was deduced using a technique called point contact Andreev reflection (PCAR) spectroscopy, which in part exploits the quantum behavior of superconductors. The researchers in this study achieved the first spin polarization measurements performed on nanowires. Other important characteristics of the iron-silicon-cobalt nanowires were measured as well. For instance, x-ray magnetic circular dichroism (XMCD) revealed that the cobalt atoms present in the nanowires constitute the primary source of the material's magnetization.

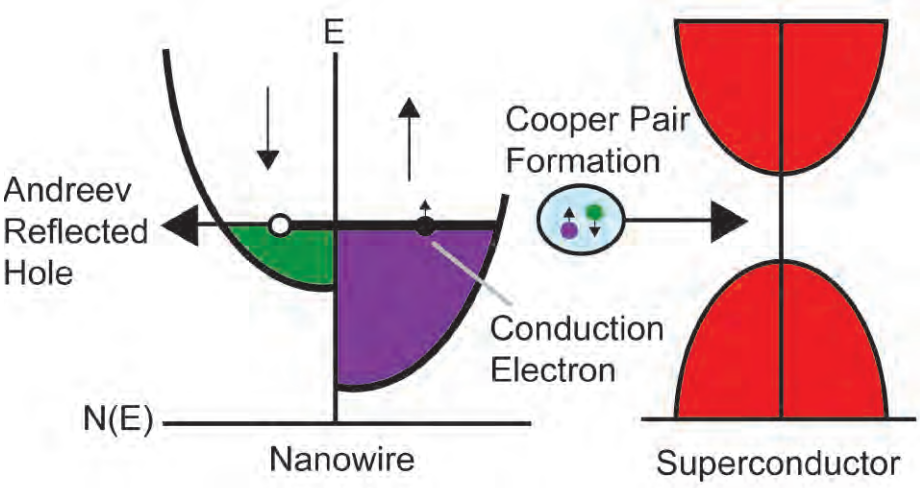

Fig. 1. Schematic spin dependent density-of-states diagram demonstrating Andreev reflection at the interface of a nanowire (with non-zero spin polarization) and a superconductor. When an incident conduction electron hits the superconductor interface it forms a Cooper pair by picking up an electron of opposite spin and reflecting a hole in the opposite direction, conserving charge and momentum.

The magnetic alloy investigated in this research has the chemical form $Fe_{1-x}Co_xSi$. The cobalt atoms are substituted for iron atoms, and the extent of this replacement is represented by the *x*-value. The researchers, from the University of Wisconsin-Madison and Argonne, used a custom-built vapor deposition apparatus to produce several batches of $Fe_{1-x}Co_xSi$ nanowires. The nanowires were initially probed to determine two important attributes: the distribution of the cobalt within each of the nanowires tested; and the origin of the alloy's intrinsic electron spin polarization in terms of its constituent elements — i.e., whether the spin polarization arises in the cobalt atoms, the iron atoms, or both.

The atomic probe tomography (APT) technique was utilized to map out the distribution of cobalt atoms in several nanowire samples. APT is a highly sensitive technique, yielding a three-dimensional representation of elemental distributions with angstrom (10^{-10} m) resolution. Individual nanowires were placed atop silicon posts using a micromanipulator for this analysis. The APT measurements indicated that the cobalt atoms were evenly distributed throughout the nanowires.

To determine the source of the electron spin polarization, nanowire samples were subjected to XMCD. This technique utilizes alternating left and right circularly polarized x-rays to probe the magnetic and spin properties of atoms. The sample to be studied is placed in a strong magnetic field—in this instance, a field strength of 2 T. Magnetic properties of atoms are mostly associated with certain electronic orbitals (for instance, the 3d orbitals in iron and cobalt). Both left and right circularly polarized synchrotron x-rays were supplied from the APS. Utilizing a monochromator, different x-ray photon energies were used to excite the electrons in various orbitals. The XMCD results showed that practically all the electron spin polarization within the $Fe_{1-x}Co_xSi$ nanowires arose from cobalt, not iron or silicon.

In order to measure the spin polarization within the $Fe_{1-x}Co_xSi$ nanowires, a modified version of PCAR was employed. In PCAR spectroscopy, the material being tested is connected to a superconductor. Whenever an electron passes from the test material (in this case, an $Fe_{1-x}Co_xSi$ nanowire) into the superconductor (cooled below the superconducting critical temperature T_c), then the incident electron will partner with another electron of opposite spin to form a Cooper pair; to conserve momentum, an electron hole is reflected back into the test material (Fig. 1). This quantum behavior (i.e., the formation of a Cooper pair and associated recoiling hole) doubles the material's effective conductivity. This doubling of conductance holds true *unless* there is a bias in electron spin.

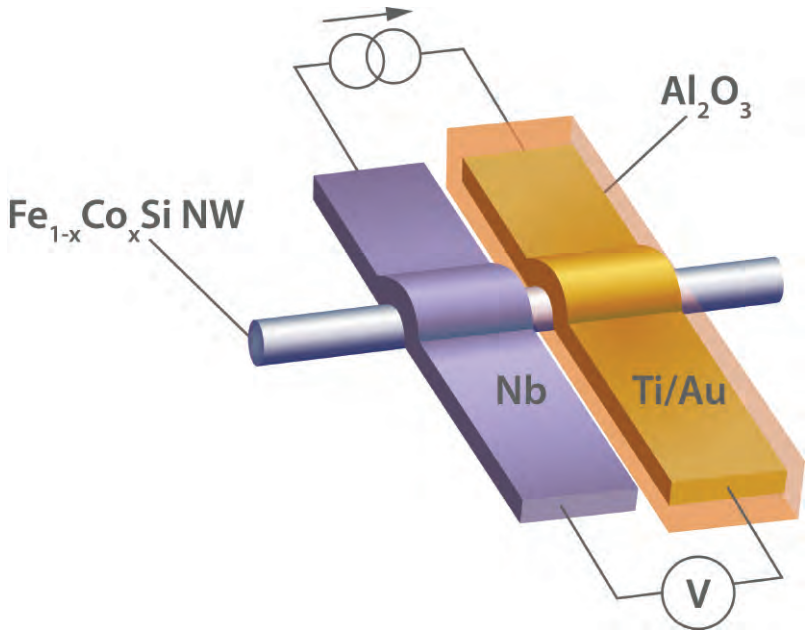

Fig. 2. Schematic view of $Fe_{1-x}Co_xSi$ nanowire device for Andreev reflection measurement with a niobium (Nb) superconducting contact. Note titanium-gold (Ti/Au) contact covered with an insulating aluminum oxide layer to prevent shorting between the two contacts.

If, for instance, the test material has more "spin up" than "spin down" electrons, then Cooper pair formation will be hindered by the lack of available spin-down electrons. The suppression of Cooper pair formation results in a proportional decrease in electrical conductivity measured by the experiment.

The "point contact" aspect of Andreev reflection spectroscopy, though wholly acceptable for thin films, is problematic for nanowire applications. The researchers therefore adapted their experimental setup using standard electronics fabrication techniques. Specifically, superconducting niobium contacts and titanium-gold contacts were deposited across individual nanowires (the schematic in Fig. 2 illustrates the basic setup). To prevent potential shorting between the nanoscale Nb and Ti-Au leads, the latter was covered with a 40-nm-thick, insulating aluminum oxide layer. The average spin polarization value, Ps, derived from six nanowire setups was 28%, with a top measured value of 35% spin polarization.

The successful measurement of spin polarization within a nanowire constitutes an important step forward in spintronic development. Key to these measurements was adapting point contact Andreev reflection spectroscopy to nanowire dimensions. Besides the iron-silicon-cobalt material examined here, scientists would like to investigate the electron spin characteristics of many other promising materials at the nanowire scale. The conventional electron-beam fabrication techniques used in this research for the spin polarization measurements, along with the APT and XMCD methods employed for determining the nanowires' elemental composition and spin distribution, should be readily applicable to determining the electron spin polarization of many other nanowire compositions. *— Philip Koth*

See: John P. DeGrave[1], Andrew L. Schmitt[1], Rachel S. Selinsky[1], Jeremy M. Higgins[1], Song Jin[1]*, and David J. Keavney[2], "Spin Polarization Measurement of Homogeneously Doped $Fe_{1-x}Co_xSi$ Nanowires by Andreev Reflection Spectroscopy," Nano Lett. **11**, 4431 (2011). DOI:10.1021/nl2026426

Author affiliations: [1]University of Wisconsin-Madison, [2]Argonne National Laboratory

Correspondence: *jin@chem.wisc.edu

This research was supported by the Research Corporation for Science Advancement through a Cottrell Scholar Award. S.J. also thanks the National Science Foundation (CBET-1048625) and the Sloan Research Fellowship for support. Use of the Advanced Photon Source at Argonne National Laboratory was supported by the U.S. Department of Energy Office of Science under Contract No. DE-AC02-06CH11357.

4-ID-C • XSD • Physics, materials science • Magnetic circular dichroism (x-ray magnetic circular dichroism, soft x-ray), x-ray magnetic linear dichroism, x-ray photoemission spectroscopy, x-ray photoemission electron microscopy, anomalous and resonant scattering (soft x-ray) • 500-2800 eV • On-site • Accepting general users •

LAYING DOWN THE RULES FOR SUPERLATTICE SYNTHESIS

Sometimes, control is everything. That is certainly the case in the design and engineering of superlattices, which are nanoscale layers of different materials assembled for various practical applications. But precise control of events at the nanoscale is fiendishly difficult, because it is hard to predict exactly how different atoms or nanoparticles will come together and interact as they form a new crystal lattice. The ability to predict and thus control superlattice formation would be a major step in engineering nanomaterials for increasingly specific and precisely tailored purposes on the macroscale. Based partly on a series of experiments performed at the APS, a team of researchers has devised a set of design rules that can be used to control the synthesis of superlattices by using DNA as a programmable assembly agent.

Working at the DND-CAT 5-ID-B,C,D beamline at the APS, the experimenters from Northwestern University and Argonne used small-angle x-ray scattering (SAXS) to observe and characterize the formation of superlattices constructed using building blocks of gold nanoparticles coated with a dense layer of highly oriented DNA strands sticking out perpendicular to the nanoparticle surface (DNA-NPs or spherical nucleic acids [SNAs], Fig. 1).

The superlattices were also embedded in a resin and examined under transmission electron microscopy (TEM). The team used Linus Pauling's Rules governing the lattice structures of atomic crystals [1] as an inspiration to develop their own guidelines on determining superlattice structure and stability. However, while Pauling's Rules are essentially only predictive and descriptive, the researchers have gone further, constructing a workable model that can describe, predict, and control superlattice structure by influencing the hybridization events among the individual nanoparticles.

Nine different DNA-NP superlattices were constructed using oligonucleotide linker strands. These linkers bind to a DNA-NP and present a single-stranded "sticky end" at a controllable distance from the nanoparticle's surface, which allows for control over the distance between adjacent particles. The DNA sequence used as a "sticky end" then dictates which DNA-NPs can form bonds with one another. Because the DNA-NPs are polyvalent, they can bond to multiple other NPs, forming a large number of DNA connections; the driving hypothesis in the researchers' work is that the most stable crystal structure will always be the one that maximizes the number of these DNA connections.

The rules based on this hypothesis delineate the controlled synthesis of nine distinct crystallographic symmetries, wherein the researchers show that they can independently control the superlattice periodicity, lattice parameters (from 25 nm to 150 nm), and particle size (from 5 to 60 nm). The specific rules that dictate crystal stability are:

1. In a system where DNA-NPs have equal hydrodynamic radii, each NP will maximize the number of neighboring nanoparticles with complelmentary sticky ends;
2. In lattices of similar stability, slowing the hybridization rate of individual DNA linkers allows one to stabilize kinetic products;
3. The overall hydrodynamic radius of a DNA-NP dictates its packing and assembly behavior, rather than the sizes of its individual components (nanoparticle or DNA strand);
4. The size and DNA linker ratio between two particles dictate the most-favored thermodynamic structure;
5. Two systems with the same size ratio and DNA linker ratio will exhibit the same thermodynamic product; and
6. All possible DNA-specific hybridizations will be maximized in the most stable crystal structure.

Because determining the specific number of DNA duplexes formed within a particular lattice is problematic, the team found it difficult to experimentally confirm their key hypothesis that the maximization of DNA hybridization events is the most

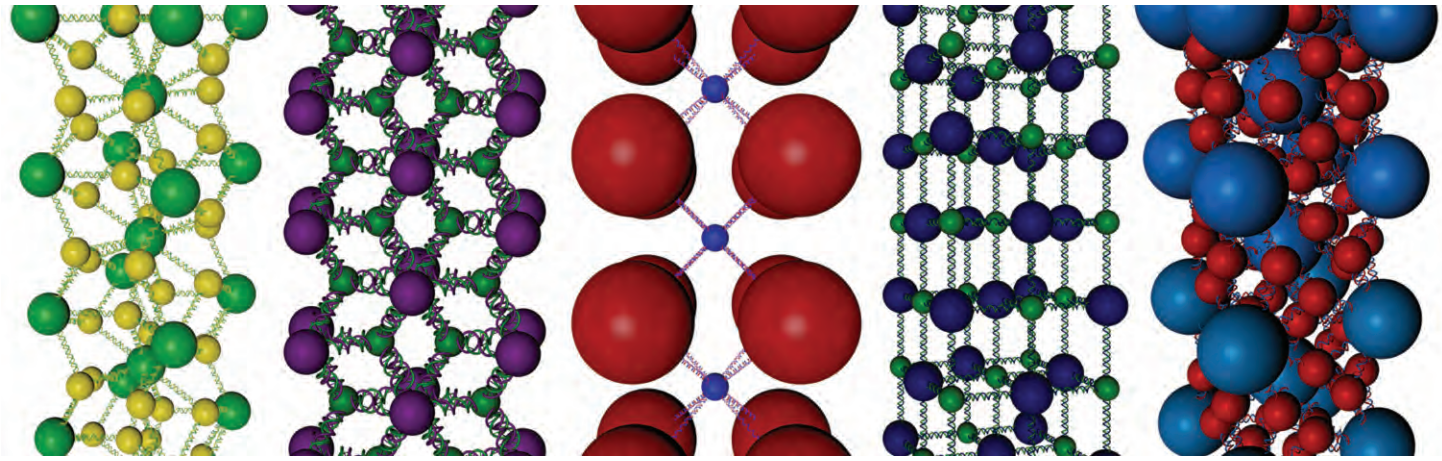

Fig. 1. Gold nanoparticles with DNA linkers assemble into lattices that maximize hybridization interactions between neighboring particles. The lattices shown have the same structures as (from left) Cr_3Si, AlB_2 , CsCl, NaCl, and Cs_6C_{60} crystals.

important factor in determining the stability of nanoparticle superlattices. So the researchers developed a model to calculate relative crystal stabilities that correctly predicts the structures resulting from an extensive range of DNA-NP size and linker ratios. Most of the data derived from this model are consistent with that obtained from the synthesized superlattices, indicating that the model (named CCM, or complementary contact model, by the experimenters) could be useful in further computational studies.

With the CCM and the six design rules that have been codified, this work not only provides major and important new insights into the design and assembly of nanoparticle superlattices, but also a practical set of tools that will now be available for the creation of new nanostructures possessing unique properties and functions for myriad applications. Refinement and extension of these experiments promises to open up new possibilities and potentials in many areas of nanotechnology.

— Mark Wolverton

REFERENCE

[1] Linus Pauling, "The principles determining the structure of complex ionic crystals," J. Am. Chem. Soc. **51,** 1010 (April 1929).

See: Robert J. Macfarlane[1], Byeongdu Lee[2], Matthew R. Jones[1], Nadine Harris[1], George C. Schatz[1], Chad A. Mirkin[1,2]*, "Nanoparticle Superlattice Engineering with DNA," Science **334**, 204 (14 October 2011). DOI:10.1126/science.1210493

Author affiliations: [1]Northwestern University, [2]Argonne National Laboratory

Correspondence: *chadnano@northwestern.edu

This work was supported by the Defense Research & Engineering Multidisciplinary University Research Initiative of the Air Force Office of Scientific Research, and by the U.S. Department of Energy (DOE) Office of Science [award DE-SC0000989; Northwestern University (NU) Non-equilibrium Energy Research Center] (C.A.M. and G.C.S.); a National Security Science and Engineering Faculty Fellowship from the U.S. Department of Defense (C.A.M.); a NU Ryan Fellowship (R.J.M.); and a NU Ryan Fellowship and a National Science Foundation Graduate Research Fellowship (M.R.J.). DND-CAT is supported by E.I. DuPont de Nemours & Co., The Dow Chemical Company and Northwestern University. Use of the Advanced Photon Source at Argonne National Laboratory was supported by the DOE Office of Science under Contract No. DE-AC02-06CH11357.

5-ID-B,C,D • DND-CAT • Materials science, polymer science • Powder diffraction, x-ray standing waves, x-ray optics development/techniques, small-angle x-ray scattering, surface diffraction, x-ray reflectivity, wide-angle x-ray scattering • 5-20 keV • On-site • Accepting general users •

CREATING CURRENT-CONTROLLED NANOSTRUCTURES UTILIZING VANADIUM OXIDE

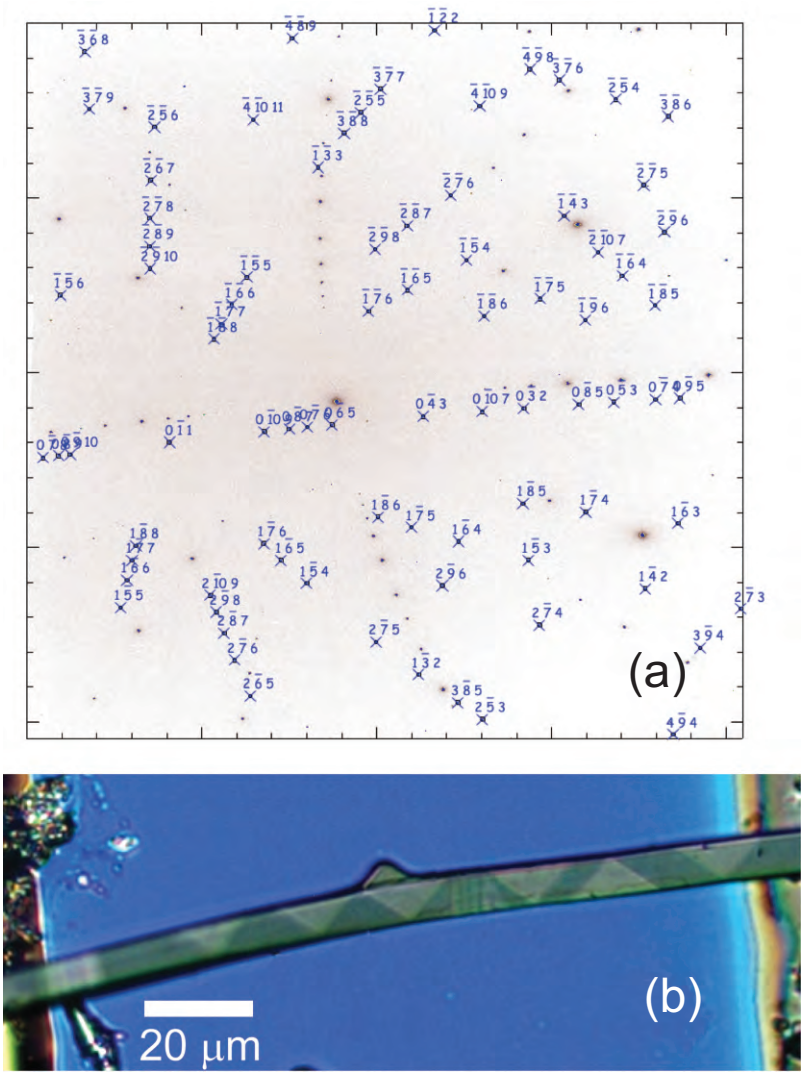

Fig. 1. (a) A Laue microdiffraction pattern and (b) polarized light optical image of a vanadium dioxide nanoplatelet in the mixed, multiphase, state. Laue patterns like that shown in panel (a) can be taken with a spatial resolution of about 0.4 μm, which allows identification of phases in complex domain structures as shown in panel (b) for a suspended single-crystalline nanoplatelet of vanadium dioxide.

Actuators are devices capable of transforming energy into a mechanical force, or movement, by thermal, electrical, magnetic, or some other form of energy. They can range from the very large to the very small. Researchers with an eye to the future foresee creating functional, electromechanical actuators at the micro- and nanoscale. Such microelectromechanical systems may one day be deployed as tiny robots or sensors that could circulate in the blood stream or other environments. At least two hurdles have thus far limited the practicality of such tiny devices. With a critical assist from an APS beamline, researchers have demonstrated the principles behind an electrothermal, current-controlled actuator that can overcome these hurdles and function near room temperature. This work represents a marked improvement over previous designs of electrothermal actuators.

Actuators using voltage to produce motion — piezoelectric devices — are limited by the small size of the mechanical deformations produced, while bimorph actuators combining thermal and electrical activation are heated to high temperatures, above 600º C, to produce large mechanical displacements, limiting the material environments where they might be used. In order to demonstrate that the principles behind an electrothermal, current-controlled actuator could function near room temperature using the metal-insulator transition (MIT) of vanadium dioxide (VO_2), the team grew single-crystalline nanoplatelets of VO_2 10- to 30-μm wide and 0.5- to 2.0-μm thick. The relatively large size of the platelets allowed probing of domain properties with polarized light optical microscopy.

The researchers from Oak Ridge National Laboratory and Southern Illinois University suspended VO_2 nanoplatelets between two electrical contacts over a silicon substrate, anchored at both ends to liquid metal droplets with a low melting point. VO_2 transitions from the metallic to the semiconducting phase at about 68º C, near room temperature. The MIT transition was induced by manipulating the voltage applied to the nanoplatelets—resulting in physical deformation, or mechanical bending, of the platelets due to Joule heating—or by varying the temperature of the substrate.

Further examination of the structure and crystal domain orientation was performed using synchrotron Laue microdiffraction at XSD beamline 34-ID-E, which produced Laue patterns of one nanoplatelet showing that at a constant voltage of 10 V applied to a nanoplatelet, as the temperature of the substrate drops the nanoplatelets transition from a purely metallic phase at 60º C to a mixed state of coexisting semiconducting and metallic phases at 44º C, and finally, fully to the insulating phase at 25º C. Lattice expansion in the semiconducting phase causes significant bending of the nanoplatelet in the mixed state (Fig. 1), and similar patterns were observed in all nanoplatelets subjected to large currents. Similar reversible phase transitions occurred when the voltage was lowered from 10 to 4 V; switching the current back and forth caused repeated bending and straightening of the nanoplatelets.

At the phase transition, electrical conductivity increased by several orders of magnitude, with a significant change in lattice structure, accompanied by expansion along the axis of the nanoplatelets, about 1%, and a contraction of about 0.5% perpendicular to the axis. These structural and electronic characteristics of the phase transition of VO_2 can be used to control the mechanical motion of the nanoplatelets. Using an electrical current, rather than direct thermal actuation, may allow finer and faster control of mechanical motion for a wide range of temperatures at or below 68º C.

Recent advances in materials synthesis have allowed significant size reductions and improved control in actuating devices since the first observations of the deformation of VO_2 crystals nearly 30 years ago. In this study, the authors have demonstrated a new method to achieve a marked improvement over previous designs of electrothermal actuators: the ability to produce significant mechanical deformation at temperatures near room temperature.

— Elise LeQuire

See: Alexander Tselev[1]*, John D. Budai[1], Evgheni Strelcov[2], Jonathan Z. Tischler[1], Andrei Kolmakov[2], and Sergei V. Kalinin[1], "Electromechanical Actuation and Current-Induced Metastable States in Suspended Single-Crystalline VO_2 Nanoplatelets," Nano Lett. **11**, 3065 (2011). DOI:10.1021/nl200493k

Author affiliations: [1]Oak Ridge National Laboratory, [2]Southern Illinois University
Correspondence: *tseleva@ornl.gov

J.D.B. and J.Z.T. were supported by the U.S. Department of Energy (DOE) Office of Science, Materials Sciences and Engineering. Use of the Advanced Photon Source at Argonne National Laboratory was supported by the DOE Office of Science under Contract No. DE-AC02-06CH11357.

34-ID-E • XSD • Materials science, physics • Microdiffraction, Laue crystallography, microbeam • 7-30 keV • On site • Accepting general users •

SUPERPARAMAGNETIC RESONANCE IMAGING

Tiny magnetic particles of iron oxide packed with cobalt ions could be used as tunable contrast agents to boost the scan images obtained during magnetic resonance imaging (MRI), according to research carried out at the DND-CAT 5-BM-D beamline at the APS. The ability to leach a controlled amount of cobalt from the prepared nanoparticles before use, and so change their magnetic properties, offers the possibility of tunable contrast for imaging specific tissues and organs. This work also underscores how important understanding the properties of nanomaterials is in the development of reliable contrast agents for diagnostic and therapeutic applications.

Magnetic resonance imaging has quickly emerged as one of the most efficacious diagnostic and research techniques in medicine. It uses powerful magnets to temporarily line up the atomic nuclei of hydrogen atoms in water molecules within the tissues of the body and then pulses the tissue with radio waves, energizing the nuclei. The speed with which the nuclei relax depends critically on the surroundings in which the water molecules find themselves, which produces a series of signals characteristic of the composition of particular tissues. A computer interprets these signals to build up the familiar MRI image.

Unfortunately, the signals produced by MRIs are anything but strong. So the radiographer may have to dose the patient with a chemical contrast agent, which emphasizes the differences in the signals from different tissues and provides an enhanced image. High-relaxivity contrast agents are the most efficient and therefore produce better contrast in the image. Chemists have spent many years looking for novel and non-toxic contrast agents for MRIs that would make the process safer while simultaneously improving the diagnostics.

One group of materials that have recently emerged as potential contrast agents are composite nanomaterials. The researchers in this study, from Northwestern University, point out that advances in synthetic methods for preparing such materials using iron oxide in the form of magnetic spinel ferrites are now lending themselves to the development of tunable contrast agents for MRIs. Such materials could extend the repertoire of MRI radiographers by allowing them to choose a specific contrast agent to get the optimal image of a given tissue or lesion.

The researchers synthesized silica-coated iron oxide and cobalt ferrite nanoparticles using standard high-temperature thermal decomposition and base-catalyzed techniques. Superparamagnetic ferrite nanoparticles act as powerful MRI contrast agents because they function as tiny yet powerful magnets when bathed in a magnetic field. It was the cobalt ferrite nanoparticles that emerged as most promising because under neutral aqueous conditions, the team found that they could leach out between 50% and 75% of the cobalt from the core of the nanoparticle. The effect of this change is to boost the magnetization and relaxivity of the nanoparticles making them more than seven times more effective as contrast agents. Crucially, however, the leaching process can be controlled to "tune" the agent to a particular level of magnetization prior to use in a patient.

The team carried out x-ray absorption fine structure (XAFS) studies on the 5-BM-D beamline to reveal precisely how the atomic structure of the ferrite core is altered by the leaching process from a partially inverted spinel cation arrangement to an inverse spinel arrangement. In addition, they employed transmission electron microscopy (TEM) and dynamic light scattering to prove that the overall morphology — fundamental properties, magnetization aside — are unchanged. The team emphasizes just how important the insights available through XAFS and parallel techniques are in understanding the way in which nanomaterials are of potential medical importance.

The team asserts that biocompatibility and stability in the body, as well as the optimization of the nanoparticles' magnetic properties are critical to the success of such contrast agents. In parallel with the structural work they have therefore closely monitored particle size, crystallinity, composition, crystallographic structure, surface features, and the surface coating of the nanoparticles and are confident that these materials can be further developed as viable MRI contrast agents.

— David Bradley

See: Elise A. Schultz-Sikma, Hrushikesh M. Joshi, Qing Ma, Keith W. MacRenaris, Amanda L. Eckermann, Vinayak P. Dravid, and Thomas J. Meade*, "Probing the Chemical Stability of Mixed Ferrites: Implications for Magnetic Resonance Contrast Agent Design," Chem. Mater. **23**, 2657 (2011). DOI:org/10.1021/cm200509g

Author affiliation:
Northwestern University
Correspondence:
*tmeade@northwestern.edu

The work performed at Northwestern University was supported by the Center for Cancer Nanotechnology Excellence initiative of the National Institutes of Health's National Cancer Institute under Award U54CA119341 and the National Institute of Biomedical Imaging and Bioengineering under Award 1RO1EB005866-01. DND-CAT is supported by E.I. DuPont de Nemours & Co., The Dow Chemical Company and Northwestern University. Equipment installed at DND-CAT has been provided by the DND-CAT partners, the U.S. National Science Foundation, the U.S. Department of Energy, and the State of Illinois. Use of the Advanced Photon Source at Argonne National Laboratory was supported by the U. S. Department of Energy Office of Science under Contract No. DE-AC02-06CH11357.

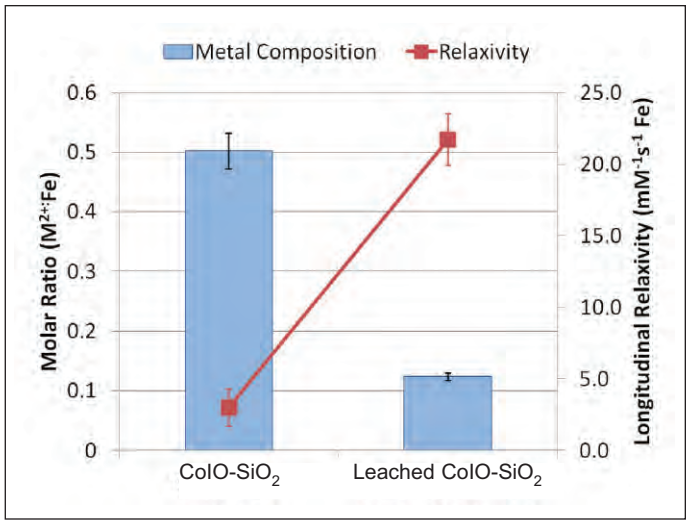

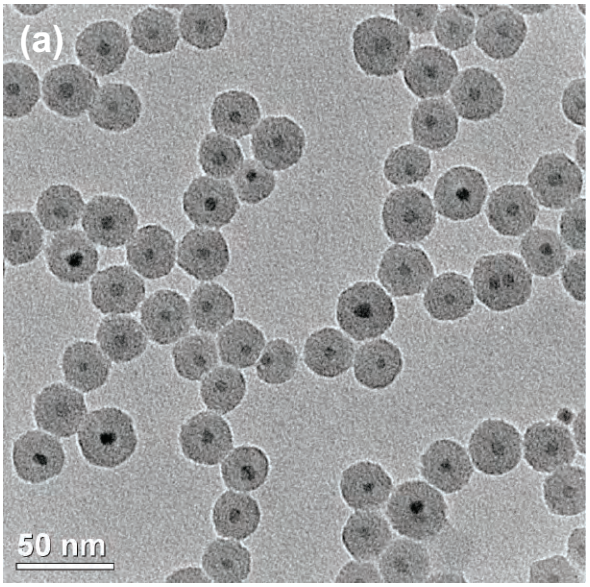

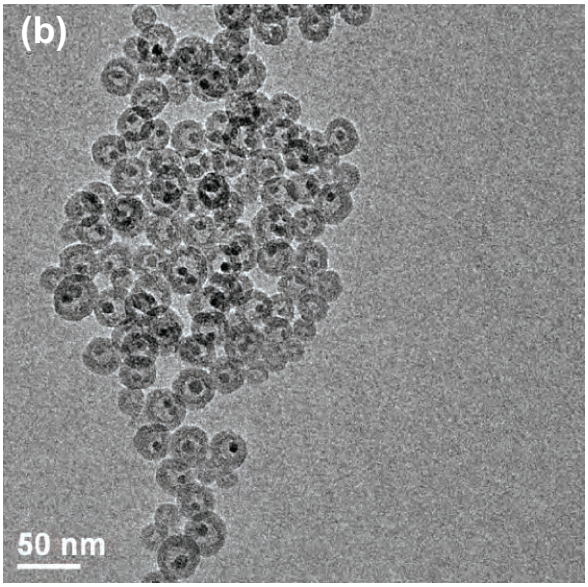

Fig. 1. Above: Plot of the changes in metal composition and relaxivity of silica-coated cobalt ferrite nanoparticles (CoIO-SiO_2) observed following leaching of cobalt from the core of the particle in aqueous conditions. The nanoparticles become more effective MRI contrast agents (higher relaxivity) following leaching. Right: (a) TEM of unleached and (b) leached CoIO-SiO_2. Leaching of the cobalt from the nanoparticle results in observable changes in the core structure.

5-BM-D • DND-CAT • Materials science, polymer science • X-ray absorption fine structure, high-energy x-ray diffraction, general diffraction • 4.5-25 keV, 4.5-80 keV • Accepting general users •

A BALANCING ACT IMITATES NATURE'S COMPLEXITY

Nanoparticles of uniform shapes — monodisperse particles — have been observed in bulk solutions to organize themselves spontaneously into larger assemblies known as supraparticles. This process continues unchecked until the particles solidify or precipitate out of solution. Researchers are now taking a conceptually novel approach to the process of self assembly by which polydisperse inorganic nanoparticles (those with a broad range of size, shape, and mass) form monodisperse supraparticles (those of uniform size or distribution) that are self-limiting. These supraparticles rival in complexity certain naturally occurring nanostructures such as viruses. A team of researchers has discovered that the self-limiting growth process of the inorganic nanoparticles, in contrast to their natural counterparts, relies on equilibrium between repulsive electrostatic and attractive van der Waals forces. This work points to ways of engineering of complex macroscale materials inspired by nature . >>>

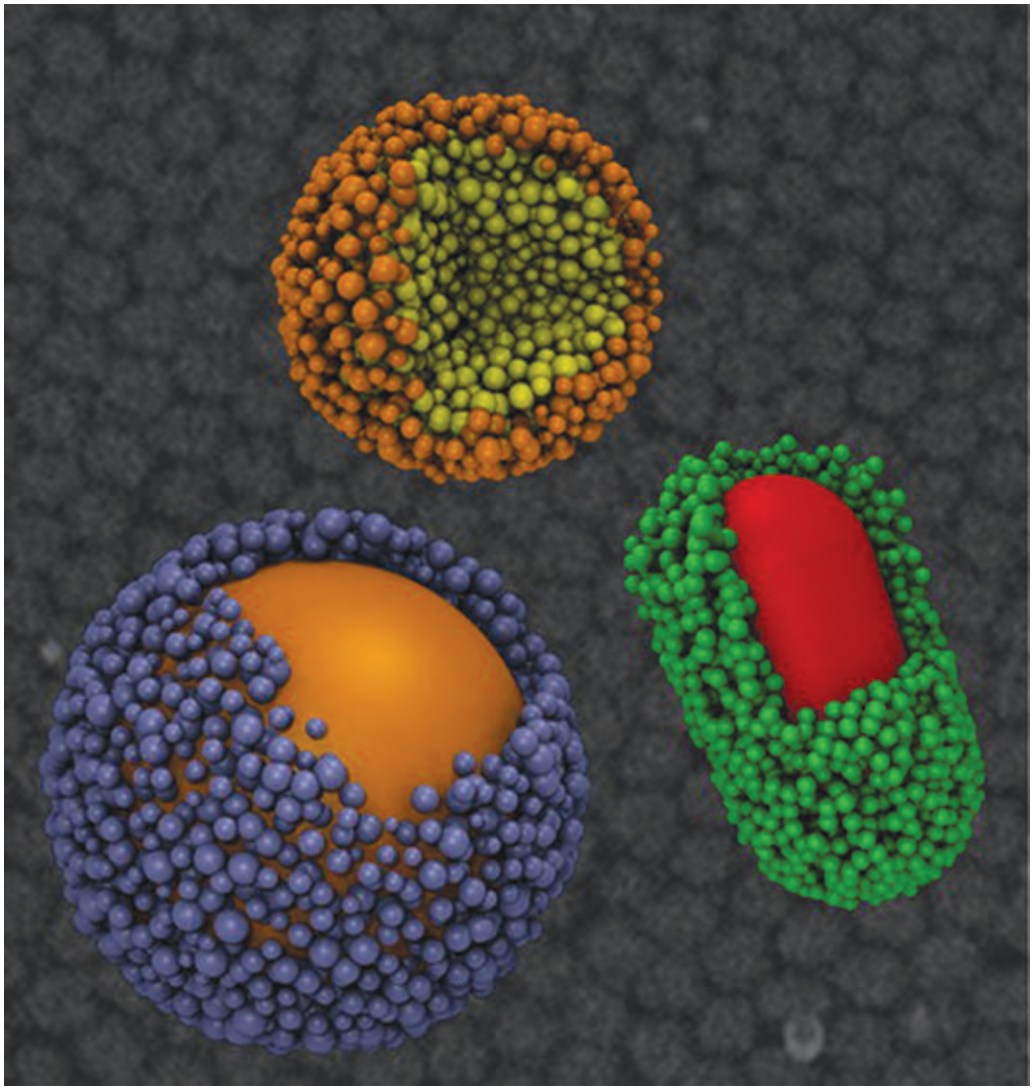

Fig. 1. Bottom: Scanning electron microscope image for monodisperse CdSe supraparticles. Color: Theoretical simulation image of supraparticles.

The groundwork for the suite of experiments was laid in The Kotov Lab at the University of Michigan by first observing the self-assembling behavior of inorganic nanoparticles of cadmium selenide (CdSe), a semiconductor known for its potentially useful optical properties in applications such as medical imaging. Synchrotron small-angle x-ray scattering (SAXS) measurements performed at the XSD 12-ID-B beamline captured the diameters of the supraparticles as they grew over time in an aqueous solution at 80º C from an initial size at 20 min of 20 nm, to about 30, 40, and 50 nms at 2, 18, and 40 h. These findings correlated well with data from transmission electron microscopy, scanning electron microscopy, and dynamic light scattering.

SAXS measurements also revealed details about the structure of the material. Although the supraparticles were highly monodisperse within the solution, inside the supraparticles, the nanoparticles themselves were highly polydisperse, a finding essentially different from observations in previous experiments. In addition, as the diameters of the nanoparticles increased within the supraparticles, the assembly formed a core-shell structure with nanoparticles loosely packed near the core and more densely packed near the outer shell. When the researchers added gold nanoparticles to CdSe nanoparticles in the initial solution, the material formed a self-limiting assembly with a gold nanorod core and a shell of CdSe nanoparticles.

The research team, from the University of Michigan, the National Center for Nanoscience and Technology in China, and Argonne attributes the cessation of growth of the supraparticles to the balance of van der Waals attraction between the nanoparticles, and electrostatic repulsion between supraparticles and nanoparticles. Moreover, the team found that a similar balance of forces occurs in a variety of other self-assembling materials such as the semiconductors cadmium sulfide, zinc selenide, and lead sulfide.

Computer simulations allowed the team to model a wide variety of nanoparticles with different shapes, sizes, and net charges. The model results indicated a process that parallels that of the experimental results, as the simulated nanoparticles grew first into loose aggregates and finally formed spherical uniform supraparticles. The simulations also confirmed that the supraparticles are in a thermodynamic equilibrium state of attraction/repulsion rather than being governed by kinetic forces.

Both structures, the cylindrical and the spherical supraparticles, resemble in many respects self-limiting organic superstructures that occur in nature, such as viral capsids that encapsulate the DNA and RNA of the cowpea mosaic virus, with its spherical architecture, and other viruses, like rabies, with rod-like structures. Unlike viruses, which have a lock-and-key mechanism that allows the virus to enter its host in order to replicate, these inorganic supraparticles maintain their equilibrium solely through the balance of electrostatic repulsion and van der Waals attraction. Together, these findings suggest new pathways for the engineering of complex macroscale materials inspired by nature. *— Elise LeQuire*

See: Yunsheng Xia[1], Trung Dac Nguyen[2], Ming Yang[2], Byeongdu Lee[3], Aaron Santos[2], Paul Podsiadlo[2], Zhiyong Tang[1], Sharon C. Glotzer[2], and Nicholas A. Kotov[2]*, "Self-assembly of self-limiting monodisperse supraparticles from polydisperse nanoparticles,' Nat. Nano. **6**, 580 (September 2011).
DOI:10.1038/NNANO.2011.121
Author affiliations: [1]National Center for Nanoscience and Technology, [2]University of Michigan, [3]Argonne National Laboratory
Correspondence: *kotov@umich.edu

The authors thank the 100 Talents Program of the Chinese Academy of Sciences (Z.Y.T.), the National Natural Science Foundation for Distinguished Youth Scholars of China (21025310, Z.Y.T.), the National Research Fund for Fundamental Key Project no. 2009CB930401 (Z.Y.T.), and the National Natural Science Foundation of China (nos. 91027011 and 20973047, Z.Y.T.). This material is based on work supported in part by the U.S. Army Research Office (grant award no. W911NF-10-1-0518, S.C.G. and N.A.K.). S.C.G. and T.D.N. also acknowledge support from the James S. McDonnell Foundation 21st Century Science Research Award/Studying Complex Systems (award no. 220020139); by the Department of Defense, Office of the Director, Defense Research and Engineering (DOD/DDRE) (award no. N00244-09-1-0062, S.C.G.); by the Center for Solar and Thermal Energy Conversion, an Energy Frontier Research Center funded by the U.S. DOE Office of Science (award no. DE-SC0000957, N.A.K.); by the National Science Foundation (grant nos ECS-0601345, EFRI-BSBA 0938019, CBET 0933384 and CBET 0932823, N.A.K.); and by National Institutes of Health 1R21CA121841- 01A2 (NAK). Use of the Advanced Photon Source at Argonne National Laboratory was supported by the U. S. Department of Energy Office of Science under Contract No. DE-AC02-06CH11357.

12-ID-B • Chemistry, materials science, life sciences, geoscience, polymer science • Small-angle x-ray scattering, grazing incidence small-angle scattering, wide-angle x-ray scattering • 7.9-14 keV • On-site • Accepting general users •

TUNING THE COLLECTIVE PROPERTIES OF ARTIFICIAL NANOPARTICLE SUPERCRYSTALS

Precise ordering in two-dimensional (2-D) and three-dimensional (3-D) superlattices formed by the self-assembly of individual nanocrystals (NCs) allows for control of the magnetic, optical, and electronic coupling between the individual NCs. This control can lead to useful collective properties such as vibrational coherence, reversible metal-to-insulator transitions, enhanced conductivity, spin-dependent electron transport, enhanced ferro- and ferrimagnetism, tunable magnetotransport, and efficient charge transport. These properties have many potential applications in solar cells, field-effect transistors, light-emitting devices, photodetectors, and photoconductors. A team of researchers utilizing two beamlines at the APS has reported on the first combined quasi-hydrostatic, high-pressure, small-angle x-ray scattering (SAXS) and micro x-ray diffraction (XRD) studies on individual faceted, 3-D supercrystals self-assembled from colloidal 7.0-nm PbS nanocrystals.

Due to precise positioning of the NCs within a 3-D superlattice, such systems are frequently referred to as "supercrystals" (SCs) in analogy to crystals built of atoms. But unlike the atomic crystals, SCs offer the flexibility of tuning the interparticle distance due to presence of the "soft" shell of organic ligands that can be used to control collective properties in such structures. Structural stability and compressibility are fundamental characteristics of any 3-D system.

The researchers from the Argonne, The University of Chicago, and Northwestern University combined the SAXS and XRD techniques to achieve precise evaluation of the interparticle spacing during the pressure cycling, since the volume change of the individual NCs was taken into account. Neon was used as a pressure transmitting media to avoid the possibility of the leaching of organic ligands from the surface of the NCs and losing the structural integrity of the SCs due to sintering. Diamond anvil cell (DAC) SAXS experiments in the pressure range from ambient to 12.5 GPa, performed at XSD beamline 12-ID-C,D at the APS, revealed nearly perfect structural stability of the SCs, with fcc organization of the NCs. The XRD experiments, which were carried out at GeoSoilEnviroCARS beamline 13-ID-C,D at the APS, demonstrated that NCs have strong preferential orientation of individual NCs in SCs up to ~55 GPa that is preserved during pressure cycling.

The mechanical properties of the individual NCs, their SCs, and the ligand matrix were analyzed using the equation of states derived from the compression data produced by SAXS and XRD. Ambient pressure bulk modulus of the SCs was calculated to be ~5 GPa during compression and ~14.5 GPa during the release cycle, respectively. NCs were found to undergo first-order phase transition above 8 GPa, and the transformation proceeds through a single nucleation event (within a pressure range of 8.1-9.2 GPa) during the first transition, and heterogeneous nucleation during the second transformation from the intermediate phase (that is not yet identified) to CsCl structure. A bulk modulus for the ligand matrix of ~2.2-2.95 GPa is an order of magnitude greater than that observed from nanoindentation study.

The high structural stability of the SCs and the ability to tune the interparticle spacing seem to offer the promise of further manipulation of the collective properties of self-organized artificial solids including the structures that consisted of NCs transformed at high pressures into a different phase. Combining high-pressure XRD and SAXS provides unique opportunities to obtain direct information about the mechanical properties of individual building blocks and their hierarchical architectures.

See: Paul Podsiadlo[1]*, Byeongdu Lee[1], Vitali B. Prakapenka[2], Galyna V. Krylova[1], Richard D. Schaller[1,3], Arnaud Demortière[1], and Elena V. Shevchenko[1]**, "High-Pressure Structural Stability and Elasticity of Supercrystals Self-Assembled from Nanocrystals," Nano Lett. **11**, 579 (2011). DOI:10.1021/nl103587u

Author affiliations: [1]Argonne National Laboratory, [2]The University of Chicago, [3]Northwestern University

Correspondence: *ppodsiadlo@anl.gov, **eshevchenko@anl.gov

Work at the Argonne Center for Nanoscale Materials was supported by the Office of Science of the U.S. Department of Energy (DOE) under Contract No. DE-AC02-06CH11357. P. P. acknowledges the support of Willard Frank Libby postdoctoral fellowship from Argonne National Laboratory. GeoSoilEnviroCARS is supported by the National Science Foundation—Earth Sciences (EAR-0622171) and Department of Energy—Geosciences (DE-FG02-94ER14466). Use of the Advanced Photon Source at Argonne National Laboratory was supported by the U.S. DOE Office of Science under Contract No. DE-AC02-06CH11357.

12-ID-C,D • XSD • Chemistry, physics, materials science • Small-angle x-ray scattering, grazing incidence small-angle scattering, wide-angle x-ray scattering, surface diffraction • 4.5-36 keV • On-site • Accepting general users •

13-ID-C,D • GSECARS • Geoscience, environmental science • Inelastic x-ray scattering • small-angle x-ray absorbtion fine structure, microdiffraction, x-ray absorption fine structure, microfluorescence (hard x-ray), high-pressure diamond anvil cell, high-pressure multi-anvil press • 4-45 keV • On-site • Accepting general users •

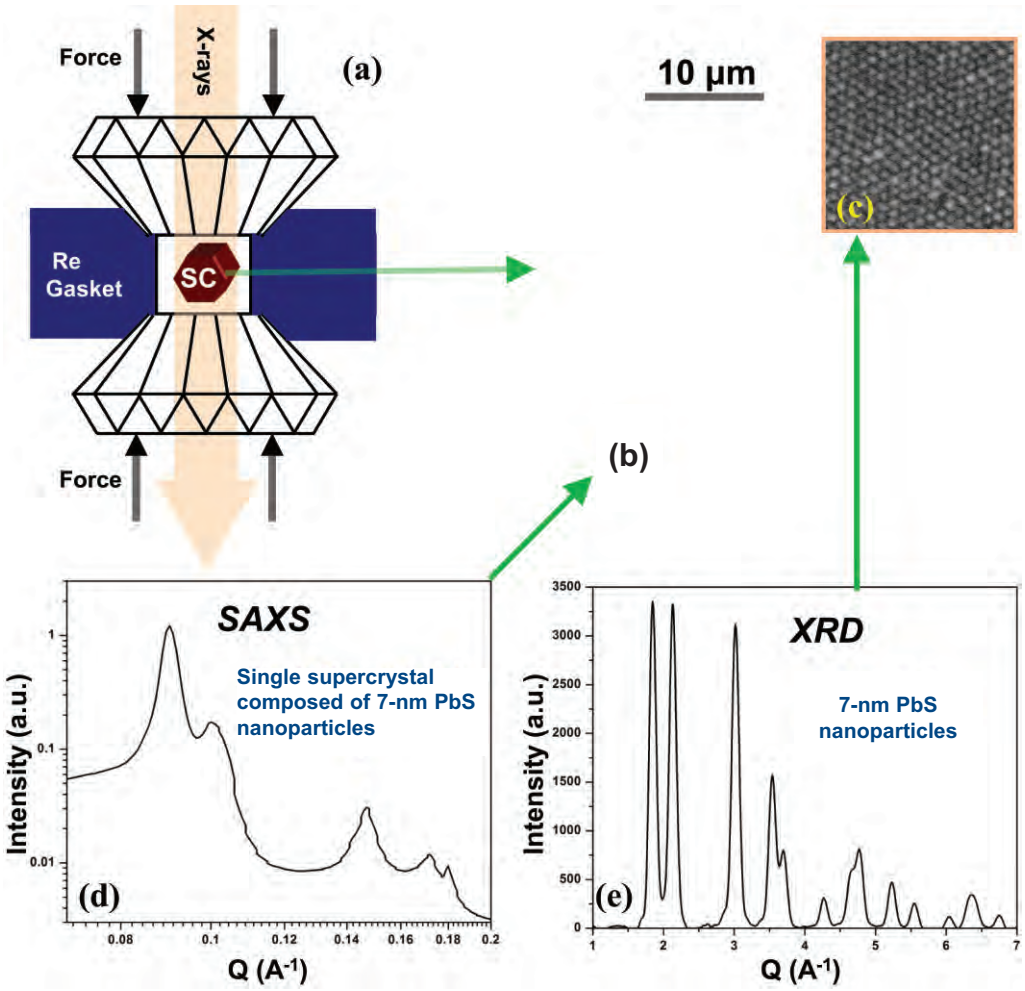

Fig. 1. (a) Schematic illustration of the high-pressure experiment in a diamond anvil cell. High-resolution scanning electron microscopy images of faceted 3-D supercrystals (b) self-assembled from colloidal 7.0-nm spherical PbS nanocrystals (c) and corresponded small-angle x-ray scattering (d) and micro x-ray diffraction patterns (e).

TAKING A PAGE FROM NATURE TO BUILD BETTER NANOMATERIALS

Sometimes nature cannot be improved upon. One example is in the synthesis of nanomaterials, which in the laboratory or factory generally requires toxic chemicals and extreme conditions of temperature and pressure. But over millions of years, nature has developed ways of putting together inorganic nanocrystals at mild temperatures and pressures. Usually this process, known as biomineralization, involves calcium carbonate or phosphate for purposes such as building bone or shells, but another interesting variation is seen in the crystallization of gold from solution by certain types of bacteria. A group of researchers has devised a unique experiment to mimic this natural process of biomineralization in order to create oriented gold nanocrystals and examine their formation at the ChemMatCARS 15-ID-B,C,D beamline at the APS, opening a path for the development of improved (and evironmentally friendly) manufacturing processes for nanomaterials.

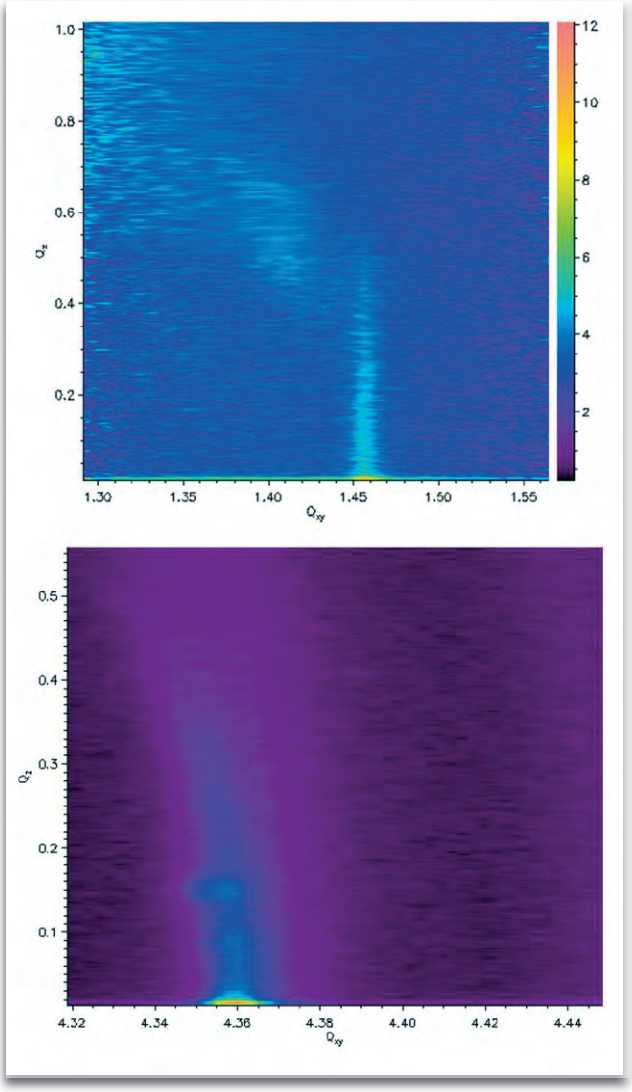

Fig. 1. Grazing incidence diffraction data revealing the interface structure of alkylthiol Langmuir monolayer (top) and the gold nanocrystals (bottom) simultaneously.

The researchers from Northwestern University and The University of Chicago floated Langmuir monolayers of octadecanethiol (C18S) on solutions of chloroauric acid ($HAuCl_4$) at room temperature and pressure, then employed a monochromatic 10-keV x-ray beam at ChemMatCARS both as a reduction agent to induce gold crystallization and as a probe to examine the interface through grazing-incidence x-ray diffraction (GID, Fig. 1). (The experiments were repeated at sector X14A of National Synchrotron Light Source to confirm that the results were not artifacts of the setup or the beam.)

Self-assembly of organic molecules is well-known and well-studied on gold surfaces. The team wanted to use this knowledge to grow gold nanoparticles utilizing an organic template. By covering the undersurface of the floating Langmuir monolayer with gold, the experimenters essentially reversed the SAM (self-assembled monolayer) creation process and used it as an analogue for biomineralization (Fig. 2). Alkylthiol SAMs have a structure perfectly matching the (111) face of gold. Inspired by this, the team made Langmuir monolayers on aurochloric acid solutions, and then grew gold crystals under them by using x-rays to reduce the gold.

In doing so, they could see the molecular interactions at the interface, how the organic molecule structures change during the process, and also the surface structures of the gold nanoparticles at the same time. Instead of trial-and-error methods of growing gold nanoparticles, they observed the process going on at the nanoscale.

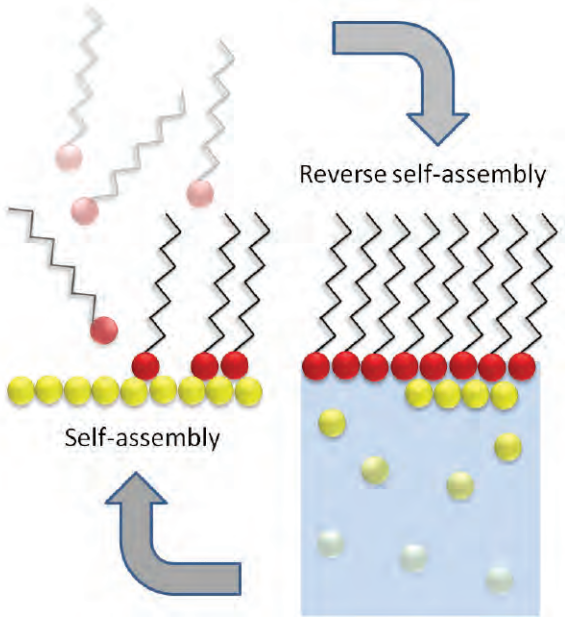

Fig. 2. Schematic diagram comparing the well-known self-assembly of alkylthiol monolayers on gold to the "reverse self-assembly" process described here. Alkylthiol molecules are organized by Au(111) surfaces in the direct process; therefore, alkylthiol monolayers were used in the biomimetic reverse process to grow oriented gold nanoparticles.

The work offers important insights into the actual molecular interactions. The GID peaks revealed that gold crystals formed at the thiol surface, with a (111) orientation commensurate with the organic template. Samples of the gold crystals were imaged with transmission electron microscopy (TEM), showing plate-like hexagonal nanocrystals about 50-nm wide (Fig. 3). The thiol monolayer behaves as a soft template, changing itself to accommodate formation of the nanocrystals.

This adaptability of the monolayer promotes the growth of the oriented gold nanoparticles. The researchers note that their ability to "trick" gold into growing in a crystallographically oriented way is the major news in the study. Just as with SAMs, the structure of the organic monolayer matches the structure of the gold surface, and this lattice match makes gold crystals want to grow with all the (111) planes pointed the same way.

Showing a method by which organic molecules can be used to control the shape, size, and crystallographic orientation of inorganic nanocrystals in a mild environment has opened a path for the development of improved manufacturing processes for nanomaterials. Although current techniques using high temperatures and hard vacuum provide large yields, they are also more expensive and less environmentally friendly. Understanding the basics of the interaction may help to increase the yield of these more "green" methods. This is a process that happens in normal conditions. It is true that x-rays are used to reduce the gold, but such reduction can also be done chemically, which is how bacteria do it.

The next step, the researchers say, is to quantify the role of the chemistry and the structure of the monolayer in gold nanoparticle orientation and shape. There are other functional groups in living organisms such as amine and carboxyl groups. They want to see what works and what doesn't. The ultimate goal is, of course, to be able to design templates for desired nanoparticle shapes and orientations. By being smart about putting the right molecules on the template, they expect to be able to make better materials for photonics or other purposes.

— Mark Wolverton

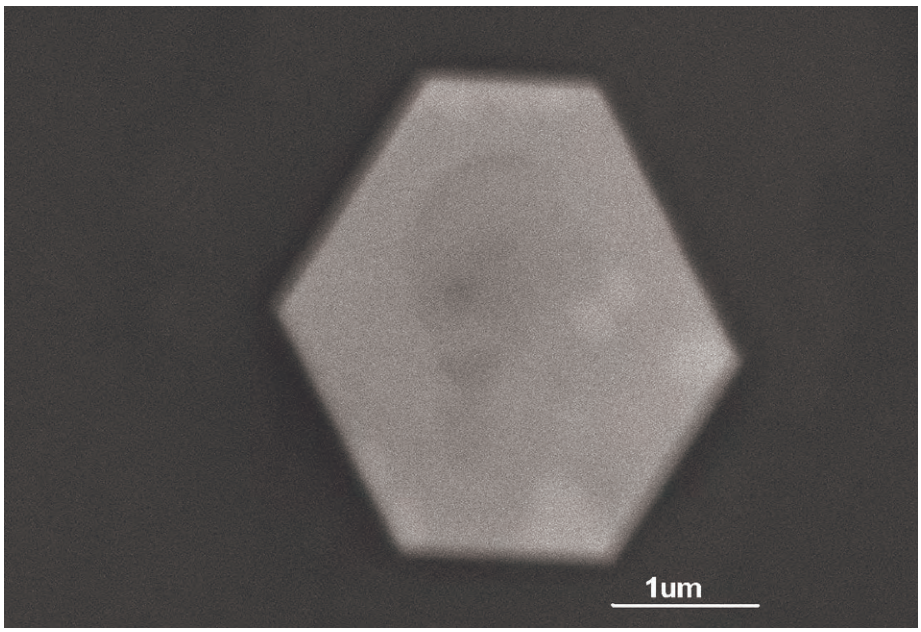

Fig. 3. Transmission electron micrograph of a (111)-oriented gold crystal examined after the experiment.

See: Ahmet Uysal[1], Benjamin Stripe[1], Binhua Lin[2], Mati Meron[2], and Pulak Dutta*[1], "Reverse Self-Assembly: (111)-Oriented Gold Crystallization at Alkylthiol Monolayer Templates," Phys. Rev. Lett. **107**, 115503 (2011). DOI:10.1103/PhysRevLett.107.115503

Author affiliations: [1]Northwestern University, [2]The University of Chicago
Correspondence:
*pdutta@northwestern.edu

This work was supported by the U.S. National Science Foundation (NSF) under Grant No. DMR-1006432. ChemMatCARS Sector 15 is principally supported by the National Science Foundation/Department of Energy (DOE) under grant number NSF/CHE-0822838. Use of the Advanced Photon Source at Argonne National Laboratory was supported by the U. S. Department of Energy, Office of Science under Contract No. DE-AC02-06CH11357.

15-ID-B,C,D • ChemMatCARS • Materials science, chemistry • Single-crystal diffraction, anomalous and resonant scattering (hard x-ray), wide-angle x-ray scattering, microdiffraction, liquid surface diffraction, small-angle x-ray scattering, ultra-small-angle x-ray scattering, high-pressure diamond anvil cell • 6-32 keV, 10-60 keV • On-site • Accepting general users •

APS users Angus Wilkinson and graduate student Leighanne Gallington (both Georgia Tech in the School of Chemistry and Biochemistry) working at APS Sector 5 as they prepare to examine the response of negative thermal expansion materials to pressure, at elevated temperatures, using high-energy powder diffraction.

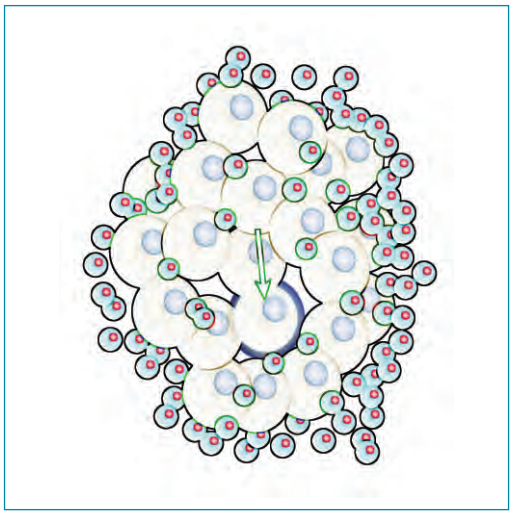

Structural Studies

OSMOSIS IN COLLOIDAL SUSPENSIONS

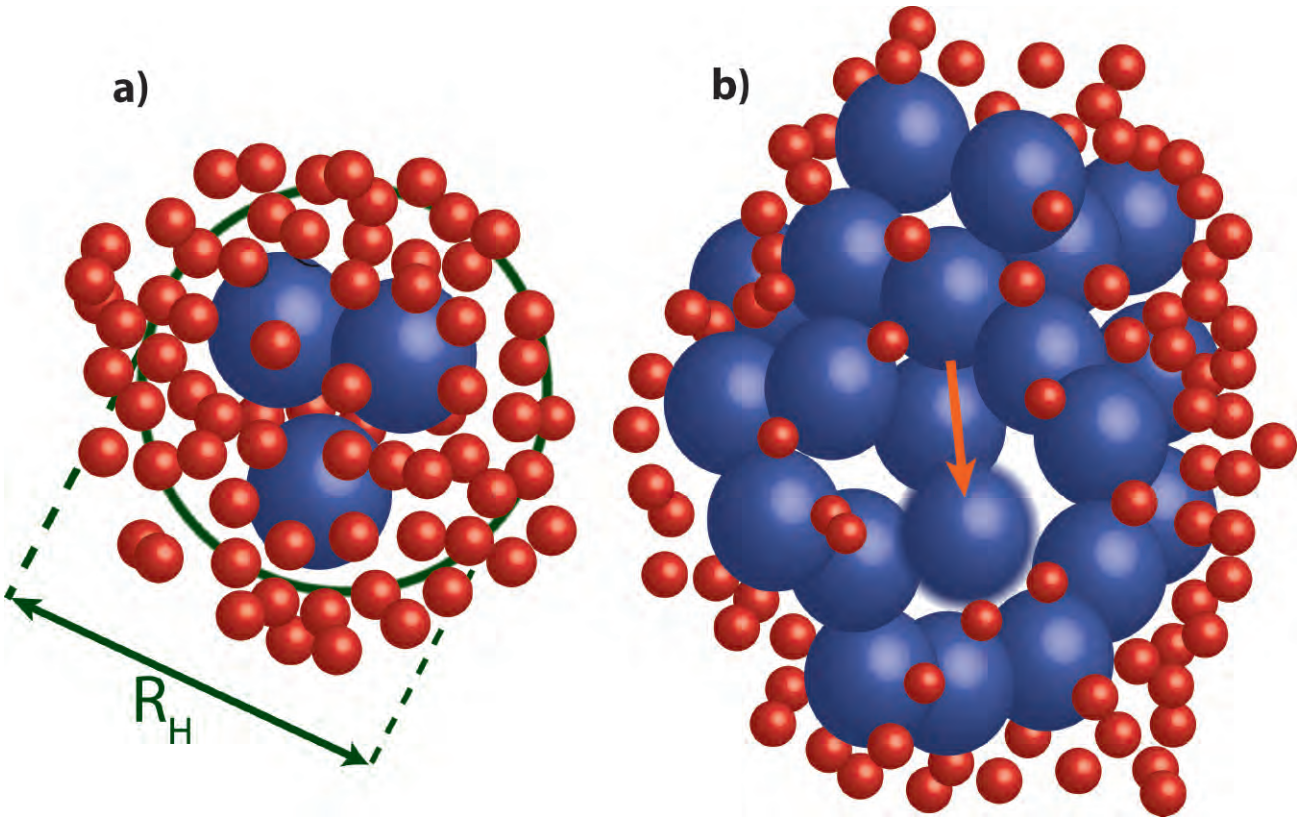

Fig. 1. Physical picture of the structure of bimodal colloidal suspensions dictated by the strength of the osmotic pressure exerted by the small spheres on the large spheres. (a) small, and (b) large relative content of the large spheres in the suspension. The effective hydrodynamic radius of an aggregate R_H is marked with a solid line in (a). The arrow in (b) indicates a possible rearrangement within the large-sphere-rich domain. From M. Sikorski et al., Phys. Rev. Lett. **106**, 188301 (2011). ©2011 by The American Physical Society.

It is difficult to overestimate the importance of colloidal suspensions. Besides being an integral part of our everyday life (food, cosmetics, drugs), they also serve as an excellent model system for basic science. Extensive studies of monomodal (single, well-defined size distribution) colloidal suspensions have helped us to understand a wide range of phenomena, such as glass transitions, relaxation in amorphous media, and hydrodynamic interactions at the nanoscale to name a few. Researchers have shifted their attention toward bimodal suspensions, which are more complex mixtures of particles with two distinct size distributions. From skimmed milk to volcanic ashes, nature provides us with numerous examples of bimodal systems. Gaining insight into the mechanism governing the structure and the dynamics of bimodal mixtures would be valuable for fundamental understanding as well as for industrial applications. Utilizing XSD beamline 8-ID-I at the APS, a research team from Argonne has obtained a clearer picture of the relationship between the composition and the equilibrium dynamics in highly asymmetric bimodal colloidal suspensions.

It has been theoretically predicted and experimentally verified that a large mismatch in the particle dimensions in bimodal suspensions may result in an attractive force between the large constituents, referred to as the "depletion interaction." The strength of this interaction is determined mainly by the ratio of the particle sizes, their relative concentration, and the volume fraction of the colloidal particles. As a result, the structure of bimodal mixtures is a complex function of its composition.

A significant amount of theoretical and experimental work has been devoted to understanding the link between composition and structure in bimodal systems. Along with the structure, the dynamics of the suspended particles is expected to be very sensitive to the composition. To date, there is very little understanding of the equilibrium dynamics of bimodal mixtures.

Studies devoted to dynamic relaxation in colloidal gels have shown that adding even a very small amount of small particles to a large sphere matrix strongly affects its temporal and spatial dynamical heterogeneity. To what extent the equilibrium dynamics in ergodic suspensions are affected by the substitution of the host particle matrix with particles of very different dimensions is still an open question.

Using x-ray photon correlation spectroscopy, a well-established tool to study nanoscale dynamics, the Argonne researchers studied a series of hard-sphere bimodal suspensions with a size ratio of 5 (Fig.1). Analysis of the time evolution of the interference pattern, called "speckles," formed by the coherent superposition of the x-ray photons scattered from the probed sample, yielded insight onto the dynamics at nanometer length scales matching the interparticle separation distances. By systematically changing the relative content of the large and the small spheres, the researchers were able to tune the strength of the attractive interaction between the large particles to reveal the sensitivity of the dynamics in bimodal suspensions to subtle variations in this parameter.

A physical picture based on a complete de-mixing of the constituent spheres into monomodal domains was proposed to explain the presence of multiple dynamic time scales. According to this picture, the mobility of the particles within such domains is governed by the strength of the osmotic pressure exerted by the small spheres on the large sphere domains.

The proposed model successfully links the observed distribution of dynamical time scales to the structural spatial heterogeneity.

Changes in the relative content of both species were found to affect the dynamics in the large and small sphere domains in different ways. Interestingly, the diffusion of the small spheres was found to be independent of the composition. On the contrary, as the content of the large spheres increases, the dynamical time scales of the large spheres spans more than a decade in time, reflecting the transition from a cooperative motion of the entire aggregate to the diffusion of a single particle within the large domains.

See: M. Sikorski, A.R. Sandy, and S. Narayanan*, "Depletion-Induced Structure and Dynamics in Bimodal Colloidal Suspensions", Phys. Rev. Lett. **106**, 183301 (2011). DOI:10.1103/PhysRevLett.106.188301

Author affiliations: Argonne National Laboratory

Correspondence:

*sureshn@aps.anl.gov

This work and the use of the Advanced Photon Source at Argonne National Laboratory were supported by the U.S. Department of Energy Office of Science under Contract No. DE-AC02-06CH11357.

8-ID-I • XSD • Materials science, physics, polymer science • Intensity fluctuation spectroscopy, small-angle x-ray scattering, x-ray photon correlation spectroscopy • 6-12.5 keV, 7.35-7.35 keV, 7.35 keV • On-site • Accepting general users •

A CHEMICAL DETOUR TO QUANTUM CRITICALITY

Physicists and chemists use different techniques to study essentially the same thing—the nature and behavior of matter. Usually the particular path is of little consequence, because they all lead ultimately to the same truths at the end of the experimental journey. Sometimes, however, choosing one path over another can offer unique and interesting insights along the way, such as when a traveler takes the scenic route instead of a more direct path. A good example is in the study of superconductivity, which is generally the realm of solid-state physicists. But some Princeton University chemists and Argonne physicists teamed up to uncover a new insight about a common intermetallic superconducting-type crystal structure.

Working at the XSD high-resolution powder diffraction beamline 11-BM-D at the APS, the researchers found that by manipulating the parameters of a particular chemical bond within the $ThCr_2Si_2$ structure, specifically by breaking a Ge-Ge dimer embedded within $SrCo_2(Ge_{1-x}P_x)_2$, they could induce the absolute-zero phase transition known as a ferromagnetic quantum critical point (QCP).

Unlike the everyday phase transitions with which we're all familiar, such as ice melting into liquid or water boiling into steam, a quantum critical point is a phase transition driven not by temperature but by the quantum fluctuations that dominate at absolute zero. Depending on the combination of elements and their structure in a compound, inducing a QCP can produce interesting and useful phenomena such as ferromagnetism and superconductivity. Usually the transition is driven by electron doping or manipulating a physical parameter such as pressure, but the team found a different way.

Their research was inspired by the work of Nobel Prize-winning chemist Roald Hoffmann, who made some interesting observations in the 1980s about $ThCr_2Si_2$-type structures. He noted that, in some unexpected way, there's a small embedded molecule inside some subset of these compounds. It was not understood why certain crystal structures were the way

Lynn Ribaud (left) and Matthew Suchomel (both XSD-SRS) inside the 11-BM-B beamline experiment station at Sector 11 of the APS. The custom multi-crystal detector assembly (top right) delivers the highest resolution powder diffraction data available in the Americas.

they were. To explain some structural problems in this family of intermetallic compounds, Hoffmann came up with the idea that instead of thinking about it like a typical metallic compound, one must to consider the chemical bonding to understand what the electronic state of the system actually is.

The researchers realized that the $ThCr_2Si_2$ structure, with its embedded molecule, was one example for which the chemical bonding in this molecule might have an impact on the physical properties of superconductors. The team prepared several series of compounds to determine the impact of the embedded molecule on structural properties. They discovered that something dramatic happened in the $SrCo_2(Ge_{1-x}P_x)_2$ structure when the Ge-Ge dimer in the embedded phosphorus-germanium molecule is broken by changing composition across the series (Fig. 1).

The chemical parameter that they were manipulating somehow induced ferromagnetism and turned it on at near zero Kelvin. When a quantum critical point is approached from above in temperature, there are certain characteristics of susceptibility and specific heat that indicate this phase transition is being approached at very low temperature. It is in that temperature dependence right around this quantum critical composition that one sees the ferromagnetism coming, even though it is not there yet.

Another surprising aspect is that such phenomena are typically seen in rare-earth compounds, rather than the transition element compounds used in these experiments.

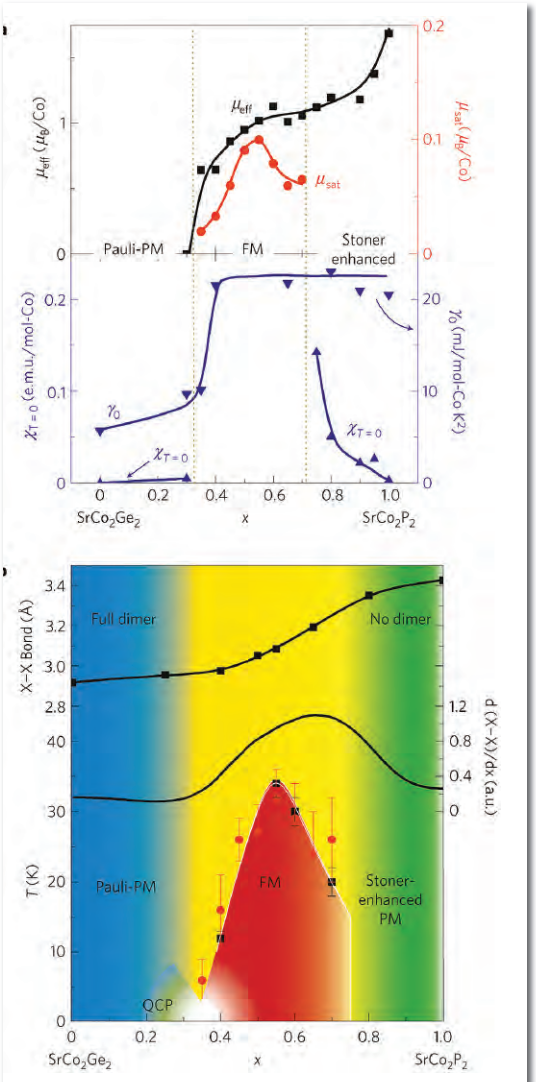

Fig. 1. The structural and magnetic phase diagram for $SrCo_2(Ge_{1-x}P_x)_2$. Black symbols: TC determined by the Arrott plot; the error bars are the temperature interval of the measured isotherms. Red symbols: TC determined by assuming M(TC)=20±10% M (2K). From Jia et al., Nat. Phys. **7**, 207 (2011).

The team's next step will be to grow single crystals of compounds around the QCP in order to study in greater detail the thermodynamics of the approach to the QCP as temperature decreases. Although their work did not result in the discovery of a path to superconductivity, it offers a new perspective on the structural possibilities in this family of superconducting compounds. The team asked a fundamental chemical question and found a surprising, fundamental physical property. The idea that this kind of molecule can exist in this structure type impacts the way we think about the iron-arsenide superconductors, which are the ones that could have some kind of application in the future. *— Mark Wolverton*

See: Shuang Jia[1], Pawina Jiramongkolchai[1], M.R. Suchomel[2], B.H. Toby[2], J.G. Checkelsky[1], N.P. Ong[1], and R.J. Cava[1]*, "Ferromagnetic quantum critical point induced by dimer-breaking in $SrCo_2(Ge_{1-x}P_x)_2$," Nat. Phys. **7**, 207 (March 2011).
DOI:10.1038/nphys1868
Author affiliations: [1]Princeton University, [2]Argonne National Laboratory
Correspondence:
*rcava@princeton.edu

The work at Princeton was supported by the U.S. Department of Energy (DOE), Office of Science, Basic Energy Sciences, Grant No. DE-FG02-98ER45706. Use of the Advanced Photon Source at Argonne National Laboratory was supported by the U.S. DOE Office of Science under Contract No. DE-AC02-06CH11357.

11-BM-B • XSD • Chemistry, materials science, physics • Powder diffraction • 15-35 keV • On-site, mail-in • Accepting general users •

SMALL AVALANCHES MAKE A BIG DIFFERENCE

Investigating how atoms move and rearrange themselves is fundamental to our understanding of the behavior of materials, and is particularly important for engineering new materials or materials with enhanced functionality. Phase transitions involve the rearrangement of the atomic structure of a material as it is subjected to changing conditions such as alterations in pressure, temperature, etc. Sometimes the transition is quite obvious—for instance when ice melts into water—but often it occurs on a much smaller and less readily apparent scale. These are diffusionless phase transitions, with the best-known example being the martensitic phase transition in which the crystalline structure of a unit cell is changed by a shearing force. These changes can produce strains in the crystal lattice that can interfere with the progress of the transition, but the strains can be released through sudden rearrangements. Often these rearrangements are localized and small, but sometimes they occur in cascades called "avalanches"—which bear a strong resemblance to the large-scale variety that involve rocks or snow. Researchers utilizing the XSD 8-ID-E beamline at the APS have obtained new information about microstructural avalanches that is revealing important spatial characteristics about these phenomena.

Although microstructural avalanches have been observed indirectly through thermal, acoustic, and electrical means, their structural details have proven challenging to visualize. Conventional x-ray or neutron scattering techniques provide a picture made up of measurements averaged over broad regions of a sample material and thus tend to miss the narrowly localized changes seen in microstructural avalanches. A group of collaborators from Boston University and McGill University recently overcame that problem by using the highly-coherent x-ray techniques afforded by the x-ray beams from the APS.

Using x-ray photon correlation spectroscopy (XPCS) at the 8-ID-E beamline, the researchers visualized for the first time the microstructural avalanches that occur during the martensitic phase transition in cobalt (Fig. 1). At high temperature, cobalt maintains a face-centered cubic (fcc) phase, which changes into a hexagonal close-packed (hcp) phase at lower temperatures, beginning at about 720K. Both of these phases are similar, with close-packed planes, and differ only in their atomic stacking order and interplanar spacing, making the microstructural avalanches a natural and efficient means of strain relief.

Beginning with a sample completely in the fcc phase at 870K, the experimenters observed the x-ray scattering after cooling quickly through the transition temperature. They found that the martensitic transformation appears to occur in two fairly distinct stages. After an initial growth period of the hcp phase, a more heterogeneous stage of strain redistribution occurs throughout the sample, as stacking faults built up during the earlier stage are eliminated through sudden scattered avalanches. The XPCS Bragg peaks show that these occur over a wide range of sizes, from about 100 nm to 10 μm, and decrease in rate over time following the beginnings of the phase transition.

Perhaps the most intriguing finding is that the observed behavior of the microstructural avalanches is similar mathematically to the dynamics of earthquakes and their aftershocks. Both the Gutenberg-Richter law describing earthquake power-law magnitude distribution, and the Omori law describing a 1/t aftershock rate decrease match the results seen in the this work. Just as aftershocks release the stresses in the Earth's crust caused by the fault shifts of a large earthquake, microstructural avalanches relieve the strains of the martensitic transformation from fcc to hcp phases. Though the differences in scale are immense between an atomic-scale rearrangement and an earthquake, the physical mechanisms involved appear to be remarkably alike. Whether the similarities are merely coincidental or are actually empirically related is a matter for further investigation.

This research not only demonstrates the value of XPCS as a powerful technique for probing structural dynamics with great precision, but also provides a valuable model for the study of other thermally-driven martensitic phase transitions, some of which may involve similar mechanisms of strain relief. They may not be as spectacular nor as dangerous as the earthquakes and avalanches of the macroscopic world, but their function is just as important. *— Mark Wolverton*

See: Christopher Sanborn[1], Karl F. Ludwig[1], Michael C. Rogers[2], and Mark Sutton[2]*, "Direct Measurement of Microstructural Avalanches during the Martensitic Transition of Cobalt Using Coherent X-Ray Scattering," Phys. Rev, Lett. **107**, 015702 (1 July 2011). DOI:10.1103/PhysRevLett.107.015702
Author affiliations: [1]Boston University, [2]McGill University
Correspondence:
*mark@physics.mcgill.ca

The Boston University component of this research was supported by National Science Foundation grant DMR-0508630 (experiment) and U.S. Department of Energy Office (DOE) of Science Contract No. DE-FG02-03ER46037 (development of algorithms for analysis of x-ray data from nonequilibrium systems). Use of the Advanced Photon Source at Argonne National Laboratory was supported by the U.S. DOE Office of Science under Contract No. DE-AC02-06CH11357.

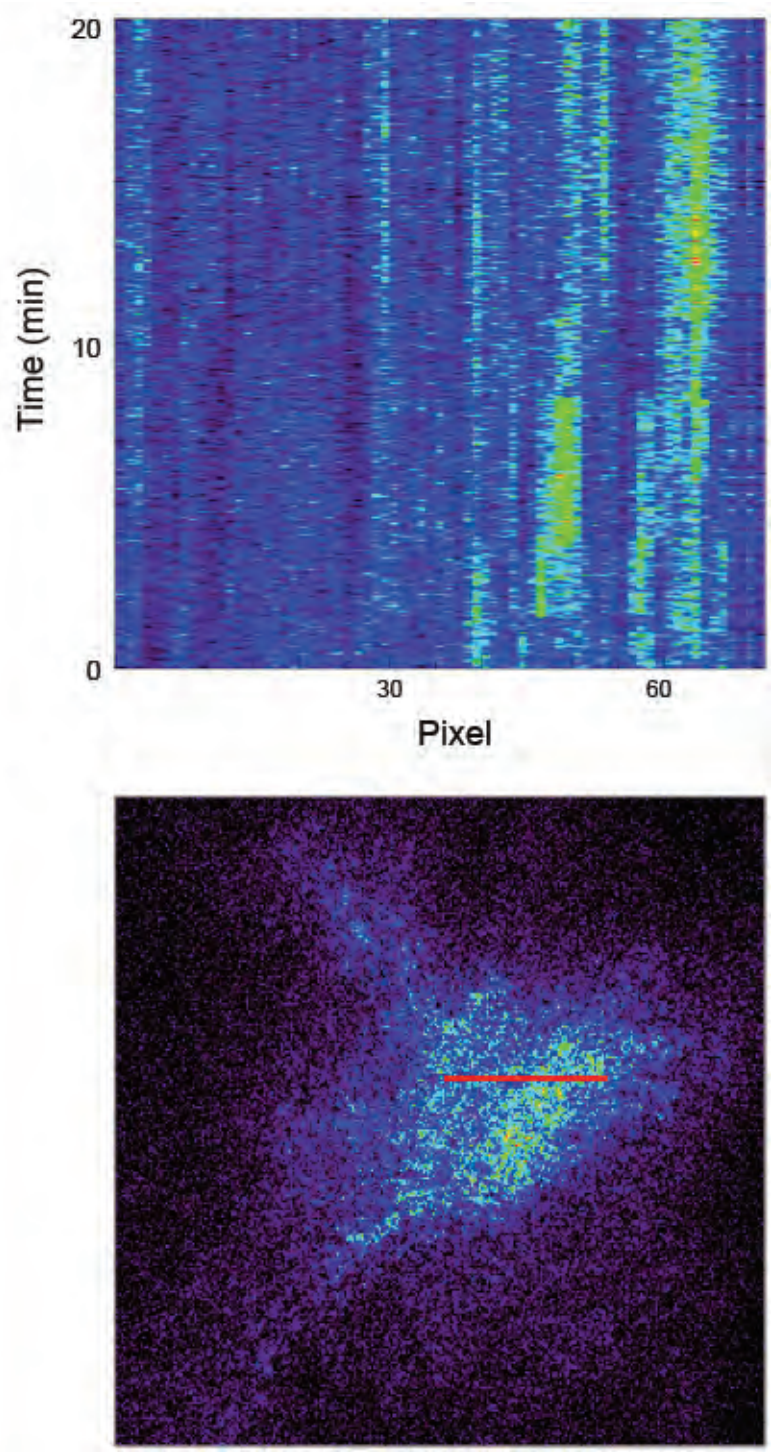

Fig. 1. Top: A "waterfall" plot showing the evolution of a cross section of a speckle pattern near the (00.2) HCP peak of cobalt during its martensitic phase transformation. Pattern discontinuities, such as the one at approximately 8 min, indicate the occurrence of avalanches. Bottom; A single frame of the complete speckle pattern. The cross section used for the waterfall plot is indicated by the red line, which has a length of 5×10^{-3} inverse angstroms.

8-ID-E • XSD • Materials science, polymer science, physics • Grazing incidence small-angle scattering • x-ray photon correlation spectroscopy • intensity fluctuation spectroscopy • grazing incidence diffraction • 7.35-7.35 keV, 12-12 keV * On-site • Accepting general users *

FINDING THE HIDDEN ORDER IN METALLIC GLASS

Glass is the classic example of an amorphous solid, a material that lacks the tidy long-range order in its atomic structure found in other materials such as metals that feature a well-defined and periodic crystalline lattice. It is possible to combine the qualities of both in a metallic glass (MG) such as $Ce_{75}Al_{25}$. But while such materials can exhibit useful properties, and have even been shown to sometimes display medium-range order in clusters at the nanometer range, they still lack the characteristic long-range order of a crystal. Or do they? Researchers working at the HP-CAT 16-ID-B beamline at the APS found that a thin ribbon of $Ce_{75}Al_{25}$ metallic glass could display a distinct long-range crystalline phase under the right conditions, providing hints that the long-sought "perfect glass state" might yet be a possibility. >>>

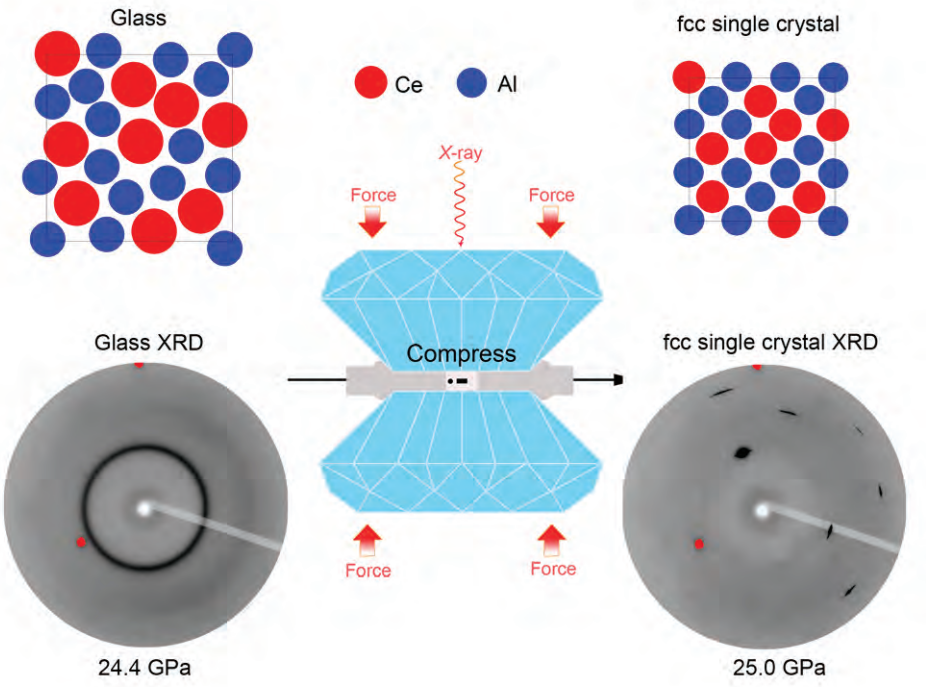

Fig. 1. Pressure-induced single-crystal devitrification in $Ce_{75}Al_{25}$ metallic glass observed by *in situ* high-pressure XRD in a DAC. The two-dimensional (2-D) XRD image below 24.4 GPa shows a typical glass pattern, and the 2-D XRD image at 25.0 GPa shows a typical single-crystal zone-axis pattern. A focused (15×15 μm^2) monochromatic x-ray (wavelength 0.36806 Å) through the DAC axis without rotation was used. Red spots are masks of diamond single-crystal XRD spots. The cartoon shows a schematic illustration of the change of atomic structures during the devitrification.

The experimenters, from Zhejiang University, the Carnegie Institution of Washington, George Mason University, Jilin University, Stanford University, and the SLAC National Accelerator Laboratory obtained x-ray diffraction (XRD) images of a $Ce_{75}Al_{25}$ MG ribbon produced by a single-roller melt-spinning method. The ribbon was cut into samples of approximately 50-μm × 40-μm × 15-μm, which were then loaded into a diamond anvil cell (DAC) and subjected to various pressures. High-resolution transmission electron microscopy (HRTEM) and electron diffraction (ED) imaging were also performed at Argonne's Electron Microscopy Center.

At pressures up to 24.4 GPa, the samples displayed the expected broad amorphous XRD patterns. But as pressure was slightly increased to 25 GPa, an abrupt transformation suddenly occurred in the XRD pattern, characteristic of a face-centered cubic (fcc) single crystal, with its [111] direction oriented lengthwise along the ribbon and the [110] direction oriented along the ribbon thickness.

Repeated tests with samples cut from different parts of the MG ribbon showed the same results, with a definite topological relationship between the fcc crystal and the MG structure. The single-crystal pattern remained even at ambient pressure.

The researchers believe that this long-range order actually occurs in the metallic glass as it is formed. Because both Ce and Al normally crystallize in an fcc structure, it is possible that this tendency may still exist even when Ce and Al atoms are randomly mixed in the roller-spinning and melt-quenching process. Under pressure, the Ce atoms undergo 4*f* electron delocalization, allowing the Hume-Rothery rule to come into effect (the conditions under which an element could dissolve in a metal, forming a solid solution) and the fcc structure to manifest itself in the long range.

To further model the dynamics of the system, the experimenters performed simulations using classical molecular dynamics calculations to see how the amorphous structure of the Ce-Al metallic glass would behave under different temperature, pressure, and electronic changes, starting with an fcc lattice and allowing the structure to evolve. They found that the metallic glass retained a hidden memory of the original fcc pattern, which then emerged as higher pressures were simulated and the 4f electron delocalization occurred. Another metallic glass generated without the fcc constraint changed to a polycrystal, showing no long-range order.

Aside from the surprising discovery of unexpected order arising from a supposedly amorphous structure changing to a vitreous crystalline condition, the experiments demonstrate more specifically that the $Ce_{75}Al_{25}$ metallic glass system could be a leading candidate to achieve the perfect glass state. But other metallic glasses that display similar qualities, particularly the large disparity in their atomic sizes and Hume-Rothery frustration that can be overcome under pressure, could also display such a state. While the unique hybrid properties of metallic glasses such as $Ce_{75}Al_{25}$ could be useful for valuable applications in microelectronics and elsewhere, a perfect glass (if attainable, and in whatever composition of atoms) would offer even greater promise both for practical uses and as a fascinating scientific phenomenon, providing new insights into the myriad ways by which atoms can come together to form matter.

— Mark Wolverton

See: Qiaoshi Zeng[1,2], Hongwei Sheng[3], Yang Ding[2], Lin Wang[2,4], Wenge Yang[2], Jian-Zhong Jiang[1]*, Wendy L. Mao[1,5,6], and Ho-Kwang Mao[1,2]**, "Long-Range Topological Order in Metallic Glass," Science **332**, 1404 (17 June 2011). DOI:10.1126/science.1200324

Author affiliations: [1]Zhejiang University, [2]Carnegie Institution of Washington, [3]George Mason University, [4]Jilin University, [5]Stanford University, [6]SLAC National Accelerator Laboratory

Correspondence: **mao@gl.ciw.edu, *jiangjz@zju.edu.cn

This work was funded by the U.S. Department of Energy (DOE) Energy Frontier Research Center grant DE-SC0001057 (EFree). The use of HP-CAT was supported by the Carnegie Institute of Washington, the Carnegie-DOE Alliance Center, the University of Nevada at Las Vegas, and the Lawrence Livermore National Laboratory through funding from the DOE National Nuclear Security Administration, the DOE Office of Science, and the U.S. National Science Foundation. The Zhejiang University participants were supported by the National Natural Science Foundation of China (grants 10979002, 50920105101, and 51050110136), the China Postdoctoral Science Foundation, the Zhejiang University-Helmholtz Cooperation Fund, the Ministry of Education of China, and Zhejiang Provincialc Department of Science and Technology. Use of the Advanced Photon Source was supported by the U.S. DOE Office of Science under Contract No. DE-AC02-06CH11357.

16-ID-B • HP-CAT • Materials science, geoscience, chemistry, physics • Microdiffraction, single-crystal diffraction, high-pressure diamond anvil cell • 24-35 keV • On-site • Accepting general users •

UNCERTAINTY KEEPS LITHIUM FROM FREEZING

Subjected to high pressures, most materials become more difficult to liquefy, so their melting points rise. But researchers working at HP-CAT beamline 16-1D-B at the APS and at the European Synchrotron Radiation Facility (ESRF) have discovered that, over a limited pressure range, lithium behaves in the opposite way: The more it is squeezed, the lower the temperature at which it melts. It can remain liquid down to 190K, the lowest melting temperature ever seen for a metal. Their investigation raises the possibility of "constructing" a system, other than pure hydrogen, possessing a metallic liquid ground state, and that by tuning the electronic properties of such a system by pressure, or by further doping, arrive at a previously unobserved novel state of matter.

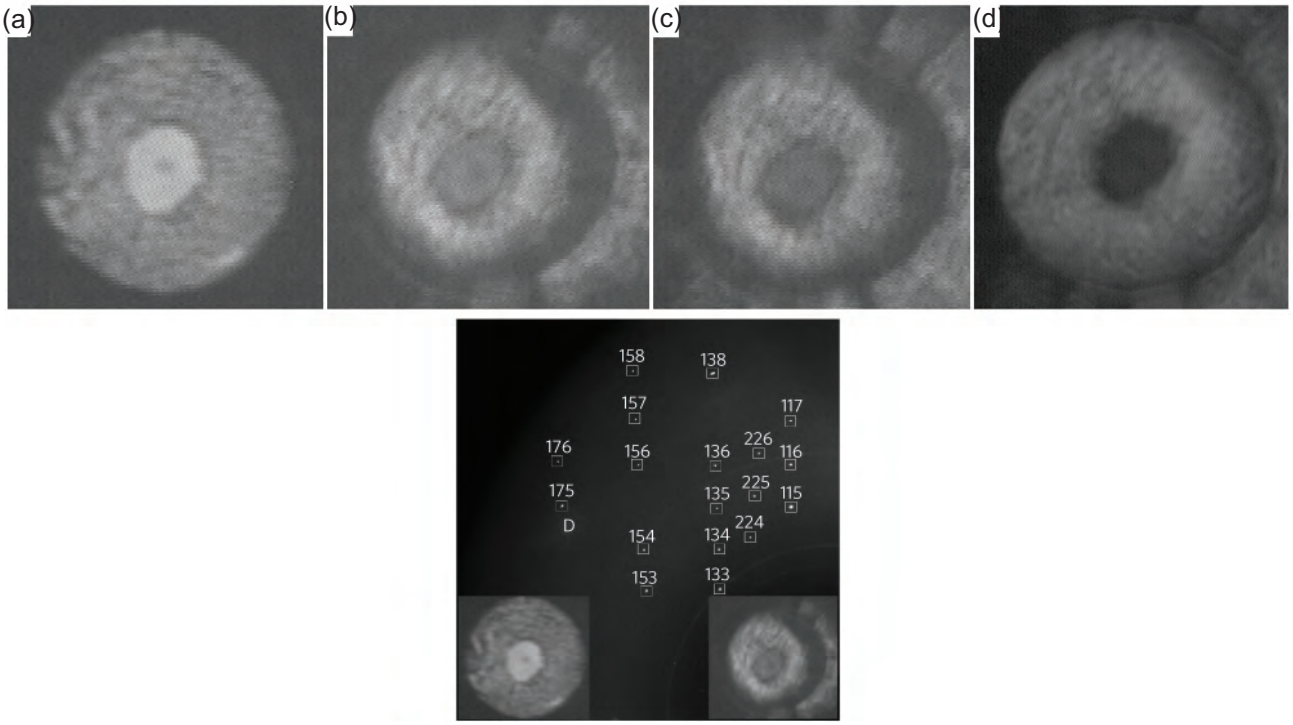

Fig. 1. Top row: Lithium subjected to increasing pressure goes through a series of changes to its lattice structure that also alter its visual appearance, seen here in the central area of these diffraction images, bordered by a rhenium gasket. In (a), at 45 GPa at 180K, lithium has a 16-atom unit cell and appears shiny. In (b), at 65 GPa and 180K, the unit cell has 88 atoms, and the sample has darkened. In (c) and (d), the pressures are higher still, the unit cells become smaller, and the samples darken further. This progression corresponds to lithium becoming less metallic. Bottom: Diffraction data from the oC88 phase at 65GPa and 180K collected over a 13° scan range. The left inset shows the visual appearance of the sample in the cI16 phase at 45 GPa and 180 K. The right inset shows the same sample in the oC88 phase at 65 GPa and 180K. From C.L. Guillaume et al., Nat. Phys. **7**, 211 (2011).

In 2005, members of this research team found that the melting point of sodium falls from about 1000K at a pressure of just over 30 GPa, equivalent to 30,000 atmospheres, down to 300K at 120 GPa, before rising again [1]. In the present study, the team set out to see if the closely related metal lithium would show comparable behavior. Recent experiments up to 15 Gpa hint at a downward trend in lithium's melting point, but no experiments had explored higher pressures.

At the APS and the ESRF, the team conducted 35 x-ray diffraction experiments on lithium, at pressures ranging from 5 GPa to 130 GPa and temperatures between 77K and 300K. Compressing lithium in diamond anvil cells presents challenges. Atoms of lithium, the third lightest element and the lightest metal, sneak into tiny cracks in the diamond, causing the effective pressure on the sample to fall. And at temperatures above 200K, lithium can chemically react with diamond. To get around these difficulties, the scientists kept the lithium samples small (from 6 to 15 μm across), and at higher temperatures gathered data for no more than 2 or 3 h.

The presence of liquid lithium was inferred from the absence of an x-ray diffraction pattern corresponding to a solid crystal lattice. In this way, the team found that the melting point fell to a minimum of 190K at 40 GPa, rising slowly at pressures up to 60 GPa, and increasing more steeply thereafter. The researchers propose an explanation of this surprisingly low melting point that involves the quantum mechanical phenomenon known as zero point energy.

A solid melts when the kinetic energy of atoms is enough to overwhelm the forces holding the lattice together. Kinetic energy decreases with falling temperature, but the uncertainty principle mandates that no measurement can show it be exactly zero. The zero-point energy is the smallest amount of kinetic energy that remains even as the temperature falls as low as possible. Zero-point energy is normally not an important factor in lattice dynamics. But the team argues that in highly compressed lithium, which has very light atoms and small lattice binding forces, it can be the deciding factor in keeping the metal liquid at unexpectedly low temperatures.

The researchers also used their x-ray diffraction data to deduce that the lithium lattice undergoes a series of changes as the pressure rises. A 2-atom cubic unit cell first changes into a cubic form with 4 atoms per unit cell; then, at about the minimum melting point, into a new geometry with 16 atoms per unit cell, and at still higher pressures into a novel lattice with an estimated 88 atoms per unit cell. Normally, high pressure squeezes lattices into simpler, smaller, and more symmetric unit cells. Lithium's contrary behavior, which parallels similar changes observed in sodium, may also reflect the role of zero-point energy in allowing atoms to resist the usual effect of compression.

Among other elements, hydrogen is predicted to have a liquid-metal state at zero temperature and under very high pressures, but the conditions to achieve that transformation are far beyond laboratory capabilities. But it may be possible to synthesize a molecule with a small average mass-per-atom and weak electrostatic interactions that would have a metallic liquid ground state. *— David Lindley*

16-ID-B • HP-CAT • Materials science, geoscience, chemistry, physics • Microdiffraction, single-crystal diffraction, high-pressure diamond anvil cell • 24-35 keV • On-site • Accepting general users •

REFERENCE:

[1] E. Gregoryanz, O. Degtyareva, M. Sommayazulu, R.J. Hemley, and H.K. Mao, "Melting of Dense Sodium," Phys. Rev. Lett. **94**, 185502 (2005).

See: Christophe L. Guillaume[1], Eugene Gregoryanz[1]*, Olga Degtyareva[1], Malcolm I. McMahon[1], Michael Hanfland[2]**, Malcolm Guthrie[3], Stanislas V. Sinogeikin[3], and H.K. Mao[3], "Cold Melting and Solid Structures of Dense Lithium," Nat. Phys. **7**, 211 (2011). DOI:10.1038/NPHYS1864

Author affiliations: [1]University of Edinburgh, [2]European Synchrotron Radiation Facility, [3]Carnegie Institution of Washington

Correspondence:

*e.gregoryanz@ed.ac.uk,

**hanfland@esrf.fr

This work is supported by a research grant from the UK Engineering and Physical Sciences Research Council and facilities made available by the European Synchrotron Radiation Facility. Some of the single-crystal data were collected under ESRF LTP project HS-3090. HP-CAT is supported by the U.S. Department of Energy (DOE) Office of Science, the DOE National Nuclear Safety Administration, and the U.S.National Science Foundation. Work carried out at HP-CAT was supported as part of the EFree initiative, funded by the DOE Office of Science, under Award Number DE-SC0001057. O.D.acknowledges support from the Royal Society. Use of the Advanced Photon Source at Argonne National Laboratory was supported by the DOE Office of Science under Contract No. DE-AC02-06CH11357.

SUPER-FAST SUPERLATTICES

Superlattices — structures made up of atomic-scale layers of different materials — allow new materials with entirely new phenomena to be created from parent components with quite different properties. Ferroelectric/dielectric superlattices are fabricated from materials based on transition metal oxides with similar structures but distinct bulk properties. Novel electronic phenomena, including nanoscale self-organized domain structures, arise from the interactions between these layers. As in bulk ferroelectrics, these superlattice materials have a remnant polarization that can be manipulated using applied electric fields. This response is closely linked to domains, regions of uniform polarization. But unlike bulk ferroelectrics, the size of polarization domains in the superlattices is defined by the new degree of control arising from the choice of the sequence of atomic layers during their growth. Under the right conditions, these domains organize into stripes, which have particularly interesting responses to applied fields. Now, researchers have used the APS to understand the nanosecond-scale dynamics of these striped domains, which may lead to wide application in communications, sensing and actuating technologies, and nanoelectronics. >>>

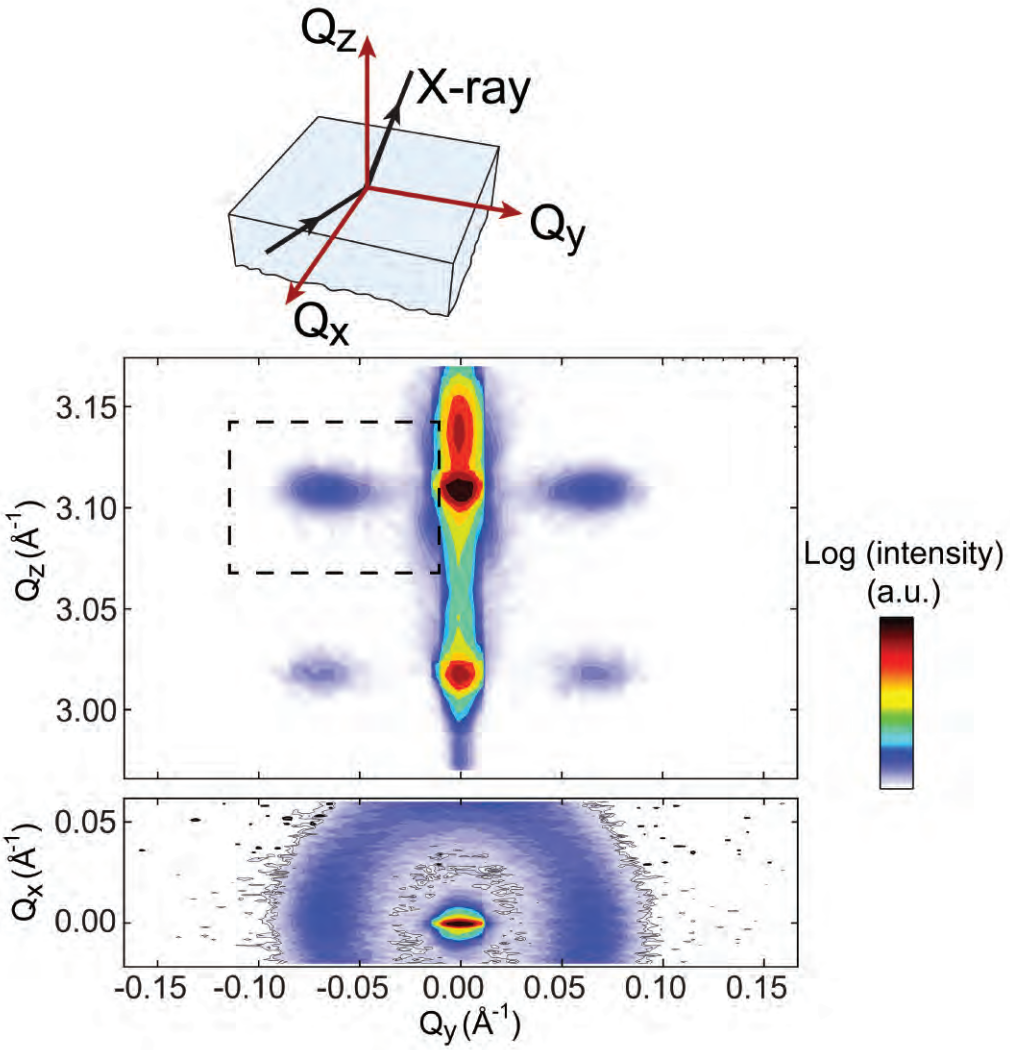

Fig. 1. Diffracted intensity in planar sections through reciprocal space at (a) $Q_x = 0$ and (b) $Q_z = 3.106$ Å^{-1}. Reflections from the stripe nanodomains are apparent at nonzero values of Q_y in (a) and as a ring in the Q_x-Q_y plane in (b). Inset: A schematic of the scattering geometry. The color scale is labeled with intensities relative to the superlattice structural reflection. Figures this and facing page: Ji Young Jo et al., Phys. Rev. Lett. **107** (2011). ©2011 American Physical Society.

The key step in understanding these materials is the transition between the striped nanodomains, where the domains have a structure defined by the sequence of layers, to a uniform polarization state favored by the external applied field. The team of researchers from the University of Wisconsin-Madison, Stony Brook University, and Argonne probed this transition using time-resolved x-ray microdiffraction techniques at the XSD 7-1D-B,C,D beamline at the APS. X-rays are particularly valuable in this work because the domains produce a diffuse scattering signature linked directly to their structure (Fig. 1).

The dynamics apparent in these experiments led the team to propose a new model for the evolution of the striped nanodomains. The time required for the completion of the transition decreases at high fields, promising that the polarization transition can provide ultrafast control of electronic properties.

By noting the decrease in the intensity of domain satellite reflections in the x-ray microdiffraction patterns (Fig. 2), the researchers could observe the changes in the superlattice domain structure as the electric field was altered. In addition to the rapid disappearance, the experimenters found that the piezoelectric response of the striped domains of the superlattice appears to be strongly suppressed due to electromechanical clamping, with no apparent piezoelectric shift of stripe domain reflections.

Based on these results, the team proposed a heterogeneous model for the transitions, in which the dynamics are based not on the motion of domain walls but on the transformation of striped domains to widely spaced areas of uniform polarization throughout the superlattice. Unlike the striped domains, the piezoelectric characteristics of the switched areas are free of the clamping effect and thus show piezoelectric expansion. Eventually the switched areas increase until the entire sample is uniformly polarized. The measurements of the domain reflection intensities shows that their dynamics are strongly dependent upon the magnitude of the applied electric field.

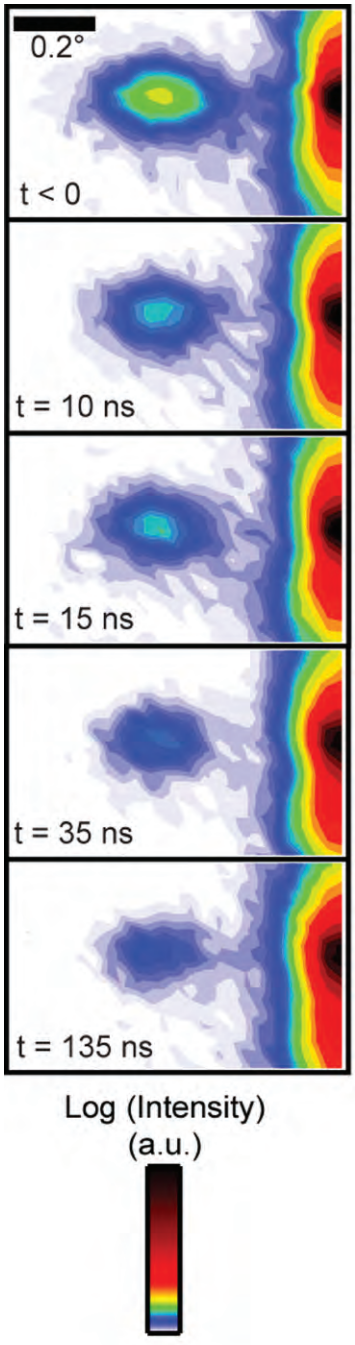

Fig. 2. Diffraction patterns at several times following the onset of an electric field of 0:84 MV/cm. The patterns show the domain reflection at the center of each image and a tail from a superlattice structural reflection at the right edge of the images.

This work demonstrates the possibility of controlling and switching superlattice nanodomains on very short time scales of 5 to 100 nsec, which raises the intriguing prospect of employing such phenomena in electronic devices with extremely high operating frequencies in the gigahertz range. Further experimental work may lower the switching time scale to 1 nsec or even less. Such capabilities could have wide application in communications, sensing and actuating technologies, and nanoelectronics. *— Mark Wolverton*

See: Ji Young Jo[1‡], Pice Chen[1], Rebecca J. Sichel[1], Sara J. Callori[2], John Sinsheimer[2], Eric M. Dufresne[3], Matthew Dawber[2], and Paul G. Evans[1*], "Nanosecond Dynamics of Ferroelectric/Dielectric Superlattices," Phys. Rev. Lett. **107**, 055501 (28 July 2011).
DOI:10.1103/PhysRevLett.107.055501
Author affiliations: [1]University of Wisconsin–Madison, [2]Stony Brook University, [3]Argonne National Laboratory. ‡Present address: Gwangju Institute of Science and Technology
Correspondence:
*evans@engr.wisc.edu

This work was supported by the U.S. Department of Energy (DOE) Office of Science under Grant No. DEFG02-10ER46147 (P.G.E.). M. D. gratefully acknowledges startup funding from Stony Brook University. Use of the Advanced Photon Source at Argonne National Laboratory was supported by the U.S. DOE Office of Science under Contract No. DE-AC02-06CH11357.

7-ID-B,C,D • XSD • Materials science, atomic physics, chemistry • Time-resolved x-ray scattering, time-resolved x-ray absorption fine structure, phase contrast imaging • 6-21 keV • On-site • Accepting general users •

Novel X-ray Techniques & Instrumentation

X-RAY MICROSCOPY AT NANOMETER RESOLUTION: 2-D FOCUSING WITH MULTILAYER LAUE LENSES

The unique capabilities that hard x-rays offer as a materials probe—including considerable penetrating power, very high sensitivity to trace elements, and the capability to elucidate structure and strain—make them appealing for many imaging applications requiring nanometer resolution. A major challenge has been the development of optics that can focus hard x-rays (typically considered those with energies 10 keV and higher) to the scale of a few nanometers. While several complementary techniques, such as mirrors and Fresnel zone plates, are used to focus hard x-rays, they are limited in their potential to significantly exceed a resolution of 10 nm with good efficiency. In this research, carried out with hard x-rays at the CNM/XSD beamline 26-ID-C at the APS, a novel approach suitable for sub-10-nm imaging—the multilayer Laue lens (MLL)—has demonstrated the ability to focus hard x-rays in two dimensions at high efficiency. Continued advances in MLL resolution points to new possibilities for x-ray imaging of, for instance, individual nanoparticles in catalytic systems, efficiency-limiting defects in solar cells, trace metal quantities of tens of atoms in biological cells, and the nanoscale structural properties of materials and thin films. >>>

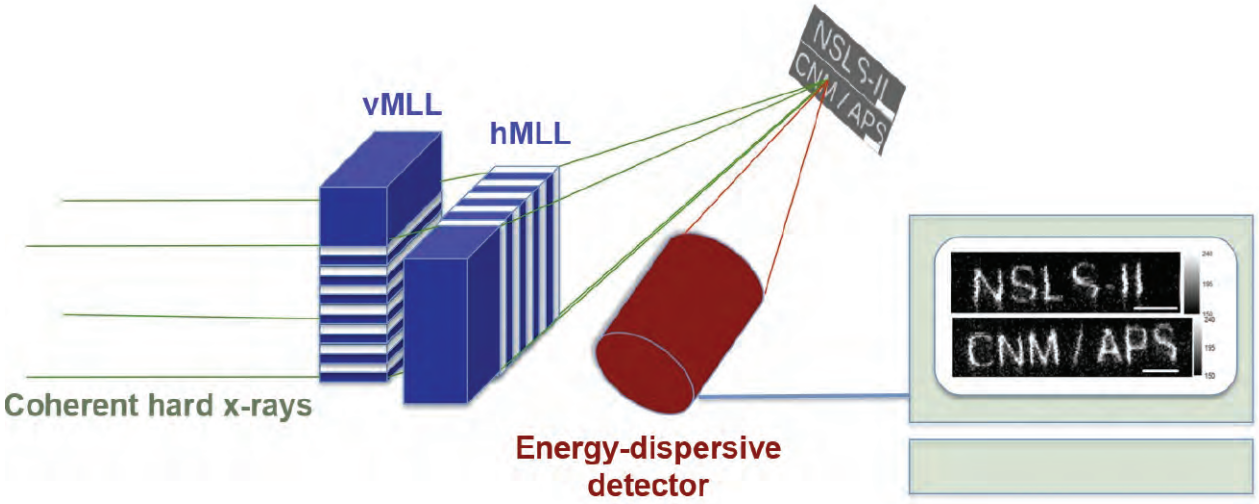

Fig. 1. A vertically focusing MLL (vMLL) and a horizontally focusing MLL (hMLL) are positioned sequentially into a coherent hard x-ray beam from the APS. The vMLL and hMLL are fabricated to yield different focal lengths, such that the vertical and horizontal foci come to lie in the same focal plane. A sample is aligned into the focal plane and rastered through the hard x-ray nanofocus. An energy dispersive detector records the fluorescence radiation emitted by the sample and displays the fluorescence image on a computer screen.

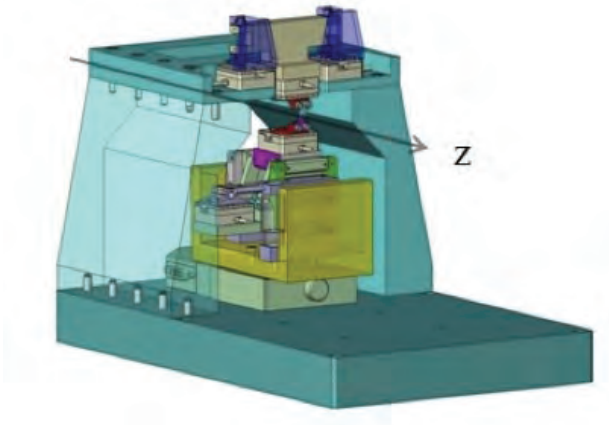

> Fig. 2. Mechanical design of the MLL instrument at the APS. Currently, 8° of freedom are required to position two cylindrically focusing MLL optics in such a way that they yield a single focal spot. X-rays enter from the left. A nanofocus is formed in the center of the instrument.

26-ID-C • CNM/XSD • Physics, materials science • Microfluorescence (hard x-ray), microdiffraction, tomography • 8-12 keV • On-site • Accepting general users •

MLLs are produced using sputter deposition methods to create more than a thousand thin layers that focus x-rays by diffraction as they pass through the layer system. Individual MLLs diffract x-rays into a cylindrical wavefront. By placing two MLLs in series, x-rays are focused in two directions to a point focus. The basic setup is illustrated in Fig. 1. Incoming x-rays first diffract through the vertically-focusing MLL (vMLL), followed by diffraction through the horizontally-focusing MLL (hMLL). Each MLL must be individually aligned to the Bragg condition (i.e., the condition for constructive interference). The longer focal length of the vertical lens allows the two MLLs to achieve a common focal plane. Figure 2 depicts the positioning apparatus used to precisely align the two MLL lenses with respect to the x-ray beam.

Two-dimensional focusing with the MLL at a spatial resolution from 25 nm to 40 nm was achieved at photon energies of 12 keV and 19.5 keV. While 12 keV is still within the energy range where zone plates can focus to approximately 50 nm with reasonable efficiency, operation at 20 keV demonstrates the powerful high-energy capabilities of MLLs. The MLLs utilized were optimized for operation at 20 keV, where they demonstrated a focusing efficiency of 17% in two dimensions (2D). When operated at 12 keV, absorption reduced the focusing efficiency to 2%. However, by proper thinning of the MLL structures, high focusing efficiency should be achievable for x-ray photon energies down to 8 keV. From a practical perspective, positioning stability at the nanoscale is vital to perform experiments with hard x-ray nanobeams. The MLL microscope used in these experiments demonstrated outstanding stability more than initial alignment, without the use of advanced encoders or feedback.

Test patterns were utilized to characterize the resolution of the MLL microscope. Figure 3a shows a micrograph from a scanning electron microscope (SEM) revealing a series of horizontal and vertical gold stripes deposited on a substrate as test images. Below Fig. 2a are the MLL-focused x-ray images of those same horizontal (3b) and vertical (3c) gold lines. The largest lines are 200-nm in width, while the smallest are 50-nm wide with 50-nm spacing between the lines.

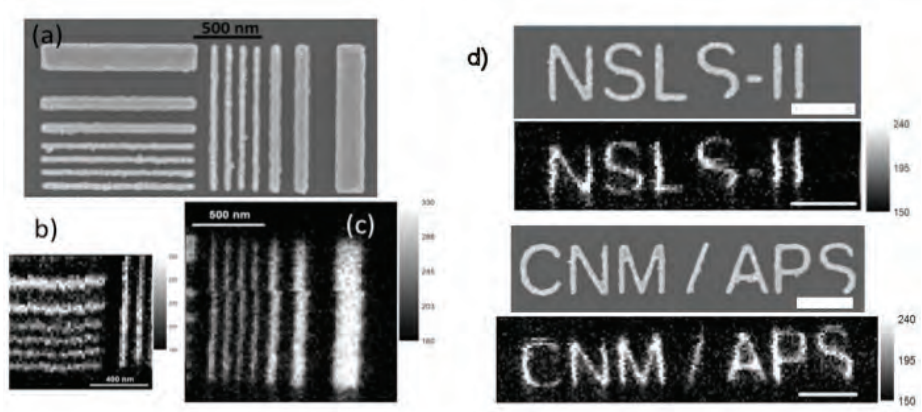

Fig. 3. Images of test patterns obtained with a scanning electron microscope (SEM, a), and maps obtained with the MLL nanofocus (b, c). Excellent spatial resolution of 25 nm × 27 nm has been obtained in the x-ray images. Part (d) shows two additional sets of test patterns, with the upper letters in each set imaged by SEM; beneath each SEM image is the corresponding MLL x-ray image.

The figure clearly shows that the x-ray images resolved features considerably less than 50 nm. The microscope's resolution was quantified utilizing a single 50-nm line, with both 12- and 19.5-keV x-rays. A resolution of 25 nm (horizontal) × 27 nm (vertical) was obtained utilizing 12-keV photons, and of 25 nm × 40 nm using 19.5-keV photons. Figure 3d shows additional SEM micrographs and their associated x-ray images.

This research demonstrates significant progress in pushing toward usable hard x-ray beams with sizes below 10 nm. With additional improvements in deposition of MLL structures and advances in nanopositioning and metrology, a goal of 5-nm resolution with high efficiency for hard x-ray microscopy seems reasonable. These results employing the MLL technique compare favorably with other x-ray microscopy techniques being developed. For instance, the 17% efficiency of the MLL technique achieved with 19.5-keV photons is 5 times to 10 times higher than Fresnel zone plates used at 10 keV can currently achieve with comparable resolution.

Utilizing existing MLL designs, an efficiency well in excess of 10% is theoretically achievable for photon energies of below 10 keV to 25 keV and above. MLLs with 5-nm resolution and below could in principle achieve focusing efficiencies of 50% and greater.

Continued improvements in MLL resolution will open new possibilities for x-ray imaging. Nanometer-scale x-ray microscopy could be applied to tasks such as probing catalytic systems on the scale of individual nanoparticles; understanding efficiency-limiting defects in solar cells; uncovering the trace metal quantities of tens of atoms in, for instance, biological cells by applying x-ray fluorescence to their tiny structures; and to probing the nanoscale structural properties of materials and thin films.

— Philip Koth

See: Hanfei Yan[1,2], Volker Rose[1], Deming Shu[1], Enju Lima[2], Hyon Chol Kang[3], Ray Conley[1,2], Chian Liu[1], Nima Jahedi[1], Albert T. Macrander[1], G. Brian Stephenson[1], Martin Holt[1], Yong S. Chu[2], Ming Lu[2], and Jörg Maser[1]*, "Two Dimensional Hard X-ray Nanofocusing with Crossed Multilayer Laue Lenses," Opt. Express 1**9**(16), 15069 (1 August 2011). DOI:10.1364/OE.19.015069
Author affiliations: [1]Argonne National Laboratory, [2]Brookhaven National Laboratory, [3]Chosun University
Correspondence: *maser@anl.gov

Work at Argonne, including use of the Advanced Photon Source and the Center for Nanoscale Materials, was supported by the Department of Energy Office of Science under Contract No. DE-AC-02-06CH11357. H.C.K. acknowledges support by the Basic Science Research Program through the National Research Foundation of Korea funded by the Ministry of Education, Science and Technology (MEST No. R15-2008-006-01000-0).

REDUCING STRESS IN MULTILAYER LAUE LENSES

Multilayer Laue lenses (MLLs) developed at the APS focus high-energy x-rays so tightly they can detect objects as small as 16 nm in size, and are in principle capable of focusing well below 10 nm. Studies carried out by researchers at the APS (and now the National Synchrotron Light Source II at Brookhaven National Laboratory) reveal a simple means to reduce stress in MLLs, thereby removing a possible obstacle to maximizing the potential of these lenses.

As reported in 2011 on the Argonne home page (http://www.anl.gov/articles/argonne-pioneered-x-ray-lens-aid-nanomaterials-research), MLLs double the resolution over existing lenses, and future advances could increase resolution by 10 times. Furthermore, large-diameter MLLs have the potential to achieve a very high efficiency, enabling detailed studies of individual nanoparticles.

Future MLLs with an overall growth thicknesses in excess of 50 μm will be needed to focus the full brilliance of APS x-ray beams to spot sizes of 5 nm and below. Any built-up stress, if not reduced, can limit the maximum useful thickness of the MLL. Excessive stress can cause delamination of the lenses during processing of deposited multilayers into ready-to-use lenses. However, there is a way to reduce the grown-in stress.

Since their invention at Argonne, MLLs and the technology needed to make them have progressed to the point where a focus spot of 25 nm × 27 nm was reported in *Optics Express* [1]. The deposited thicknesses for the two crossed lenses were 12.4 μm and 13.4 μm, which limited the focused flux to approximately 1% of what could ideally be obtained. Future lenses will require thicker deposits, and methods to reduce stress are needed.

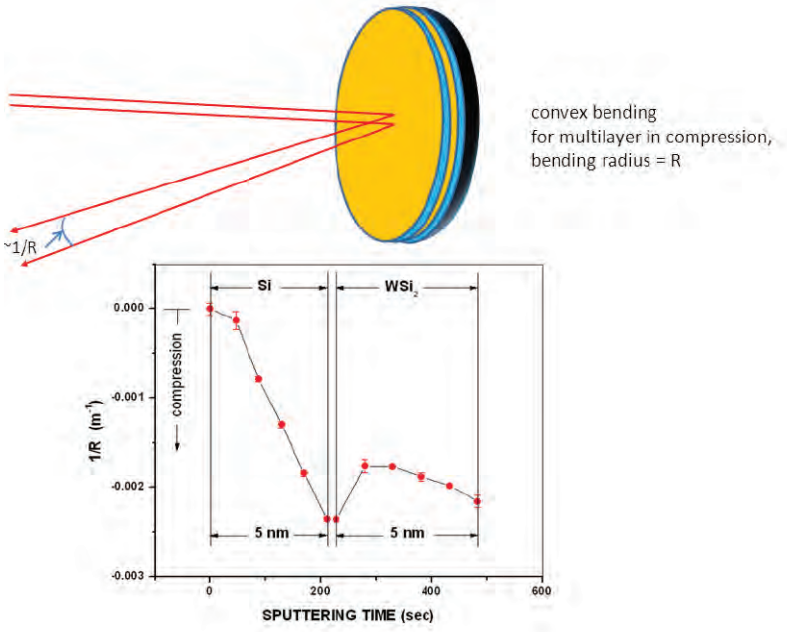

Fig. 1. Schematic illustration of the laser-based measurement of the radius of curvature caused by the stress inherent in the sputter deposition of a multilayer. The measured data were obtained by averaging over several periods.

Grown-in stress resulting from a newly deposited layer can be measured by monitoring the change in the radius-of-curvature of the entire wafer, as schematically shown in the top part of Fig. 1. The formula that relates the stress to this curvature was first published by G.G. Stoney in 1909, and measurements of curvature offer a very simple and powerful means to monitor changes after only 1 nm of a thin film is deposited on a substrate via sputter deposition, as shown in the bottom part of the figure. The fact that stress in very thin layers can be studied is reported in *Applied Physics Letters*. The data reveal that more of the grown-in stress arises from the Si layers than from the WSi_2 layers, so that a reduction in the fraction of the multilayer period that is Si should be effective.

This simple means to reduce stress is presently an active area of research at the APS, and the preliminary results point to an effective path towards larger-diameter optics.

— Al Macrander

REFERENCE

[1] Hanfei Yan, Volker Rose, Deming Shu, Enju Lima, Hyon Chol Kang, Ray Conley, Chian Liu, Nima Jahedi, Albert T. Macrander, G. Brian Stephenson, Martin Holt, Yong S. Chu, Ming Lu, and Jörg Maser, "Two dimensional hard x-ray nanofocusing with crossed multilayer Laue lenses," Opt. Express **19**, 15069 (2011).

See: Kimberly MacArthur[1‡], Bing Shi[1], Ray Conley[1,2‡‡], and Albert T. Macrander[1]*, "Periodic variation of stress in sputter deposited Si/WSi_2 multilayers," Appl. Phys. Lett. **99**, 081905 (2011). DOI:10.1063/1.3628242]
Author affiliations: [1]Argonne National Laboratory, [2]Brookhaven National Laboratory. Present address: ‡University of Tennessee, ‡‡National Synchrotron Light Source II
Correspondence:
*macrander@aps.anl.gov

This work was supported by the U.S. Department of Energy Office of Science under Contract No. DE-AC-02-06CH11357.

COHERENT DIFFRACTIVE IMAGING IN LIVING COLOR

One hundred and fifty years after the first color photograph appeared, scientists have devised a way of employing the full spectrum of colors from synchrotron and free-electron laser x radiation to image nanometer-sized subjects with unprecedented clarity and speed, and in three dimensions. This new research technique, developed with a major assist from the APS, is expected to improve imaging on the nanoscale in the quest for advances in pharmaceuticals and new materials for next-generation technologies.

The researchers, from the ARC Centre of Excellence for Coherent X-ray Science (The University of Melbourne and La Trobe University), SLAC National Accelerator Laboratory, and Argonne used the XSD 2-ID-B beamline at the APS to develop this new technique, dubbed "polyCDI."

PolyCDI extends the capabilities of coherent diffractive imaging (CDI), a lens-less imaging technique that has been a mainstay for experiments observing matter on the scale of x-ray wavelengths.

But CDI has its limits. Even though the light from synchrotron x-rays produced at facilities like the APS is the brightest available for research, it is not bright enough to capture precise images at the nanoscale even if exposures are very long, and it cannot be used to capture "movies" of chemical processes, biological changes, and the transformation of materials under stress.

PolyCDI promises to change the game for diffractive imaging. Rather than employing a single wavelength of light from a high-brightness x-ray source such as the APS, polyCDI utilizes broadband light, also available from the APS, that contains many wavelengths at the same time. The results of the group's research, just published in Nature Photonics, show that polyCDI can produce images almost two orders of magnitude faster than conventional CDI.

Deployed in concert with a new generation of fast x-ray detectors, CDI could make possible the first time-resolved nano-movies of changes to materials brought on by extreme temperatures or high magnetic fields, processes that are vital in developing advanced materials for new technologies. Coupled to innovative focusing optics, polyCDI could greatly reduce the time needed to gather information about the composition of diseased cells.

For best imaging, researchers typically need to convert samples to crystals, but this is not always possible in all samples. This new way of utilizing full-color synchrotron light to improve the precision and speed of imaging has great potential, perhaps revolutionizing x-ray imaging much as the advent of broadband communications technology has changed our lives.

The researchers will next apply it to CDI with higher energy x-rays to peer deeper into dense materials, ultimately to see features on the scale of single atoms. — *Richard Fenner*

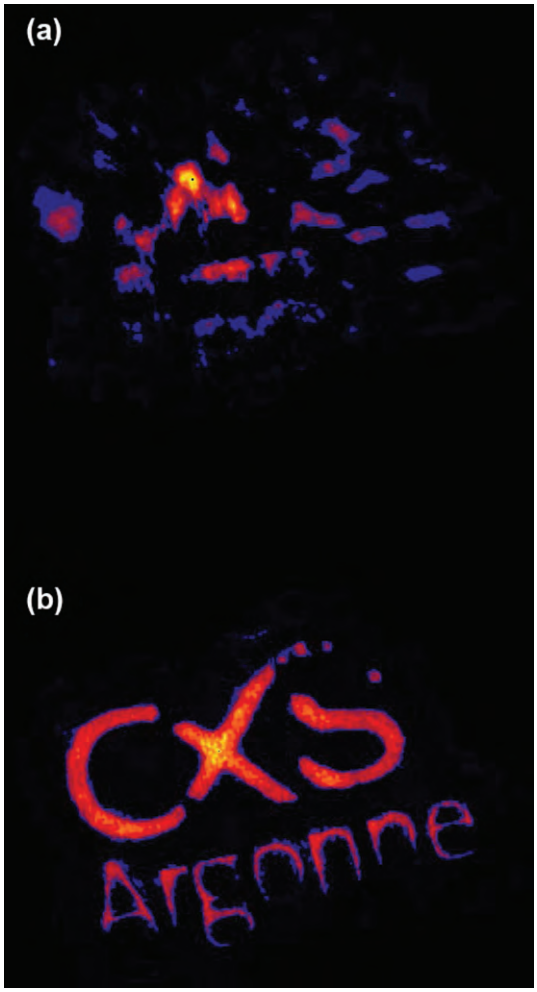

Images of a gold test pattern reconstructed from coherent diffraction patterns taken with polychromatic (broadband) ~1.4-keV x-rays, (a) assuming the x-ray beam consists of a single wavelength, and (b) using the new polychromatic diffraction algorithm.

See: Brian Abbey[1], Lachlan W. Whitehead[1], Harry M. Quiney[1], David J. Vine[1], Guido A. Cadenazzi[1], Clare A. Henderson[1], Keith A. Nugent[1]*, Eugeniu Balaur[2], Corey T. Putkunz[2], Andrew G. Peele[2], G.J. Williams[3], and I. McNulty[4], "Lensless imaging using broadband X-ray sources," Nat. Photo. **5**, 420 (2011). DOI:10.1038/NPHOTON.2011.125

Author affiliations: [1]The University of Melbourne, [2]La Trobe University, [3]SLAC National Accelerator Laboratory, [4]Argonne National Laboratory

Correspondence: *keithan@unimelb.edu.au

The authors acknowledge the support of the Australian Research Council Centre of Excellence for Coherent X-ray Science and the Australian Synchrotron Research Program. Use of the Advanced Photon Source at Argonne National Laboratory was supported by the U.S. Department of Energy Office of Science under Contract No. DE-AC02-06CH11357.

2-ID-B • XSD • Materials science, environmental science, physics • Coherent x-ray scattering (soft x-ray), microfluorescence (soft x-ray) • 635-4100 eV • On-site • Accepting general users •

Seeing on the Nanoscale without Lenses

To understand what happens on the nanoscale, we have to be able to see at the nanoscale. While many experimental techniques exist for seeing the very small, such as x-ray and electron microscopy, each has its own limitations and constraints, whether from technological capabilities or simply the laws of nature. The development of new nanoscale imaging methods for the nanotechnology toolbox is therefore a matter of continuing and pressing importance. Researchers from the University of California, San Diego, and Argonne carrying out investigations at the APS have conceived and demonstrated a new approach to lensless imaging of magnetic structure at the nanoscale, x-ray coherent diffractive imaging (CDI). This work points toward greater insights about magnetic oxides at the nanoscale and the ways assembly of nanostructures can be controlled. >>>

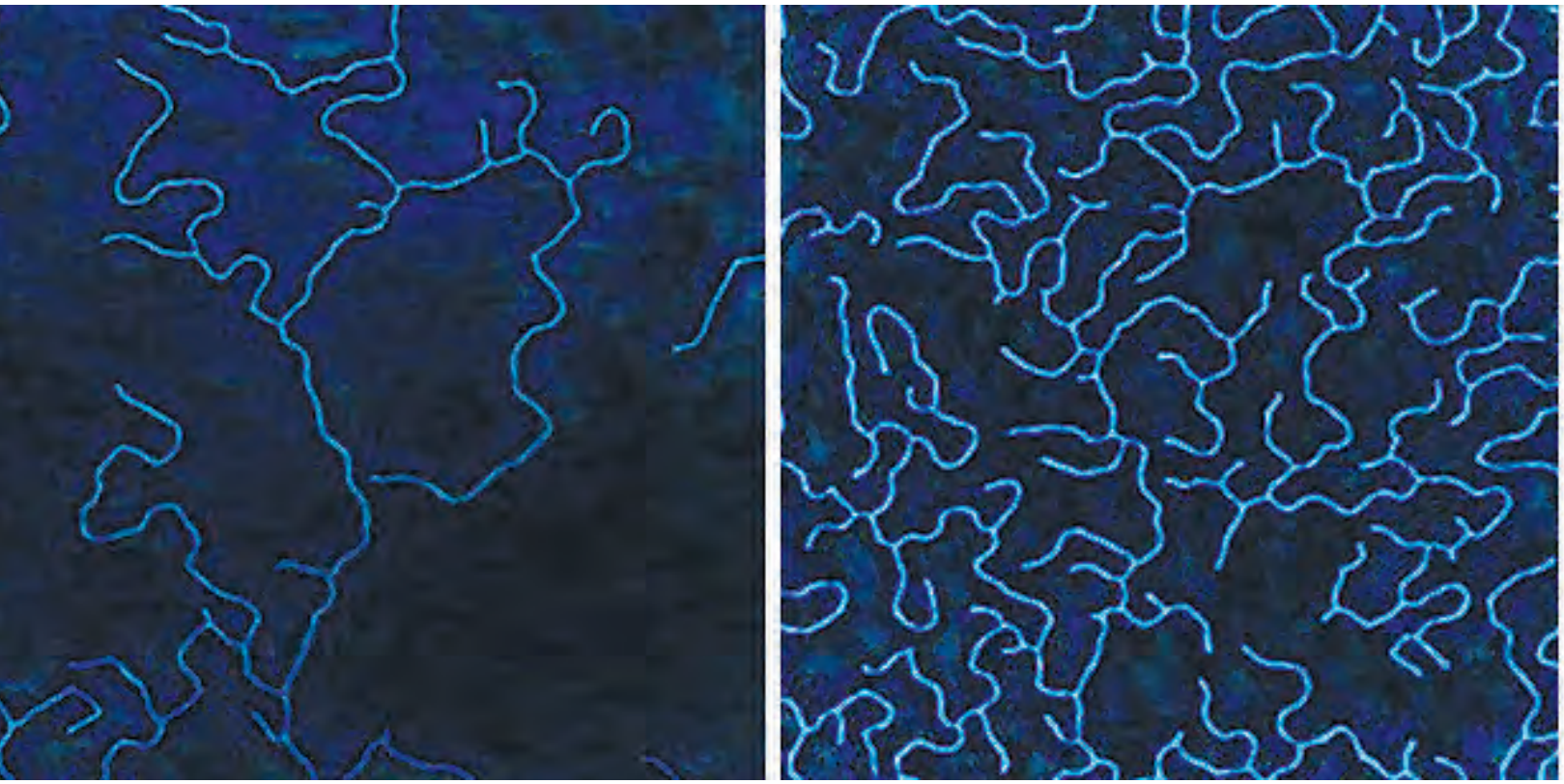

Fig. 1. Evolution/nucleation and growth of nanoscale magnetic domains as a function of applied magnetic field.

Working at the XSD 2-ID-B beamline at the APS, the experimenters employed the principle of dichroism, in which a crystal structure absorbs light with one polarization while transmitting light of a different polarization. Their new CDI technique obtains a coherent x-ray scattering pattern from a sample, maps the Ewald sphere (the sphere of reflection), then inverts the pattern mathematically. In this way, images can be generated without the need for any reference wave or precision optics.

The team used this lensless CDI technique to map ferrimagnetic domains in a multilayer Gd/Fe film and to partly follow domain structural evolution through its hysteresis loop.

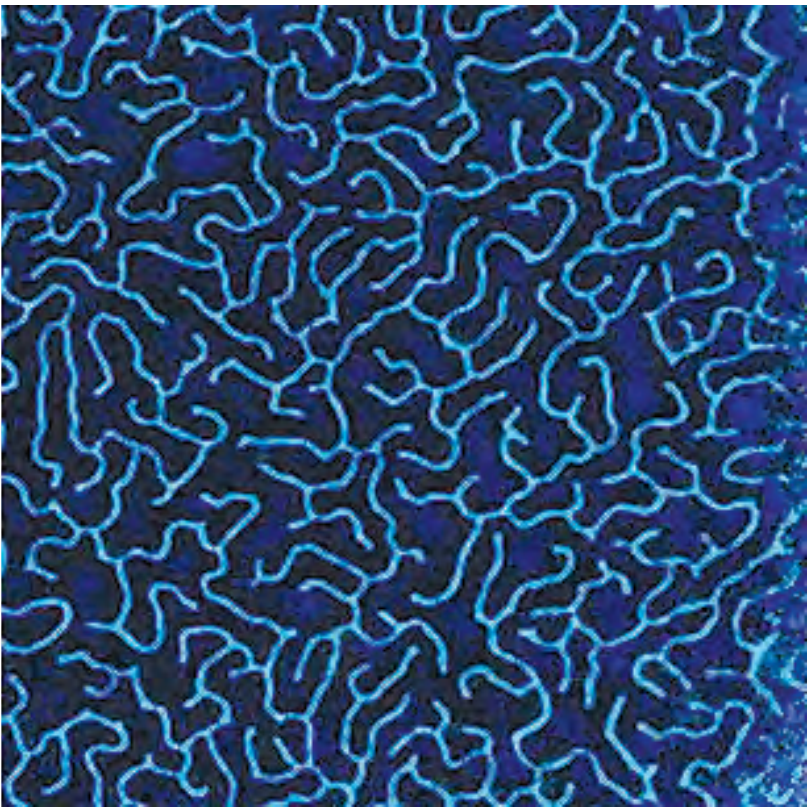

Multilayer films such as gadolinium/iron (Gd/Fe) and similar structures have become increasingly important because of their behavior as an artificial ferrimagnet with perpendicular magnetic anisotropy, which makes them extremely useful for the study of the magnetic stripe-forming systems used in swipe cards and now smart cards. The prospect of using these films for laser-induced domain switching at femtosecond rates may lead to extremely fast magnetic recording devices. The CDI technique provides invaluable insight into the physics of such systems. The team's work was made possible by the extremely bright and tunable nature of the APS x-ray source, which allows the use of ptychographic techniques that provide high resolution; ptychography determines the relative phase of adjacent coherent Bragg reflections through their interference pattern.

The experimenters examined a Gd/Fe film beginning with the sample in a magnetically saturated state in which the entire film is in a single magnetic domain, then reduced the applied field to observe the emergence of the ferromagnetic domain patterns (Fig. 1). These began to appear at about 44 mT. As the applied magnetic field was decreased, classic stripe patterns arose, of a type found in many other systems such as diblock copolymers, liquid crystals, and Langmuir monolayers. The domain behavior is highly sensitive to the fluctuations of the applied magnetic field, which is not the case with other multilayer films such as cobalt/palladium.

Unlike other techniques, the spatial resolution of the CDI technique is not dependent upon extreme nanoscale precision of optical equipment, but simply on a high-frequency signal-to-noise ratio in the coherent diffraction measurements, and on the stability and precision of the x-ray beam. Thus, because their "lens" was mathematical rather than physical, the team was able to obtain reconstructions of the evolution of magnetic configurations of the film with extremely high resolution. The technique is also not limited to only magnetic materials, but can be applied to any dichroic structure and can image samples of any size. It will become even more valuable as new-generation x-ray sources become available, featuring beams with greater brilliance and transverse coherence.

With this powerful yet technically uncomplicated technique, the team has opened a new window into understanding the structure and behavior of complex magnetic oxides at the smallest scales. That understanding promises to extend the scope and powerful possibilities of nanotechnology by providing another way to see and thus control the assembly of nanostructures. As with so many endeavors both at the very large and the very small scales, the first critical step is seeing clearly.

— Mark Wolverton

See: Ashish Tripathi[1,2], Jyoti Mohanty[1], Sebastian H. Dietze[1], Oleg G. Shpyrko[1]*, Erik Shipton[1], Eric E. Fullerton[1], Sang Soo Kim[2], and Ian McNulty[2], "Dichroic coherent diffractive imaging," Proc. Nat. Acad. Sci. USA **108**(33), 13393 (August 16, 2011). DOI:10.1073/pnas.1104304108

Author affiliations: [1]University of California, San Diego, [2]Argonne National Laboratory

Correspondence:
*oshpyrko@physics.ucsd.edu

E.S. and E.E.F. were partially supported by U.S. Departmrnt of Energy (DOE) Office of Science Award DE-SC0003678. Use of the Advanced Photon Source at Argonne National Laboratory was supported by the U.S. DOE Office of Science under Contract DE-AC02-06CH11357.

2-ID-B • XSD • Materials science, environmental science, physics • Coherent x-ray scattering (soft x-ray), microfluorescence (soft x-ray) • 635-4100 eV • On-site • Accepting general users •

BRAGG REFLECTIVITY OF X-RAYS: AT THE LIMIT OF THE POSSIBLE

Studies aided by two APS beamlines have demonstrated that synthetic, nearly defect-free diamond crystals can reflect more than 99% of hard x-ray photons backward in Bragg diffraction, with a remarkably small variation in the magnitude of reflectivity across the sample. These results represent a quantum leap to the largest reflectivity measured, at the limit of what is theoretically possible. It was attained under the most challenging conditions of normal incidence and with extremely high-energy x-ray photons. >>>

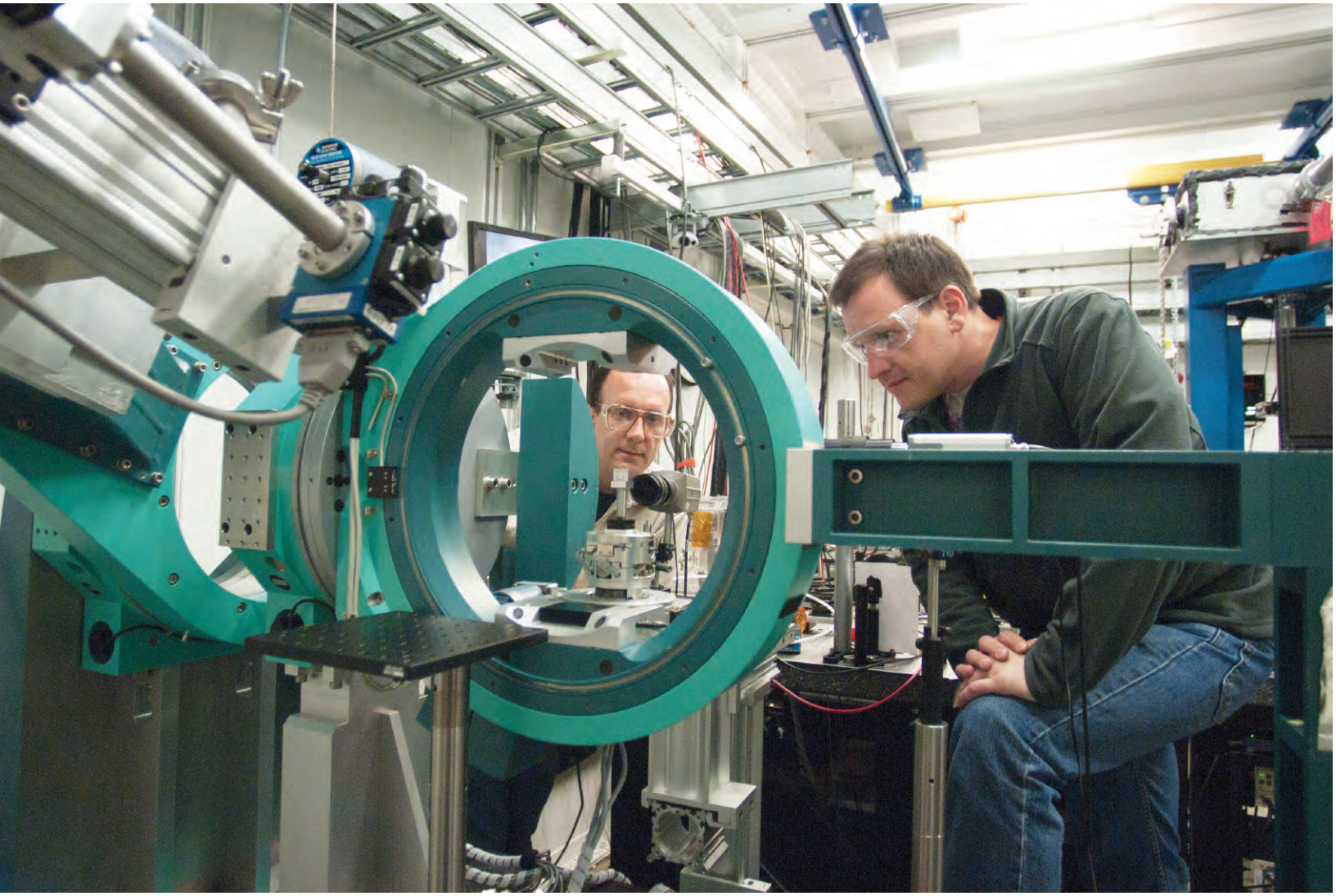

Donald Walko, left, and Stanislav Stoupin (both XSD-IXN) check the sample mount on the six-circle goniometer in the 7-ID-B,C,D research station before taking measurements.

7-ID-B,C,D • XSD • Atomic physics, chemistry, materials science • Phase contrast imaging, time-resolved x-ray absorption fine structure, time-resolved x-ray scattering • 6-21 keV • On-site • Accepting general users •

30-ID-B,C • XSD • Materials science, physics • Inelastic x-ray scattering • 5-14 keV, 5-30 keV, 23.7-29.7 keV• On-site • Accepting general users •

Ultra-high-reflectance mirrors are essential components of the most sophisticated optical instruments, which are designed to cover the entire frequency spectrum and find use in a wide range of applications, from telescopes for astronomy to high-energy x-ray facilities such as the APS. In the x-ray regime, super-polished mirrors with close to 100% reflectivity are routinely used at grazing angles of incidence. However, at large angles of incidence, and especially at normal incidence, such high reflectivity had not been achieved.

The research in this study was conducted by a team comprising investigators from Argonne and the Technological Institute for Superhard and Novel Carbon Materials (TISNCM) in Russia. This investigation was motivated by the need for high-reflectivity x-ray mirrors at close-to-normal incidence for use in x-ray free electron laser oscillators (XFELOs).

XFELOs are x-ray light sources of the future that will provide scientists with fully coherent x-rays with record high spectral purity and average brightness, qualities that are highly desirable for experiments. Unlike high-gain x-ray lasers, XFELOs are designed to be low-gain machines, requiring a low-loss optical cavity with high-reflectivity x-ray mirrors close to backscattering, similar to conventional table-top lasers.

The feasibility of XFELOs was questioned by many experts because of the high-reflectivity x-ray mirror limitations. These limitations are now removed by the demonstration of very high (more than 99%) reflectivity of hard x-rays in Bragg backscattering from diamond crystals. Theoretical analysis presented in the *Nature Photonics* paper establishes that diamond has the highest (higher than any other crystal) Bragg reflectivity due to the uniquely small ratio of the extinction length in Bragg diffraction to the absorption length. Even in backscattering, where the reflectivity is lowest, it was thought to be more than 99%, and this has now been demonstrated.

Diamond crystals of sufficient size and crystalline perfection for use as high-reflectivity x-ray mirrors can be synthesized using state-of-the-art crystal growth techniques. In this experiment, synthetic diamond single crystals of very high crystal quality were grown at the TISNCM via the temperature gradient method under high-pressure and high-temperature conditions. The reflectivity measurements were performed at the XSD beamlines 30-ID-B,C and 7-ID-B,C,D at the APS, utilizing 23.7-keV and 13.9-keV photons, respectively.

Systematic observations of the more than 99% reflectivity show that high-reflectivity mirror limitations in the regime of hard x-rays have been eliminated (Fig. 1). This is an important step toward realization of x-ray cavities for XFELOs. Also, the results in this study support a broad range of potential applications of diamond crystals for high-reflectance, coherence-preserving, and resilient x-ray optics, such as x-ray monochromators, beam splitters, delay lines, high-finesse Fabry-Perot resonators, etc.

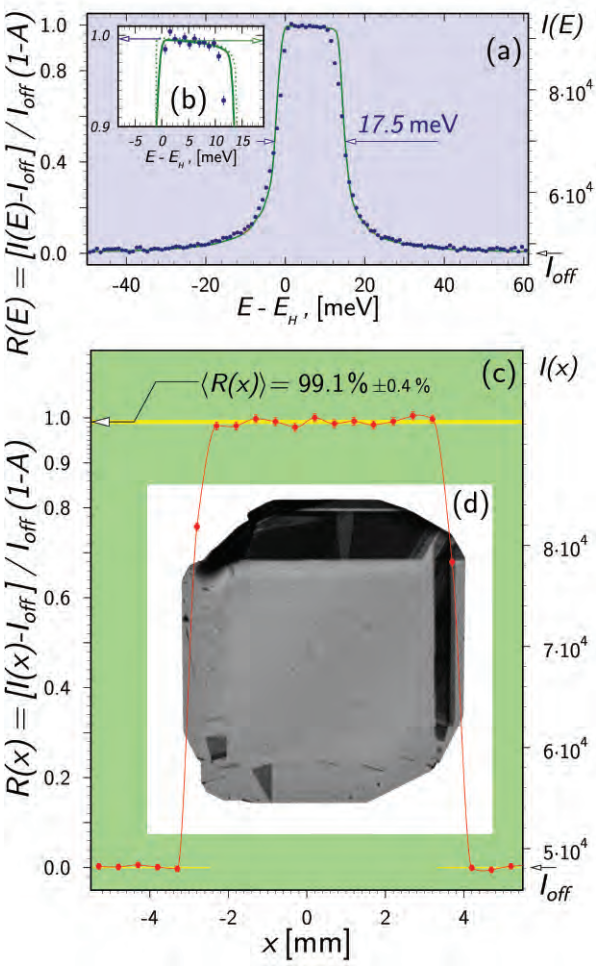

Fig. 1. Absolute reflectivity of 13.9-keV x-rays from the (008) atomic planes of a diamond crystal in Bragg backscattering (a)-(c), and x-ray Lang transmission topogram of the diamond crystal (d). The diamond crystal, nearly defect-free in a volume of 5 × 5 × 1 mm^3 , reflects more than 99% of hard x-ray photons backwards in Bragg diffraction, with a remarkably small variation in magnitude across the sample.

See: Yuri Shvyd'ko[1]*, Stanislav Stoupin[1], Vladimir Blank[2], and Sergey Terentyev[2], "Near-100% Bragg reflectivity of X-rays," Nat. Photonics **5**, 539 (2011). DOI:10.1038/nphoton.2011.197

Author affiliations: [1]Argonne National Laboratory, [2]Technological Institute for Super-hard and Novel Carbon Materials

Correspondence:
*shvydko@aps.anl.gov

This work and use of the Advanced Photon Source was supported by the U.S. Department of Energy (DOE) Office of Science under Contract No. DE-AC02-06CH11357. White-beam topography studies were carried out at beamline X19C of the National Synchrotron Light Source, Brookhaven National Laboratory, which is supported by DOE Contract no. DE-AC02-98CH10886.

IMAGING INTERFACIAL PROCESSES IN REAL TIME

Chemical reactions that occur at interfaces are central to many natural and industrial processes. Examples are chemical reactions at mineral surfaces that control the release of nutrients and the formation of bone and skeletal minerals, and those of heterogeneous catalysis, in which reactants diffuse to the catalyst surface and adsorb onto it via the formation of chemical bonds. Yet the ability to image interfaces in complex environments remains severely limited. Scanned probe microscopies (e.g., atomic force microscopy) are widely used but require a probe tip, which can introduce artifacts, be a source of unwanted reactivity, and fail to reach buried solid-solid interfaces. The recent development of x-ray reflection interface microscopy (XRIM) opens a new window to studying interfacial processes *in situ* and in real time, including those processes that take place under aggressive chemical conditions, which currently can only be studied by *ex situ* approaches. Researchers at Argonne recently demonstrated some of the technique's thin-film capabilities by using it at XSD beamline 33-ID-D,E to characterize three complex oxide thin-film systems, $SrRuO_3$ on $SrTiO_3$, $EuTiO_3$ on $DyScO_3$, and $Bi2O_3$ on $SrTiO_3$.

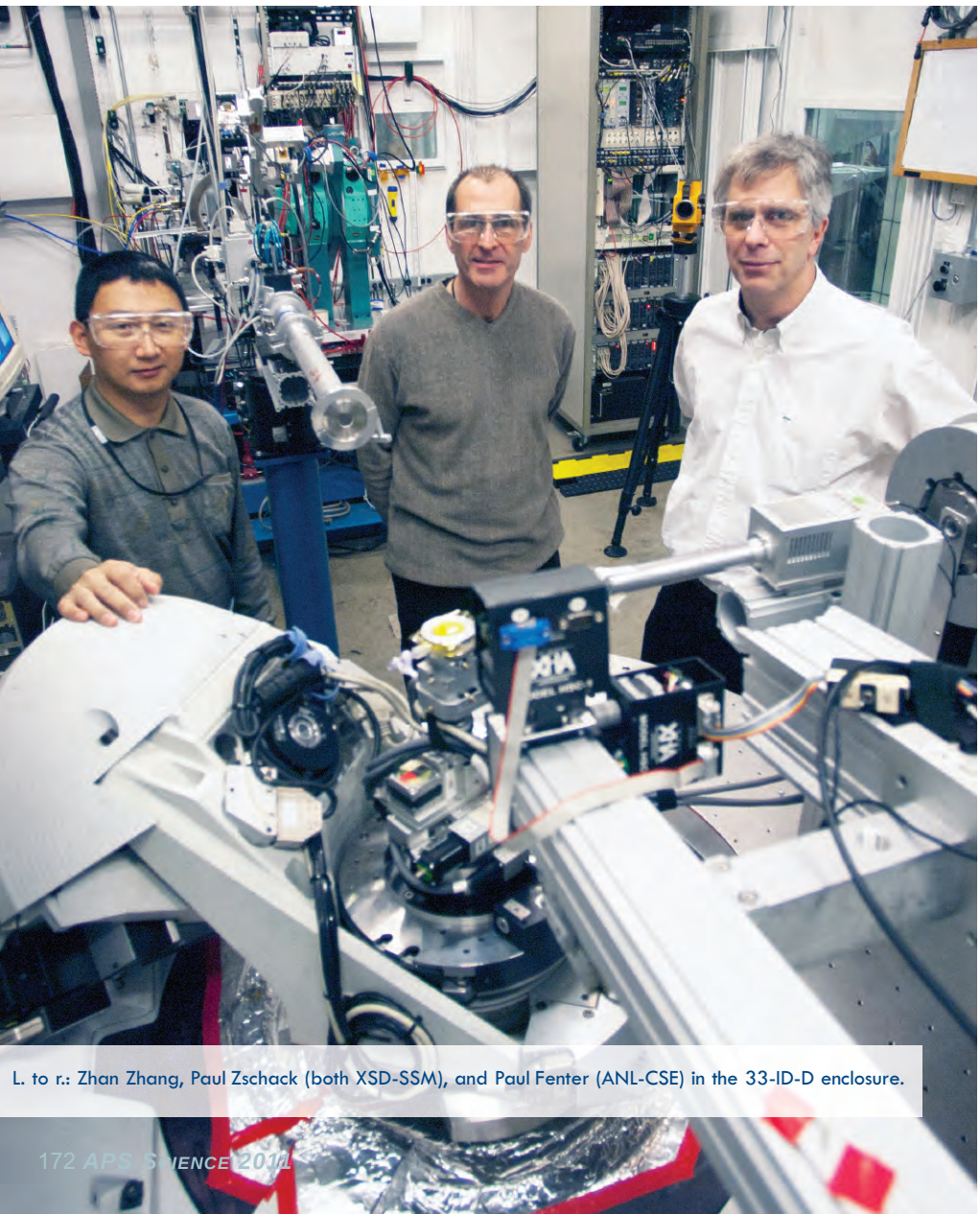

L. to r.: Zhan Zhang, Paul Zschack (both XSD-SSM), and Paul Fenter (ANL-CSE) in the 33-ID-D enclosure.

Because of the penetration of hard x-rays, buried molecular-scale interfacial features can be directly probed by XRIM without damaging the sample. Furthermore, the weak interaction of x-rays with matter makes it feasible to quantitatively analyze the measured images when x-rays from high-brightness synchrotron sources such as the APS are used. XRIM applies full-field imaging using a specularly reflected monochromatic x-ray beam from a surface or interface and directly visualizes the interfacial topography of a solid surface by exploiting phase contrast. Vertical changes in surface topography give rise to differences in x-ray path length for the reflected x-rays, leading to destructive interference, so variations in surface topography are seen by the x-ray beam as pure phase objects undergoing sudden phase changes. Measurements of contrast variations in the images as a function of momentum transfer allow features to be identified as steps or terraces or as film inhomogeneities. This novel use of interfacial phase contrast permits objects to be observed that are substantially (~300 ×) smaller than the spatial resolution of the x-ray optics being used. Because the contrast of the objects in the images can be controlled by manipulating the scattering conditions, XRIM can be valuable for monitoring interfacial features during film growth.

In all of the experiments, a monochromatic x-ray beam at 10 keV was focused on samples using a Fresnel zone plate (FZP) followed by an order sorting aperture (OSA), which was used to stop the higher-order focused beams. The specularly reflected x-rays were then focused onto a charge-coupled device (CCD) detector by another FZP followed by a second OSA, this time in the form of a 4-blade slit, which was used to cut out the directly

reflected x-rays. The sample was mounted on a six-circle Kappa geometry diffractometer, while the objective FZP, the slit, and the CCD were all mounted on the δ-arm of the Kappa diffractometer so that reciprocal space could be accessed.

$SrRuO_3$ on $SrTiO_3$. A high-quality 100-layer epitaxial film of $SrRuO_3$ (SRO) was grown on $SrTiO_3$ (STO) using pulsed laser deposition. A traditional reflectivity curve was obtained for the sample, and XRIM images were collected at various momentum transfers near the STO (002) reflection. Image collection time varied from approximately 3 to 30 min. The step and terrace structure of the interface was clearly evident from the XRIM images collected along the thickness fringes. In addition to the step contrast features in these images, small growth defects could also be observed in these films.

$EuTiO_3$ on $DyScO_3$. High-quality coherent epitaxial films of $EuTiO_3$ (ETO) on $DyScO_3$ (DSO) substrates were synthesized using molecular beam epitaxy. The 22-nm-thick ETO films were protected with overlayers of CaO and amorphous silicon. Reflectivity near the DSO (110) Bragg peak showed well-defined thickness fringes and a shifted ETO Bragg peak, as expected because of the epitaxy. The XRIM characterization at various momentum transfer values, however, revealed regions that are not homogeneous, which highlights the capability of XRIM to spatially resolve laterally heterogeneous structures (Fig. 1).

$Bi2O_3$ on $SrTiO_3$. Although δ-phase Bi_2O_3 is an important oxide ionic conductor, its bulk phase is stable only in a narrow temperature range. By epitaxial growth on the slightly lattice-mismatched oxide substrate, a δ-Bi_2O_3 nanostructure or thin film can be stabilized at room temperature. A series of images were taken along the STO surface normal direction, near the β-Bi_2O_3 (002) and δ-Bi_2O_3 (002) Bragg peak positions. Imaged nanodots were identified as β-Bi_2O_3 and δ-Bi_2O_3.

X-ray reflection interface microscopy has been shown to be capable of imaging surfaces, buried interfaces, and thin-film topographies. When combined with laterally averaged x-ray scattering measurements, both the averaged and the localized information about surfaces or interfaces can be quantitatively obtained. In the future, the efficiency and the lateral resolution of XRIM can be further improved through the use of optimized optics. Therefore, the *in situ*, real-time observations of many surface/interface processes such as thin-film growth, surface dissolution, and precipitation can be realized. With a proper normalization of the reflected intensities, a fully quantitative analysis of XRIM images could compare observations as a function of position (i.e., different parts of the sample) and momentum transfer. Spatially resolved information such as the phase of the deposited material, the lattice parameters, stress state, and thickness of the thin film can also be retrieved.

— Vic Comello

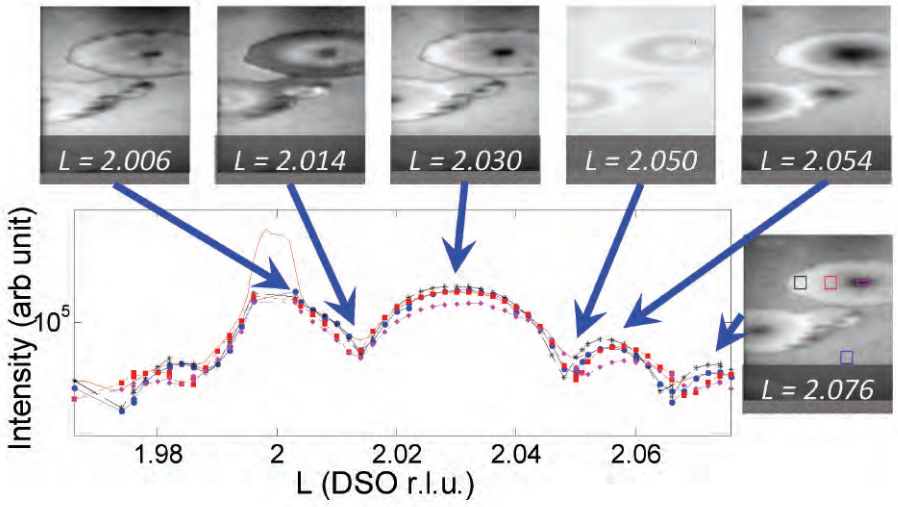

Fig. 1. $EuTiO_3$ thin film epitaxially grown on $DyScO_3$ were studied with XRIM along the surface truncation rod near the DSO (002) Bragg peak. For quantitative analysis, integral intensities inside the black, blue, red, and pink boxes (image on right) are calculated for each image and plotted (dashed lines have the corresponding colors) as functions of the DSO reciprocal lattice unit, *L*. The solid line relates to the crystal truncation rod measured with the same focused x-ray beam. It is clearly shown that the signals inside the red and pink boxes have longer oscillating periods, indicating that the film thicknesses are getting smaller approaching the center of the circular defects.

See: Zhan Zhang*, Paul Zschack, and Paul Fenter, "Application of X-ray Refection Interface Microscopy to Thin-Film Materials," Nat. Phys. **2**, 700 (2011).
DOI:10.1016/j.nima.2010.11.159
Author affiliation: Argonne National Laboratory
Correspondence: *zhanzhang@anl.gov

P.F. was supported by the Geosciences Research Program, Department of Energy (DOE) Office of Science. Use of the Advanced Photon Source at Argonne National Laboratory was supported by the U.S. DOE Office of Science under Contract No. DE-AC02-06CH11357.

33-ID-D,E • XSD • Materials science, physics, chemistry • Anomalous and resonant scattering (hard x-ray), diffuse x-ray scattering, general diffraction, surface diffraction, x-ray reflectivity, x-ray standing waves • 4-40 keV, 6-21 keV • On-site • Accepting general users •

AN *IN SITU* OXIDE MOLECULAR BEAM EPITAXY SYSTEM AT APS SECTOR 33

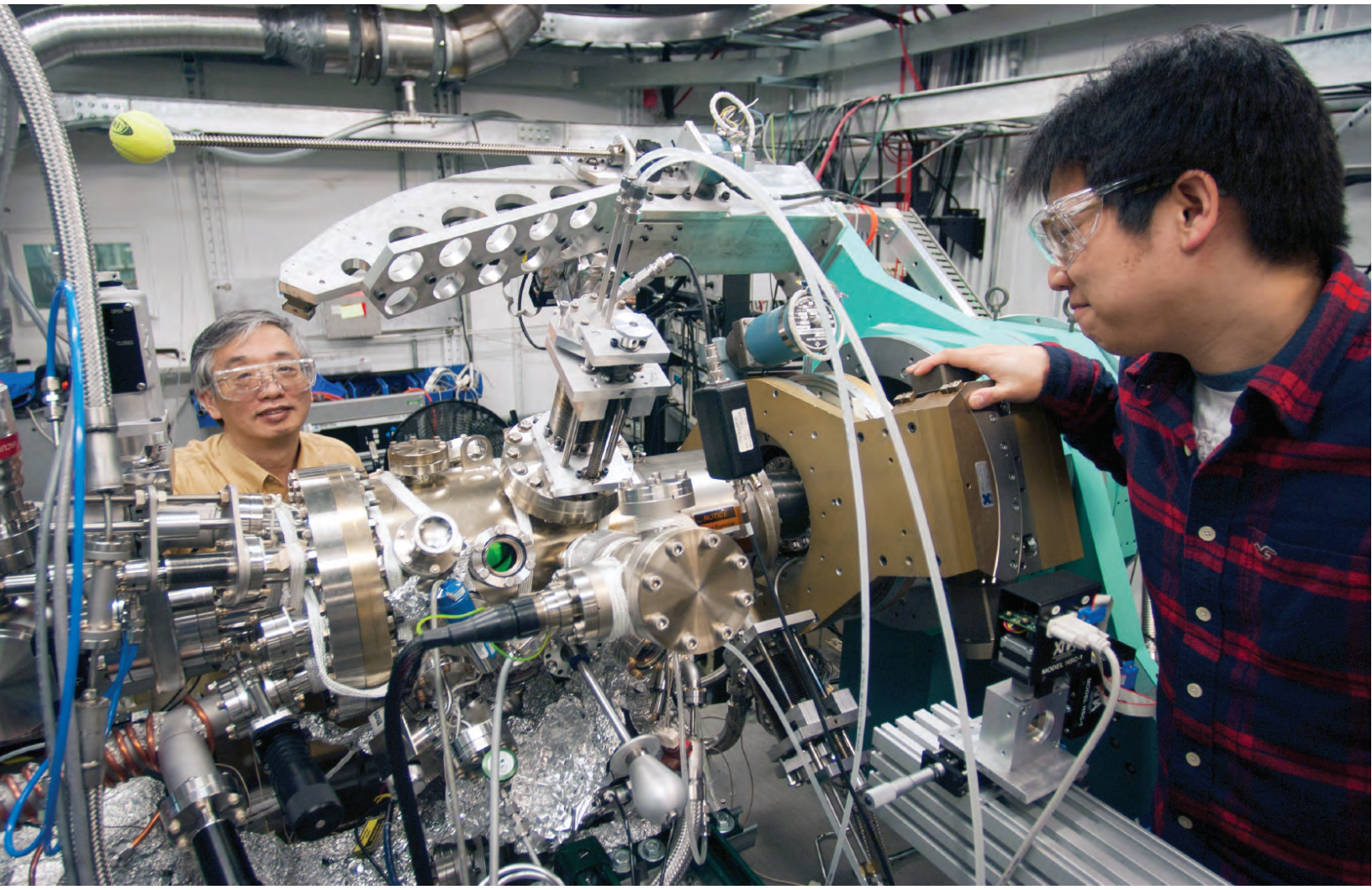

Using funds provided by Argonne's Materials for Energy Strategic initiative, the world's first *in situ* oxide molecular beam epitaxy (MBE) system (Fig.1) has been built at XSD Sector 33 of the APS. It is designed to play an important role in helping move forward Argonne's development of "innovative approaches for designing, creating and harnessing novel, environmentally responsible molecules and materials that exhibit revolutionary scientific phenomena or use-inspired functionality are poised to transform science and technology."

Functional materials based on complex oxides offer new and exciting strategies for meeting many of our outstanding energy challenges. Materials theorists can now design virtual crystals for specific applications and predict their properties [1].

Unfortunately, synthesis of a new oxide material is typically difficult even when utilizing oxide MBE, a powerful deposition technique that allows the construction of materials atomic plane by atomic plane. At issue is the stability of the desired structure. Even if unstable, the crystal may be synthesized by a kinetic route if quantitative, atomic-resolution information regarding the film structure can be supplied

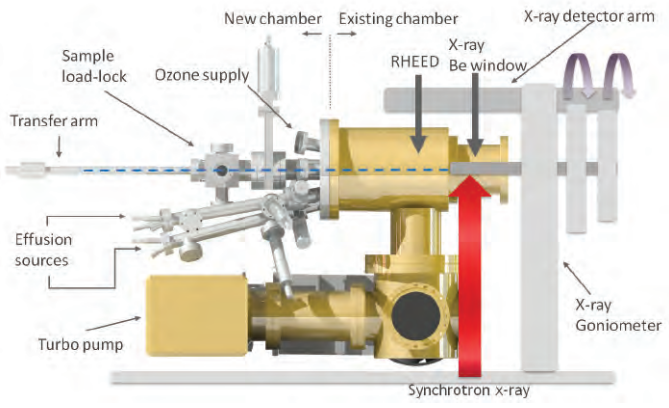

Fig. 1. Photo: Hawoong Hong (left) and June Hyuk Lee (both XSD-SSM) at the oxide growth upgrade to the existing molecular beam epitaxy system in research ststion 33-ID-E of the APS. Above: A diagram of the system.

during growth. Coupling x-ray tools *in situ* with oxide film synthesis offers real-time quantitative understanding of the synthesis process.

The layered complex oxides (so-called because their unit cell consists of stacked atomic sheets as shown in Fig. 2) offer an enormously broad range of functionalities. For example, some have demonstrated excellent mixed ionic-electronic conducting properties, making them highly attractive candidates for intermediate-temperature solid oxide fuel cell cathodes [2]. Others have a unique structure that makes them ideal for a wide range of catalytic reactions [3], including photochemical water splitting [4].

Furthermore, with the recent advances in *ab initio* modeling techniques and computational power, we can now design layered oxides that display novel functionalities. One such material is shown in Fig. 2. This layered complex oxide, $PbSr_2Ti_2O_7$, is expected to exhibit colossal and highly tunable dielectric and piezoelectric properties [5] and may serve as a working template for achieving revolutionary advances in energy generation, storage, and conversion in future state-of-the-art electroactive devices.

Unfortunately, researchers have been constrained in their ability to synthesize such layered materials because of limited control over composition and structure during deposition, even with the most powerful tool available for layer-by-layer oxide growth: oxide MBE. For materials with highly tunable properties, like the complex oxides, loss of stoichiometric control is tantamount to unintentional doping, easily turning what was to be an excellent dielectric material into a conductor [6]. Such synthesis issues have severely impeded the widespread application of the complex oxides to the many energy technologies in which they have so much potential. In short, scientific/technological progress in this field demands the realization of exceptional compositional and structural control during synthesis.

While the researcher has some control over deposition parameters, nature ultimately controls crystal growth. We therefore need to not only monitor growth, but also to understand

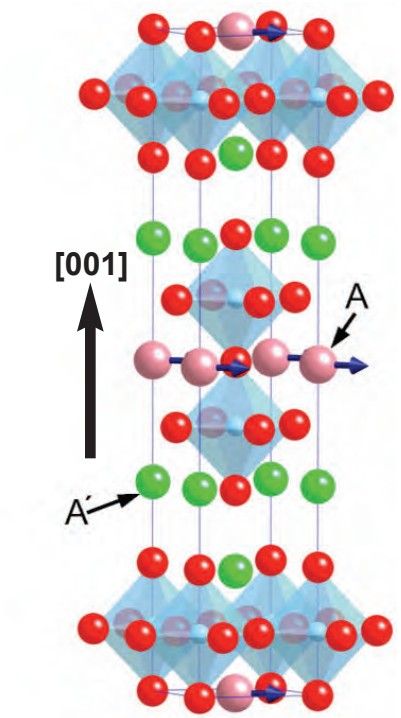

Fig. 1. Crystal structure of a Ruddlesden-Popper-type $PbSr_2Ti_2O_7$ superlattice, where A = Pb and A´ = Sr. An in-plane polar distortion of the superlattice is outlined by bold arrows. From Ref. [5].

what atomic-scale processes take place, along with their associated energies and time scales. For example: Is the deposited structure thermodynamically stable? Does dynamic surface segregation of one of the cation species occur during deposition? Do the interfaces naturally interdiffuse at the growth temperature? Many such questions can be addressed by harnessing state-of-the-art *in situ* synchrotron x-ray techniques to provide a heretofore unknown level of insight into the synthesis of complex materials [7]. Integrating the oxide molecular beam epitaxy system into a high-flux, hard x-ray beamline will enable us to track layer-by-layer structure and composition in real-time.

As an important component of the funded program, the experimental effort is connected to an integrated theoretical synthesis effort (J. Jellinek and M. Malshe of the Argonne Chemical Sciences and Engineering Division; and S.M. Nakhmanson of the Argonne Materials Science Division) whose ultimate goal is to provide guidance on the optimal growth conditions of compounds with the desired structure. This goal is being achieved via extensive molecular dynamics and Monte Carlo simulations of oxide MBE growth, conducted as a function of the chemical identity of the depositing species and operational conditions such as epitaxial stress, temperature, and pressure.

This combined experimental and theoretical effort has not only developed a unique *in situ* oxide MBE capability at the APS, but in the long term will have tremendous impact on a fundamental understanding of the synthesis of complex oxide films and heterostructures. These systems offer unique pathways to new materials relevant to meet the energy needs of the future.

Correspondence:

J.W. Freeland (XSD-MM), freeland@anl.gov; J.-H Lee (XSD-SSM), jhlee@anl.gov; I.C. Tung (Northwestern Univ.), IChengTung@u.northwestern.edu; H. Hong (XSD-SSM), hong@aps.anl.gov; D.D. Fong (ANL-MSD), fong@anl.gov; S.-H. Chang (ANL-MSD), cshyoung@gmail.com; A. Bhattacharya (ANL-MSD), anand@anl.gov; S.M. Nakhmanson (ANL-MSD), nakhmanson@anl.gov; N. Markovic (ANL-MSD), nmmarkovic@anl.gov; J.A. Eastman (ANL-MSD), jeastman@anl.gov; M. Malshe (ANL-CSE), milind@anl.gov; and J. Jellinek (ANL-CSE), jellinek@anl.gov

REFERENCES

[1] J.M. Rondinelli and N.A. Spaldin, Adv. Mater. **23**(30), 3363 (2011).
[2] A. Tarancón et al., J. Mater. Chem. **20**, 3799 (2009).
[3] G. Centi and S. Perathoner, Micropor. Mespor. Mater. **107**, 3 (2008).
[4] J. Kim et al., Topics Catal. **35**, 295 (2005).
[5] S.M. Nakhmanson and I. Naumov, Phys. Rev. Lett. **104**, 097601 (2010).
[6] T. Ohnishi et al., J. Appl. Phys. **103**, 103703 (2008).
[7] J.Z. Tischler et al., in Synchrotron Radiation Instrumentation: Eleventh U.S. National Conference, ed. P. Pianetta et al., p. 151 (2000); P.R. Willmott et al., Appl. Surf. Sci. **247**, 188 (2005); V. Vonk et al., J. Synch. Rad. **12**, 833 (2005).

This work is supported by the U.S. Department of Energy Office of Science under Contract DE-AC02-06CH11357.

THE APS BEAMLINE 1-ID UPGRADE: PHASE IIA

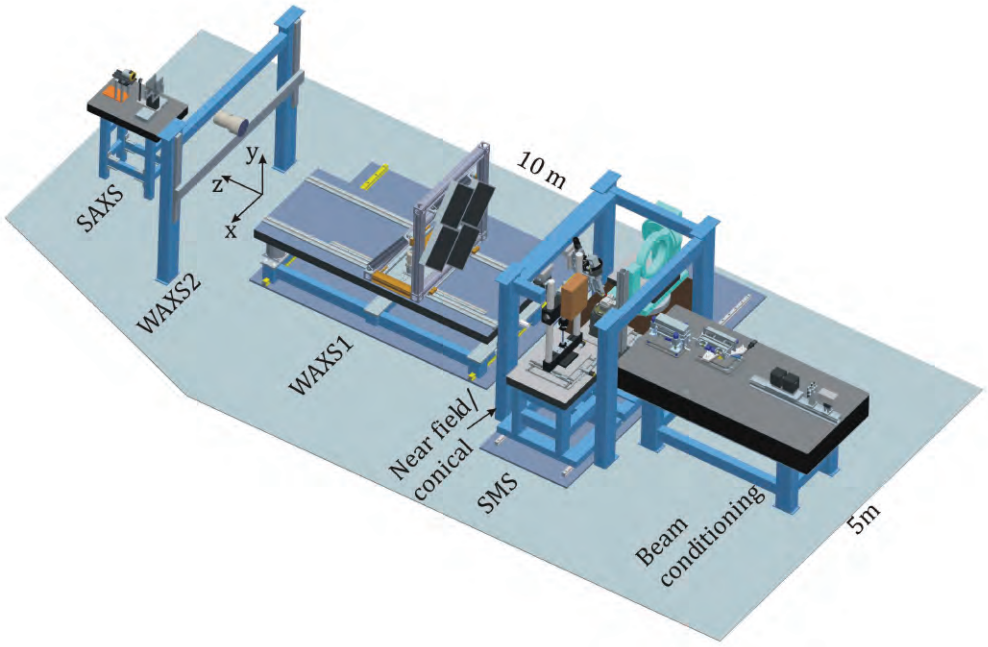

The major part of the beamline 1-ID upgrade involves construction and instrumentation of a new white-beam hutch, 1-ID-E. It provides a new suite of experimental techniques to enable non-destructive materials characterization under a variety of external stimuli, the most prominent being thermo-mechanical loading. This follows the 1-ID phase I upgrade, in which the beamline was dedicated to high-energy x-ray operations, and precedes planned APS Upgrade Project enhancements for the sector, including white-beam capability in 1-ID-E.

Construction of the 1-ID-E hutch was completed in May 2011 and first monochromatic beam taken in July 2011. User access is anticipated for late 2012. The hutch is located downstream of the monochromatic-beam 1-ID-C hutch, and has considerable volume ($4 \times 5 \times 10$ m^3) to accommodate the instrumentation described below. The downstream position of the hutch is 76 m from the insertion device (ID) straight section and allows for high demagnification of the source (and corresponding resolution) through planned optics.

The hutch instrumental layout is designed to combine flexible and unique sample environments with a variety of detection modes, and is shown in the illustration above. The upstream optical table will condition and characterize the incident undulator x-ray beam, which will be either monochromatic (50-130-keV, $1e^{-3} \leq dE/E \leq 1e^{-4}$) or white beam, using a series of slits, beam positioning monitors, and either monochromatic or white-beam focusing optics. Focused beams down to 0.5 μm are anticipated, with modest focal lengths (~1 m) to provide sufficient *q*-resolution for scattering experiments. Downstream of the table will be a series of sample-manipulation-systems (SMS), which can be interchanged through an *x*-translation. SMS-1 comprises a 3-axis Eulerian cradle to enable full sample orientation for scattering experiments.

Custom user environments will also be possible at this site. The centerpiece of SMS-2 is an Aerotech air-bearing stage, which will allow high-accuracy angular measurements. SMS-3 is a custom-built MTS servo-hydraulic device, which will include provisions (through partnership with external users) for in-grip rotation and measuring of radioactive samples. A support structure will be built around the SMSes to house a high-resolution "near-field" detector and conical slit, the former allowing for absorption/phase tomography and near-field orientation measurements, the latter providing ~100-μm longitudinal resolution and thus three-dimensional volume mapping capability. Further downstream will be an *x-z* translatable array of large-area detectors (WAXS1) configured to provide large angular coverage and with a center through-hole for simultaneous measurement of small-angle x-ray scattering (SAXS) at the end of the hutch. Just upstream of the fixed SAXS table, a detector (WAXS2) will be sited for very high *q*-resolution measurements, with large *x-y* translations (several meters) to provide sufficient *q*-coverage.

This upgrade will allow, for the first time, *in situ* studies combining near-field mapping (of grain and subgrain orientations, shapes, and sizes); diffraction (high-resolution phase and strain evaluation); tomography (micron-scale microstructure); and SAXS (nanoscale microstructure). Complementary probes will be available, including digital image correlation for macroscopic strain and sample positioning. Thermomechanical studies will reveal degradation mechanisms through measurement of the shapes, orientation, and strain states of individual grains within polycrystalline aggregates and correlated void/crack observations. In addition, the microfocusing capabilities will be utilized for high-pressure studies and non-destructive mapping of gradient (nano-) materials including fuel cells and batteries. Such high-fidelity, non-destructive measurements — in the bulk and at grain and subgrain length scales — will offer powerful new views of materials evolution, and allow development of new models capable of predicting material response to complex stimuli.

As is the case for the current 1-ID-C hutch, demand from a wide range of disciplines is anticipated, including materials science, physics, and a variety of engineering disciplines (mechanical, nuclear, chemical, and biomechanical).

Correspondence:
J. Almer, almer@aps.anl.gov; and A. Mashayekhi, mashayek@aps.anl.gov (both XSD-MPE); U. Lienert (DESY), ulienert@ameritech.net; and E. Benda (AES-MED), benda@aps.anl.gov

This work is supported by the U. S. Department of Energy Office of Science under Contract No. DE-AC02-06CH11357.

NEW CANTED IDS AT THE APS

Synchrotron x-ray beamlines and beam time seem to always be at a premium. Time-based solutions (schedule more user-beam hours) or space-based solutions (expand the facility) are often impractical, if not impossible, so ingenuity has become a necessity.

The canted undulator (CU) storage ring straight section configuration creates two insertion device (ID) beams per sector where there had been one by adding a second ID to the lattice, thus doubling the capacity of that beamline. A chicane is created with a trio of dipole magnets, with an undulator in each leg (Fig. 1). This creates an angular separation between the x-ray beams that can be exploited downstream to create two independent beamlines from a single straight section. The CU system consists of two slightly shortened undulators, a special ID vacuum chamber, the dipoles, a corrector magnet for the chicane, and a specialized front end (FE) [1].

At the APS, canted IDs have been in operation at sectors 4 and 12 (managed by XSD), Sector 21 (LS-CAT), Sector 23 (GM/CA-CAT), and Sector 24 (NE-CAT). These are now joined by new canted configurations at Sector 16 (HP-CAT) and Sector 34 (also managed by XSD). Next up for canted IDs will be GSECARS at Sector 13.

16-ID-B & 16-ID-D

Funding for the HP-CAT canted FE (like the other two new front ends) was provided by monies the APS received from the American Recovery and Reinvestment Act (ARRA) of 2009. The canted FE allows two stations (16-ID-B and 16-ID-D) to be run simultaneously and independently (rather than parasitically). The 16-ID-B beamline is dedicated to high-pressure micro-x-ray diffraction, while the 16-ID-D beamline is dedicated to x-ray scattering and spectroscopy research of materials under high pressure. Installation of the canted front end was carried out in September 2011 and HP-CAT plans to accept general users on the new independent beamlines in FY2012.

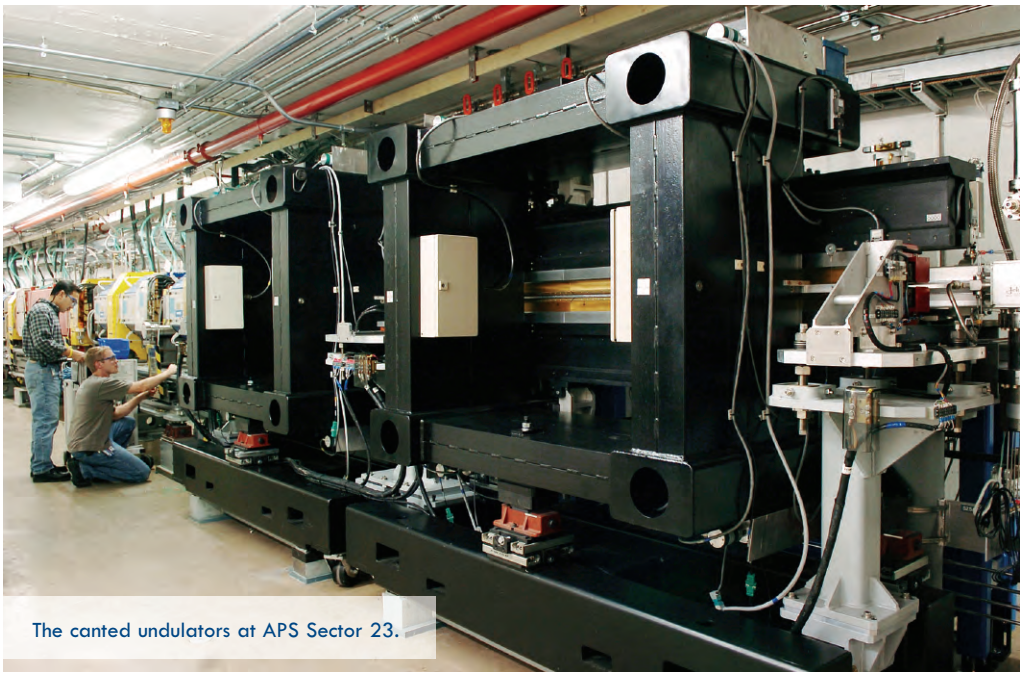

The canted undulators at APS Sector 23.

34-ID-C & 34-ID-E

The canted FE for Sector 34 was also supported by ARRA funding. It will allow two stations (34-ID-C and 34-ID-E) to be run simultaneously and independently (rather than in an either/or mode, or occasionally in a parasitic mode). The 34-ID-C beamline is dedicated to coherent x-ray scattering techniques. 34-ID-E is dedicated for Laue microdiffraction techniques utilized to examine the structure of materials with sub-micron spatial resolution in all three dimensions. Installation of the canted FE occurred during the May 2011 maintenance period and the two new independent beamlines are accepting general users.

13-ID-C, 13-ID-D, & 13-ID-E

GSECARS operates the third sector at the APS to receive ARRA funding support for its canted undulator upgrade. This upgrade will allow two stations (13-ID-C or D and 13-ID-E) to be run simultaneously and independently in FY2012. The x-ray microprobe will run in 13-ID-E with a new ID (U36). The second new ID (U30) will supply interface diffraction and spectroscopy in 13-ID-C or high-pressure studies in 13-ID-D. Installation of the vacuum chamber and the U30 undulator was carried out during the scheduled maintenance period in December 2011; the FE and U36 undulator will be installed during the April-May 2012 shutdown. Associated beamline upgrades are being supported by the U.S. Department of Energy, the National Science Foundation, and NASA.

REFERENCE

[1] P.K. Den Hartog et al., Proceedings of the 2003 Particle Accelerator Conference (2003, IEEE), pg. 833.

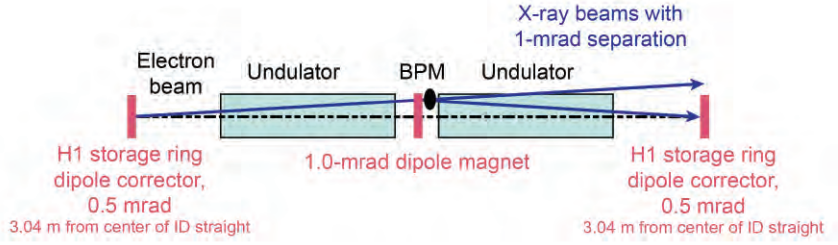

Fig. 1. Schematic layout of a CU straight section showing the angular separation of the x-ray beams produced by the three dipoles.

SAXS and Surface Scattering at 12-ID

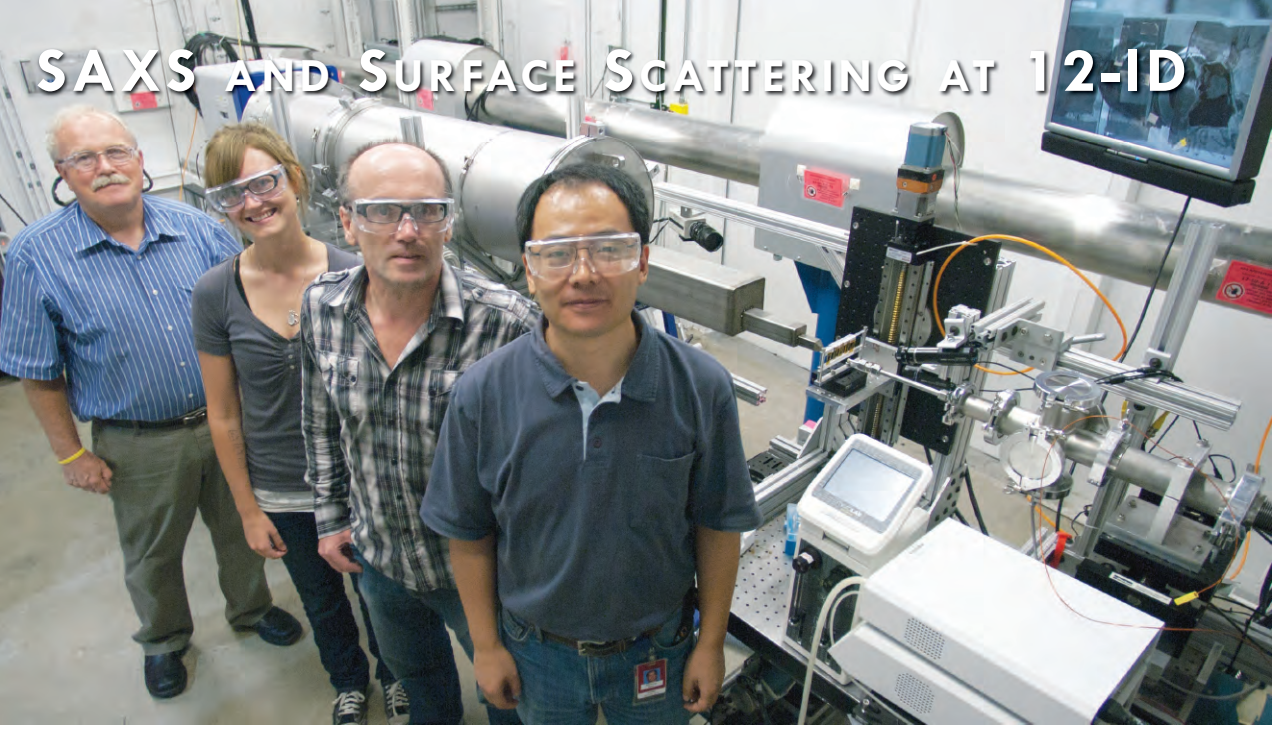

In the 12-ID-B enclosure with the new SAXS instrument. Left to right: Randy Winans, Janae DeBartolo, Soenke Seifert, and Xiobing Zuo (all XSD-CMS). Not pictured: Byeongdu Lee.

For the last eight years, the demand for small-angle x-ray scattering (SAXS) beam time by users of XSD Sector 12-ID at the APS exceeded the available time by a factor of two. The existing SAXS facility steadily grew to represent 50% of 12-ID usage. With the instrument configuration oversubscribed, the only way to support the growth of the SAXS community was to provide simultaneous operation of two 12-ID experiment stations by adding canted undulators and new beamline optics. This provides the APS with a dedicated SAXS beamline to better serve the general user community in a number of areas in materials science, chemistry, and biology. At least half of current 12-ID users are doing bioSAXS.

The increasing demand for SAXS beam time is driven by research into the structure and dynamics of nanoscale materials (for which SAXS is an extremely valuable probe), and increased interest in soft matter and usage of the 12-ID SAXS facility for time-dependent structural investigations. General-user experiments have included these areas, as well as extensive use of the 12-ID SAXS instrumentation for biological research. The more than 400 users who have done experiments on the XSD Chemical and Materials Science (CMS) Group's SAXS instrument come from U.S. and foreign universities, national laboratories and government institutions, and industrial research laboratories.

Increased interest in time-dependent SAXS experiments led the CMS Group to add a pink-light mirror system to 12-ID. Installed in late FY2005, it enhanced the flux-on-sample by over three orders of magnitude, providing new time-resolved opportunities for small-angle scattering experiments. With the development of dedicated instrumentation for anomalous grazing-incidence small-angle x-ray scattering, the beamline serves as an important complement to the infrastructure for the Argonne Center for Nanoscale Materials and increases the demand for this beamline, enabling XSD to pursue options such as high-throughput SAXS, to be used for combinatorial materials studies.

Two installed undulators (a U30S and U33S) have been canted. In the future the U33S will be replaced with a U27 undulator, which is optimized for the energy range on the 12-ID-B beamline. One of the resulting undulator beamlines uses a more stable version of the current monochromator with an energy range of 4.5 to 35 keV and a mirror system that includes the existing pink-beam mirror. This beam will feed 12-ID-C/D and be used for anomalous, time resolved, grazing incidence SAXS in the C hutch, and surface scattering and metal organic chemical vapor deposition studies in the D hutch. The experiments in the C hutch will use a new mosaic large-area charge-coupled device detector built by XSD.

The second undulator feeds 12-ID-B as a dedicated SAXS station using a large offset monochromator (870 mm). This monochromator uses a cryo-cooled silicon [220] first crystal to provide an energy range of 7.4–13.9 keV. A Pilatus 2M large-area detector will be used in conjunction with a large vacuum-scattering chamber where the position of the detector can be changed automatically to access different Q ranges, and a wide-angle Pilatus 300K detector will be attached permanently to the front of the chamber. A two-dimensional detector with high linearity, dynamic range, stability, and low or no dark current is crucial for SAXS. The Pilatus detector has overwhelming capability in these respects, with a 20-bit dynamic range and no dark current. These detectors make 12-ID-B a very versatile SAXS beamline.

Correspondence:

Randy Winans, rewinans@anl.gov

This work is supported by the U. S. Department of Energy Office of Science under Contract No. DE-AC02-06CH11357.

Progress on the IEX-CDT 29-ID-A Beamline

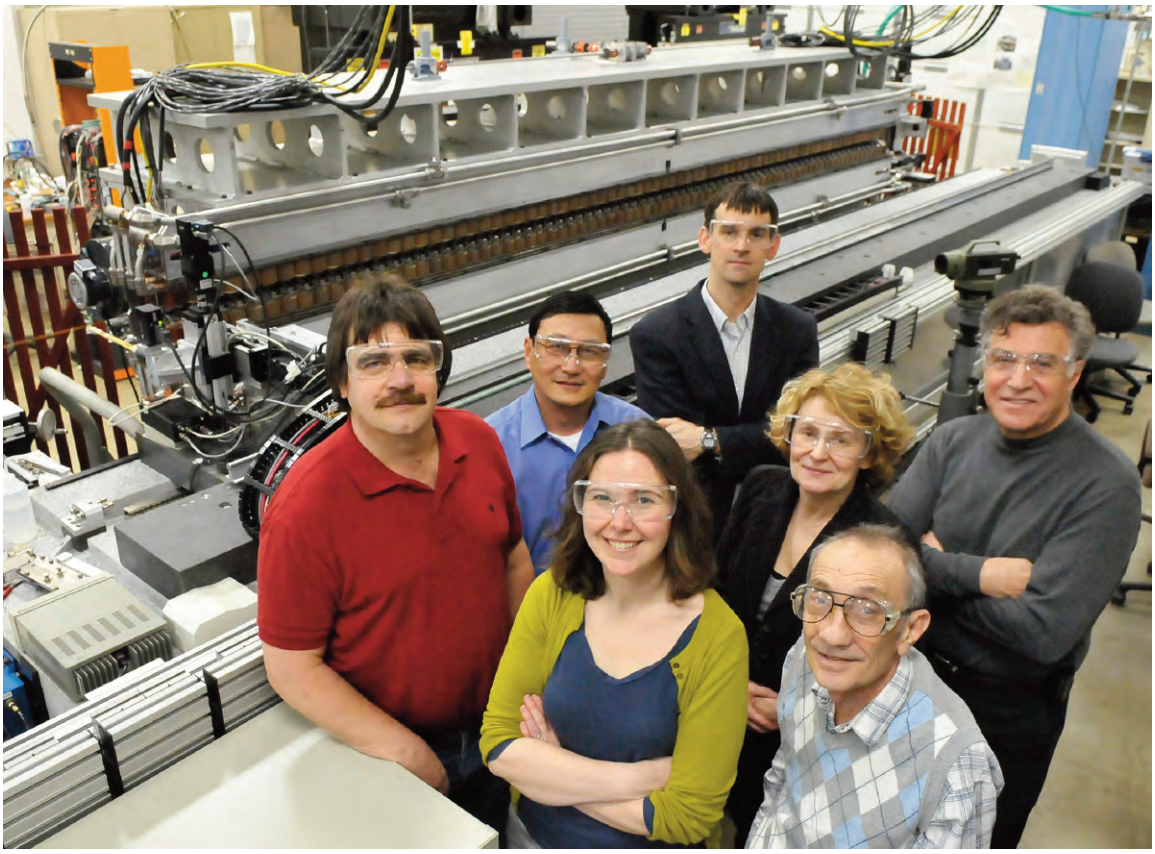

Some of the people who worked on the IEX-CDT and the EM-VPU (which is behind the group) in the APS Magnet Measurement Facility. Left to right: Mark Jaski (ASD-MD), Joe Xu (AES-CTL), Jessica McChesney (XSD-MM), Peter Abbamonte (UIUC), Christa Benson (AES-MD), Isaac Vasserman (ASD-MD), and Boris Deriy (ASD-PS).

The Intermediate Energy X-ray Collaborative Development Team (IEX-CDT) is constructing a new insertion device beamline at APS Sector 29. This facility will address one of the core challenges in condensed matter physics: understanding the fundamental mechanisms driving collective electronic behavior in materials. The IEX-CDT is a close collaboration between the APS and principal investigators from the University of Illinois at Chicago and the University of Illinois at Urbana-Champaign (UIUC), and represents a strong commitment from both the Department of Energy and the U.S. National Science Foundation to build the first beamline of its kind in North America.

The beamline will utilize intermediate-energy x-rays (250 ev to 2500 eV) with high resolution, high flux, and small spot size to support investigations of correlated electron physics with two complementary techniques: angle-resolved photoemission spectroscopy and resonant soft x-ray scattering.

This premier facility (diagram below) begins with a state-of-the-art insertion device, the electromagnetic variable polarizing undulator (EM-VPU), which is being developed by ASD. The EM-VPU will allow users to optimize the beam profile by selection of polarization (horizontal, vertical, or circular) and higher-order harmonic suppression via the ability to run in quasiperiodic mode. Following the development and testing of two prototypes, the final 4.8-m device has been assembled and at the time of writing is undergoing magnetic field characterization. Installation is slated for the May 2012 shutdown.

The front end, which connects the storage ring to the beamline proper, has been installed and the first optical enclosure has been constructed. Phase-1 installation, which includes all white/pink beam components, will begin after the EM-VPU has been installed in the storage ring, followed by commissioning and full characterization of the undulator in summer 2012.

The beamline design and controls, which are the result of a close collaboration between IEX-CDT and various groups in AES, are nearing completion. Phase-2 installation, which includes the end stations, a variable line spacing plane grating monochromator, and refocusing optics will follow.

Commissioning of the entire beamline is planned for spring 2013. Upon completion, the IEX beamline will become part of the Magnetic Materials Group in XSD.

Correspondence: Jessica McChesney, jmcchesn@aps.anl.gov

This work supported in part by the University of Illinois at Chicago and UIUC through a grant via National Science Foundation Award DMR-0703406, and by the U.S. Department of Energy Office of Science.

SOLVING A "ROGUE MICROWAVE" PROBLEM IMPACTING APS BPMS

Bob Lill with one of the vacuum chamber snubbers.

Fig. 1. Installation geometry for mode-suppressing snubbers.

One feature of the APS storage ring vacuum system is the presence of transverse-electric (TE) microwave modes in the large-aperture chambers comprising the arc sections between insertion device (ID) straight sections. These modes were known as far back as 25 years ago, to a time before the original conceptual design of the APS facility [1]. At that time, the primary consideration was the impact of chamber resonances on the ring's impedance impacting such things as coupled-bunch instabilities. Because the modes are transverse, to lowest order they do not couple to the particle beam and indeed do not affect beam stability directly.

Fast-forward 12 years to 1998 in the early days of APS operation, when what can only be termed as bizarre behavior was observed impacting only the vertical readbacks of large numbers of radio-frequency (rf) beam position monitors (BPMs). In one case, approximately five minutes after injecting to 102 mA, a pair of beam position monitors in Sector 5 would make a step change in their vertical readbacks with amplitude in the range from 100 μm to 150 μm. Additionally, a majority of the vertical BPMs exhibited large amounts of variable intensity dependence as the beam current decayed between injections, which was particularly important in the days before top-up operation. One other interesting observation was that the problems generally occurred in pairs: adjacent BPM channels attached to the same vacuum chamber section would misbehave simultaneously.

After extensive investigation, the microwave modes first described in 1986 were "re-discovered" in 1998 using a network analyzer attached to BPM pickup electrodes in Sector 5 [2]. Because the electric field associated with these modes is oriented vertically, only vertical position monitor readings were impacted. In a stroke of (particularly bad) luck, it was found that the 80 curved vacuum chambers almost always had one of the modes at a frequency matching the 352-MHz processing frequency of the rf BPM system. At that time, a number of solutions were proposed, and a few tested with limited success. However, it became clear that the only means to solve the problem would involve venting the chambers and making modifications to the internal chamber geometry.

Fortunately, the modes did not affect the small-aperture ID vacuum chambers, so the machine could be operated with stable x-rays by ignoring the large-chamber BPMs. Furthermore, bending the magnet photon BPMs provided stable operation for bending magnet beamline experiments. Nevertheless, a significant fraction of the orbit correction hardware was crippled by these modes.

Having lived with this state of affairs for over a decade, Robert Lill, an rf engineer in the ASD Diagnostics Group, in 2009 took the initiative to solve the problem once and for all. His solution was simple but ingenious: insertion of a series of spring-like "snubbers" into the antechamber portion of the chambers [3]. These springs are commonly used to suppress electromagnetic interference from sensitive electronics and in effect shorted out the modes by connecting the top to the bottom of the chamber. In many cases, the spacing between chambers is only some 10s of centimeters, but because the snubbers are mounted between short steel strips, they can be inserted relatively easily from the chamber ends. Figure 1 shows two snubbers with the associated steel strips, indicating the method of installation.

This solution was tested for the first time in Sector 29, where modifications were made to all five of the large-aperture storage ring vacuum chambers. Shown in Fig. 2 are the results of measurements on one of the chambers made with a network analyzer indicating the elimination of modes with frequencies below about 460 MHz. Transmission from an electronic E-probe to a BPM capacitive pickup electrode is shown on a logarithmic scale. The E-probe was inserted at the chamber end nearest to the button pickup. As of January 2012, three sectors have been upgraded using this method (3, 4, and 29), with additional sectors being modified during each machine shutdown period.

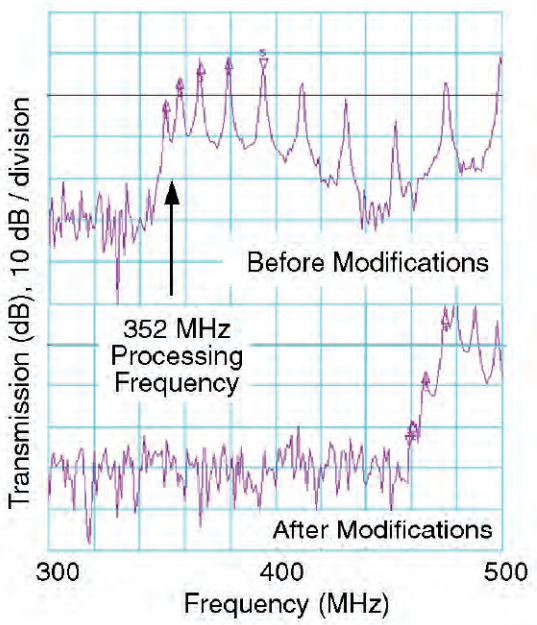

Fig. 2. Data indicating the effect of the suppressors on the chamber mode structure.

Correspondence:
G. Decker, decker@aps.anl.gov; R. Lill, blill@aps.anl.gov; and X. Sun, xiang@aps.anl.gov (all ASD-DIA); and John Hoyt (AES-MOM), hoytman@aps.anl.gov

REFERENCES

[1] R. Kustom and J. Cook, "Electromagnetic Properties of the Vacuum Chamber," Light Source Note LS-56 (1986). http://www.aps.anl.gov/Science/Publications/lsnotes/content/files/aps_1417624.pdf

[2] Y. Kang, G. Decker, and J. Song, "Damping Spurious Harmonic Resonances in the APS Storage Ring Beam Chamber," PAC99, New York (1999). http://accelconf.web.cern.ch/AccelConf/p99/PAPERS/THP61.PDF

[3] R. Lill, G. Decker, J. Hoyt, and X. Sun, "Measurement, Simulation, and Suppression of APS Storage Ring Vacuum Chamber TE Modes Impacting Vertical BPM Readings," BIW10, (2010). http://accelconf.web.cern.ch/AccelConf/BIW2010/papers/tupsm049.pdf

ON-DEMAND, HIGH-PERFORMANCE COMPUTING

Researchers at APS sectors 1, 2, 8, 32, and 34 are able to utilize an on-demand, high-performance computing (HPC) cluster for carrying out near-real-time experiment computation. In a typical HPC system, the goal is to keep the cluster's processors as busy as possible, so jobs typically reside in a queue, sometimes for hours or days, waiting for the resources they need in order to run. In the case of the APS HPC system, the goal is to provide an on-demand computing resource that is available when the scientist needs it, with little or no waiting. This is accomplished by dedicating cluster compute nodes to specific research teams. While experiments are running, the nodes may be idle for part of the time, but a user-submited job runs immediately, hence the term "on demand." When APS beamline scientists aren't running experiments, they are often reprocessing data for previous users.

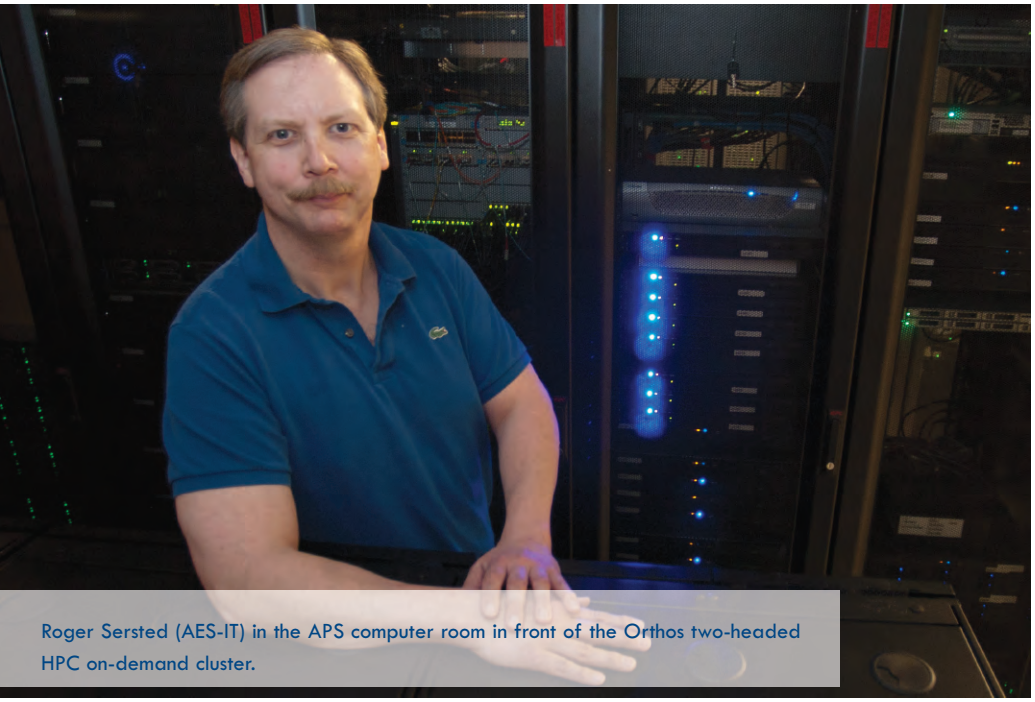

Roger Sersted (AES-IT) in the APS computer room in front of the Orthos two-headed HPC on-demand cluster.

The HPC system, which is managed by the AES Information Technology Group, runs applications written by the AES Software Services Group (SSG) in collaboration with XSD beamline scientists.

The combination of dedicated hardware plus custom software results in more efficient use of beam time by scientists and helps to increase sample throughput. The HPC system also provides a high-speed data-transfer capability using the "gridFTP" application, which empowers users to transfer large numbers of files using multiple parallel data streams, allowing significant amounts of data to be moved from one system to another much faster than with conventional file copy techniques. gridFTP is part of the Globus Toolkit that was developed by Argonne's Mathematics and Computer Science (MCS) Division. MCS has been very supportive of APS efforts; their technical assistance has been invaluable.

The APS HPC system provides a core infrastructure of Infiniband (a high-speed, low-latency network) and distributed file storage using the Lustre file system. In a small cluster (fewer than 200 nodes), the high-speed network and shared storage are disproportionately expensive in comparison to the cost of the compute nodes. At the APS, users have the option to run on standard compute nodes provided by AES, or they can purchase their own components. Sector 34, for example, purchased their own compute nodes, while Sector 8 uses standard nodes. Sector 1 is working with an external collaborator to purchase nodes tailored to the types of jobs they will be running. The Accelerator Systems Division required an on-demand computing resource for performing accelerator tuning on machine studies days. They purchased nodes with specifications that would satisfy their needs.

Graphics processor unit (GPU) computing is a strong area of interest in the data processing community as well as at the APS, and GPU processing capabilities are being added to the APS HPC environment. GPU computing uses the "many-core" design of video cards (448 cores in APS systems). Two GPU-based nodes were added to the APS HPC system, each of which has two GPUs, allowing users to run parallel GPU jobs or to perform visualization on one GPU and data analysis on the other.

The APS HPC environment supports the popular MPI (Message Passing Interface) protocol (developed by the MCS Division) for parallel jobs. When an SSG developer wanted to use the Hadoop framework for performing analysis, it was installed on a dedicated set of nodes. Hadoop is a software system that performs distributed processing and storage, using local storage on the compute node, rather than using the Lustre shared storage system. This flexibility is possible because the nodes are dedicated to a specific user.

The APS HPC system was designed and implemented to be a valuable asset to the APS research community. It provides the ability to perform near-real-time calculations during an experiment, as well as allowing physicists to reprocess data sets that end-users might not be able to handle at their home institutions. The use of dedicated computing resources provides the flexibility of radically different technologies for solving data analysis and visualization challenges at the APS. The combination of MPI, shared storage, Hadoop, and GPU computing technologies is something that few other HPC environments support.

Correspondence:

Roger Sersted, rs1@aps.anl.gov

Sustainability through Collaboration: An APS/Argonne Energy Success Story

Improving energy efficiency is a key element in achieving our national goals for energy independence. Believe it or not, buildings, from houses to skyscrapers and even research labs constitute a major energy consumer in the United States, accounting for over 42% of the total national energy consumption, according to the U.S. Energy Information Agency. So increasing the energy efficiency of buildings is a prime candidate for efficiency initiatives.

The U.S. Department of Energy recognizes the need to address the management of building energy usage, and the U.S. government has, through various legislation and executive orders, set specific goals for improvement in building energy efficiency. Argonne has been at the forefront of this building technology research, aggressively pursuing application of these stringent standards to its existing buildings and in the construction of its new facilities.

The APS is the largest electrical energy consumer at Argonne, thanks to the accelerator and light source technical components, and the number of large facility buildings. The APS is collaborating with the Laboratory's other research divisions and the Argonne Facilities Management and Services (FMS) Group to upgrade the energy efficiency of the APS facilities and make available its buildings as test beds for new and emerging technology currently under investigation at Argonne.

This collaboration has resulted in the first phase of implementing major heat recovery technology to reduce the APS overall energy consumption. This is being accomplished through an aggressive energy reclamation process and ongoing planning for its application Argonne-site wide.

The use of techniques and system designs developed as prototype installations at APS have been employed as working installations in the APS lab office modules (LOMs) around the perimeter of the experiment hall, the experiment hall itself, and the Argonne Center for Nanoscale Materials. Many have also been incorporated in the design of the new Advanced Protein Crystallization Facility being built adjacent to the experiment hall, and the Energy Science Building under construction elsewhere on the Argonne site. These early efforts have so far resulted in yearly savings of more than 10 GWh of energy, 6,000 mT of CO_2, and $600,000 in energy costs.

Marvin Kirshenbaum (left, AES-SO) and Robert Brachle (ANL-FMS) with one of the new LED fixtures being installed in the APS computer room. The LEDs help control heat levels in this room in addition to reducing energy consumption.

The latest achievement in this ongoing effort has been the qualification of LOM 438 to meet the DOE standards for high-performance and sustainability buildings (HPSB). In 2011, LOM 438 became one of the first existing DOE facilities, nationally, to meet these requirements. The LOM 438 upgrade included:

- Replacing existing T-12 florescent lighting with light-emitting diode (LED) fixtures along with 77 occupancy sensors to automatically turn lights off when a room is unoccupied. This provided a 60% reduction in lighting energy consumption, saving 77,107 kWh per year. At the same time, the new lighting system improved work surface light intensity from 40 to 50 ft-c while yielding superior color rendering, improving visual acuity and depth perception in the work environment. LOM 438 is the first DOE facility to have full interior LED lighting.
- Replacing restroom fixtures using high-efficiency sinks and urinals with motion activated fixtures.
- Utilization of waste heat generated from the APS process cooling water system used to cool storage ring magnets and power supplies. This low-grade (80º F) waste heat is used in the winter to pre-heat LOM 438 outdoor ventilation air, saving an estimated 125 million Btu (43 MWh-equivalent) of energy per year.

Plans call for these same upgrades to be implemented in the other seven LOMs.

A post-implementation energy audit determined that the lighting upgrade and the installation of occupancy sensors, combined with heat recovery from the APS technical componnts, have reduced the LOM 438 total energy costs by 23.8%, meeting the minimum HPSB goal of a 20% energy cost savings.

Correspondence: M. Kirshenbaum, kirshen@aps.anl.gov

Gluskin of ASD Elected to AAAS Fellowship

Argonne physicist **Efim Gluskin** was elected a Fellow of the American Association for the Advancement of Science (AAAS). Each year, the AAAS elects members whose "efforts on behalf of the advancement of science or its applications are scientifically or socially distinguished." Gluskin is currently the Magnetic Devices Group Leader in ASD, and is an Argonne Distinguished Fellow, His election to AAAS fellowship underscores his role as one of a handful of scientists who were instrumental in "the development of ultra-bright x-ray sources utilized at third generation synchrotron sources and x-ray lasers, used by thousands of scientists from around the world," as noted by the AAAS in announcing Gluskin's election. The honor also recognizes his later work in the evolution of the first x-ray free-electron laser, the Linac Cohrent Light Source at the SLAC National Accelerator Laboratory.

Jacobsen of XSD Elected to APS Fellowship

"Seminal contributions to x-ray microscopy" earned **Chris Jacobsen** election to Fellowship in the American Physical Society (APS). Jacobsen is the Associate Division Director for Imaging and Microscopy in XSD, and a Professor in Physics & Astronomy at Northwestern University. He was nominated for Fellowship by the APS Topical Group on Instrument and Measurement Science. Jacobsen has been awarded a Presidential Faculty Fellow Award by the White House/National Science Foundation in 1992-1997; the 1996 International Dennis Gabor Award from Hungary; and the Kurt Heinrich Award as an outstanding young scientist, from the Microbeam Analysis Society, in 2001. He is a Fellow of the Optical Society of America, the American Association for the Advancement of Science, and now the American Physical Society.

Linda Young of XSD Elected Vice Chair of DAMOP

Argonne Distinguished Fellow and XSD Director **Linda Young** was elected vice chair of the Division of Atomic, Molecular, and Optical Physics of the American Physical Society (DAMOP). The position became official at the 2011 DAMOP Meeting held at Atlanta, Georgia, on June 13-17, 2011. The four-year-term position starts with vice chair and progresses to chair elect, chair, and then past chair. Among Young's recent scientific accomplishments, the atomic, molecular, and optical research carried out by her research group at Argonne has been featured in the Presidential Budget request as a "Selected Accomplishment" two years in a row. The most recent work explored the femtosecond electronic response of simple atoms to ultrashort, high-intensity x-ray pulses from the world's first x-ray free-electron laser, the Linac Coherent Light Source at the SLAC National Accelerator Laboratory [Nature **466**, 56 (2010)]. The previous year's work demonstrated how light, through the phenomenon of electromagnetically induced transparency, can control x-ray absorption [Nat. Phys. **6**, 69 (2010)].

Assoufid of XSD Elected a Fellow of SPIE

Lahsen Assoufid was been elected a Fellow of SPIE, the international society for optics and photonics. He is Section Leader for Mirror Multilayer and Metrology in the XSD Optics and Detectors Group. He was acknowledged for his "achievements in metrology and x-ray optics. A leader in the field of x-ray optics and metrology, Assoufid has made significant technical contributions to several aspects of synchrotron x-ray optics, including the design, optical metrology, and in-beam characterization of focusing profiled Kirkpatrick-Baez (K-B) mirrors. Especially notable is his development of at-wavelength metrology using coherent diffraction and phase retrieval techniques for characterizing astigmatism/misalignment, focal spot size, and surface aberrations of K-B nanofocusing mirrors." He founded and served as Chair for the SPIE conference in Advances in Metrology for X-ray and EUV Optics, and served in the leadership of the Chicago Chapter of SPIE during 2004-7, contributing to optics and educational outreach activities in the Chicago area. He is a member of the American Physical Society and a Fellow of the Opical Society of America.

Groundbreaking for a $34.5M MX Research Facility

Argonne broke ground on August 30, 2011, for a $34.5 million Advanced Protein Crystallization Facility (APCF) that will enable scientists from around the world to produce, purify, and characterize a wide range of proteins more rapidly and play a critical role in the development of important medical therapeutics. The State of Illinois will provide funding for the design and construction of the APCF, which is slated to open in 2014. The APCF will be located next to the APS. The 50,000 sq-ft state-of-the-art structural genomics facility will complement the U.S Department of Energy's Structural Biology Center (SBC), also located at the APS. The SBC is a scientific user facility that hosts hundreds of researchers for x-ray protein crystallography (MX) studies. The APCF will provide those visiting researchers with modern laboratory space for sample preparation prior to using the SBC beamlines to collect data.

An artist's conception of the APCF is shown above. Right: The traditional shovel ceremony. Left to right: State Representative **Jim Durkin** (R-Ill.), 82nd District; **Joanna Livengood**, U.S. Department of Energy Argonne Site Office manager; Argonne Director **Eric Isaacs**; Ill. Congresswoman **Judy Biggert** (R-13th); **John Kamis**, Senior Advisor to the Governor, State of Illinois, Office of Governor Pat Quinn; and **Wayne Anderson**, Professor at Northwestern University and Director of the Center for Structural Genomics of Infectious Diseases.

Keith Moffat of APS, BioCARS, and U. of C. Receives 2011 Patterson Award from ACA

Keith Moffat, Principal Investigator for the BioCARS research facility at the APS, from 2002-2010 the Deputy Provost for Research at the University of Chicago, and recently appointed as Senior Advisor for Life Sciences at the APS was selected as the recipient of the 2011 Patterson Award from the American Crystallographic Association (ACA). Moffat, who is also the Louis Block Professor in Biochemistry & Molecular Biology and a founding member of the Institute for Biophysical Dynamics at the University, is recognized for his work in pioneering ultrafast time resolved x-ray diffraction using synchrotron radiation to capture the function of fundamental protein processes at atomic resolution. The Patterson Award was established in 1980 in honor of A. Lindo Patterson to recognize and encourage outstanding research in the structure of matter by diffraction methods, including significant contributions to the methodology of structure determination and/or innovative application of diffraction methods and/or elucidation of biological, chemical, geological, or physical phenomena using new structural information.

2011 APSUO Arthur H. Compton Award to Stern, Lytle, Sayers, and Rehr

The 2011 Compton Award winners. Clockwise from top left: Farrel Lytle, John Rehr, Edward Stern, and Dale Sayers.

The APS and the APS Users Organization (APSUO) awarded the 2011 Arthur H. Compton Award jointly to **Edward Stern**, **Farrel Lytle**, **Dale Sayers** (posthumously), and **John Rehr** for their development of the technique of x-ray absorption fine structure spectroscopy (XAFS), whereby information can be acquired on local structure and on unoccupied electronic states in non-crystalline materials. These outstanding scientists have defined how XAFS is understood, enabling its application to an extremely wide range of problems across all disciplines of the physical, chemical, and biological sciences. The award was presented at the 2011 APS/Center for Nanoscale Materials/Electron Microscopy Center Users Meeting.

As a result of work by Stern, Lytle, Sayers, and Rehr, researchers at universities, national laboratories, and industry using the APS can take XAFS and use it to solve and understand complex problems in materials research. Stern, together with Lytle and Sayers, developed the modern theory of XAFS in 1970. This theory describes XAFS as due to the scattering of the photoelectron ejected from an atom when it absorbs an x-ray. By Fourier-transforming the XAFS oscillations, Stern, Lytle, and Sayers showed that the phenomenon was sensitive to the local atomic structure around the absorbing atom and how XAFS can be used to retrieve quantitative information on interatomic distances and coordination around selected absorbing atoms. This established XAFS as a premier tool for probing short-range atomic order in solids and liquids alike.

With the modern form of the XAFS equation in hand, Stern, Lytle, and Sayers, together with generations of students, proceeded to develop the basic experimental and analysis procedures for XAFS data collection and interpretation, many of which are still used today. As a result, XAFS has emerged as a powerful technique on a par with the more established diffraction probes. Their careful experiments, first using laboratory x-rays and later at synchrotrons laid the groundwork for virtually all subsequent measurements. They showed an entire generation how to collect accurate data and helped to set the direction for all major experimental advances in the technique.

Rehr significantly extended the initial XAFS theories, and together with Robert Albers of Los Alamos National Laboratory, developed techniques for quantitative calculations. Perhaps most importantly, Rehr and his group developed a suite of programs that made *ab initio* calculations of XAFS spectra a practical reality. Rehr's FEFF program (named after feff, the effective curved wave scattering amplitude in the modern XAFS equation) revolutionized the practice of XAFS. It is now possible to obtain very accurate calculations of the expected XAFS for a completely unknown structure, and thus to analyze experimental measurements in terms of the structure and other properties of a material.

The ability to quantitatively interpret XAFS measurements has profoundly impacted a huge range of scientific disciplines, and consequently XAFS and related spectroscopies are among the more commonly used synchrotron tools, with large and diverse user communities at most synchrotron sources, including the APS. In addition, the theoretical understanding of XAFS as a scattering phenomenon influenced the development of other modern synchrotron-based techniques such as x-ray photoelectron diffraction from surfaces, bulk x-ray holography, resonant x-ray scattering and inelastic x-ray scattering, as well as electron-based techniques such as electron energy loss spectroscopy.

The Arthur H. Compton award was established in 1995 by the APSUO to recognize an important scientific or technical accomplishment at the U.S. Department of Energy's Advanced Photon Source. *Correspondence: Susan Strasser, strasser@aps.anl.gov*

Chapman of XSD Wins Oxford Cryosystems Poster Prize

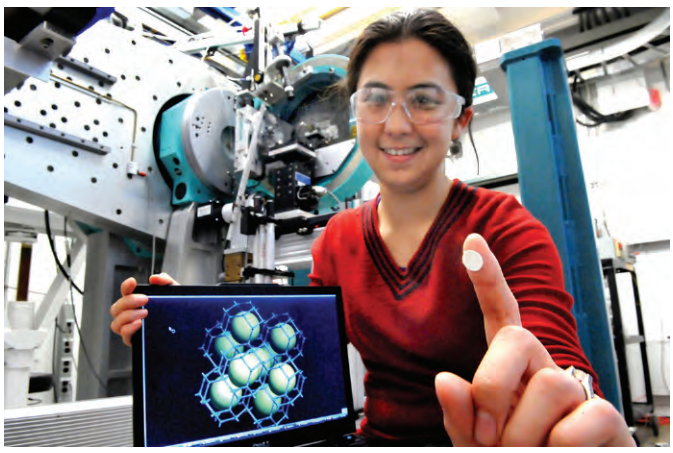

Karena Chapman (ANL-XSD) won the 2011 Oxford Cryosystems Poster Prize for "11-ID-B, a Dedicated Instrument for X-ray Pair Distribution Function Measurements." Oxford Cryosystems gives this cash prize to the best poster describing work in low-temperature crystallography. Chapman's poster reported her work with Kevin Beyer and Peter Chupas (also XSD) to optimize the instrument at APS. They improved data quality, reduced data collection times, and facilitated a whole range of sample environments for *in situ* studies under non-ambient conditions. Now studies varying temperature, pressure, and chemical environment are routine, and users collect hundreds or even thousands of individual pair-distribution functions per day.

DMLS 2011: 4th International Workshop on Diamonds for Modern Light Sources • May 5-6 • The fourth in a series of workshops devoted to the use of diamonds at synchrotrons and free-electron lasers (FELs) was held at the APS. The scope was to assess the status, size, quality, and availability of synthetic type-IIa diamonds; the status of chemical vapor deposition (CVD) diamonds; applications for beamline optics; applications for beam position monitors and detectors; applications at FELs; and novel applications, such as for an x-ray free electron laser oscillator (XFELO). Highlights of the workshop included: reports of supplier facilities for thinning and polishing; reports on tests of supplier-provided bonds to CVD cooling manifolds; a report of more than 99% reflectivity from diamond for hard x-rays, significant for XFELO feasibility, measured at the APS; a report on thermal expansion measurements at low temperatures made at the APS (no negative thermal expansion, thermal expansion below 1e-9); a report from Brookhaven National Laboratory on substantial progress in diamond beam flux monitors, and fast detectors; and a presentation on plans for a self-seeding at the Linac Coherent Light Source with diamond crystals. *Contact: atm@aps.anl.gov*

Argonne Strategic Initiatives Collaboration Workshop: Opportunities in Electrical Energy Storage • April 4 • "Electrical Energy Storage" is one of Argonne's Major Initiatives. Research and development related to electrical energy storage has been occurring in many corners of the Laboratory, particularly in areas defined by the other three Major Initiatives: "Materials for Energy" (formerly M2D2), "Leadership Computing," and "Hard X-ray Sciences." Underpinning this workshop was a desire to establish stronger connections among various groups in the Laboratory in order to shape and execute a larger Argonne vision for electrical energy storage research. The goal was to coalesce the four major initiatives around electrical energy storage in order to sharpen Argonne's competitive edge and better position the Laboratory for capturing large funding opportunities. The workshop featured talks from representatives of the four major initiatives. Areas of interest included current problems with existing Li-ion materials, advanced materials for the next generation of Li-ion technology, and electrochemical energy systems beyond Li-ion.

National School on Neutron and X-ray Scattering • June 11-June 25 • The National School on Neutron and X-ray Scattering educates graduate students on the utilization of major neutron and x-ray facilities. Lectures presented by researchers from academia, industry, and national laboratories include basic tutorials on the principles of scattering theory and the characteristics of the sources, as well as seminars on the application of scattering methods to a variety of scientific subjects. Students conduct short experiments at Argonne's APS and Oak Ridge National Laboratory's Spallation Neutron Source and High Flux Isotope Reactor facilities to provide hands-on experience for using synchrotron and neutron sources. The target audience is graduate students attending U.S. universities and majoring in physics, chemistry, materials science, or related fields. The school is jointly conducted by Argonne's Division of Educational Programs, APS, and Materials Science Division; and Oak Ridge National Laboratory's Neutron Scattering Science Division. *Contact: nxschool@dep.anl.gov*

HEXD-MM Workshop • October 13-15 • The goal of this workshop was to advance research in the general area of micromechanics of polycrystalline materials. Presentations were given by international experts who i) conduct synchrotron x-ray diffraction experiments, ii) model material behaviors on multiple size scales, and iii) work in industry on relevant materials. The workshop aimed to enhance contacts between these distinct communities. The impact of the high-value data (both experimental and virtual) is optimized by assuring that the most relevant and timely studies are performed and that these results can then serve as templates for experimental/theoretical collaborations in the future. It is the hope of the organizers that this workshop might initiate a community around the theme of diffraction/micromechanics. For this reason, a group of young investigators were invited to attend the workshop and present their work in a special poster session.
Contact: jlienert@aps.anl.gov

APS X-RAY SOURCE & USER DATA

APS storage ring reliability (MTBF)

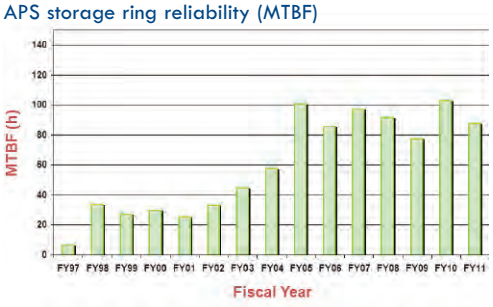

APS x-ray availabilty

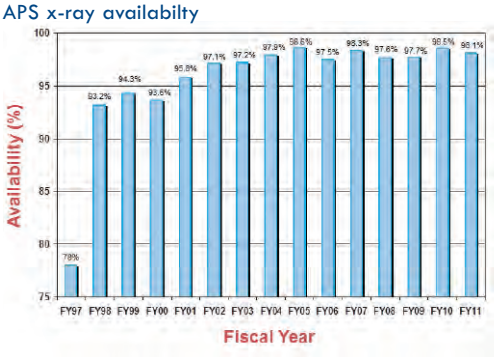

Number of APS users

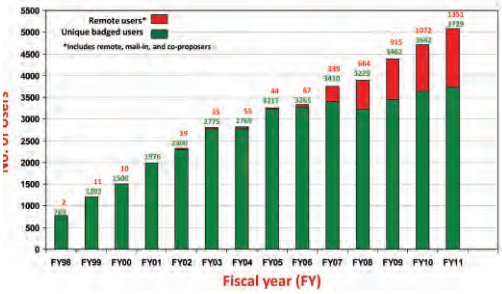

Number of experiments at the APS

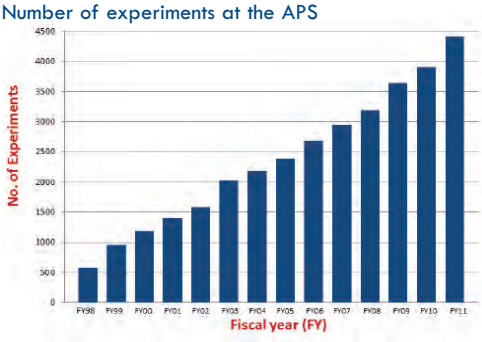

Number of APS publications

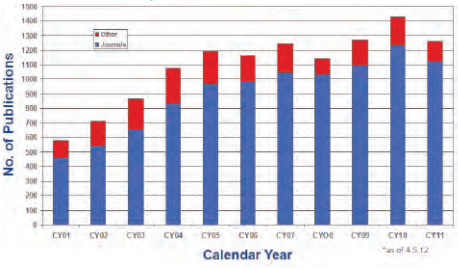

For complete lists of APS publications see the Publications Database at http://www.aps.anl.gov/Science/Publications/

In fiscal year 2011* the APS x-ray source continued to function as a highly reliable delivery system for synchrotron x-ray beams for research. Several factors support the overall growth in both the APS user community and the number of experiments carried out by that community. But there is a direct correlation between the number of x-ray hours available to users; the success of the APS experiment program; and the physicists, engineers, and technicians responsible for achieving and maintaining optimum x-ray source performance. Below are definitions of important measures for the delivery of x-ray beam to users (shown graphically at left).

Storage Ring Reliability: A measure of the mean time between beam losses (faults), or MTBF. MTBF is calculated by taking the delivered beam and dividing by the total number of faults. The APS targets, and routinely exceeds, 70 h MTBF. A fault is defined as complete unavailability of beam either via beam loss or removal of shutter permit not related to weather. A fault also occurs when beam has decayed to the point where stability and orbit can no longer be considered reliable. At the APS, this threshold is 50 mA.

X-ray Availability: The number of hours that the beam is available to the users divided by the number of hours of scheduled beam delivery prior to the beginning of a run. The specific definition of available beam is that the APS Main Control Room has granted permission to the users to open their shutters, *and* there is more than 50-mA stored beam in the storage ring.

* While the highlights in, and title of, this report cover calendar year 2011 data on accelerator performance and user statistics are measured on the basis of fiscal years.

APS users by institutional geographic distribution

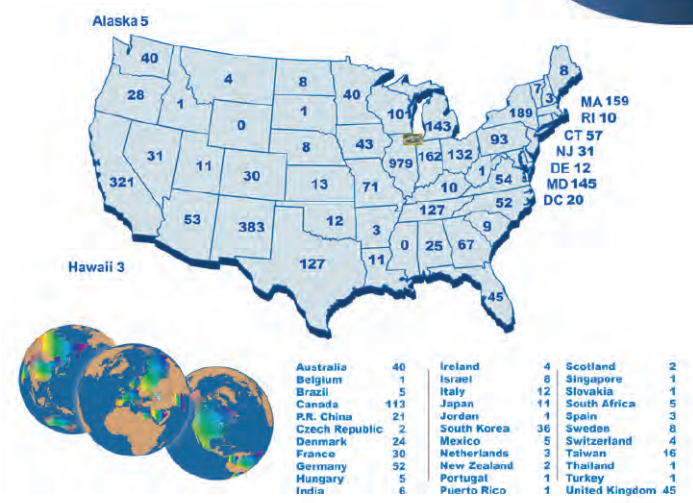

Australia	40	Ireland	4	Scotland	2
Belgium	1	Israel	6	Singapore	1
Brazil	5	Italy	12	Slovakia	1
Canada	113	Japan	11	South Africa	5
P.R. China	21	Jordan	1	Spain	3
Czech Republic	2	South Korea	36	Sweden	8
Denmark	24	Mexico	5	Switzerland	4
France	30	Netherlands	3	Taiwan	16
Germany	52	New Zealand	2	Thailand	1
Hungary	5	Portugal	1	Turkey	1
India	6	Puerto Rico	1	United Kingdom	45

APS users by institution type

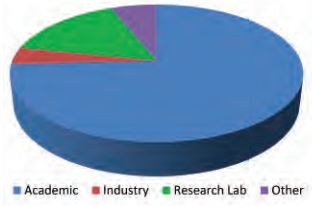

APS users by employment

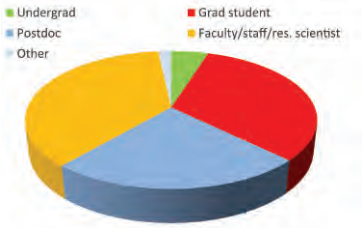

APS users by discipline

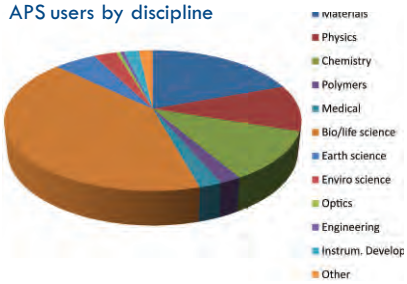

APS users by user type

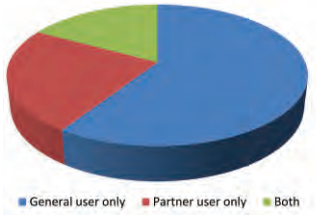

APS users by funding source

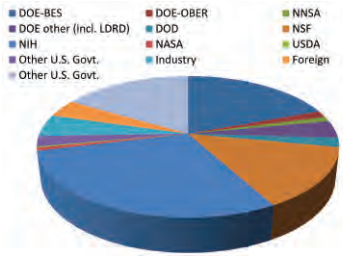

APS ORGANIZATION CHART

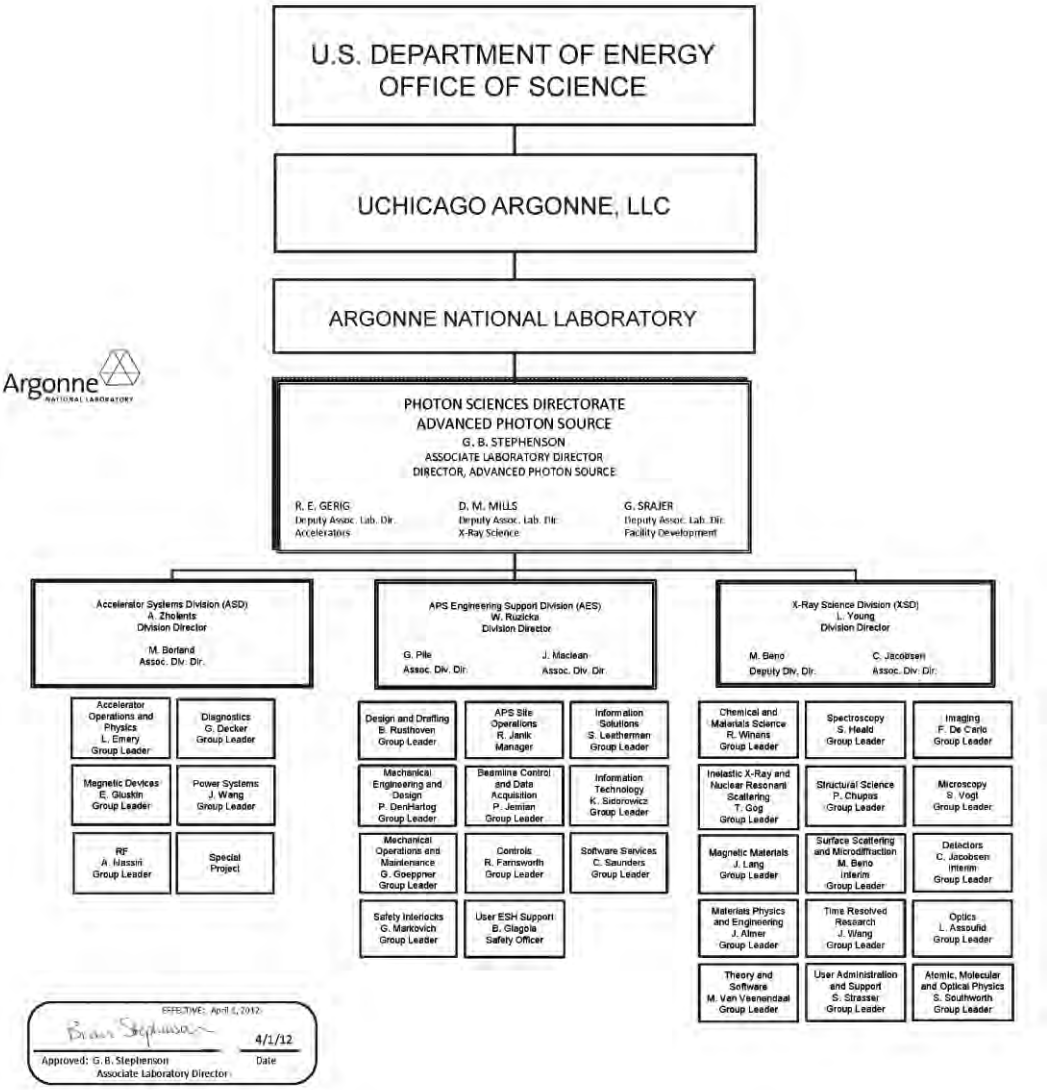

APS STAFFING AND FUNDING

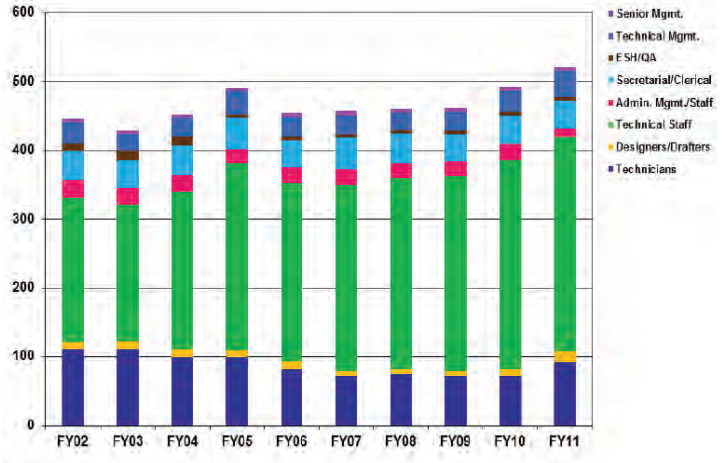

APS staffing levels, FY02-FY11

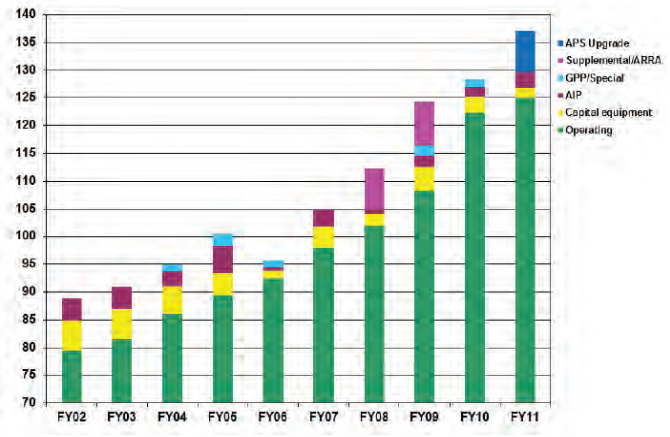

APS funding levels, FY02-FY11

TYPICAL APS MACHINE PARAMETERS

LINAC

Output energy	325 MeV
Maximum energy	450 MeV
Output beam charge	1–3 nC
Normalized emittance	10–20 mm-mrad
Frequency	2.856 GHz
Modulator pulse rep rate	30 Hz
Gun rep rate (1–6 pulses, 33.3 ms apart every 0.5 s)	2–12 Hz
Beam pulse length	8–15 ns
Bunch length	1–10 ps FWHM

PARTICLE ACCUMULATOR RING

Nominal energy	325 MeV
Maximum energy	450 MeV
Circumference	30.66 m
Cycle time	500 ms
Fundamental radio frequency (RF1)	9.77 MHz
12th harmonic rf frequency (RF12)	117.3 MHz
RMS bunch length (after compression)	0.34 ns

INJECTOR SYNCHROTRON (BOOSTER)

Nominal extraction energy	7.0 GeV
Injection energy	325 MeV
Circumference	368.0 m
Lattice structure	10 FODO cells/ quadrant
Ramping rep rate	2 Hz
Natural emittance	65 nm-rad-92 nm-rad
Radio frequency	351.930 MHz

STORAGE RING SYSTEM

Nominal energy	7.0 GeV
Circumference	1104 m
Number of sectors	40
Length available for insertion device	5.0 m
Nominal circulating current, multibunch	100 mA
Natural emittance	2.5 nm-rad
RMS momentum spread	0.096%
Effective emittance	3.1 nm-rad
Vertical emittance	0.040 nm-rad
Coupling	1.5%
Revolution frequency	271.554 kHz
Radio frequency	351.930 MHz
Number of bunches	24 to 1296
Time between bunches	153 to 2.8 ns
RMS bunch length	25 ps to 40 ps
RMS bunch length of 16 mA in hybrid mode	65 ps

APS SOURCE PARAMETERS

UNDULATOR A

Period: 3.30 cm
Length: 2.1 m in sectors 12, 21, 23, 24; 2.4 m in others
K_{max}: 2.75 (effective; at minimum gap)
Minimum gap: 10.5 mm
Tuning range: 3.0–13.0 keV (1st harmonic)
3.0–45.0 keV (1st-5th harmonic)
On-axis brilliance at 7 keV: 4.1 x 10^{19} ph/s/mrad^2/mm^2/0.1%bw (2.4 m)
3.3 x 10^{19} ph/s/mrad^2/mm^2/0.1%bw (2.1 m)
Source size and divergence at 8.0 keV:
Σ_x: 276 μm Σ_y: 11 μm
$\Sigma_{x'}$: 12.7 μrad (2.4 m), 12.9 μrad (2.1 m)
$\Sigma_{y'}$: 6.7 μrad (2.4 m), 7.1 μrad (2.1 m)

2.30-CM UNDULATOR (SECTORS 1, 11, 14)

Period: 2.30 cm
Length: 2.4 m
K_{max}: 1.20 (effective; at minimum gap)
Minimum gap: 10.5 mm
Tuning range: 11.8–20.0 keV (1st harmonic)
11.8–70.0 keV (1st-5th harmonic, non-contiguous)
On-axis brilliance at 12 keV: 6.9 x 10^{19} ph/s/mrad^2/mm^2/0.1%bw
Source size and divergence at 12.0 keV:
Σ_x: 276 μm Σ_y: 11 μm
$\Sigma_{x'}$: 12.3 μrad $\Sigma_{y'}$: 5.9 μrad

2.70-CM UNDULATOR (SECTORS 3 & 14)

Period: 2.70 cm
Length: 2.4 m
K_{max}: 1.76 (effective; at minimum gap)
Minimum gap: 10.5 mm
Tuning range: 6.7–16.0 keV (1st harmonic)
6.7–60.0 keV (1st-5th harmonic, non-contiguous)
On-axis brilliance at 12 keV: 5.7 x 10^{19} ph/s/mrad^2/mm^2/0.1%bw
Source size and divergence at 8.0 keV:
Σ_x: 276 μm Σ_y: 11 μm
$\Sigma_{x'}$: 12.7 μrad $\Sigma_{y'}$: 6.7 μrad

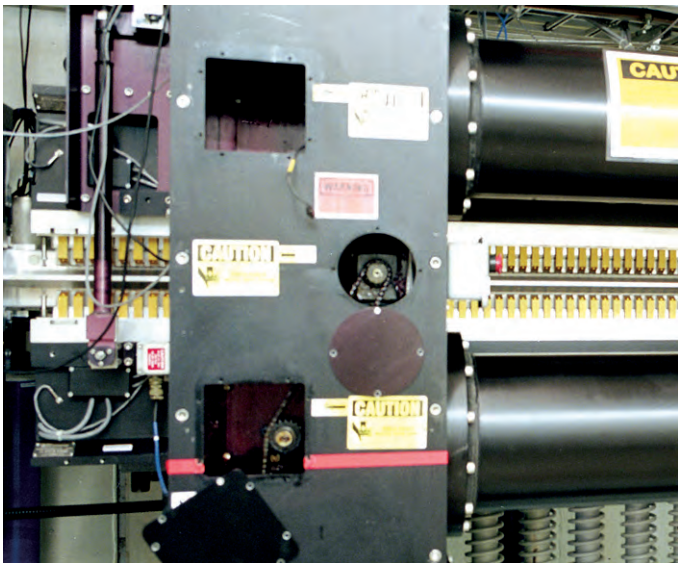

APS SOURCE PARAMETERS

3.00-cm UNDULATOR (SECTORS 12, 21, 23, 30)

Period: 3.00 cm
Length: 2.1 m in sectors 12, 21, and 23; 2.4 m in Sector 30
K_{max}: 2.20 (effective; at minimum gap)
Minimum gap: 10.5 mm
Tuning range: 4.6–14.5 keV (1st harmonic)
4.6–50.0 keV (1st-5th harmonic)
On-axis brilliance at 8 keV: 4.8 x 10^{19} ph/s/mrad^2/mm^2/0.1%bw (2.4 m)
3.9 x 10^{19} ph/s/mrad^2/mm^2/0.1%bw (2.1 m)
Source size and divergence at 8.0 keV:
Σ_x: 276 μm Σ_y: 11 μm
$\Sigma_{x'}$: 12.7 μrad (2.4 m), 12.9 μrad (2.1 m)
$\Sigma_{y'}$: 6.7 μrad (2.4 m), 7.1 μrad (2.1 m)

3.50-cm SmCo UNDULATOR (SECTOR 4)

Period: 3.50 cm
Length: 2.4 m
K_{max}: 3.08 (effective; at minimum gap)
Minimum gap: 9.5 mm
Tuning range: 2.3–12.5 keV (1st harmonic)
2.3–42.0 keV (1st-5th harmonic)
On-axis briliance at 7 keV: 3.7 x 10^{19} ph/s/mrad^2/mm^2/0.1%bw
Source size and divergence at 8.0 keV:
Σ_x: 276 μm Σ_y: 11 μm
$\Sigma_{x'}$: 12.7 μrad $\Sigma_{y'}$: 6.7 μrad

5.50-cm UNDULATOR (SECTOR 2)

Period: 5.50 cm
Length: 2.4 m
K_{max}: 4.97 (effective; at minimum gap)
Minimum gap: 14.0 mm
Tuning range: 0.6–7.0 keV (1st harmonic)
0.6–25.0 keV (1st-5th harmonic)
On-axis brilliance at 4 keV: 1.7 x 10^{19} ph/s/mrad^2/mm^2/0.1%bw
Source size and divergence at 4.0 keV:
Σ_x: 276 μm Σ_y: 11 μm
$\Sigma_{x'}$: 13.9 μrad $\Sigma_{y'}$: 8.8 μrad

APS SOURCE PARAMETERS

CIRCULARLY POLARIZING UNDULATOR (SECTOR 4)

Period: 12.8 cm
Length: 2.1 m
Circular mode:
K_{max}: 2.65 (effective; for both horizontal and vertical fields at maximum currents of 1.2 kA horizontal and 0.34 kA vertical)
B_{max}: 0.26 T (peak fields)
Tuning range: 0.5–3.0 keV (1st harmonic)
On-axis brilliance at 1.8 keV: 3.1 x 10^{18} ph/s/mrad^2/mm^2/0.1%bw
Linear mode:
K_{max}: 2.80 (effective; for both horizontal and vertical fields at maximum currents 1.4 kA horizontal and 0.40 kA vertical)
B_{max}: 0.29 T (peak fields)
Tuning range: 0.8–3.0 keV (1st harmonic)
0.8–10.0 keV (1st–5th harmonic)
On-axis brilliance at 2.1 keV: 2.3 x 10^{18} ph/s/mrad^2/mm^2/0.1%bw
Switching frequency: 0-5 Hz
Switching rise time: 20 ms
Source size and divergence at 1.5 keV:
Σ_x: 276 μm Σ_y: 12 μm
$\Sigma_{x'}$: 18.1 μrad $\Sigma_{y'}$: 14.5 μrad

APS BENDING MAGNET

Critical energy: 19.51 keV
Energy range: 1–100 keV
On-axis brilliance at 16 keV: 5.4 x 10^{15} ph/s/mrad^2/mm^2/0.1%bw
On-axis angular flux density:
9.6 × 10^{13} ph/s/mrad^2/0.1%bw at 16 keV
On-axis horizontal angular flux density:
1.6 × 10^{13} ph/s/mradh/0.1%bw at 6 keV
Source size and divergence at the critical energy:
Σ_x: 92 μm Σ_y: 31 μm
$\Sigma_{x'}$: 6 mrad $\Sigma_{y'}$: 47 μrad

Acknowledgments

APS Science 2011 Editorial Board:

Cele Abad-Zapatero (University of Illinois at Chicago), Mark A. Beno (ANL-XSD), Rodney E. Gerig (ANL-PSC), Dennis M. Mills, (ANL-PSC), William G. Ruzicka (ANL-AES), George Srajer (ANL-XSD), G. Brian Stephenson (ANL-PSC), Linda Young (ANL-XSD), Alexander A. (Sasha) Zholents (ANL-ASD)

The research highlights in this report were written by:

William Arthur Atkins (waarc@grics.net)
David Bradley (david@sciencebase.com)
Yvonne Carts-Powell (yvonne.cartspowell@gmail.com)
Vic Comello (ANL-CEP, vcomello@anl.gov)
Dana Desonie (desonie@cox.net)
Sandy Field (sfield@fieldscientific.com)
Karen Fox (kfox@nasw.org)
Emma Hitt (emma@hittmedicalwriting.com)
Philip Koth (philkoth@comcast.net)
Elise LeQuire (cygnete@mindspring.com)
David Lindley (dlindley@nasw.org)
Mona A. Mort (monasbox@gmail.com)
Nicola Parry (nicola@parrymedicalwriting.com)
Mark Wolverton (exetermw@earthlink.net)

Photography: Wes P. Agresta and George J. Joch (both ANL-CEP)
Aerial photograph of the APS: John Hill (Tigerhill Studio, http://www.tigerhillstudio.com)
Publications, contracts, rights and permissions, circulation: Jessie L. Skwarek (ANL-PSC)
Printing: Gary R. Weidner (ANL-CEP)
CD production: Linda M. Graf and Lorenza M. Salinas (both ANL-CEP)
Editorial and project coordination, design, photography: Richard B. Fenner (ANL-PSC)

Our thanks to the corresponding authors and others who assisted in the preparation of the research highlights, to the users and APS personnel who wrote articles for the report, and our apologies to anyone inadvertently left off this list. To all: your contributions are appreciated.

Acronyms for Argonne division and group names that appear in this report

AES	Argonne APS Engineering Support Division
AOP	Accelerator Operation & Physics Group (ASD)
ASD	Argonne Accelerator Systems Division
CMS	Chemical and Materials Science Group (XSD)
CSE	Argonne Chemical Sciences and Engineering Division
CTL	Controls Group (AES)
DD	Design & Drafting Group (AES)
DIA	Diagnostics Group (ASD)
FMS	Argonne Facilities Management and Services Group
IT	Information Technology Group (AES)
IXN	Inelastic X-ray & Nuclear Resonant Scattering Group (XSD)
MD	Magnetic Devices Group (ASD)
MED	Mechanical Engineering & Design Group (AES)
MIC	Microscopy Group (XSD)
MM	Magnetic Materials Group (XSD)
MOM	Mechanical Operations & Maintenance (AES)
MPE	Materials Physics & Engineering (XSD)
MSD	Argonne Materials Science Division
OPT	Optics Group (XSD)
PS	Power Systems Group (AES)
PSC	Argonne Photon Sciences
SO	Site Operations Group (AES)
SRS	Structural Science Group (XSD)
SSM	Surface Scattering & Microdiffraction Group (XSD)
XSD	Argonne X-ray Science Division

Advanced Photon Source
Argonne National Laboratory
9700 S. Cass Ave.
Argonne, IL 60439 USA

www.anl.gov
www.aps.anl.gov

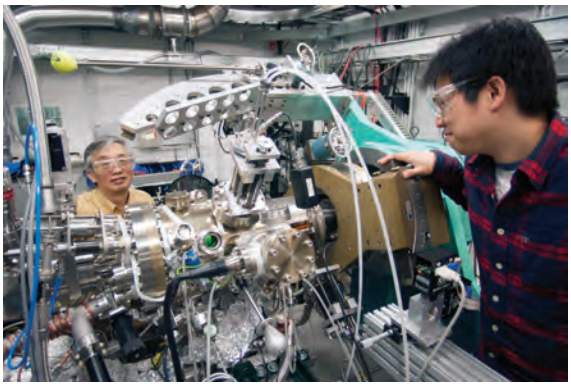

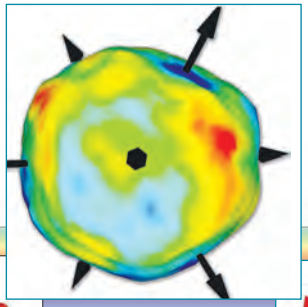

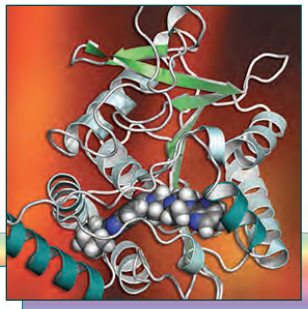

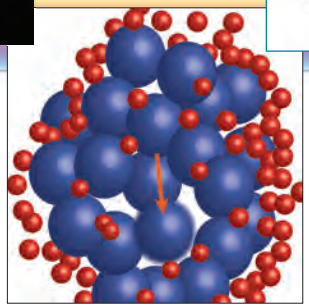

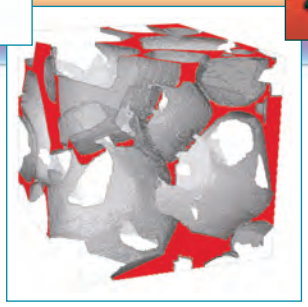

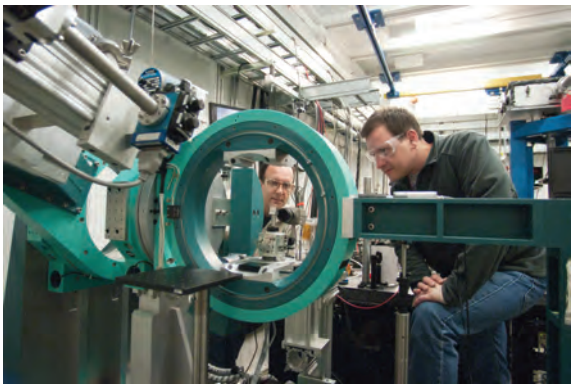

U.S. DEPARTMENT OF ENERGY | Office of Science